Semi-metallic polymers for thermoelectric applications

Solène Perrot

université de BORDEAUX

THÈSE PRÉSENTÉE

POUR OBTENIR LE GRADE DE

DOCTEUR DE L'UNIVERSITÉ DE BORDEAUX

ÉCOLE DOCTORALE des Sciences Chimiques

SPÉCIALITÉ : Polymères

Par Solène PERROT

SEMI-METALLIC POLYMERS FOR THERMOELECTRIC APPLICATIONS

-

POLYMERES SEMI-METALLIQUES POUR DES APPLICATIONS EN THERMOELECTRICITE

Sous la direction de Guillaume FLEURY et Georges HADZIIOANNOU

Soutenue le 19 février 2021

Membres du jury :

Dr ROUGIER Aline, Directrice de Recherche, ICMCB – Bordeaux	Présidente du jury
Dr HEBERT Sylvie, Directrice de recherche, CRISMAT - Caen	Rapporteur
Pr SEMMAR Nadjib, Professeur, Université d'Orléans	Rapporteur
Pr CRISPIN Xavier, Professeur, Université de Linköping – Suède	Examinateur
Dr FLEURY Guillaume, Maître de Conférences, Université de Bordeaux	Directeur de thèse
Pr HADZIIOANNOU Georges, Professeur, Université de Bordeaux	Directeur de thèse

ACKNOWLEDGMENT

Ce projet de thèse a été conduit dans le laboratoire de chimie des polymères organiques (LCPO) au sein de l'équipe 4, polymères pour l'électronique, l'énergie et l'information. Je tenais tout d'abord à remercier Georges HADZIIOANNOU, directeur de cette équipe, de m'avoir accueillie mais aussi d'avoir co-dirigé cette thèse. Je souhaiterais surtout remercier mon directeur de thèse Guillaume FLEURY. Durant ces trois ans et demi de thèse, Guillaume a toujours été disponible, que ce soit pour parler de résultats, préparer des présentations ou corriger des écrits. Guillaume a vraiment permis le bon déroulement de cette thèse en m'apportant les conseils rassurant sur l'avancée des travaux. Il reste quand même un goût amer de ne pas avoir pu aller plus loin sur la dernière partie de mes travaux.

Je tenais ensuite à remercier Sylvie HEBERT, directrice de recherche au CRISMAT, et Nadjib SEMMAR, professeur à l'université d'Orléans, pour avoir accepté d'être les rapporteurs de cette thèse mais aussi Aline ROUGIER, directrice de recherche à l'ICMCB, et Xavier CRISPIN, professeur à l'université de Linköping, d'avoir accepté d'être les examinateurs. La discussion avec le jury a été très constructive et a permis de mieux comprendre certains résultats obtenus et c'est pourquoi je tenais une nouvelle fois à les remercier.

L'analyse des matériaux de cette thèse n'aurait pas été possible sans l'accès à la plateforme ELORPrintTec, c'est pourquoi je remercie l'ensemble des personnes travaillant sur cette plateforme qui m'ont formée à l'utilisation des machines Notamment, je tenais à remercier Roland LEFEVRE pour son aide pour la spectroscopie de photoélectrons et les discussions autour de mes résultats.
La majeure partie des manipulations de ma thèse ont été effectuées grâce à une salle blanche présente au LCPO, c'est pourquoi je tenais à remercier Gilles PECASTAINGS qui gérait cette salle blanche mais aussi l'AFM. Merci pour les analyses, les moments de discussion et de partage qu'il y a pu avoir que ce soit au sein du laboratoire ou à l'extérieur.

Le laboratoire ne pourrait pas fonctionner sans l'aide de Mélanie, Aude et Ellena, merci à vous pour l'aide mais aussi pour les moments de discussion. Merci aussi aux autres permanents du laboratoire.

Ces trois ans de thèse n'auraient pas été les mêmes sans les **B8ers** ! Que ce soit d'un point de vue scientifique ou personnel, les discussions ont toujours été enrichissantes. Merci à Benjamin (le super papa), Micah (et son incroyable voix), Ariana, Cian (twerkman forever), Ségo, Naser, Alberto, Emin, Alizée, Lauriane (mention spéciale pour ses pâtisseries), Florian (toujours de bons conseils), Kosta (My friend), Jeremy (le gardien du chat), Alexander, Quentin, Rim, Anirudh, Shekhar, Kaili, Sasikumar, Milutin. Merci aux italiens : Tommaso, Francesco, Lorenzo, Federico, Nicoletta et Sylvia (♡). Merci aux origines du Bu3West : Camille, Geoffrey, Pane et Florent, pour les moments de discussion, les activités travaux manuels du vendredi, les fous rires et les moments sérieux. Tout particulièrement merci à Florent pour toute l'aide que tu m'as apportée, merci de m'avoir rassurée et d'avoir été présent jusqu'au bout. Merci à mes sportifs préférés de m'avoir traînée à la salle de sport : Antoine et Pino ! Remerciement spécial à Cindy Cordula, même si je n'ai jamais compris ton style vestimentaire, tu auras été d'un grand soutien pendant ces trois ans. Merci pour tes conseils scientifiques, merci pour les moments de discussion et les voyages. Deuxième mention spéciale pour mon illustrateur préféré : Nils, sans toi les gens n'auraient pas aussi bien compris ma thèse !

Je voulais aussi remercier mes amis qui même s'ils n'ont pas pu être présent physiquement, étaient là moralement pour me soutenir ! Merci aux meilleurs bro Boris et Quentin, vous pouvez maintenant dire que vous avez une amie docteur ! Merci aussi à Sam ! Vinicius, tu es la meilleure rencontre de mes études supérieures, ma Cristina n°2 ! Merci de m'avoir soutenue et je suis sûre que tout se passera bien pour toi aussi !

Je voulais enfin remercier ma famille, notamment ma mère et ma sœur qui ont toujours été là pour moi. Merci pour tout ce que vous avez fait et ce que vous faîtes encore. Merci de me soutenir.

Merci aussi à celui qui partage ma vie et qui a permis à cette thèse qu'elle soit jolie. Merci mon artiste Sacha ♡. Merci de m'avoir supportée pendant les derniers moments super stressant de ma thèse, je ne sais pas comment tu as fait.

Merci Rito !

Merci à toutes les autres personnes qui ont contribuées de près ou de loin au bon déroulement de cette thèse.

Papa, je sais que tu veilles sur moi de là-haut et que tu serais fier de moi.

RESUME EN FRANÇAIS

Polymères semi-métalliques pour des applications en thermoélectricité

La thermoélectricité consiste à utiliser une différence de température pour la transformer en électricité. Ce principe se base sur les découvertes des scientifiques Volta, Seebeck, Peltier et Thomson. La thermoélectricité se base notamment sur l'effet Seebeck où le coefficient Seebeck s'exprime comme suit :

$$\nabla V = -S\nabla T \qquad \textit{Équation 1}$$

Lorsqu'une différence de température est appliquée à un matériau, un déplacement de charges va survenir (sans déplacement de matière) et il est alors possible de mesurer une différence de tension aux bornes de ce matériau. Il existe deux types de matériaux thermoélectriques, les matériaux de type p, où les porteurs de charges majoritaires sont des trous, et les matériaux de type n où les porteurs de charges majoritaires sont des électrons. L'efficacité des matériaux thermoélectriques se mesure avec le facteur de mérite ZT :

$$ZT = \frac{\sigma S^2}{\kappa} T \qquad \textit{Équation 2}$$

où σ est la conductivité électrique, S le coefficient Seebeck et κ la conductivité thermique.

Pour obtenir un bon matériau thermoélectrique, il est donc nécessaire que celui-ci soit un bon conducteur de charges (σ grand), ait un bon thermovoltage (S grand) mais soit un mauvais conducteur thermique (κ faible). Cependant, σ et S ont des comportements antagonistes en fonction du taux de porteurs de charges. Il est donc nécessaire de trouver une balance entre ces deux paramètres pour obtenir un bon matériau thermoélectrique. Comme κ est un paramètre plus compliqué à mesurer, et

notamment en configuration de film mince, les matériaux thermoélectriques sont souvent évalués en fonction du facteur de puissance PF exprimé comme suit :

$$PF = S^2\sigma \qquad \text{Équation 3}$$

Pour des applications à température ambiante, le meilleur composé thermoélectrique est un matériau inorganique, le Bi_2Te_3 avec des facteurs de mérite supérieur à 1. De nombreux autres composés inorganiques sont utilisés en thermoélectricité comme les oxydes, les sulfites et sélénites, etc. Malgré les propriétés intéressantes des matériaux inorganiques, l'étude de matériaux plus simple à mettre en œuvre et composés d'éléments plus abondants, les matériaux organiques, semble être une bonne alternative. Ces matériaux ont notamment des propriétés thermoélectriques intéressantes avec comme exemple notable le poly(3,4-ethylènedioxythiophène) (PEDOT), qui, dopé avec du tosyle de fer (Tos), peut atteindre des facteurs de puissance de l'ordre de quelques centaines de $\mu W.m^{-1}.K^{-2}$. De plus, ce polymère peut être synthétisé par différentes méthodes que sont la polymérisation in-situ et en phase vapeur (ISP et VPP respectivement).

Dans cette optique, le PEDOT:Tos a été choisi pour étudier ses propriétés électroniques et thermoélectriques au vu de la méthode de polymérisation. La compréhension des méthodes de caractérisation était un point important avant de pouvoir interpréter les résultats obtenus pour le PEDOT:Tos, c'est pourquoi un chapitre lui est consacré avec notamment une étude sur la mesure de conductivité électrique avec des contacts métalliques.

Le premier chapitre expérimental (chapitre 3 du manuscrit) est dédié à la comparaison entre les deux méthodes de polymérisation du PEDOT:Tos : ISP et VPP. Dans le premier cas, l'ensemble des produits (EDOT et tosyle de fer) est mélangé, déposé par dépôt à la tournette et chauffé pour induire la polymérisation alors que dans le deuxième cas seulement le tosyle de fer est déposé puis exposé à des vapeurs d'EDOT ce qui va induire la polymérisation. Cette différence de polymérisation va avoir un impact sur la croissance des chaînes polymériques et notamment sur la

structure macroscopique et microscopique. En effet, par microscopie à force atomique (AFM), on remarque que les films préparés par VPP sont plus rugueux que ceux préparés par ISP, Figure 1.

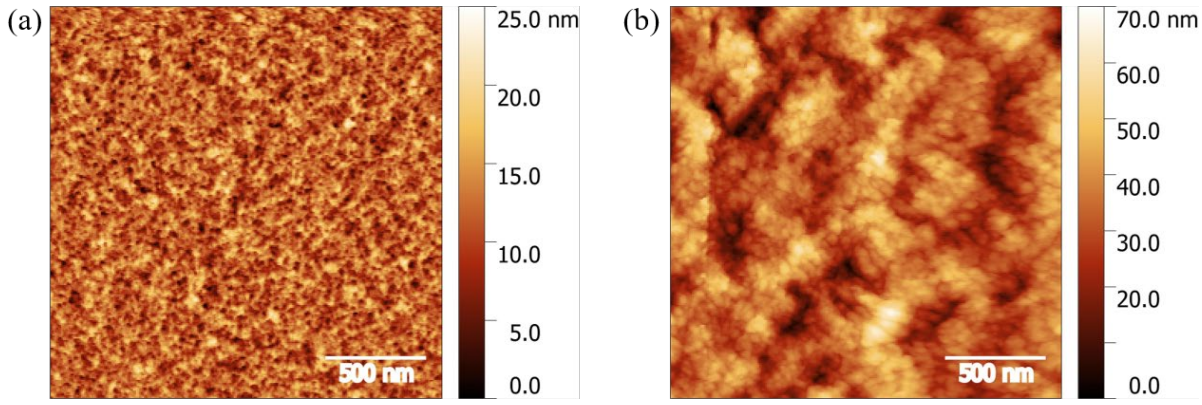

Figure 1 Images de topographie AFM 2x2µm² (a) film déposé par ISP (b) film déposé par VPP.

La différence de structure se retrouve aussi à l'échelle microscopique où, grâce à la diffraction des rayons X en incidence rasante (GIXRD), il est possible d'avoir accès aux distances caractéristiques entre les chaînes de polymère. Ces distances, $d_{\pi-\pi}$ et $d_{lamelles}$, ainsi qu'un calcul du degré de cristallinité des films, permettent de conclure sur le caractère plus cristallin des films polymérisés en in-situ. La cristallinité des films va avoir un impact sur les propriétés de transport en facilitant la conduction par saut. Notamment, on retrouve un facteur de puissance plus important dans le cas de films synthétisés par in-situ, Figure 2. Il est important de noter que cette étude a permis d'obtenir des valeurs de conductivité électrique très hautes comparées à la littérature.

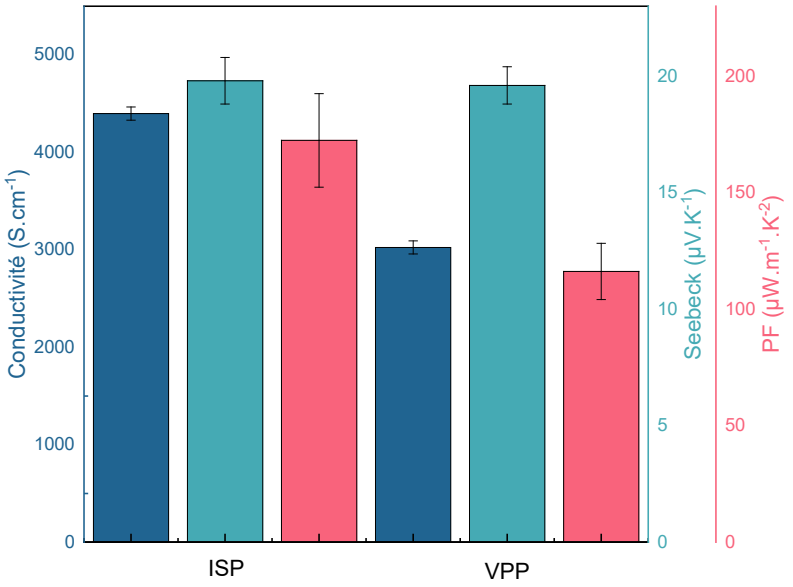

Figure 2 Propriétés thermoélectriques des films synthétisés par ISP et VPP. La conductivité électrique est représentée en bleu foncé, le coefficient Seebeck en bleu clair et le facteur de puissance en rose.

Malgré les meilleures propriétés intrinsèques des films synthétisés par ISP, il a été décidé de mieux comprendre les phénomènes liés à la VPP à travers un deuxième chapitre expérimental (chapitre 4 du manuscrit) car cette méthode se montre plus versatile et doit permettre de modifier plus efficacement les propriétés thermoélectriques du PEDOT:Tos.

Le but de ce chapitre était tout d'abord de comprendre l'influence des additifs (pyridine et DMSO) sur la synthèse des films de PEDOT:Tos en VPP. Ces deux additifs permettent d'augmenter la masse molaire du polymère et d'avoir une meilleure cristallinité. La spectroscopie de photoélectrons à rayons X (XPS) permet notamment de calculer des degrés d'oxydations différents avec une valeur plus faible dans le cas de films polymérisés sans additifs (14,9% contre 22%). Cette valeur indique que sans pyridine et DMSO, la croissance des films est rapide et inhomogène et ne permet pas de doper le film tout en le faisant croitre. De plus la spectroscopie de photoélectrons à UV (UPS) permet d'avoir accès à la structure électronique des films et tend à dire que moins d'états électroniques sont disponibles dans le cas de films sans additifs ce qui entrainerait une diminution de la conductivité électrique, Figure 3.

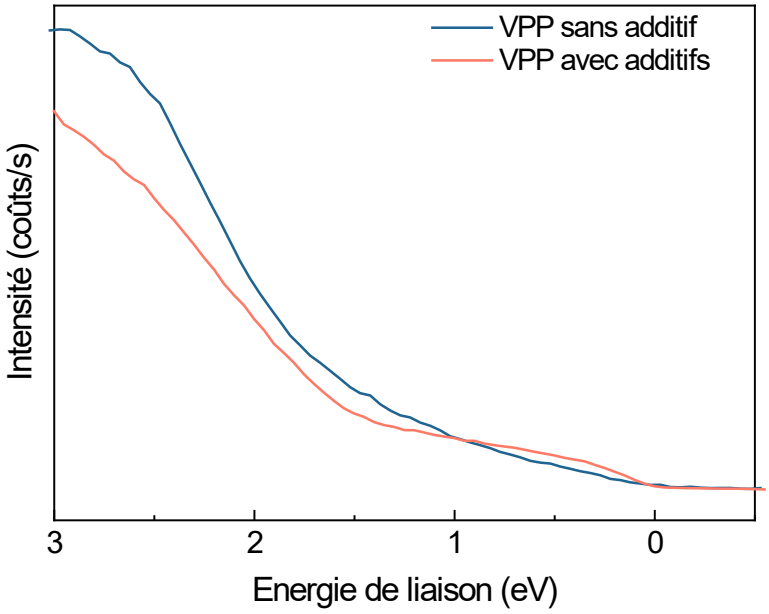

Figure 3 Spectres UPS de films synthétisés avec (rouge) et sans (bleu) additifs.

Les propriétés thermoélectriques (conductivité électronique et coefficient Seebeck) ont été mesurées et permettent de conclure que l'ajout d'additifs est indispensable car il permet d'obtenir des facteurs de puissance 100 fois supérieurs.

Le chapitre se poursuit avec l'étude de l'effet de la concentration en tosyle de fer lors de la polymérisation. Il en ressort que la concentration joue notamment un rôle sur l'épaisseur et la résistance du film du fait que plus la concentration est faible, plus l'épaisseur du film va être faible et donc plus le film va être inhomogène. La concentration va donc jouer un rôle sur la conductivité électrique des films tout en maintenant le coefficient Seebeck relativement constant, Figure 4.

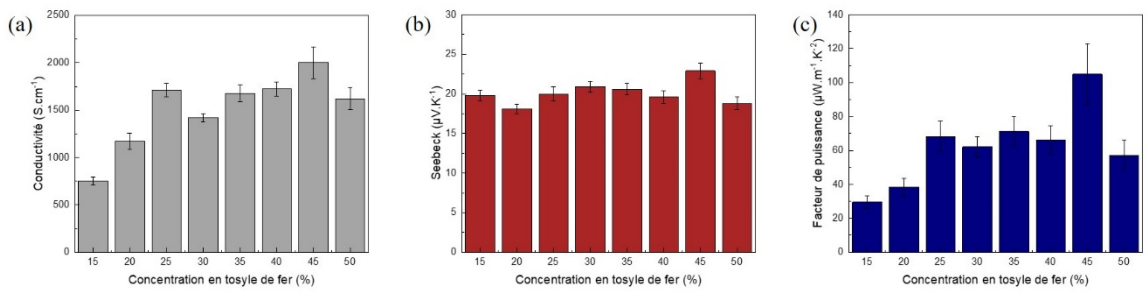

Figure 4 Conductivité électrique, coefficient Seebeeck et facteur de puissance des films de PEDOT:Tos en fonction de la concentration en tosyle de fer.

Les structures électroniques, sondées par XPS et UPS, ne vont pas être modifiées par la concentration en tosyle de fer avec un degré d'oxydation constant de 22% quelle que soit la concentration.

Ce second chapitre expérimental se termine avec l'étude des propriétés électroniques des films de PEDOT:Tos à leur surface mais aussi à l'interface entre le film et le substrat. Cette étude a été menée en retirant les films de leur substrat et en les retournant sur un nouveau substrat. Les résultats de spectroscopie de photoélectrons montrent que le degré d'oxydation est le même des deux côtés du film et que la structure électronique est similaire. La principale différence réside dans la morphologie où l'AFM montre une structure en éponge liée à la méthode de croissance. En effet, comme la croissance de PEDOT:Tos par VPP est un processus de nucléation suivie de la croissance du film, l'interface est moins homogène.

Le dernier chapitre de cette thèse (chapitre 5 du manuscrit) se veut novateur. Après avoir étudié les propriétés électroniques et structurales des films de PEDOT:Tos, le but étant d'améliorer ses propriétés de conduction. Pour se faire, l'idée est de confiner les chaines de polymères dans de petits espaces afin d'augmenter la cristallinité et donc la conduction par saut. Pour se faire, des copolymères à blocs ont été utilisés car ils ont l'avantage de s'auto-organiser sous certaines conditions, permettant d'obtenir des motifs à l'échelle nanométrique. En effet, les copolymères à blocs (CPBs) sont deux polymères liés entre eux par une liaison covalente qui, lorsque l'on joue sur leur incompatibilité, leur degré de polymérisation ou la fraction d'un bloc par rapport à l'autre, peuvent se structurer selon des cylindres ou des lamelles (ou d'autres structures qui n'ont pas été étudiées dans le cadre de ce travail). Trois stratégies ont été adoptées pour cette étude.
1/ La première stratégie consiste à utiliser le CPB comme masque pour un procédé de lithographie dont le processus est décrit. Le PS-*b*-PMMA a été choisi pour cette étude car il s'agit d'un copolymère connu dans le domaine de la lithographie en microélectroniques. Un film de PEDOT:Tos a été déposé sur un substrat et un film de CPB par-dessus. Cette bicouche est ensuite passé dans un réacteur plasma afin de retirer le bloc de PMMA pour laisser apparaître un masque troué de PS. Le traitement

plasma est ensuite poursuivi pour gravé à la fois le PEDOT:Tos suivant le masque mais aussi le masque pour permettre d'obtenir des motifs de PEDOT:Tos.

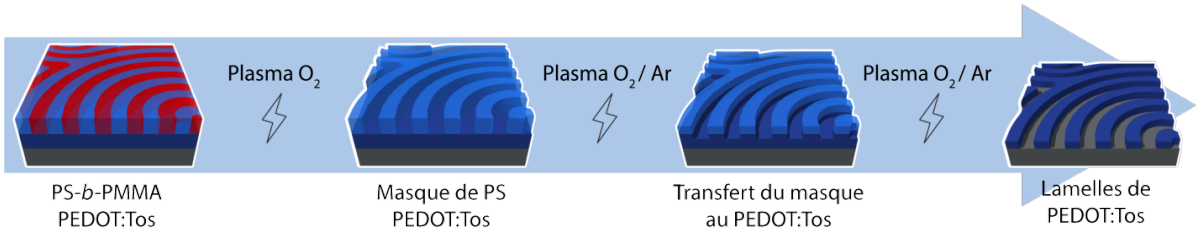

Figure 5 Processus de lithographie du PEDOT:Tos par un masque de PS.

Cette étude permet de démontrer que la lithographie permet d'obtenir des motifs de PEDOT:Tos, comme le montre la Figure 6.

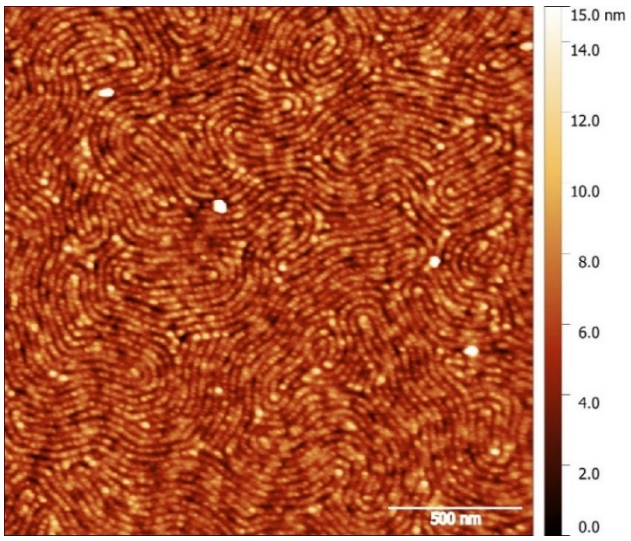

Figure 6 Image de topographie AFM 2x2µm² d'un film de PEDOT :Tos après lithographie avec un copolymère à blocs lamellaire.

Malgré une bonne reproduction des motifs, le PEDOT:Tos obtenu a perdu ses propriétés de conduction électrique. Lorsque l'on analyse sa structure avec la méthode XPS, on se rend compte que la structure du polymère n'est plus la même avec une contribution des liaisons S=O beaucoup plus importante qui peut être liée à de nouvelles liaisons, dans le squelette du polymère, créées lors du traitement par plasma.

2/ La deuxième stratégie consiste à faire gonfler un film de CPB avec une solution de tosyle de fer. Pour ce faire, le CPB PS-*b*-P2VP a été choisi du fait de la grande réactivité du bloc pyridine. La solution de tosyle de fer est diluée dans du butanol et le butanol fait gonfler le bloc P2VP. Naturellement, le tosyle de fer devrait se retrouver dans le bloc gonflé. Lorsque l'on regarde en AFM les structures obtenues après avoir plongé un film de PS-b-P2VP dans une solution de tosyle de fer, puis rincé avec du butanol, on retrouve la structure lamellaire du CPB avec certaines parties plus gonflées que d'autres, Figure 7. L'analyse de ces films par XPS permet de démontrer que du tosyle de fer est présent à l'intérieur du CPB mais aussi qu'il y a eu un dédoublement du pic d'azote montrant une complexation de celui-ci. Cependant, après exposition de ces films aux vapeurs d'EDOT, l'analyse de ce nouveau système ne nous permet pas de mettre en évidence la présence de PEDOT.

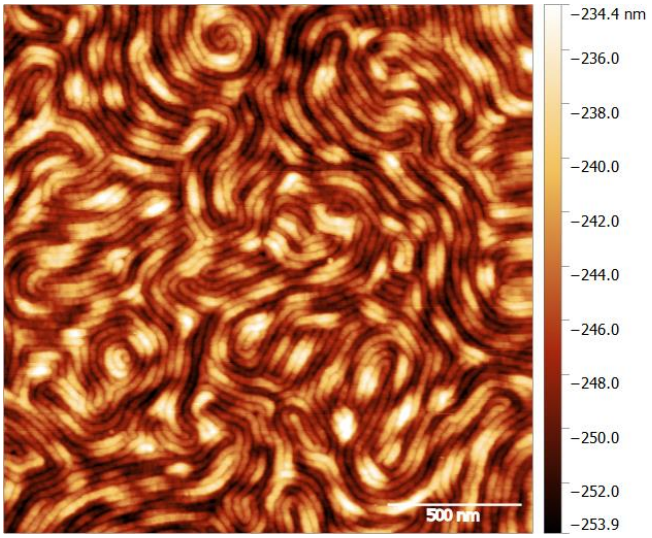

Figure 7 Image de topographie AFM 2x2µm² d'un film de PS-b-P2VP après avoir été plongé dans une solution de tosyle de fer et rincé.

En complexant avec le la P2VP, les ions Fe^{3+}, nécessaires à la polymérisation de l'EDOT, sont réduits en Fe^{2+} et ne sont donc plus disponibles pour la polymérisation du monomère.

3/ La troisième stratégie consiste à préparer une solution avec le CPB, PS-*b*-P2VP, et le tosyle de fer puis à la déposer sur un substrat et chauffer le film pour induire une organisation. Le tosyle de fer est supposé avoir une affinité pour le groupement pyridine du CPB et donc se lié à celui-ci. De ce fait, la fraction du bloc P2VP va devenir

plus importante par rapport au bloc PS. Lors de l'analyse par AFM de ces films, on note une transition de phase de la structure lamellaire à la structure cylindrique, Figure 8 (a) et (b) respectivement.

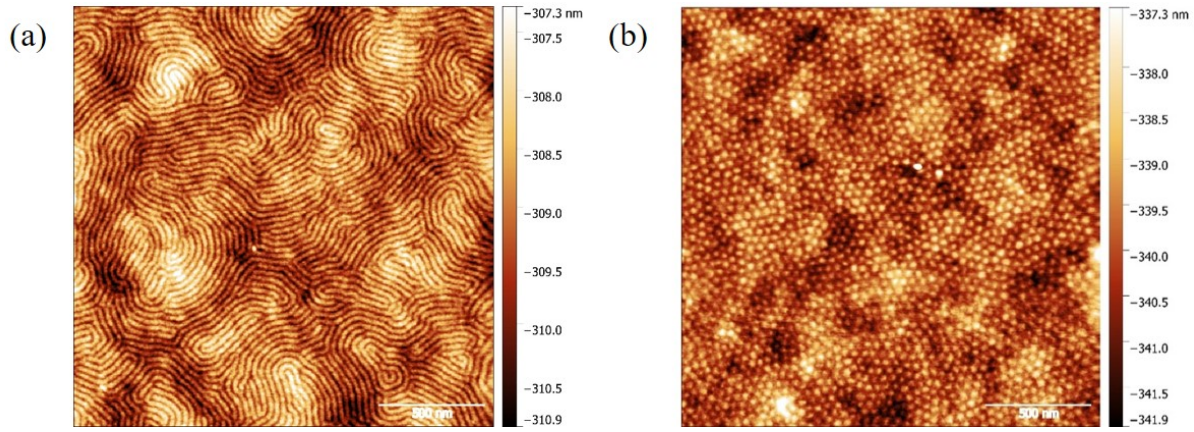

Figure 8 Image de topographie AFM 2x2µm² d'un film de (a) PS-b-P2VP et (b) PS-b-P2VP/Tos après structuration.

Le changement de phase observé permet de conclure que le tosyle de fer a complexé avec la P2VP. Les films sont maintenant composés d'une matrice P2VP/Tos avec des cylindres de PS. L'exposition à des vapeurs d'EDOT solubilise le film et un traitement plasma a été choisi pour rendre le film insoluble. Cependant, après analyse le film contient une faible proportion de PEDOT.

Ce dernier chapitre est une ouverture sur les perspectives possibles pour polymériser de l'EDOT avec du tosyle de fer en formant des nanostructures dans le but d'améliorer les propriétés thermoélectriques.

LIST OF ABBREVIATIONS

AFM: Atomic Force Microscopy

Ag: Silver

Al Kα: Monochromatic aluminum anode

Ar: Argon

Au: Gold

BCP: Block Copolymer

Bi_2Te_3: Bismuth Telluride

Br: Bromium

BTFMSI: Bis(trifluoromethylsulfonyl)imide

Bu_4NTos: Tetrabutylammonium Tosylate

BuOH: Butanol

C: Carbon

C1s: Carbon 1s orbital

CB: Conduction Band

Cl: Chlorine

ClO_4^-: Perchlorate anion

CNT: Carbon Nanotube

CSA: Camphorsulfonic Acid

Cu Kα: Monochromatic copper anode

CVD: Chemical Vapor Deposition

DC: Direct Current

DMF: dimethylformamide

DMSO: dimethylsulfoxide

DoS: Density of States

EDOT: Ethylene Dioxythiophene

E_F: Fermi level

EG: Ethylene Glycol

EtOH: Ethanol

F_4TCNQ: 2,3,5,6-Tetrafluoro-7,7,8,8-tetracyanoquinodimethane

FBDPPV: Fluorine functionalized benzodifurandione-based poly(p-phenylene vinylene)

$Fe(OTf)_3$: Iron(III) trifluoromethanesulfonate

$Fe(Tos)_3$: Iron(III) Tosylate

$FeCl_3$: Iron Chloride

FWHM: Full Width at Half Maximum

GIWAXS: Grazing Incidence Wide Angle X-Rays Scattering

GIXRD: Grazing Incident X-ray Diffraction Grazing Incident X-ray Diffraction

H_2O_2: Peroxyde d'hydrogène

He: Helium

HMS: Higher Manganese Silicide

HOMO: Highest Occupied Molecular Orbital

$HSO4^-$: Hydrogenosulfate ion

IP: Ionization Potential

IPES: Inverse PhotoEmission Spectroscopy

ISP: In-Situ Polymerization

$LiBF_4$: lithium tetrafluoroborate

$LiClO_4$: Lithium Perchlorate

LUMO: Lowest Unoccupied Molecular Orbital

$NaBIm_4$: sodium tetrakis(1-imidazolyl)borate

NaOH: Sodium Hydroxide

N-DMBI: 4-(1,3-dimethyl-2,3-dihydro- 1H-benzoimidazol-2-yl)phenyl)dimethylamine

NW: Nanowires

O: Oxygen

O1s: Oxygen 1s orbital

O_2: Dioxygen

oCVD: Oxidative Chemical Vapor Deposition

P(NDI2OD-T2): Poly{[N,N0 -bis(2-octyldodecyl)-naphthalene-1, 4,5,8-bis(dicarboximide)-2,6-diyl]-alt-5,50 -(2,20 -bithiophene)}

P(NDI2OD-T2); poly{[N,N0 -bis(2-octyldodecyl)-naphthalene-1, 4,5,8-bis(dicarboximide)-2,6-diyl]-alt-5,50 -(2,20 -bithiophene)}

P3HT: Poly(3-hexylthiophene)

PA: Polyacetylene

PANi: Poly(Anilyne)

PEDOT: Poly(ethylene dioxythiophene)

PEG-PPG-PEG: Poly(ethylene glycol-propylene glycol-ethylene glycol)

PEG-ran-PPG: Poly(ethylene glycol-ran-propylene glycol)

PEO-PPO-PEO: Poly(ethylene oxide)-block-poly(propylene oxide)-block-poly(ethylene oxide)

PF: Power Factor

PF_6: Hexafluorophosphate

PFBT: poly(fluorene-*alt*-benzothiadiazole)

PGMEA: Propylene Glycol Methyl Ether Acetate

PPP: Polyparaphenylene

PPV: Poly(Phenylene Vinylene)

PPy: Poly(Pyrole)

PS-*b*-P2VP: Polystyrene-*block*-poly(2vinylpyridine)

PS-*b*-PMMA: Polystyrene-*block*-poly(methyl methacrylate)

PSS: Poly(styrenesulfonate)

PS-*stat*-PMMA: Polystyrene-*statistic*-poly(methyl methacrylate)

PT: Polythyophene

PTFE: Polytétrafluoroéthylène

pTSA: p-Toluenesulfonic Acid

PyrBr: Pyridinium Bromide

QCM: Quartz Crystal Microbalance

rC: Relative Crystallinity

RIE: Reactive Ion Etching

RPM: Rotation Per Minute

S: Sulfur

S2p: Sulfur 2p orbital

Sb_2Te_3: Antimony Telluride

SEM: Scanning Electron Microscopy

Si: Silicon

SiO_2: Silicon oxide

SWCNT: Single Walled Carbon Nanotube

$TBABF_4$: Tetra-n-butylammonium tetrafluoroborate

$TBAClO_4$: Tetrabutylammonium perchlorate

TDAE: Tetrakis(dimethylamino)ethylene

TE: Thermoelectric

TEM: Transmission Electron Microscopy

Tos: Tosylate

UHV: Ultra-high vacuum

UPS: Ultraviolet Photoelectrons Spectroscopy

VB: Valence Band

VPP: Vapor Phase Polymerization

VVPP: Vacuum Vapor Phase Polymerization

WF: Work Function

XPS: X-Ray Photoelectrons Spectroscopy

XRD: X-Ray Diffraction

ZT: Figure of Merit

LIST OF SYMBOLS

Symbol	Symbol name	Unit
λ	Mean free path length	Å
μ	Chemical potential	$J.mol^{-1}$
χ	Flory-Huggins parameter	-
2ϑ	Angle of the diffraction pattern	°
D	Diffusion coefficient	$m^2.s^{-1}$
D(E)	Number of available state	-
d_{hkl}	Interplanar distance	Å
$d_{lamellae}$	Lamellae stacking distance	Å
$d_{\pi-\pi}$	π-π stacking distance	Å
E_B	Binding energy	eV
E_F	Fermi level	eV
E_{kin}	Energy Kinetic	eV
$f_0(E)$	Fermi-Dirac distribution	-
I	Current	A
J	Current density	$A.m^{-2}$
K	Thomson coefficient	$V.K^{-1}$
K	Shape factor	-
k_B	Boltzmann coefficient	$J.K^{-1}$
L_0	Copolymer periodicity	nm
L_C	Coherence length	Å
N	Degree of polymerization	-
PF	Power Factor	$\mu W.m^{-1}.K^{-2}$
q	Elemental charge	A.s
Q	Thermal flux	W
R	Resistance	Ω
rC	Relative crystallinity	-
R_s	Sheet resistance	$\Omega.sq^{-1}$

S	Seebeck coefficient	$\mu V.K^{-1}$
T	Temperature	K
ZT	Figure of merit	-
ϵ	One-dimensional filed E	-
κ	Thermal conductivity	$W.(m \cdot K)^{-1}$
μ	Mobility	$m^2.(V.s)^{-1}$
Π	Peltier coefficient	V
σ	Electrical conductivity	$S.cm^{-1}$
a	Carrier diffusivity	$m^2.s^{-1}$
v	Drift velocity of charge carrier	$m.s^{-1}$
Φ or WF	Work Function	eV
τ	Relaxation time	s

TABLE OF CONTENTS

FOREWORD

Whether it is in daily life, production or transport, energy is in the center of human life. As today, fossil fuels (petroleum, naturel gas and coal) are the most common sources for the production of energy but new “cleaner” sources have emerged as solar, nuclear, wind, geothermal, hydrothermal or biomass. However, the efficiency of the processes which use the produced energy are not maximal. This is highlighted every year by the Lawrence Livermore National Laboratory which describes all the U.S. energy uses in a Sankey diagram, displayed in Figure I-1. In this diagram, only 32.7% of the energy is used for services. A significant percentage is always released under different forms as heat, mechanical vibrations or light. One solution would be to re-use part of this “rejected” energy in dedicated systems.

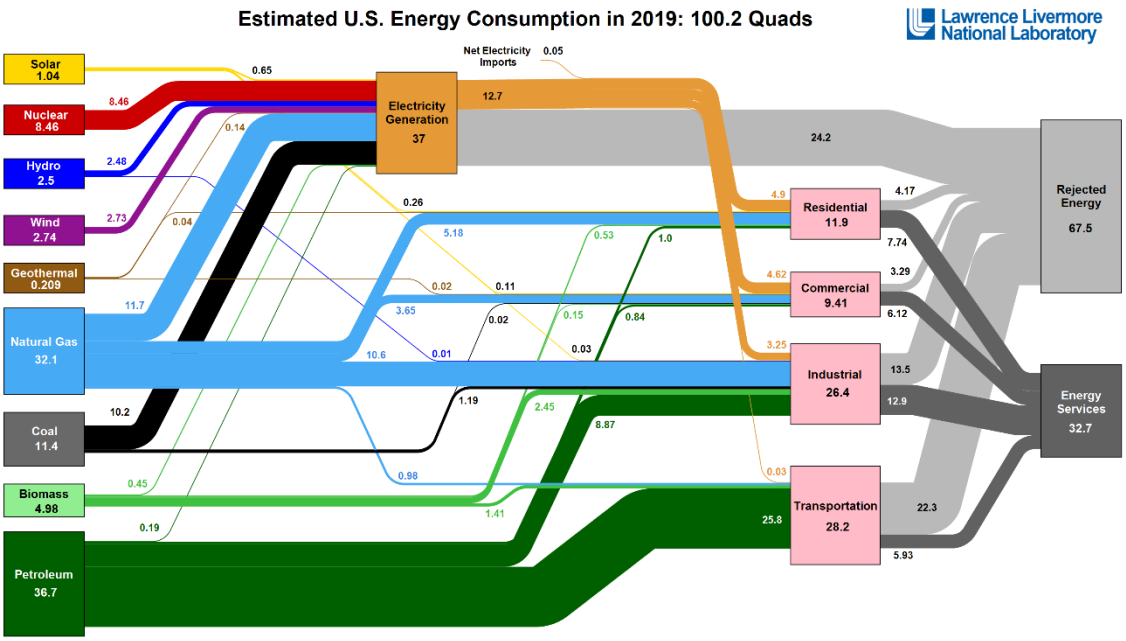

Figure I-9 Sankey diagram of the US energy consumption in 2019.

Therefore, thermoelectricity and its associated processes which convert heat into electrical current are foreseen as an answer to reduce the amount of “waste” energy, with, for instance, application in the conversion of rejected heat from vehicles into electrical power [1].

The rationale behind thermoelectricity appeared in the 19th century with the discovery of the Seebeck, Peltier and Thomson effects. Thermoelectric materials are materials which, subjected to a temperature gradient, create an electrical current. This kind of materials have to act as a phonon glass (low thermal conductivity), an electronic crystal (high electrical conductivity) and a good thermovoltage material (good capacity to convert heat into electricity). Inorganic materials are the most studied compounds in thermoelectricity with Bi_2Te_3 as a flagship due to its high efficiency [2], [3]. However, organic materials and in particular π-conjugated polymers are considered as a promising option because they are constituted of more abundant and less toxic elements. Additionally, they can be easier to process using printing technologies, opening new avenues for applications [4]. In this field, materials based on poly(3,4-ethylenedioxythiophene) (PEDOT) have been the focus of intense studies during the past years since they have demonstrated the best efficiency while being easily synthesizable [5].

This Ph.D. work consequently focuses on the relationships between the synthetic pathway, the structure and the electronic properties of PEDOT-based materials with an emphasis on PEDOT doped with tosylate moieties (PEDOT:Tos) as this particular form of PEDOT is often considered as the most promising for thermoelectric applications. The manuscript is organized in five chapters related to PEDOT materials synthesis and formulation, structural and electronic characterization and prospective work on the nano-confinement of PEDOT materials. More precisely:

The first chapter is a state-of-the-art review covering various aspects of thermoelectricity. Firstly we described the basis of thermoelectricity by examining the Seebeck, Peltier and Thomson effects while drawing overall guidelines for the design of an efficient thermoelectric material. The concept of density of states and its relation with the thermoelectric properties will be also examined in this chapter. Finally, some characteristic examples of inorganic and organic materials will be discussed with respect to their thermoelectric behavior with an emphasis on organic materials and especially PEDOT:Tos.

The second chapter is dedicated to the experimental protocols and the characterization methodologies used during this Ph.D. work. In particular, the

pathways to produce homogeneous PEDOT:Tos thin films by various methods will be described while details on the characterizations techniques will be provided. A study on the methodologies to accurately measure the electronic properties (electrical conductivity and Seebeck coefficient) of PEDOT:Tos thin films is the focus of a last part in this chapter.

In the third chapter, the two main synthetic pathways to polymerize PEDOT:Tos, which are in-situ and vapor phase polymerization, are examined in details. After a brief overview of the literature, the materials synthetized by each technique are analyzed in term of thermoelectric properties (Seebeck coefficient and electrical conductivity), morphological features and electronic properties through spectroscopic measurements. Such treatment allows us to decipher the strong interplay between PEDOT:Tos film growth, its crystalline structure and the final applicative properties.

The fourth chapter is focused on the vapor phase polymerization technique as this recent synthetic route for the production of PEDOT:Tos is only partially understood as today. In particular, we examined the effect of additives and the oxidant concentration on the structure and electronic characteristics of the films.

Finally, the last chapter of this Ph.D. thesis is dedicated to the nano-patterning of PEDOT:Tos with the aim to study the effect of confinement on the thermoelectric properties. The methodology used to obtain the nano-confinement is derived from block copolymer lithography and the results of two different integration schemes (direct patterning and in-situ confined formation of PEDOT:Tos) are exposed.

[1] C. B. Vining, "An inconvenient truth about thermoelectrics," *Nat. Mater.*, vol. 8, pp. 83–85, 2009, doi: 10.1002/jmv.20837.

[2] T. C. Harman, B. Paris, S. E. Miller, and H. L. Goering, "Preparation and some physical properties of Bi2Te3, Sb2Te3, and As2Te3," *J. Phys. Chem. Solids*, vol. 2, no. 3, pp. 181–190, 1957, doi: 10.1016/0022-3697(57)90081-1.

[3] C. Han, Q. Sun, Z. Li, and S. X. Dou, "Thermoelectric Enhancement of Different Kinds of Metal Chalcogenides," *Adv. Energy Mater.*, vol. 6, no. 15, 2016, doi: 10.1002/aenm.201600498.

[4] L. M. Cowen, J. Atoyo, M. J. Carnie, D. Baran, and B. C. Schroeder, "Review—Organic Materials for Thermoelectric Energy Generation," *ECS J. Solid State Sci. Technol.*, vol. 6, no. 3, pp. N3080–N3088, 2017, doi: 10.1149/2.0121703jss.

[5] M. N. Gueye, A. Carella, J. Faure-Vincent, R. Demadrille, and J. P. Simonato, "Progress in understanding structure and transport properties of PEDOT-based materials: A critical review," *Prog. Mater. Sci.*, vol. 108, no. September 2019, p. 100616, 2020, doi: 10.1016/j.pmatsci.2019.100616.

I. BIBLIOGRAPHICAL PART

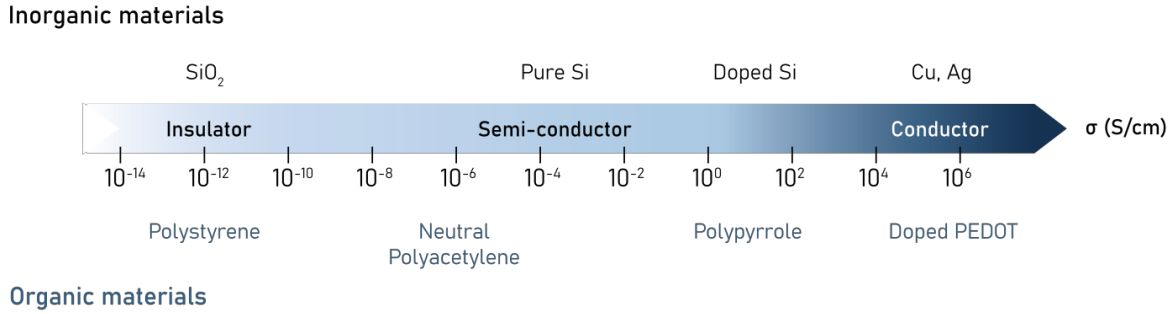

In this chapter, we present the general concepts inherent to thermoelectricity and thermoelectric materials. Firstly, we introduce the relevant thermoelectric effects and describe the important parameters characterizing thermoelectric efficiency. We also demonstrated how the concept of density of states allows one to relate the band structure of a materials to its thermoelectric characteristics. Secondly, the discovery of intrinsically conducting polymers with the example of doped polyacetylene encouraged scientists to focus on polymeric materials for electronic applications. Organic materials for thermoelectric applications are reviewed with an emphasis of the poly(ethylene dioxythiophene):tosylate complex which has shown promising characteristics in thermoelectricity.

I- THERMOELECTRICITY

I-1- BASIS OF THERMOELECTRICITY

I-1-A- HISTORY

The first hints of thermoelectric effects are related to Alessandro Volta's works in 1794, as illustrated in Figure I-1, when he noted the appearance of a force when a difference of temperature was applied to a frog's leg. However, thermoelectric phenomena were first discovered at the beginning of the 19th century by Thomas J. Seebeck. During an experiment, he noticed that a circuit made from two dissimilar metals with junctions at different temperatures would deflect a compass magnet [1], [2]. He correlated this phenomenon to the appearance of a magnetic field which further led him to propose a theory on the origin of terrestrial magnetism. Later this effect was linked to the appearance of a potential difference with the application of a temperature gradient by Oersted. Thus, the Seebeck effect linked two thermodynamic potentials that are the temperature and the electrochemical potential [3].

Figure I-1 History of thermoelectricity - Important personalities.

Following these pioneering works, Jean C. A. Peltier discovered in 1834 the as-called Peltier phenomenon [4] which permits to heat or cool a junction with the application of an electric current. This effect was explained later by Lenz in 1838 who concluded that the heating or the cooling depend of the current direction.
In 1851, William Thomson (named later Lord Kelvin), discovered the last phenomenon related to thermoelectricity. He described the production or absorption of heat along a material when a temperature gradient is applied. Thomson subsequently linked the Seebeck and Peltier effects by two thermodynamic laws [5].

In 1909, Edmund Altenkirch reconsidered the theory of thermoelectric effects and published two reference papers. One was about the efficiency of a thermopile [6], and the other on the thermoelectric cooling [7]. He was the first to describe that a good thermoelectric material needs to combine both large Seebeck coefficient and electrical conductivity.

I-1-B- Peltier, Seebeck and Thomson effects

Thermoelectric phenomena are characterized by the conversion of a temperature gradient into an electric current and vice versa. Thermoelectric materials can thus harvest waste heat into useful electrical energy. Thermoelectricity is based on three well-known phenomena that are the Peltier, Seebeck and Thomson effects.

Seebeck effect

The Seebeck effect appears when a material is submitted to a temperature difference as schematically described in Figure I-2. One side is put at a hot temperature T_H, and the other at a cold temperature T_C. The difference of temperature, $\nabla T = T_H - T_C$, induces the appearance of an electromotive force related to a charge carrier concentration gradient. A potential gradient ∇V appears between the extremities of the material and is linked to the temperature gradient by the equation:

$$\nabla V = -S\nabla T \qquad \textit{Equation I-1}$$

where S is the Seebeck coefficient.

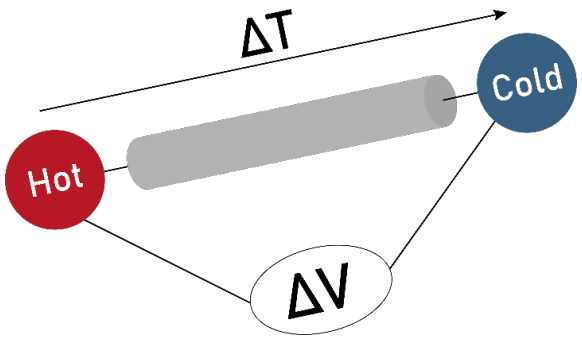

Figure I-2 Principle of Seebeck effect.

Peltier effect

The Peltier effect appears when a material is subjected to an electrical current. In this case, an absorption or production of heat is noticed along the direction of the current. The rate of heat produced or absorbed is described by the following equation:

$$\frac{dQ}{dt} = (\Pi_A - \Pi_B)I \qquad \textit{Equation I-2}$$

where I is the electric current, Π_A and Π_B the Peltier coefficients for two conductors A and B, respectively.

Thomson effect

The Thomson effect is the rate of heat produced when a material is subjected to a temperature gradient under a current flow. The heat produced or absorbed is defined by:

$$\frac{dq}{dt} = -KJ\Delta T \qquad \textit{Equation I-3}$$

where J is the current density and K the Thomson's coefficient.

These three effects are linked by the Kelvin's equation relating the Seebeck, Peltier and Thomson coefficients:

$$\Pi = T \cdot S \qquad \textit{Equation I-4}$$

where $\Pi = \Pi_A - \Pi_B$ and $K = T\frac{dS}{dT}$

I-1-c- THERMOELECTRIC MATERIALS AND CHARACTERISTIC VALUES

A thermoelectric module is composed of two legs of thermoelectric materials connected in series by metallic contacts. One leg, called the p-type leg, has holes as its majority charge carriers, while the second one, called the n-type leg, has

electrons. Accordingly, the development of both p- and n- type materials are required for practical applications. Considering a heat flux applied in parallel to a thermoelectric device assembly, Figure I-3 shows two kinds of device architecture depending of the methods used for their fabrication. For inorganic materials, Figure I-3 a) shows the typical 3D structure in which an alternation of p- and n- legs are sandwiched between two electrodes. For organic materials (and in particular polymers), 2D architecture are favored since printing methodologies leverage easier fabrication processes as displayed in Figure I-3 b) [8].

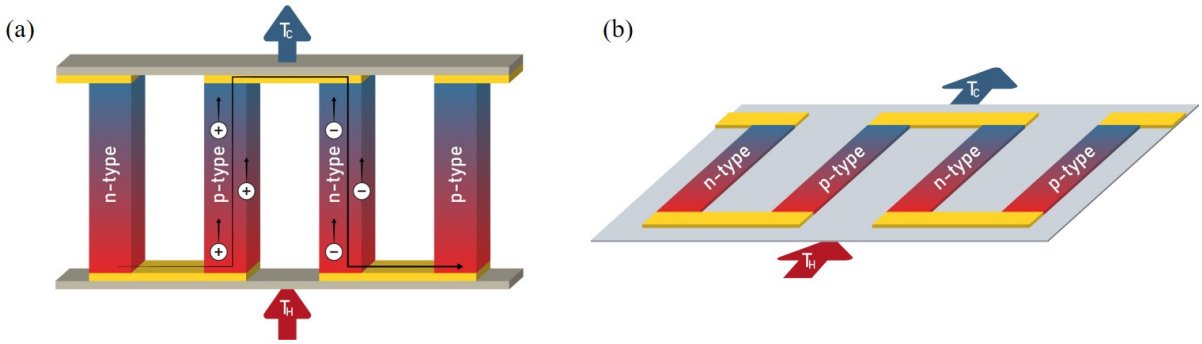

Figure I-3 a) Schematic views of thermoelectric device architectures in the case of a) inorganic materials and b) printed organic materials.

The maximum efficiency, η, of this type of device is expressed as follow:

$$\eta = \frac{T_H - T_C}{T_H} \frac{\sqrt{1+ZT}-1}{\sqrt{1+ZT}+\frac{T_C}{T_H}} \qquad \textit{Equation I-5}$$

Here, the fraction $\frac{T_H - T_C}{T_H}$ points to the Carnot efficiency, the thermodynamic limit of an ideal engine. The second fraction is composed of the figure of merit, ZT, which is an important parameter in the thermoelectric field to relate the thermoelectric efficiency of a material to its physical and electronic characteristics. The ZT is thus a dimensionless figure of merit expressed as:

$$ZT = \frac{\sigma S^2}{\kappa} T \qquad \textit{Equation I-6}$$

where σ is the electrical conductivity, S the Seebeck coefficient and κ the thermal conductivity.

In order to obtain an effective thermoelectric device, a balance between those three parameters has to be found (ZT has to be as high as possible). The materials have to exhibit a large carrier conductivity to maximize σ but also have a good thermovoltage, S. This means that the capacity of the carriers to move under a temperature gradient needs to be important. On the other hand, the thermal conductivity κ has to be as low as possible; the material has to be a thermal insulator.

As shown in Figure I-4, the Seebeck coefficient and the electrical conductivity show an antagonist behavior with regard to the carrier concentration. In order to obtain an optimal ZT value, a balance has to be found between those two parameters. Ioffe showed that there is a range of carrier concentration where the ZT is maximum [9]. Accordingly, metals which have a high carrier concentration (and thus a high electrical conductivity) exhibit a small Seebeck coefficient. Consequently, metals are not considered as good candidates for thermoelectric applications. Conversely, insulators have a low electrical conductivity and a high Seebeck coefficient that make them not useful for thermoelectric applications. Semi-conductors are thus considered as a valid option for thermoelectric applications as the balance between moderate Seebeck coefficient and electrical conductivity leads to the highest efficiency. Besides, the ZT can be drastically increased by the careful tuning of the doping level in order to rationally optimize the Seebeck coefficient and the electrical and thermal conductivities for a particular material.

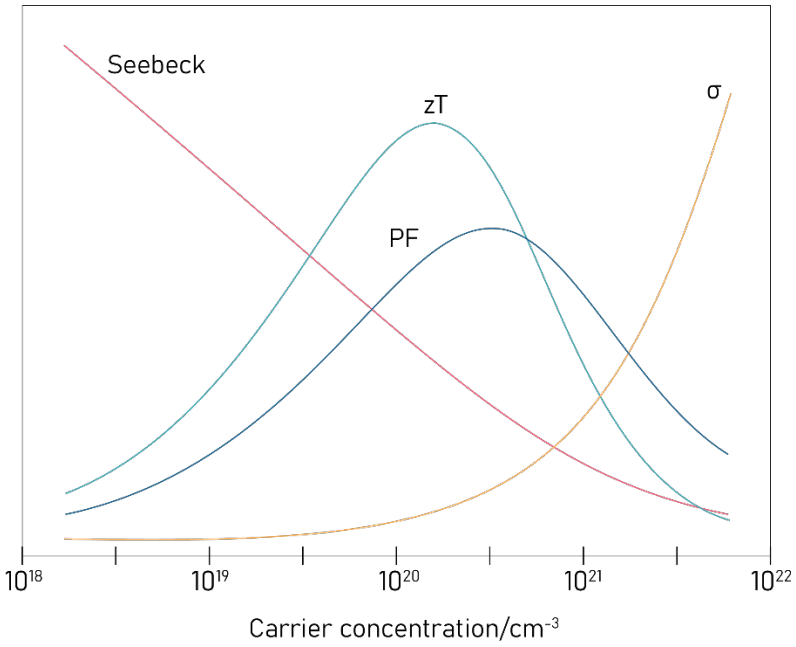

Figure I-4 Seebeck coefficient, electrical conductivity and thermal conductivity in function of carrier concentration.

It is often difficult to measure accurately the thermal conductivity of materials (even more in thin film configuration) and thermoelectric materials are then compared using the power factor (PF) which is expressed as follows:

$$PF = S^2\sigma \qquad \textit{Equation I-7}$$

Nevertheless, such treatment needs to be carefully applied, as maximizing the PF does not signify that the best ZT has been found. This is shown in Figure I-4 in which the maximum of ZT and PF differs as function of the carrier concentration.

I-2- PHYSICAL POINT OF VIEW, DENSITY OF STATES

The thermoelectric properties, i.e. the Seebeck coefficient and the electrical conductivity, are directly related to the density of states (DoS) of a material. The DoS defines the number of electronic states that are available in a system per unit volume and energy intervals. Depending on the material characteristics, electrons populate different electronic states in the valence and/or conduction bands. Materials can be divided in four categories that are metal, semimetal, semiconductor and insulator as shown in Figure I-5.

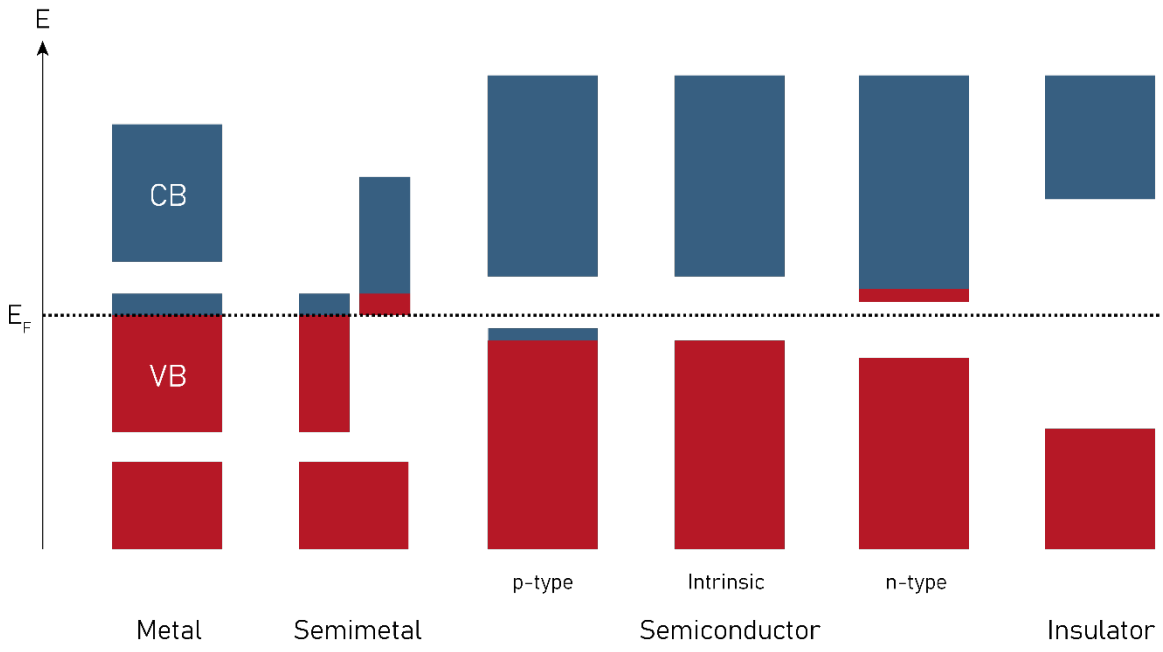

Figure I-5 Simplified diagrams of filled states for different categories of materials.

For a metal, electrons can move from the valence band to the conduction band because of the non-discontinuity of these bands. Such band configuration explains the large electronic conductivity exhibited by metals. In the case of insulators, a large band gap between the valence band and conduction bands prevents electrons to participate to the conduction. This large band gap explains the non-conductivity of these materials. The semiconductors also exhibit a band gap but smaller than the one encountered for insulators. Accordingly, the application of an external electric field allows electrons to "jump over" the gap and participate to the conduction mechanism. The last type, the semimetals, is an intermediate between metals and semiconductors, characterized by a very small bandgap. The Fermi level (E_F) is consequently defined by the highest level of electron occupancy at T = 0 K. The Fermi level is then an important characteristic to know the repartition of the electrons within the material. All of those material types can also be described by the shape of their DoS as shown in Figure I-6.

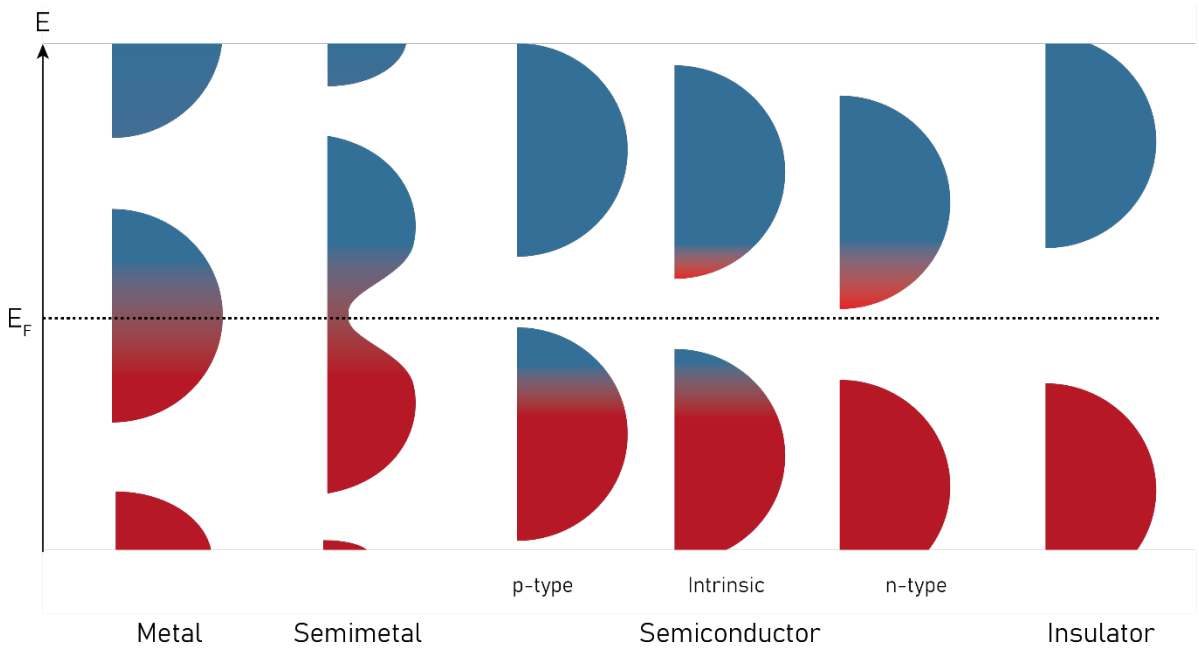

Figure I-6 Shape of the density of states for metal, semimetal, semiconductor and insulator. E_F is the Fermi energy The colors follow the Fermi–Dirac distribution (red = filled states, blue = empty states).

The DoS is a mathematical concept and, as previously mentioned, the electrical conductivity is directly linked to the filling of these states while the Seebeck coefficient is related to the shape of the DoS at the Fermi level. In the case of metals, the tangent of DoS is equal to 0 at $E = E_F$, as opposed to the insulators where the tangent is infinite. For semiconductors, the tangent value depends of the position of the Fermi level. Finally, for semimetals, the tangent depends of the amount of electronic states at the Fermi level. This mathematical description will be linked later in this chapter to the Seebeck coefficient.

The probability for an electron to occupy a state is given by the Fermi-Dirac distribution $f_0(E)$:

$$f_0(E) = \frac{1}{1 + \exp(\frac{E - \mu}{k_B T})}$$ *Equation I-8*

where, μ is the chemical potential and k_B the Boltzmann constant. If we consider that $D(E)$ is the number of available states that an electron can occupy, integrating the product of $D(E)$ and $f_0(E)$ gives the number of charge carriers in the volume:

$$N = \int_0^\infty f_0(E) \cdot D(E) dE \qquad \textit{Equation I-9}$$

N is also called the carrier concentration or the charge carrier density and it is an important parameter used to tune the thermoelectric properties of materials. The modification of these parameters directly influences the electric current J_e which flows through a material:

$$J_e = \frac{q}{3} \cdot \int v^2 \cdot \tau \cdot \left(q\epsilon \frac{\partial f_0}{\partial E} \right) D(E) dE + \frac{q}{3} \cdot \int v^2 \cdot \tau \cdot \left(q\epsilon \frac{\partial f_0}{\partial x} \right) D(E) dE \qquad \textit{Equation I-10}$$

where *q* is the elementary charge, v is the drift velocity of charge carrier, τ is the relaxation time and ϵ is the one-dimensional filed $\vec{E}$. Equation I-10 can also be expressed as follows:

$$J_e = q \cdot N \cdot \mu \cdot \epsilon + q \cdot a \cdot \frac{\partial N}{\partial x} \qquad \textit{Equation I-11}$$

where a is the carrier diffusivity and *N* the charge carrier density previously introduced. By using the Boltzmann theory, the first term of the previous equation can be linked to the electrical conductivity:

$$\sigma = q \cdot N \cdot \mu_e \qquad \textit{Equation I-12}$$

and so, by combining Equation I-10 and Equation I-1, the mobility can be expressed as:

$$\mu_e = \frac{\frac{q}{3} \cdot \int_0^\infty v^2 \cdot \tau \cdot \left(\frac{\partial f_0}{\partial E} \right) D(E) dE}{\int_0^\infty f_0(E) \cdot D(E) dE} \qquad \textit{Equation I-13}$$

Following that, the electrical conductivity can be re-written as:

$$\sigma = \frac{q^2}{3} \cdot \int_0^{\infty} v^2 \cdot \tau \cdot \left(\frac{\partial f_0}{\partial E}\right) D(E) dE \qquad \textit{Equation I-14}$$

It is easy to notice that the electrical conductivity is dependent of the number of states available and thus the shape of the DoS is an primordial parameter for the mobility and electrical conductivity. In term of material characteristics, the increase of the electrical conductivity can be performed in two ways: tuning either the mobility with enhanced material ordering or the number of states (i.e., increasing the carrier concentration) with doping [10].

The Seebeck coefficient is related to the entropy per charge carrier and is defined by the measure of a voltage under a temperature gradient under open-circuit condition [11]. The Seebeck coefficient can be expressed using the Mott's formula:

$$S(E,T) = \frac{\pi^2}{3} \cdot \frac{{k_B}^2 T}{q} \cdot \left(\frac{\partial \ln(\sigma(E))}{\partial E}\right)_{E=E_f} \qquad \textit{Equation I-15}$$

It is noteworthy that this expression is linked to the DoS. Particularly, the term $\left(\frac{\partial \ln(\sigma(E))}{\partial E}\right)_{E=E_f}$ is related to the shape of the DoS at the Fermi level and describes its tangent at the Fermi level.

As regards to the previous discussion on the various categories of materials, metals show a low Seebeck coefficient while insulators are characterized by an important one. For semiconductors and semimetals, the Seebeck coefficient particularly depends of the crystallinity (or chain ordering for polymers) of the material and the doping. The sign of the Seebeck coefficient is given by the majority charge carrier. In case of a n-type material, the majority charge carriers are electrons, so the Seebeck coefficient in negative, while in the case of p-type materials, the majority charge carriers are holes implying that the Seebeck coefficient is positive.

II- ORGANIC ELECTRONIC

II-1- FEW WORDS

II-1-A HISTORY

Organic materials, and especially polymers, have been studied for a long time for their mechanical and structural properties. Usually, polymers are insulators and it is why the interest towards their electronic properties is only recent. Consequently, electronic properties in inorganic materials are better understood and most theories applied to polymer materials are derived from inorganic ones.

Polyacetylene is the first studied polymer for electronic applications. It is composed of alternated simple and double bonds, as shown in Figure I-7 (a). Those π-bonds introduced a new category of polymers: the π-conjugated polymers. At the end of the 20th century, scientists discovered that doping polyacetylene with iodine leads to a drastic increase of its conductivity [12]. This fortuitous discovery is related to a mistake from Pr. Shirakawa who introduces an excess of catalyst inside his polymerization reactor and subsequently observed a change in the color of the solution. This color change indicates a modification of the conformation of the polymer backbone leading to a modification of the polymer electronic properties. Shirakawa synthetized thus two kinds of polyacetylene, i.e. *trans* and *cis* conformations as shown in Figure I-7, which had high electrical conductivity [13].

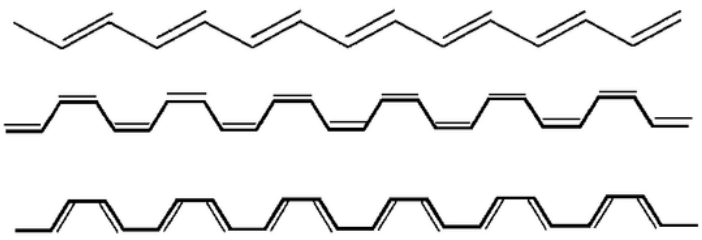

Figure I-7 Different forms of polyacetylene (a) trans (b) trans-cisoid (c) cis-transoid.

In 2000, with this discovery of conducting polyacetylene, Shirakawa, MacDiarmid and Heeger were awarded the Nobel prize. Since this discovery, π-conjugated polymers

are of high interest for scientists since they combine the intrinsic properties of polymer materials with the extended electronic behavior encountered in inorganic materials. Many architectures of π-conjugated polymers have since been developed. A first category is based on linear carbon backbone with polyacteylene or polydiacetylene. A second one includes aromatic cycles in the polymer backbone like polyparaphenylene (PPP) and its derivatives, polypyrrole (PPy), polythiophene (PT) and poly(ethylene dioxythiophene) (PEDOT). Besides, aromatic cycles can be alternated with double bonds to form poly(phenylene vinylene) (PPV) and its derivatives or poly(heteroarylene vinylene). A last class of π-conjugated polymers is based on nitrogen atoms included in the polymer backbone such as polyaniline (PANI) with all its derivatives [14], [15].

II-1-B DOPING

In order to observe a noticeable electrical conductivity, organic materials need to be doped. Polymers can be doped following two different processes. The first one is an oxidation-reduction (redox) process leading to the transfer (reduction) or the extraction (oxidation) of electrons by counter-ions on π-conjugated polymers. The second one is related to PANi which has a peculiar behavior as it can be doped by acido-basic treatment. Doping methods afford macroscopic electrical conductivity to π-conjugated polymer materials in order to be used in functional devices. As shown in Figure I-8, some polymers can then be more efficient than doped Si even if the stability of the electronic properties is often problematic. In order to understand this increase in conductivity upon doping, it is important to better apprehend the electronic band structure of polymers and intensive works have been pursued by researchers since 80-90s [16].

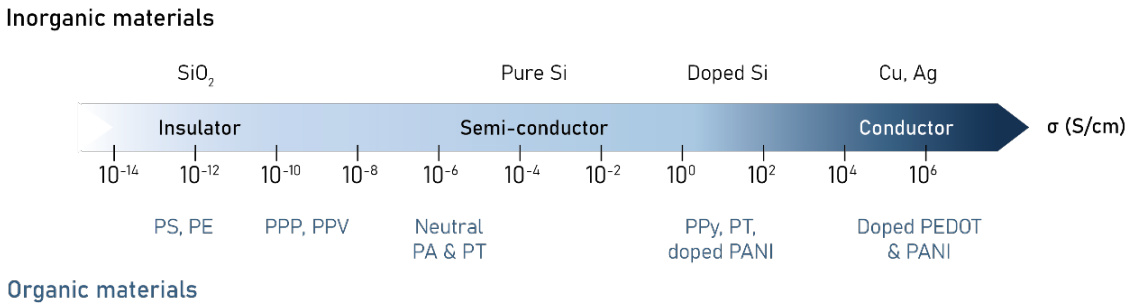

Figure I-8 Order of magnitude of conductivity of some conjugated polymers in their neutral and doped forms compared to inorganics materials.

II-2- ELECTRONIC STRUCTURE

II-2-A- BASICS ON POLYMER ELECTRONIC

The electronic structure of π-conjugated polymers has to be understood in order to decipher how charge carriers can move and so induce the conduction. The majority compound of polymers is carbon. Its electronic configuration is $1s^2 2s^2 2p^2$. The 2p orbitals contain 2 electrons in the $2p_x$ and $2p_y$ orbitals, while $2p_z$ is empty. In order to produce double bonds, orbitals have to hybridize. Three combinations are possible. 2s orbital can hybridize itself with one (sp), two (sp^2) or three (sp^3) 2p orbitals. Those hybridizations induce linear, in plane or three dimensional molecules, respectively, and the results of the hybridization are displayed in Figure I-9.

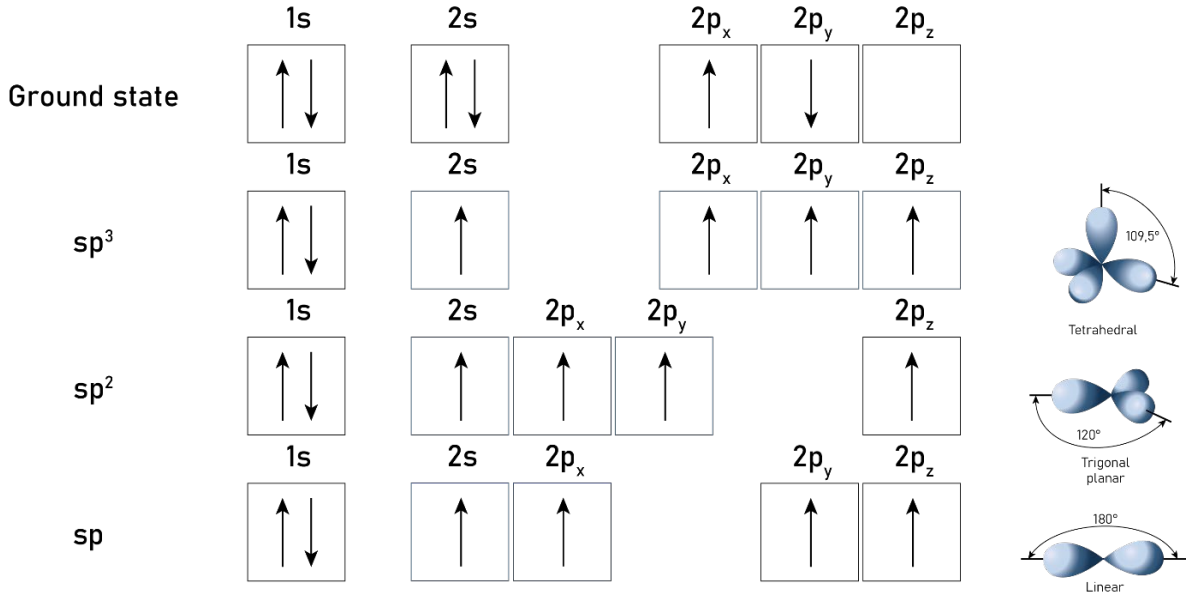

Figure I-9 Hybridization of carbon with the resulting geometric arrangements of orbitals.

The combination of sp^2 orbitals forms a σ-bond which is constituted of electrons which do not participate to the conduction. Such bond is characteristic of a saturated carbon backbone. The last $2p_z$ orbitals combine themselves to form π-bond. Those two bonds constitute the covalent double bond. π electrons are shared between atoms and lead to the formation of an electronic cloud around the backbone of the polymer. This effect leads to the conjugation of the molecule through its repetition along a polymer backbone. This conjugation can provide highly functional effects to a polymer chain like high electrical conductivity or enhanced mechanical properties. It is noteworthy that bonding between atoms are realized only if the bonding requires less energy than leaving the unit in this original conformation. Accordingly, a polymer architecture constitutes an energetic advantage as regard to monomers due to covalent bonds. By covalently bonding two monomers, the two orbitals of the first monomer are split into two occupied states. This effect is repeated within the number of monomers linked (degree of polymerization). The energy needed to pass through this energetically barrier is then decrease. Then, extending the length of the polymer chain leads to an infinite number of orbitals which overlap and form a band [17], this phenomenon is displayed in Figure I-10. The valence and conduction bands tend towards to get closer and so, the band gap decreases. Contrary to inorganic materials, the band gap for polymers is complicated to understand as the theory of band structure is not fully adapted to polymeric materials [18].

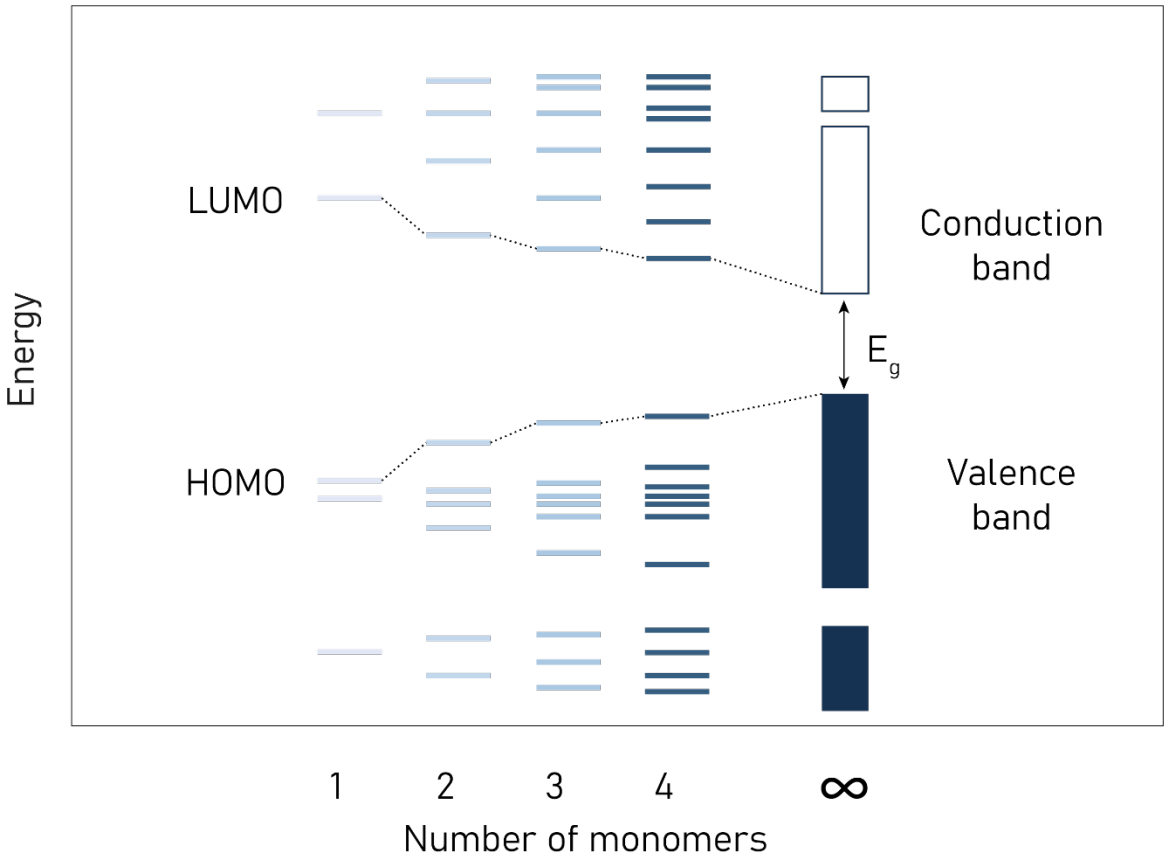

Figure I-10 Formation of bands from molecular orbitals - From monomer to polymer. Adapted from [17].

This band gap is delimited by two particular orbitals which are Highest Occupied Molecular Orbital (HOMO) and Lowest Unoccupied Molecular Orbital (LUMO).

II-2-B ROLE OF DOPING

In order to facilitate the conduction of charges, conjugated polymers can be doped. This doping facilitates the electron exchange between the HOMO and LUMO bands. Chemical doping, either oxidative or reductive, can decrease the polymer band gap in order to reach metallic behavior. In this case, the valence band and the conduction band overlap and electrons can easily transfer between them allowing a macroscopic conduction.

The oxidative or reductive doping happens with the creation of a charged defect inside the polymer chain. This defect can be a polaron or a soliton if it is positively or negatively charged, respectively. From a chemical point of view, this defect is related to a radical ion (cation or anion). Polarons or solitons can travel and participate to the

conduction. The introduction of defects in a π-conjugated architecture further modifies the conformation of polymer chains, in particular with the benzoid to quinoid transformation [18]. Energetically, this change of the chain conformation will modify the total energy of the system. Accordingly, a doped system can be non-degenerate with a modification of the system energy, or degenerate with unchanged energy as regards to the neutral state. For non-degenerated systems, the ionization inherent to the doping process permits the localization of electronic states inside the band gap, as shown in Figure I-11. This was demonstrated by Brédas *et al.* in their study on polyparaphenylene, polypyrrole, and polythiophene [19]. By heavily doping the system, localized states are created inside the band gap and the overlaping of these states creates a polaron band in the band gap. The HOMO and LUMO are then modified and the band gap of the polymer decreases leading to an enhanced conduction of the charge carriers.

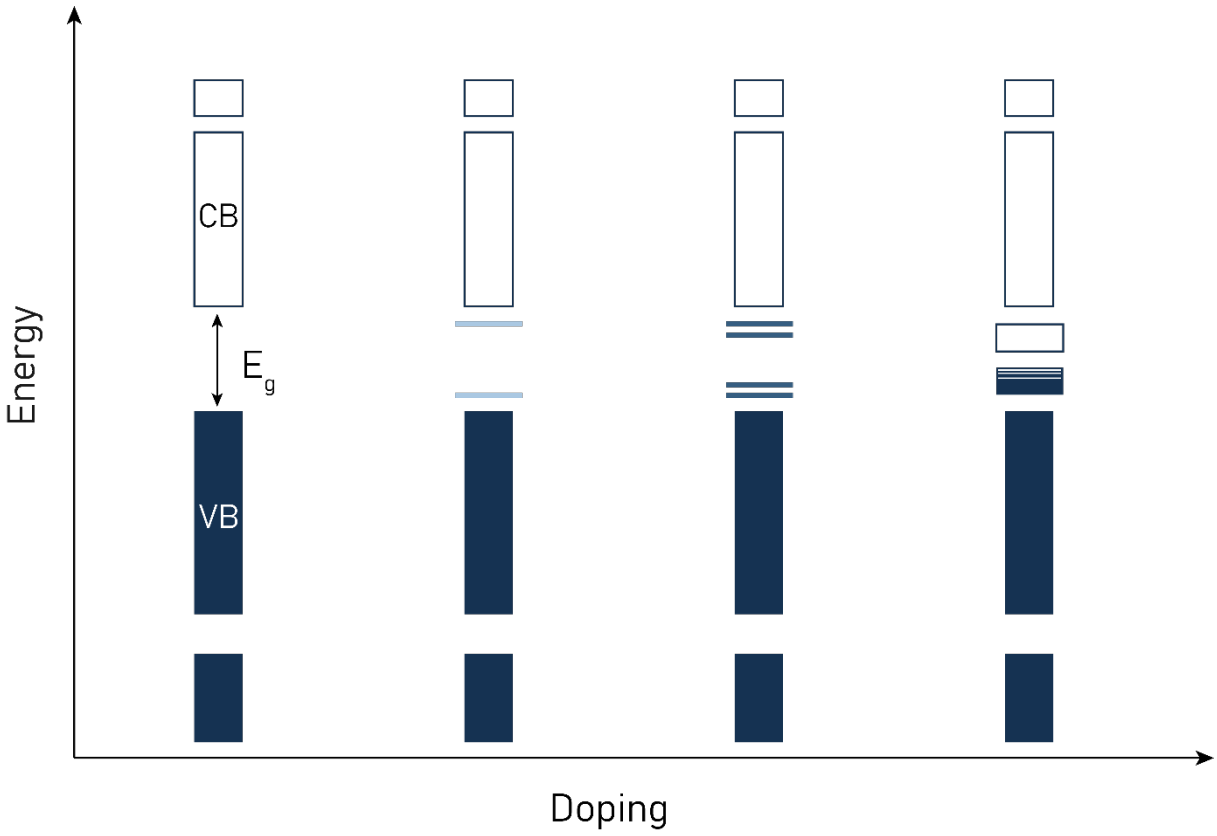

Figure I-11 Formation of localized states in the band gap with doping. At a certain doping, there is the creation of a polaron band. Adapted from [16].

The creation of defects can also result in the formation of bipolarons. Bipolarons (or dications) are a pair of two charges in association with a strong local lattice distortion [16]. The main question is when polarons or bipolarons appear? This question can be answered by referring on their respective energy. The energy needed to create a polaron is almost the same that the one needs to create a bipolaron [20]. However, bipolarons are thermodynamically more stable. By forming more and more polarons in the system, a recombination appears with the creation of bipolaron leading to a better conduction [16]. In the case of polarons or bipolarons, the overlap of the localized states forms a polaron or bipolaron band, respectively.

The second case, i.e. a degenerated system, is characteristic of trans-polyacetylene. In this case, the defect, named soliton, is created within –C- localized bonds [18]. This soliton allows the formation of localized states in the band gap. By doping, the number of solitons increases along the polymer chain but always without coupling or recombination.

II-3- CHARGE TRANSPORT

For polymer materials, charge transport is driven by several phenomena. The first one is related to the conjugated structure of the material allowing charge conduction along the polymer backbone while a hopping mechanism between chains has to be considered to fully apprehend charge transport. However, these two phenomena do not have to be dissociated as they happen at the same time. For transport, it is important to consider the mobility of the charge carriers. The mobility is dependent of the morphology of the polymer and thus linked to the ordering of the polymer chains [21], [22]. Polymers are not perfect crystallographic models and are characterized by the presence of defects along the backbone [11]. Those defects can be traps for electrons (or holes) and disrupt the conduction due to a decreased mobility. Additionally, the charge mobility inside a polymer can be affected by external parameters like temperature, pressure, external electric field, charge carrier density and molecular weight [22]. The mobility is given by the Einstein-Smoluchowski equation:

$$\mu = \frac{eD}{k_B T} \qquad \textit{Equation I-16}$$

where, e is the electron charge, D is the diffusion coefficient, k_B is the Boltzmann constant and T the temperature.

It is then easy to related mobility with polymer structure thanks to the diffusion coefficient. Diffusivity will be facilitated in crystalline materials with respect to amorphous ones. The transport of charge carriers is driven by mobility and so is influenced by polymer structure [23].

II-3-a- Band transport

Considering a polymer chain, it is possible to imagine an electron (hole) moving along the polymer backbone. This idea leads to the band transport theory for conjugated polymer. The repeating units of the polymer backbone share π-electrons creating an electronic cloud which permits to charge carriers to move. The band transport is based on the polaron band created in a conjugated polymer. Band transport need a perfect crystal to be dominant. As it has been said previously, defects over the backbone can disrupt this kind of transport. In order to better apprehend band transport, it is important to take into account defects which can be traps and thus the energy needed for a charge carrier to get out from this trap. This energy cost can be too important resulting in a drastically affected mobility. This is why it is also important to consider that hopping transport mechanism can be favored as regard to band transport.

II-3-b- Hopping transport

Hopping transport is the most important transport mechanism of charge carriers for the conduction. Charge carriers can move along the backbone by the conjugation (band transport) but in most of the case, they can jump from one monomer unit to another one on the same chain or on a different chain [18]. Depending of the structure of the conjugated polymers (amorphous, semi-crystalline), different hopping phenomena have to be considered [24].

-The first one is the quasi 1D metal for which the anisotropy has to be taken into account because charge carrier mobility is predominant along the polymer chains. In this case, the hopping transport occurs like in a metal, i.e. in one direction along the lattice, and conduction is thus greater along the polymer chain.

-The second one is the disordered metal, in which the conduction decreases in the material as the disorder increases. Here, it is important to notice a transition from metal to semiconductor where charges can hop in 2D.

-Thirdly, hopping in disordered semiconductors is often considered as the best theory to model the conductivity behavior of polymers. The charge carriers are "jumping" from chain to chain to allow the conduction at the macroscopic scale. In this case, the localized states are in the band gap.

Nevertheless, hopping in conjugated polymer can be described by all these models [22], [24]. Epstein *et al.* pointed out that quasi-1D hopping is the most important in polymer where chains alternate with amorphous part and crystalline domains [25]. This model has been highlighted by Phillips with his polymer crystal representation and its displayed in Figure I-12.

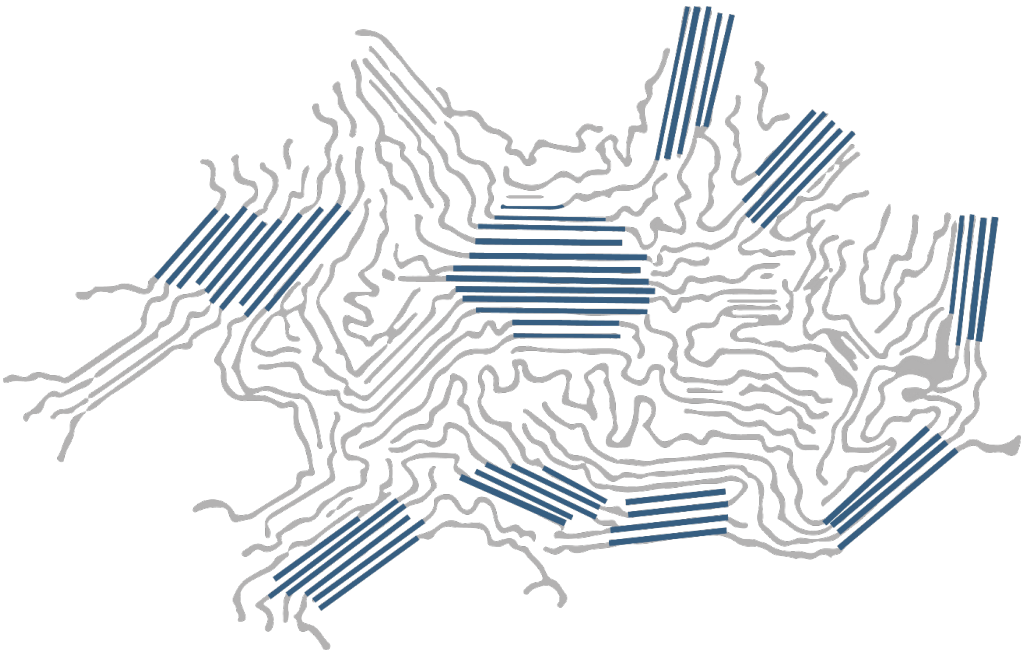

Figure I-12 Semi-crystalline structure of a polymer. Crystalline domains are highlight in blue [26].

III- THERMOELECTRIC MATERIALS

To produce a thermoelectric device two kinds of legs are needed: one leg which has electrons as majority charge carriers, the n-type leg, and another one with holes as majority charge carriers, the p-type leg. In thermoelectric applications, the best ZT values are obtained, as today, with inorganic materials, while organics are considered as a promising option because they are constituted of more abundant and less toxic elements [27]. All the results in this part are given for studies at room temperature except when it is specified.

III-1- INORGANIC MATERIALS

So far, inorganic materials have been studied for their thermoelectric properties due to their conduction properties and Seebeck coefficient. Different kinds of inorganic materials are used like chalcogenides (tellurides, sulfides and selenides) or oxides, [28].

Tellurides

For chalcogenides, Bi_2Te_3 is the most studied compound [29] in thermoelectricity due to its efficiency and stability [30]. Those chalcogenides materials are used at room temperature. Bi-Te compounds have a ZT near to one. By changing the morphology of the sample, from film to nanowire, Tan *et al.* succeeded in increasing the Figure of merit from 0.14 to 1.01 [31]. Using a similar nanostructuring approach, Venkatasubramanian and his team reached a ZT of 2.4 with p-type Bi_2Te_3/Sb_2Te_3 materials [32]. Bi_2Te_3 can also be used at higher temperature but the best performances are obtained at room temperature.

The aim of using this kind of materials is their heavy atomic weight which permits to reduce the thermal conductivity [33]. Besides, chalcogenides can be processed in different ways in order to tune their thermoelectric properties: they can be produced as p-type or n-type materials by doping them with pnictides (antimony) or halides (selenium), respectively [30].

As today, the best ZT value has been obtained for $PbSe_{0.98}Te_{0.02}$/PbTe quantum-dot superlattices materials (ZT ≈ 3 at 550 K) [34].

Oxides

Oxides materials have been expected to have low thermoelectric properties due to their ionic nature. But Terasaki pioneered in 1997 the use of oxides for thermoelectric applications with the production of $NaCo_2O_4$ with a high Seebeck coefficient concomitantly to a high electrical conductivity [35]. Since this discovery, oxides are studied for their thermoelectric properties as they show a good stability in air and are based on abundant elements. The main problem with oxides is their intrinsically low electrical conductivity.

Thermoelectric Oxides also demonstrate a large temperature range of applications, from room temperature for Na_xCoO_2 [36] to 1000 K for mixed oxide materials [37]. Figure I-13 shows the best ZT values for oxides with ZT higher than 1 for whiskers of BiSrCoO at high temperature [38]. Besides, both p- and n-types can be produced with Na_xCoO_2 for the best p-type oxide and doped perovskites for n-type.

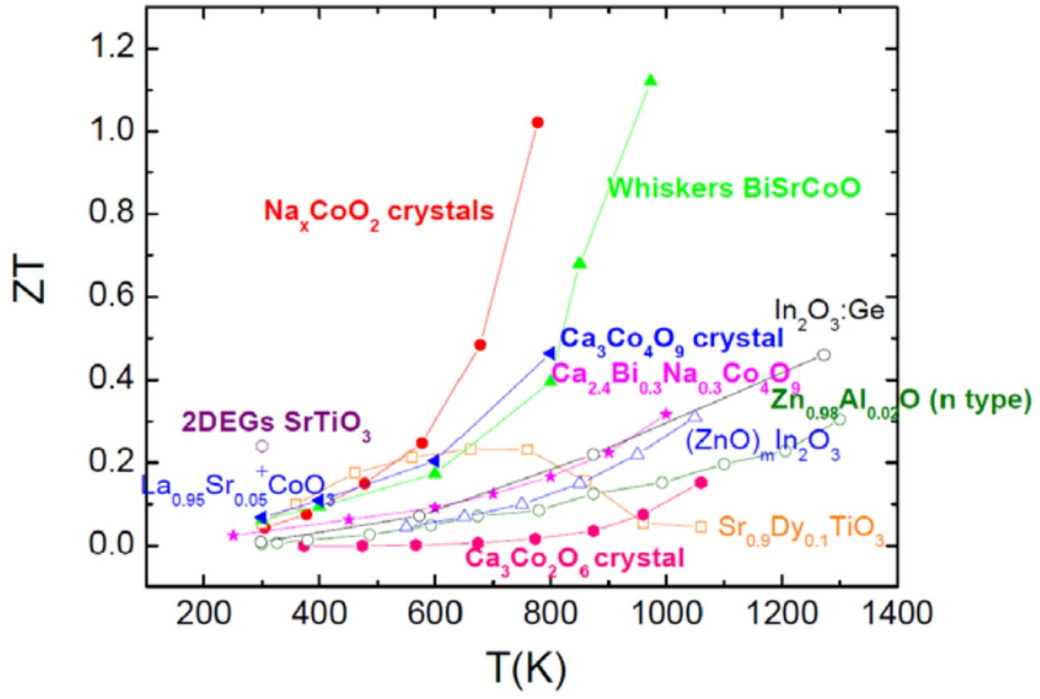

Figure I-13 ZT values for different oxides. All the references are given in [39]. *The figure is reproduced from* [28].

Sulfides and selenides

Sulfides and selenides are a sub-category of chalcogenides materials. Contrary to oxides, sulfides and selenides are covalent materials [28]. In this category, it is possible to find ceramics like Co_xTiS_2, TiS_2, pyrites, chalcopyrites and tetrahedrites. Of high interest is TiS_2 whom layered structure allows intercalation of species between the different planes of the material in order to introduce dopants increasing the thermoelectric properties. More particularly, studies have focused on the way to tune TiS_2 charge carrier concentration by adding other species like transition metals (Cu, Fe, etc.) or by substituting Ti by Ta or Nb. Another interesting examples are pyrites and chalcopyrites which are composed of heavier elements than oxygen like Se or S. The presence of heavy atoms in the structure permits to reduce the thermal conductivity even if the reported *ZT* values of those materials are quite low, less than 0.1 [40].

For high temperature applications (more than 600 K), tetrahedrite materials are promising. For example, $Cu_{12}Sb_4S_{13}$, which is a p-type material, can reach a *ZT* of 0.56 at 673 K [41]. A ZT value of 1.13 has been reported for $Cu_{11}MnSb_4S_{13}$ at 575 K [42] but it has been under debate because of the low density reported for such samples which leads to a low thermal conductivity [28]. Recently, Hinterleitner *et al.* were able to reach a ZT of 5-6 on metastable Heusler alloy thin film [43]. This value is the best value reported for thermoelectric materials but some questions subsist in the community on the possibility to reach such a high value in that compound.

In summary, this category of thermoelectric materials can reach *ZT* values higher that 1 which push researchers to study their thermoelectric properties in order to increase them. Nevertheless, they are more difficult to synthetize than organic materials due to high temperature needed to shape them. A new type of inorganic material, higher manganese silicides (HMS), is also a recent focus of interest in the scientific community because it is composed of cheap, abundant and non-toxic elements. These materials are good candidates for thermoelectric applications with *ZT* above 0.35 [44]–[46].

III-2- ORGANIC MATERIALS AND HYBRIDS

Organic materials are promising materials for thermoelectric applications. They have low thermal conductivity which permits to increase the figure of merit. Besides, recent progress in the design of conductive polymers demonstrated how π-conjugated materials can show an important electrical conductivity through doping. Moreover, thermoelectric properties can be tuned by playing on polymer morphology, i.e. mostly on the crystalline structure.

Both p- and n- type thermoelectric materials could be implement in order to fabricate a fully organic thermoelectric device which would show promise for applications requiring lightweight, flexibility, etc. As an example, researchers used paper as a substrate to fabricate fully organic thermoelectric device. Jiang *et al.* directly used paper as substrate by "writing" on it with a PEDOT:PSS ink [47], while Wei *et al.* used screen-printing to deposit PEDOT:PSS [48]. Brus and coll. also fabricated a thermoelectric generator on paper using PEDOT:PSS for the p-type material and graphite from a pen for n-type [49].
The main issue of organic materials for thermoelectric applications remains the poor stability of n-type materials under atmospheric conditions and their low thermoelectric properties [50].

III-2-A- P-TYPE MATERIALS

P-type materials are materials with holes as the majority charge carrier. The electrical conduction is then linked to the mobility of holes in the system. Conductive polymers are intrinsically semi-conductors with a low electrical conductivity. By oxidative doping [51], they become more conducting which permit to reach high electrical conductivity around 1000 $S.cm^{-1}$. Polyacetylene is the one of the oldest polymer studied for his electronic properties. In thermoelectricity, it is possible to design polyacetylene doped with iodine (PA:Ix) as thermoelectric p-doped material with a high Seebeck coefficient value of 28.4 µV/K [52]. In terms of thermal conductivity, it has been shown on polyacetylene that the value depends of the doping of the system, increasing from undoped to heavy doped systems as demonstrated by

Moses and Denenstein [53]. PANi can also be used in thermoelectric applications. The problem with this material is its low electrical conductivity and Seebeck coefficient [54]–[56]. In order to obtain improved electrical conductivity in PANi materials, it is necessary to mechanically order polymer chains in fibers or nanotubes for example. Such treatment leads to an increase of the conduction through an unidirectional enhancement of the charge carrier mobility. Dopants added in PANi have also an incidence on thermoelectric properties. For instance, camphorsulfonic acid (CSA) doped PANi has a *ZT* of 2.9×10^{-2} [54]. Another material of interest is poly(phenylene vinylene) (PPV) with demonstration by Hiroshige *et al.* of copolymers based on PPV derivatives showing *ZT* of 9.87×10^{-2} [57], [58].

Additionally, Polypyrrole (PPy) shows good electrical conductivity and environmental stability [59]. It can subsequently be doped with different moieties like benzene sulfonate [60], perchlorate anion (ClO_4^-) [60], tetrafluoroborate anion (BF_4^-) [61], p-toluene sulfonate (PPpTS) [62] or hexafluorophosphate (PF_6) [63]. Recently, Bharti *et al.* showed the effect of pTSA doping on PPy thermoelectric properties [64]. By increasing the amount of dopants, they were able to increase electrical conductivity until 162.7 $S.cm^{-1}$.

Polythiophene (PTh) and its derivatives have also been studied for their good thermoelectric properties. They can be synthetized by chemical or electrochemical polymerization, which influences the electrical conductivity [65]. Poly(3-hexylthiophene) (P3HT) electronic properties are highly dependent of the crystalline structure of the polymer. P3HT vapor-doped with 2,3,5,6-Tetrafluoro-7,7,8,8-tetracyanoquinodimethane (F_4TCNQ) leads to a crystallite structure incorporating the dopant molecules, as shown in Figure I-14 (a). This doping technique permits to control the P3HT nanostructure and thus the electrical conductivity and Seebeck coefficient [66]. Interestingly, Hynynen *et al.* showed that the electrical conductivity can be increased just by changing the solvent during the polymerization process resulting in an enhancement of the power factor from 0.2 to 2.7 $\mu W.m^{-1}.K^{-2}$ [67]. This enhancement was related to an increase of the crystalline ordering of P3HT.

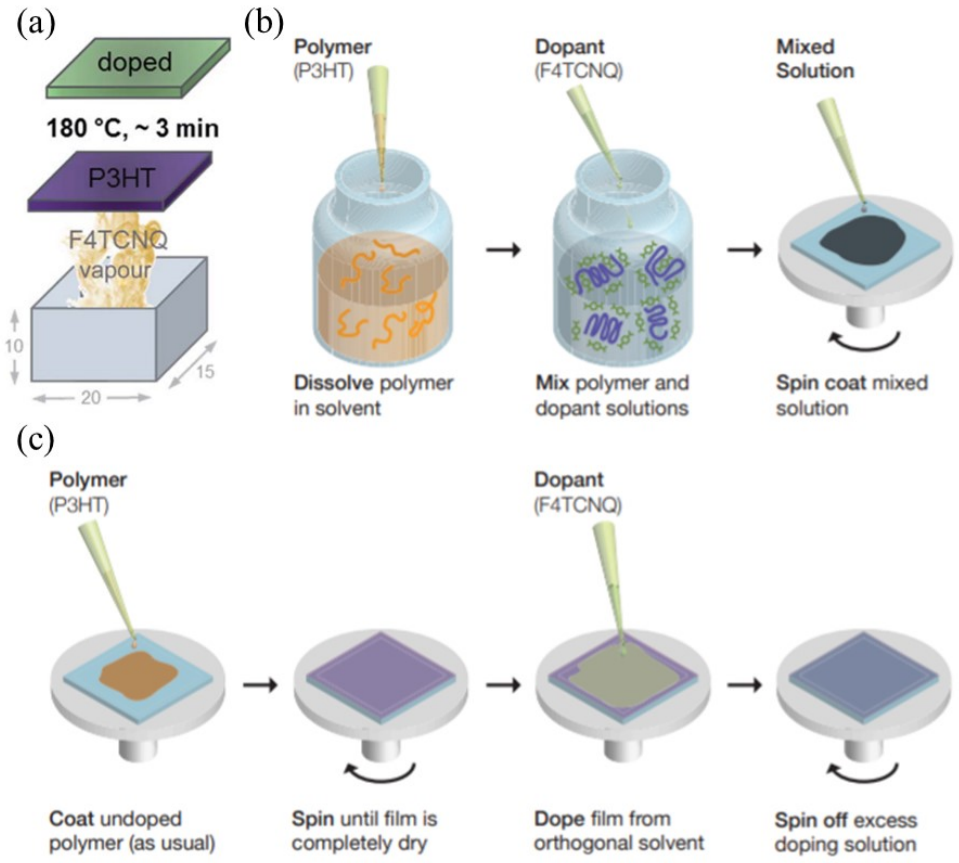

Figure I-14 Doping method for P3HT by F4TCNQ (a) vapor-phase [67] *(b) direct mixing (c) sequential method* [68].

P3HT doping can also be performed by direct mixing of the dopant and polymer, see Figure I-14 (b), or by depositing sequentially the polymer film and dopant, see Figure I-14 (c). Jacobs *et al.* compared those two methods [68]. They deduced from their study that sequential doping provides better results than mixed solution due to a better control of the final morphology. The conductivity obtained from the sequential method films are 5 to 15 times higher than the one of mixed solution films.

Nevertheless, the most studied polymer for thermoelectric applications is poly(ethylene-dioxythiophene) (PEDOT) due to its exceptional electronic properties. Among its derivatives, poly(styrenesulfonate) (PSS) and tosylate (Tos) are the more common dopants. PEDOT:Tos exhibits higher electrical conductivity than PEDOT:PSS but this last one is easier to process. This class of material will be discussed later in this chapter as the will be the main materials used in this Ph.D.

III-2-B- N-TYPE MATERIALS

N-type organic materials are less studied than their p-type counterparts due to their low stability under atmospheric conditions. This poor stability is explained by the fact that to n-dope a polymer, the LUMO level needs to be lowered by adding electron-withdrawing units to the backbone. To do that, the ionization potential of the dopant has to be lower than the electron affinity of the polymer and in general, small molecules added have a small ionization energy that makes them unstable in air [69]. Two others bottlenecks related to organic n-type materials are the low doping efficiency which results in a low charge carrier density and mobility [50].

Studies on n-type polymers really blossomed after 2010 with the doping of poly{[N,N0 -bis(2-octyldodecyl)-naphthalene-1, 4,5,8-bis(dicarboximide)-2,6-diyl]-alt-5,50 -(2,20 -bithiophene)} (P(NDI2OD-T2)) by rhodocene dimer $[RhCp_2]_2$ [70]. With this material, Qi *et al.* were able to reach a conductivity of 5.1×10^{-4} $S.cm^{-1}$ which is nevertheless lower than the one reported for common p-type materials. P(NDI2OD-T2) is part of the naphthalenediimide n-type polymer family. In this category, the best power factor was obtained for PNDI2TEG-2Tz, with 4.6 ± 0.2 $\mu W.m^{-1}.K^{-2}$ [71].
Others n-type polymers are based on *p*-phenylene vinylene derivatives. In 2013, Pei *et al.* introduced electron removal elements like chlorine (Cl) and fluorine (F) [72]. By doping the fluorine functionalized benzodifurandione-based poly(p-phenylene vinylene) (FBDPPV) with 4-(1,3-dimethyl-2,3-dihydro- 1H-benzoimidazol-2-yl)phenyl)dimethylamine (N-DMBI), Shi *et al.* reached a power factor of 25.5 ± 2.5 $\mu W.m^{-1}.K^{-2}$ for an electrical conductivity of 1.8 $S.cm^{-1}$ and a Seebeck coefficient of –159 ± 8 $\mu V.K^{-1}$ [73].

By including metal atoms inside a conjugated polymer backbone, materials can show a n-type behavior with good air stability [74]–[78]. This kind of materials can reach higher thermoelectric properties than current n-type polymers even if their processability is a challenge. Sun *et al.* reported ZT varying between 0.08 and 0.13 for temperature between 300 and 360 K for poly(Ni-ett) compounds. [78].

III-2-c- HYBRIDS

With the quest to enhance the thermoelectric properties, hybrid materials combining the advantages of inorganics and organics have been the focus of intense researches. Hybrids thermoelectric materials are based on the combination of two or more materials in order to obtain better performances by combining the electrical conductivity and/or Seebeck coefficient of those two materials. The incorporation of nanostructures in polymer matrix can drastically increase the thermoelectric properties [79] [80].

- *Carbon nanotubes inclusions*

The most common inclusion in polymer matrix is carbon nanotubes (CNT). CNT inclusion leads to the increase of the electrical conductivity due to the large specific area and the conjugated π-π structure of CNTs. Furthermore, the contacts between the matrix and CNTs increase interfacial effects which can enhance the conduction, decrease the thermal conductivity by the scattering of phonons [81], or enhance the Seebeck coefficient by increasing the energy potential barrier [82]. CNTs can be doped to result in a p-type or a n-type material and thus are extremely useful for the fabrication of thermoelectric devices [83]. Mai *et al.* doped single wall carbon nanotubes (SWCNTs) with sodium tetrakis(1-imidazolyl)borate ($NaBIm_4$) for the fabrication of a p-leg with a power factor of 7.3 ± 2.6 $\mu W.m^{-1}.K^{-2}$ while using poly(fluorene-alt-benzothiadiazole)/Pyridinium Bromide (PFBT–PyrBr) for the n-leg with a power factor of 0.041 ± 0.014 $\mu W.m^{-1}.K^{-2}$ [83]. Kumanek *et al.* also played on doping to synthetize p-type and n-type free-standing composites [84]. CNT inclusions have been used in most common p-type polymers like PEDOT:PSS [85]–[88], PANi [81], [82], [89], [90], P3HT [91] or PPy [92]. Hsu *et al.* reported a high power factor of 464 $\mu W.m^{-1}.K^{-2}$ for their PANi/SWNT composite [86].

The effect of CNTs on the thermoelectric properties can be subsequently increased by post-treating. Pan *et al.* synthetized a copolymer based on 9,9'-dioctyl-fluorene and bipyridine followed by the formation of complexes with SWCNTs [93]. By playing on the SWCNT content, they were able to reach a power factor of 62.3 $\mu W.m^{-1}.K^{-2}$ for

90 wt% SWCNT at room temperature, as shown in Figure I-15 (a). By mixing the previous complex with solutions containing metal atoms, they were further able to increase the electrical conductivity even if they noticed a concurrent decrease of the Seebeck coefficient. Nevertheless, such treatment results in an increase of the power factor. They found the best value for Ni inclusions with a power factor of 87.3 $\mu W.m^{-1}.K^{-2}$ measured at room temperature, as shown in Figure I-15 (b).

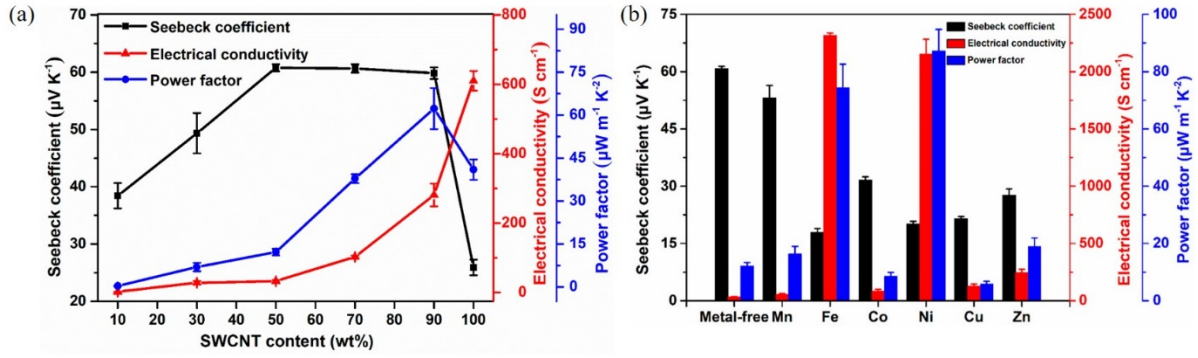

Figure I-15 Seebeck coefficient, electrical conductivity and power factor versus (a) SWCNT content (b) Metal atoms inclusions [93].

- *Inorganic inclusions*

Inorganic materials exhibit high thermoelectric properties as shown previously with the well-known Bi_2Te_3. Mixing polymers with inorganic compounds can lead to an increase of power factor with a decrease of thermal conductivity which results in a better ZT. Another advantage of those hybrids is the fact that they can be processed on flexible substrates combining thus inorganic and organic advantages. Coates *et al.* explained this enhancement of electrical conductivity by the fact that transport occurs along the interfacial contacts between PEDOT:PSS and Te nanowires (NWs) [94]. Metallic compounds like Te have huge charge carrier mobility. Mixing them with PANIi leads to increase the charge carrier mobility inside the complex resulting in a better ZT value as demonstrated by Wang *et al.* with a ZT of 0.156 [95]. Of interest is also the addition of silicides inclusions in a polymer matrix with the study of Longhin *et al.* which showed that an increase of the power factor for PEDOT:PSS/silicides complexes [96].

- *Organic/organic complexes*

Finally, the tuning of TE properties can also be done by mixing nanostructured organic materials inside an organic matrix. The advantage of such type of blending is the low thermal conductivity of both compounds. Accordingly, PEDOT nanowires have be included inside a PEDOT:Tos or PEDOT:PSS matrix and lead to an increase of the power. For instance, Zhang *et al.* multiplied by a factor two the Seebeck coefficient of their material resulting in a maximum PF of 102.7 $\mu W.m^{-1}.K^{-2}$ [80]. Those results were explained by the synergetic effect between the nanowire percolated network, the carrier filtering at interfaces and the change of carrier concentration inside the polymer matrix.

Apart filling polymers with another nanostructured polymer, composites can be made by stacking different polymers layers. Lee *et al.* made composites with alternated PANi-CSA and PEDOT:PSS layers using a layer-by-layer deposition process. They proved that this composite shows better TE properties with a power factor of 49 $\mu W.m^{-1}.K^{-2}$ [97].

III-3- PEDOT:TOS AS THE BEST OPTION FOR ORGANIC THERMOELECTRIC

PEDOT is the most studied material in the field of organic thermoelectricity. PEDOT is a polymer composed of an aromatic cycle in its benzoic form, as depicted in Figure I-16. As previously mentioned, PEDOT is a p-type semi-conducting polymer which can accept electrons. The main drawback with this polymer is its insolubility which reduces its processing ability. In order to avoid this problem, PEDOT can be doped with PSS. PEDOT:PSS is a commercially available ink and can be used in thermoelectric device but its properties are quite low with a conductivity around 1 $S.cm^{-1}$ and a Seebeck coefficient around 15 $\mu V.K^{-1}$ [98], [99].

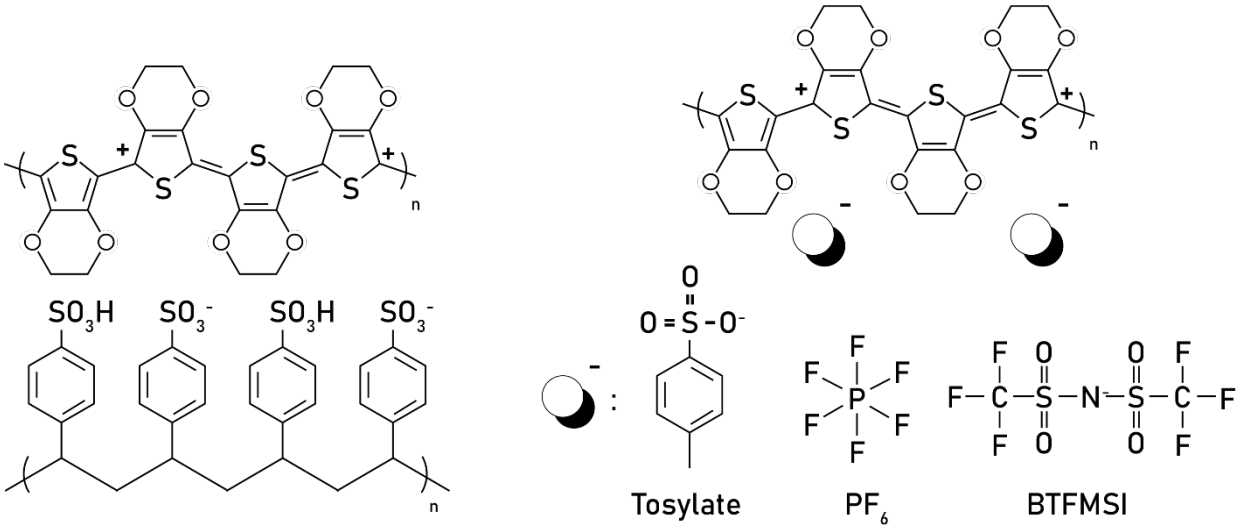

Figure I-16 Chemical structure of PEDOT doped with PSS or small counter-ions.

PEDOT can also be doped with other small counter-ions like tosylate [100]–[102], PF6 or bis(trifluoromethylsulfonyl)imide (BTFMSI) [103]. Preparing PEDOT with $FeCl_3$ can leads to a huge conductivity as shown by Wang *et al.* [104]. They managed to reach conductivity as high as 6259 $S.cm^{-1}$. Despite all the possibilities for doping PEDOT, the following parts will be focused on PEDOT:Tos which appears to be the most interesting material for thermoelectric applications.

III-3-A- PEDOT:TOS THIN FILMS

- *Films formation*

The mechanism of polymerization and doping for PEDOT:Tos was explained by Mueller *et al.* and is displayed in Figure I-17. An EDOT monomer is oxidized by Fe(III) ions to form an EDOT cation. The combination of two cations leads to an EDOT dimer which is subsequently deprotonated. This process starts again with the oxidation of one monomer which combines with the as-formed dication. The polymer is formed by the addition of EDOT monomer on the first formed dication. Tosylate is then used to dope the PEDOT structure. In order to polymerize EDOT, 2 moles of oxidant are needed, while 0.3 mole is commonly used to intrinsically dope the system during the polymerization. It has been shown previously than PEDOT:Tos can be doped at a

maximum of 33%, meaning that one tosylate can be found every three EDOT units [105], [106] but this result is always under discussion in the thermoelectric community [107].

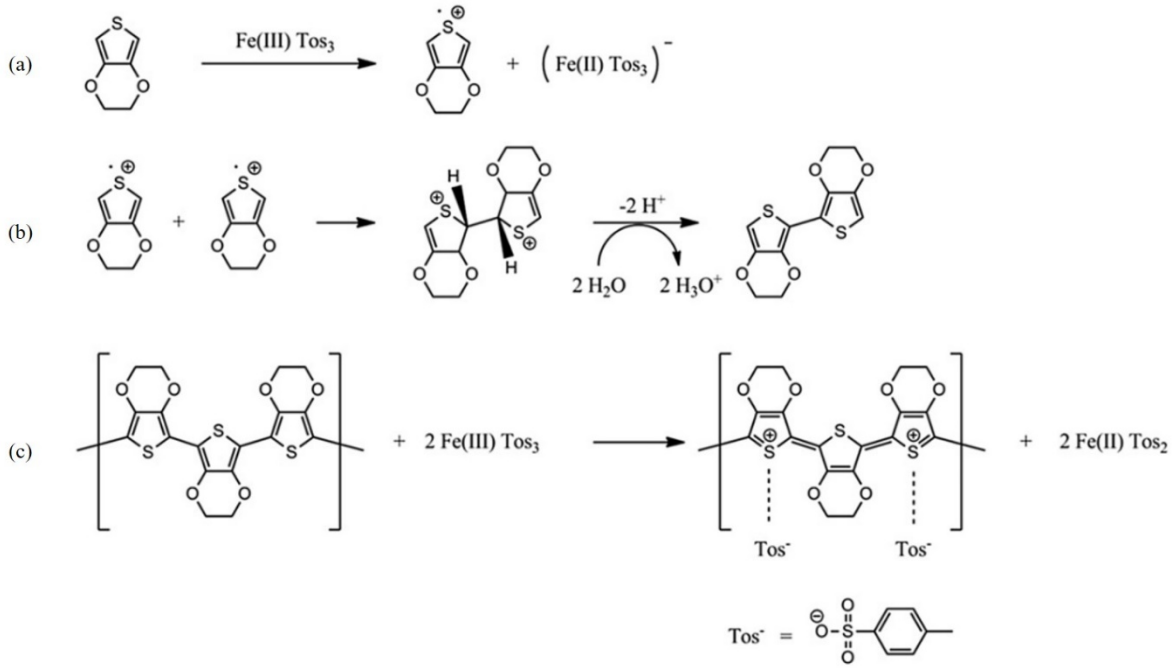

Figure I-17 Proposed polymerization mechanism by Mueller et al. for VPP PEDOT: (a) EDOT is oxidized by Fe(III) ion and becomes radical cation; (b) EDOT cation radicals combine to form dimers that get deprotonated after; (c) PEDOT polymer is doped and a tosylate ion stays in the film as a counter-ion [108].

PEDOT:Tos thin films can be obtained by three different processes. First of all, in-situ polymerization, also called chemical polymerization, is illustrated in Figure I-18 (a). In this case, the EDOT monomers, oxidants and additives are mixed together and then deposited by spin-coating to form a film by thermal treatment. The second one is the vapor phase polymerization (VPP) or vacuum vapor phase polymerization (VVPP), as shown in Figure I-18 (b). Contrary to the in-situ polymerization, only the oxidants and additives are deposited by spin-coating on a substrate. An exposure to EDOT vapors subsequently leads to the polymerization of EDOT onto the oxidant film. This technique is linked to chemical vapor deposition (CVD) with the difference of the pressure during polymerization. The last technique which can be used is electro-polymerization as shown in Figure I-18 (c). In this last case, the polymerization is performed on a conductive substrate dived in an electrolyte containing the ionic species required for the polymerization.

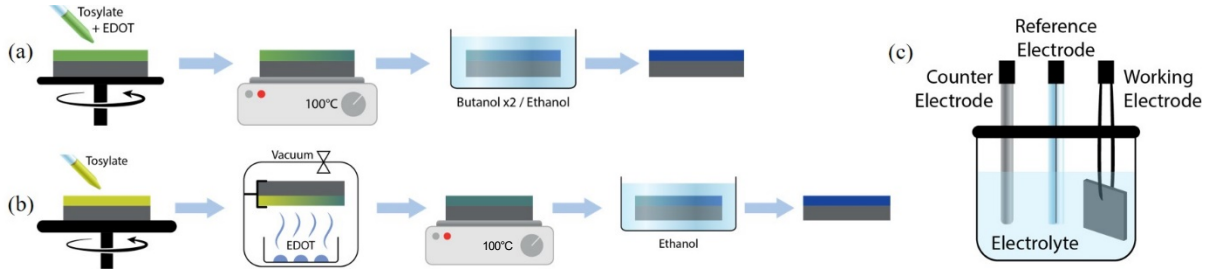

Figure I-18 Polymerization ways of PEDOT:Tos (a) steps for in-situ polymerization (b) steps for Vapor phase polymerization (c) Electropolymerization.

- *Films properties*

The PEDOT:Tos electrical conductivity and Seebeck coefficient can reach more than thousands of $S.cm^{-1}$ [109] and hundreds of $\mu V.K^{-1}$, respectively [110]. As presented in the Table I-1, PEDOT:Tos thermoelectric properties have been studied by a large number of scientists. In most of the cases, studies have been performed with the aim to increase the electrical conductivity or the Seebeck coefficient in order to reach an enhanced ZT by playing on morphology and more specifically on the polymer microstructure [111]. Structural engineering, also called "secondary doping", can be done during the polymerization or after by post treatment and is detailed below.
High boiling point solvents like dimethylsulfoxide (DMSO), dimethylformamide (DMF) or ethylene glycol (EG), have been shown to increase the crystallinity of the film by acting as a plasticizer [109]. Indeed, such solvents slow down the crystallization kinetics and allows polymer chains to rearrange themselves. This rearrangement of the chains favors an increase of the crystallization degree and further enhances the charge carrier transport in the film. This effect was demonstrated by Kim *et al.* with the increase of PEDOT:PSS properties by adding DMSO or EG [112]. Similar results have been demonstrated for PEDOT:Tos and, by increasing the crystallinity, PEDOT:Tos acquires semi-metallic properties, beneficial for thermoelectric applications [113].

Introducing a weak base in PEDOT:Tos formulation like pyridine or imidazole have been shown to reduce the auto-catalyzed process inherent to the release of free protons during the polymerization. The polymerization process is then retarded and

leads to increase of the molecular weight of PEDOT chains. By this process, delocalization of orbitals becomes larger and the electronic properties are enhanced [114][115]. As the process slows down, PEDOT chains can better organize themselves and the crystallinity is highly increased. Huang *et al.* studied the effect of imidazole on PEDOT conductivity and demonstrated an increase of the conductivity of PEDOT from 4.01 to 153.6 $S.cm^{-1}$ [114]. XRD and AFM study clearly linked this behavior to an increase of PEDOT chains ordering.

Accordingly, the increase of crystallinity in PEDOT materials has been the subject of intense efforts in the community. Fabretto *et al.* added poly(ethylene glycol-*b*-propylene glycol-*b*-ethylene glycol) triblock (PEG-*b*-PPG-*b*-PEG) or poly(ethylene glycol-*ran*-propylene glycol) (PEG-*ran*-PPG) random copolymers to PEDOT formulation [116]–[118]. These surfactants allow one to overcome the issues of volatiles compounds such as pyridine and imidazole in the formulation [118]. Finally, these glycolic compounds have been shown to provide the same effect than a weak base but also help to retain some traces of water favoring the polymerization process [108].

- *Films modification*

The thin film properties can be further increased by post treatment. The aim of those treatments is to remove non-linked dopants which decrease the charge carrier mobility [119]. This process has also an influence on the oxidation level of material and is called "de-doping". Bubnova *et al.* pioneered such methodology by exposing PEDOT:Tos films to tetrakis(dimethylamino)ethylene (TDAE) vapors [100]. By decreasing the oxidation level of PEDOT:Tos, the Seebeck coefficient increases while the electrical conductivity decreases, as shown in Figure I-19. An optimized oxidation level was found leading to a power factor as high as 324 $\mu W.m^{-1}.K^{-2}$. This behavior is comparable to the one observed in inorganic materials. This optimum thermoelectric property was established by balancing the Seebeck coefficient and the electrical conductivity.

Table I-1 Summary of thermoelectric properties of some PEDOT:Tos

Tos %	Polymerization	Additives	t (nm)	σ ($S.cm^{-1}$)	S ($\mu V.K^{-1}$)	κ ($Wm^{-1}K^{-1}$)	Power factor ($\mu Wm^{-1}K^{-2}$)	ZT	Year	Ref
16	VPP	PEG-ran-PPG	-	761 ± 73	-	-	-	-	2008	[120]
16	VPP	PEG-ran-PPG	75	701	-	-	-	-	2009	[107]
20	in-situ	pyridine	150-200	300	40	0.33 ± 0.1	38	≈ 0.025	2011	[110]
21.3	VPP	PEG–PPG–PEG	120-150	2500	-	-	-	-	2012	[102]
26.6	VPP	PEG–PPG–PEG	188 ± 6	1520 ± 102	-	-	-	-	2012	[108]
40	in-situ	PEG–PPG–PEG, pyridine	120-140	1355	79.7	-	861	-	2013	[121]
40	VPP	pyridine	100	622	-	-	-	-	2013	[122]
20	VPP	PEG–PPG–PEG	140 ± 5	944	16.5	0.495 ± 0.005	25.7	0.016	2014	[123]
12.3	VPP	PEG–PPG–PEG	-	818	17	-	-	-	2015	[124]
40	in situ	pyridine	-	810	16	-	-	-		
-	in-situ	-	627	152	11		≈ 2		2015	[125]
40	VPP	PEG–PPG–PEG	167 ± 5	≈ 500	≈ 18	≈ 1.4	≈	-	2015	[126]
40	in-situ	DMF	180	640 ± 10	35 ± 5	-	78.5	-	2016	[127]
-	VPP	PEG–PPG–PEG	100 ± 5	1532	14.9	-	33.8	-	2016	[128]
40	VPP	pyridine	≈ 70	≈ 760	-	-	-	-	2016	[129]
30.6	in-situ	pyridine	79.3 ± 4.9	376.64 ± 36.33	-	-	-	-	2017	[130]
40	in-situ	pyridine	223	≈ 800	-	-	-	-	2017	[131]
40	in-situ	pyridine, DMSO	100 ± 8	1220 ± 30	44 ± 2	-	-	-	2018	[109]
21	VPP	PEG–PPG–PEG	367 ± 12	726	-	-	-	-	2018	[132]

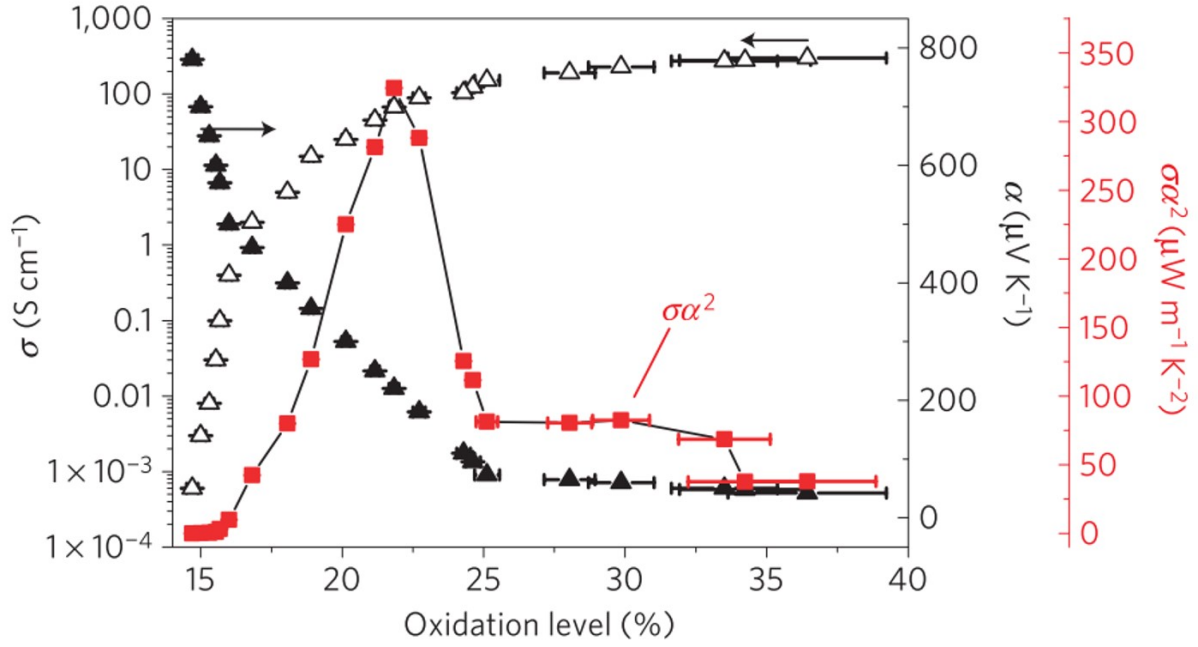

Figure I-19 Seebeck coefficient α, electrical conductivity σ and power factor $\sigma\alpha^2$ versus oxidation level [100].

Khan *et al.* applied an environment-friendly post treatment using aqueous vitamin C. This post-treatment reduces PEDOT:Tos, decreasing the oxidation level from 37 to 23%. Again, the vitamin C treatment leads to a decrease of the electrical conductivity and an increase of the Seebeck coefficient resulting in a ZT increase from 0.103 to 0.146 [133]. All the post-treatments lead to the same trend whether it is a strong base like sodium borohydride [134] or a strong acid like sulfuric acid [123] or hydrochloric acid [135]. Only hydroiodic acid permits to increase both electrical conductivity and Seebeck coefficient [128]. Dipping films inside acidic or basic solutions permits to tune thermoelectric properties [135]. Treating films with reducing agents leads to add a step in the process of film deposition and the products used during this process can be toxic. In order to further increase electronic properties of films, another way can be playing on the structuration of PEDOT:Tos.

III-3-b- Going further with structuration of PEDOT:Tos

In order to increase the conductivity of PEDOT:Tos, a good option is to play on crystallinity of PEDOT:Tos films. It has been shown that adding weak bases or high boiling point solvents lead to increase the molecular weight and so the crystallinity. Another possibility is to structure the polymer chains directly during the

polymerization. By using nano-patterns, polymers chains are confined in a small volume and are obliged to align which leads to an increase of the crystallinity and so charge carrier mobility. Kim *et al.* used a stamp in micro-contact printing in order to pattern substrate with Fe(III)Tos as ink [136], as shown in Figure I-20 (a). Using this micro-pattern, they managed to reach electrical conductivity as high as 4500 $S.cm^{-1}$. O'Connell *et al.* used an AFM tip for dip-pen nanolithography in order to pattern a substrate with Fe(III)Tos ink [137], as illustrated in Figure I-20 (b). The as-patterned substrate is then exposed to EDOT vapors in order to create PEDOT:Tos dots. With this technique, they obtained an electrical conductivity of 1 $S.cm^{-1}$ which is quite low for PEDOT:Tos system but they explained this result with the possible non-percolation of nanowires resulting from a washing step.

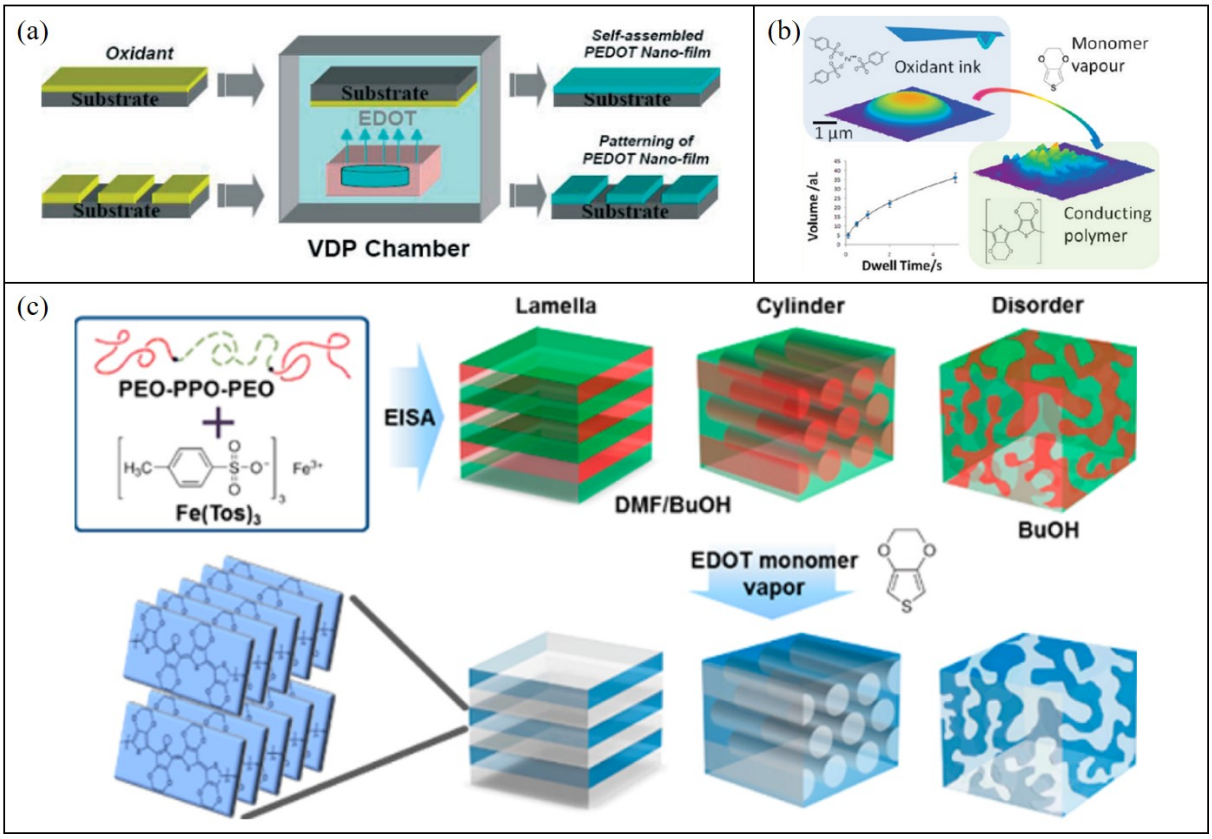

Figure I-20 Processes to obtain structured PEDOT:Tos (a) Use of stamp in microcontact printing and exposition to EDOT vapors [136] *(b) Dip pen lithography of Fe(III)Tos and exposition to EDOT vapors* [137] *(c) Infiltration of Fe(III)Tos in PEO-PPO-PEO and exposition to EDOT vapors* [138].

Patterning surface can also be done by the use of block copolymers. Lee *et al.* used poly(ethylene oxide)-*block*-poly(propylene oxide)-*block*-poly(ethylene oxide) (PEO-

b-PPO-*b*-PEO) and its self-organization into different nanostructures [138]. Fe(III)Tos mixed with PEO-*b*-PPO-*b*-PEO interacts with hydrophilic PEO domains. By thermal annealing, PEO-*b*-PPO-*b*-PEO/Fe(III)Tos films were able to self-organize and by exposing to EDOT vapors to form PEDOT:Tos nanostructures, as shown in Figure I-20 (c). The use of block copolymers permits to confine PEDOT:Tos and so increases its crystallinity and electrical conductivity with a best value at 2200 $S.cm^{-1}$.

IV- Conclusion and Ph.D. scopes

In this chapter, the basis of thermoelectricity have been introduced. As a rule of thumb, it has been shown that thermoelectric materials need to have a good electrical conductivity as well as a good Seebeck coefficient. Nevertheless, these two parameters are antagonist and thus a fine balance has to be found to design highly efficient thermoelectric materials. Inorganic materials appear as the best candidates for thermoelectric applications with respect to the intrinsic properties allowing one to finely modulate their composition and structural ordering in order to produce a high figure of merit ZT. Nevertheless, organic materials became of interest with the discover of intrinsically conductive polymers. The properties of such polymers can be tuned by taking into account polymer crystallinity, doping and charge transport. Besides, they are easier to produce, "environmentally friendly", and sometimes biocompatible as regard to inorganic materials which can open new avenues for targeted applications (wearable, internet of things) near room temperature. In this chapter, highlights were drawn on PEDOT:Tos as it has shown the best performance as regards to thermoelectric applications and a comprehensive review of the state-of-the-art regarding this particular material was presented.

The objective of this Ph.D. is thus to study PEDOT:Tos thin films as a thermoelectric material. In particular, we will focus on the influence of the polymerization processes, the post-treatments and structuration on the thermoelectric properties. Indeed, even if PEDOT:Tos is an archetypical material in organic thermoelectric, important optimizations as regards to its performance, are still needed for the advent of the technology. In particular, an extended understanding of the relationships between the chemical/crystalline/mesoscopic structures and the thermoelectric properties is needed.

Consequently, this Ph.D. firstly focuses on the polymerization pathways enabling the formation of PEDOT:Tos thin films with high thermoelectric efficiency. We have centered our study on two chemical procedures - in-situ polymerization and vapor phase polymerization - in order to decipher the interplay between the polymerization method, the structural properties and the resulting thermoelectric efficiency. In a

subsequent study, the optimization of the vapor phase polymerization process was tackled in order to better apprehend the role of the intrinsic (formulation of the reactants) and extrinsic parameters (temperature, vapor pressure) on the generation of PEDOT:Tos thin films. Finally, the last chapter of this Ph.D. is dedicated to the nanostructuration of PEDOT:Tos layers in order to evaluate the potential of such strategy on the electronic properties. The methodology used for nanostructuring is based on the self-assembly of block copolymers and its hybridization with the aforementioned polymerization processes for the generation of periodic PEDOT:Tos patterns at the nanometer scale.

[1] T. J. Seebeck, *Ueber den Magnetismus der galvenischen Kette*. 1821.

[2] T. J. Seebeck, "Ueber die magnetische Polarisation der Metalle und Erze durch Temperatur-Differenz," *Ann. Phys.*, vol. 82, no. 2, pp. 133–160, 1826, doi: 10.1002/andp.18260820202.

[3] C. Goupil, W. Seifert, K. Zabrocki, E. Müller, and G. J. Snyder, "Thermodynamics of thermoelectric phenomena and applications," *Entropy*, vol. 13, no. 8, pp. 1481–1517, 2011, doi: 10.3390/e13081481.

[4] J. C. A. Peltier, "Nouvelles expériences sur la caloricité des courants électrique," in *Annales de Chimie et de Physique*, 1834, pp. 371–386.

[5] J. D. Goddard, "On the thermoelectricity of W. Thomson: Towards a theory of thermoelastic conductors," *J. Elast.*, vol. 104, no. 1–2, pp. 267–280, 2011, doi: 10.1007/s10659-011-9309-6.

[6] V. E. Altenkirch, "Über den Nutzeffekt der Thermosäule," *Phys. Zeitschrift*, vol. 16, pp. 560–568, 1909.

[7] E. Altenkirch, "Elektrochemische Kälteerzeugung und reversible elektrische Heizung," *Phys. Zeitschrift*, vol. 12, no. 1, pp. 920–924, 1911.

[8] B. Russ, A. Glaudell, J. J. Urban, M. L. Chabinyc, and R. A. Segalman, "Organic thermoelectric materials for energy harvesting and temperature control," *Nat. Rev. Mater.*, vol. 1, no. 10, p. 16050, 2016, doi: 10.1038/natrevmats.2016.50.

[9] A. F. Ioffe, L. S. Stil'bans, E. K. Iordanishvili, T. S. Stavitskaya, A. Gelbtuch, and G. Vineyard, "Semiconductor Thermoelements and Thermoelectric Cooling," *Phys. Today*, vol. 12, no. 5, pp. 42–42, May 1959, doi: 10.1063/1.3060810.

[10] O. Bubnova and X. Crispin, "Towards polymer-based organic thermoelectric generators," *Energy Environ. Sci.*, vol. 5, no. 11, p. 9345, 2012, doi: 10.1039/c2ee22777k.

[11] A. Zevalkink *et al.*, "A practical field guide to thermoelectrics: Fundamentals, synthesis, and characterization," *Appl. Phys. Rev.*, vol. 5, no. 2, 2018, doi: 10.1063/1.5021094.

[12] K. Chiang, C, R. Fincher, C., W. Park, Y., and A. J. Heeger, "Electrical conductivity in doped polyacetylene," *Phys. Rev. B*, vol. 39, no. 17, pp. 1098–1101, 1977, doi: 10.1103/PhysRevB.24.7380.

[13] S. C. Rasmussen, "The path to conductive polyacetylene," *Bull. Hist. Chem.*, vol.

39, no. 1, pp. 64–72, 2014.

[14] X. Guo, M. Baumgarten, and K. Müllen, "Designing π-conjugated polymers for organic electronics," *Prog. Polym. Sci.*, vol. 38, no. 12, pp. 1832–1908, 2013, doi: 10.1016/j.progpolymsci.2013.09.005.

[15] K. Müllen, J. R. Reynolds, and T. Masuda, *Conjugated Polymers: A Practical Guide to Synthesis*. Royal Society of Chemistry, 2013.

[16] J. L. Bredas and G. B. Street, "Polarons, Bipolarons, and Solitons in Conducting Polymers," *Acc. Chem. Res.*, vol. 18, no. 10, pp. 309–315, 1985, doi: 10.1021/ar00118a005.

[17] B. J. Duke and B. O'Leary, "The band structure of polymers: Its calculation and interpretation: Part 3. Interpretation," *J. Chem. Educ.*, vol. 65, no. 6, pp. 513–516, 1988, doi: 10.1021/ed065p513.

[18] M. Geoghegan and G. Hadziioannou, *Polymer electronics*, Oxford mas. 2013.

[19] J. L. Brédas, B. Thémans, J. G. Fripiat, and J. M. André, "Highly conducting polyparaphenylene, polypyrrole, and polythiophene chains: an ab initio study of the geometry and electronic structure modifications upon doping," *Phys. Rev. B*, vol. 29, no. 12, 1984.

[20] J. L. Brédas, R. R. Chance, and R. Silbey, "Comparative theoretical study of the doping of conjugated polymers: Polarons in polyacetylene and polyparaphenylene," *Phys. Rev. B*, vol. 26, no. 10, pp. 5843–5854, 1982, doi: https://doi.org/10.1103/PhysRevB.26.5843.

[21] S. Holliday, J. E. Donaghey, and I. McCulloch, "Advances in charge carrier mobilities of semiconducting polymers used in organic transistors," *Chem. Mater.*, vol. 26, no. 1, pp. 647–663, 2014, doi: 10.1021/cm402421p.

[22] V. Coropceanu *et al.*, "Charge transport in organic semiconductors.," *Chem. Rev.*, vol. 107, no. 4, pp. 926–52, 2007, doi: 10.1007/128_2011_218.

[23] C. Y. Liu and S. A. Chen, "Charge mobility and charge traps in conjugated polymers," *Macromol. Rapid Commun.*, vol. 28, no. 17, pp. 1743–1760, 2007, doi: 10.1002/marc.200700327.

[24] A. B. Kaiser and V. Skákalová, "Electronic conduction in polymers, carbon nanotubes and graphene," *Chem. Soc. Rev.*, vol. 40, no. 7, p. 3786, 2011, doi: 10.1039/c0cs00103a.

[25] A. J. Epstein *et al.*, "Inhomogeneous disorder and the modified Drude metallic state of conducting polymers," *Synth. Met.*, vol. 65, no. 2–3, pp. 149–157, 1994, doi: 10.1016/0379-6779(94)90176-7.

[26] P. J. Phillips, "Polymer crystals," *Reports Prog. Phys.*, vol. 53, no. 5, pp. 549–604, 1990, doi: 10.1088/0034-4885/53/5/002.

[27] L. M. Cowen, J. Atoyo, M. J. Carnie, D. Baran, and B. C. Schroeder, "Review—Organic Materials for Thermoelectric Energy Generation," *ECS J. Solid State Sci. Technol.*, vol. 6, no. 3, pp. N3080–N3088, 2017, doi: 10.1149/2.0121703jss.

[28] S. Hébert *et al.*, "Searching for new thermoelectric materials: Some examples among oxides, sulfides and selenides," *J. Phys. Condens. Matter*, vol. 28, no. 1, 2016, doi: 10.1088/0953-8984/28/1/013001.

[29] T. C. Harman, B. Paris, S. E. Miller, and H. L. Goering, "Preparation and some physical properties of Bi2Te3, Sb2Te3, and As2Te3," *J. Phys. Chem. Solids*, vol. 2, no. 3, pp. 181–190, 1957, doi: 10.1016/0022-3697(57)90081-1.

[30] C. Han, Q. Sun, Z. Li, and S. X. Dou, "Thermoelectric Enhancement of Different Kinds of Metal Chalcogenides," *Adv. Energy Mater.*, vol. 6, no. 15, 2016, doi: 10.1002/aenm.201600498.

[31] M. Tan, Y. Deng, and Y. Wang, "Ordered structure and high thermoelectric properties of Bi2(Te,Se)3 nanowire array," *Nano Energy*, vol. 3, pp. 144–151, 2014, doi: 10.1016/j.nanoen.2013.07.009.

[32] R. Venkatasubramanian, E. Siivola, T. Colpitts, and B. O' Quinn, "Thin-film thermoelectric devices with high room-temperature figures of merit," *Mater. Sustain. Energy A Collect. Peer-Reviewed Res. Rev. Artic. from Nat. Publ. Gr.*, pp. 120–125, 2010, doi: 10.1142/9789814317665_0019.

[33] S. M. Pourkiaei *et al.*, "Thermoelectric cooler and thermoelectric generator devices: A review of present and potential applications, modeling and materials," *Energy*, vol. 186, p. 115849, 2019, doi: 10.1016/j.energy.2019.07.179.

[34] T. C. Harman, M. P. Walsh, B. E. Laforge, and G. W. Turner, "Nanostructured thermoelectric materials," *J. Electron. Mater.*, vol. 34, no. 5, pp. L19–L22, May 2005, doi: 10.1007/s11664-005-0083-8.

[35] I. Terasaki, Y. Sasago, and K. Uchinokura, "Large thermoelectric power in single crystals," *Phys. Rev. B - Condens. Matter Mater. Phys.*, vol. 56, no. 20, pp.

R12685–R12687, 1997, doi: 10.1103/PhysRevB.56.R12685.

[36] H. S. Lee, G. H. Kim, D. H. Hwang, and S. I. Woo, "High thermoelectric power in a NaxCoO2 thin film prepared by sputtering with rapid thermal annealing," *Curr. Appl. Phys.*, vol. 15, no. 3, pp. 412–416, 2015, doi: 10.1016/j.cap.2014.12.030.

[37] M. Ohtaki, T. Tsubota, K. Eguchi, and H. Arai, "High-temperature thermoelectric properties of (Zn1-xAlx)O," *J. Appl. Phys.*, vol. 79, no. 3, pp. 1816–1818, 1996, doi: 10.1063/1.360976.

[38] R. Funahashi and M. Shikano, "Bi2Sr2Co2Oy whiskers with high thermoelectric figure of merit," *Appl. Phys. Lett.*, vol. 81, no. 8, pp. 1459–1461, 2002, doi: 10.1063/1.1502190.

[39] S. Hébert and A. Maignan, "Thermoelectric oxides," in *Functionnal oxides*, D. W. Bruce, D. O'Hare, and R. I. Walton, Eds. John Wiley & Sons, Inc., 2010, pp. 397–441.

[40] P. Zhang, Y. X. Zhang, H. Lai, J. Deng, J. Feng, and Z. H. Ge, "Enhanced thermoelectric properties of natural chalcopyrite by vacuum annealing," *Mater. Lett.*, vol. 253, pp. 430–433, 2019, doi: 10.1016/j.matlet.2019.07.101.

[41] X. Lu *et al.*, "High performance thermoelectricity in earth-abundant compounds based on natural mineral tetrahedrites," *Adv. Energy Mater.*, vol. 3, no. 3, pp. 342–348, 2013, doi: 10.1002/aenm.201200650.

[42] J. Heo, G. Laurita, S. Muir, M. A. Subramanian, and D. A. Keszler, "Enhanced thermoelectric performance of synthetic tetrahedrites," *Chem. Mater.*, vol. 26, no. 6, pp. 2047–2051, 2014, doi: 10.1021/cm404026k.

[43] B. Hinterleitner *et al.*, "Thermoelectric performance of a metastable thin-film Heusler alloy," *Nature*, vol. 576, pp. 85–90, 2019, doi: 10.1038/s41586-019-1751-9.

[44] Z. Li, J. F. Dong, F. H. Sun, S. Hirono, and J. F. Li, "Significant Enhancement of the Thermoelectric Performance of Higher Manganese Silicide by Incorporating MnTe Nanophase Derived from Te Nanowire," *Chem. Mater.*, vol. 29, no. 17, pp. 7378–7389, 2017, doi: 10.1021/acs.chemmater.7b02270.

[45] N. Parse, S. at Tanusilp, W. Silpawilawan, K. Kurosaki, and S. Pinitsoontorn, "Enhancing Thermoelectric Properties of Higher Manganese Silicide (HMS) by Partial Ta Substitution," *J. Electron. Mater.*, vol. 49, pp. 2726–2733, 2019, doi: 10.1007/s11664-019-07673-x.

[46] S. Muthiah *et al.*, "Significant enhancement in thermoelectric performance of nanostructured higher manganese silicides synthesized employing a melt spinning technique," *Nanoscale*, vol. 10, no. 4, pp. 1970–1977, 2018, doi: 10.1039/c7nr06195a.

[47] Q. Jiang *et al.*, "Paper: An effective substrate for the enhancement of thermoelectric properties in PEDOT:PSS," *J. Polym. Sci. Part B Polym. Phys.*, vol. 52, no. 11, pp. 737–742, 2014, doi: 10.1002/polb.23482.

[48] Q. Wei, M. Mukaida, K. Kirihara, Y. Naitoh, and T. Ishida, "Polymer thermoelectric modules screen-printed on paper," *RSC Adv.*, vol. 4, no. 54, pp. 28802–28806, 2014, doi: 10.1039/c4ra04946b.

[49] V. V Brus, M. Gluba, J. Rg Rappich, F. Lang, P. D. Maryanchuk, and N. H. Nickel, "Fine Art of Thermoelectricity," 2018, doi: 10.1021/acsami.7b17491.

[50] Y. Lu, J. Y. Wang, and J. Pei, "Strategies to Enhance the Conductivity of n-Type Polymer Thermoelectric Materials," *Chem. Mater.*, vol. 31, no. 17, pp. 6412–6423, 2019, doi: 10.1021/acs.chemmater.9b01422.

[51] S. Peng, D. Wang, J. Lu, M. He, and C. Xu, "A Review on Organic Polymer-Based Thermoelectric Materials," *J. Polym. Environ.*, vol. 25, no. 4, pp. 1208–1218, 2017, doi: 10.1007/s10924-016-0895-z.

[52] Y. W. Park, "Structure and morphology: relation to thermopower properties of conductive polymers," *Synth. Met.*, vol. 45, no. 2, pp. 173–182, 1991, doi: 10.1016/0379-6779(91)91801-G.

[53] D. Moses and A. Denenstein, "Experimental determination of the thermal conductivity of a conducting polymer: Pure and heavily doped polyacetylene," *Phys. Rev. B*, vol. 30, no. 4, pp. 2090–2097, 1984, doi: 10.1103/PhysRevB.30.2090.

[54] H. Yan, T. Ohta, and N. Toshima, "Stretched polyaniline films doped by (±)-10-camphorsulfonic acid: Anisotropy and improvement of thermoelectric properties," *Macromol. Mater. Eng.*, vol. 286, no. 3, pp. 139–142, 2001, doi: 10.1002/1439-2054(20010301)286:3<139::AID-MAME139>3.0.CO;2-F.

[55] J. Wu, Y. Sun, W. Xu, and Q. Zhang, "Investigating thermoelectric properties of doped polyaniline nanowires," *Synth. Met.*, vol. 189, pp. 177–182, 2014, doi: 10.1016/j.synthmet.2014.01.007.

[56] C. O. Yoon, M. Reghu, D. Moses, Y. Cao, and A. J. Heeger, "Transports in blends

of conducting polymers," *Synth. Met.*, vol. 69, no. 1–3, pp. 255–258, 1995, doi: 10.1016/0379-6779(94)02439-6.

[57] Y. Hiroshige, M. Ookawa, and N. Toshima, "High thermoelectric performance of poly(2,5-dimethoxyphenylenevinylene) and its derivatives," *Synth. Met.*, vol. 156, no. 21–24, pp. 1341–1347, 2006, doi: 10.1016/j.synthmet.2006.10.004.

[58] Y. Hiroshige, M. Ookawa, and N. Toshima, "Thermoelectric figure-of-merit of iodine-doped copolymer of phenylenevinylene with dialkoxyphenylenevinylene," *Synth. Met.*, vol. 157, no. 10–12, pp. 467–474, 2007, doi: 10.1016/j.synthmet.2007.05.003.

[59] L. X. Wang, X. G. Li, and Y. L. Yang, "Preparation, properties and applications of polypyrroles," *React. Funct. Polym.*, vol. 47, no. 2, pp. 125–139, 2001, doi: 10.1016/S1381-5148(00)00079-1.

[60] K. Bender, E. Gogu, and D. Schweitzer, "Electric conductivity and thermoelectric power of various polypyrroles," *Synth. Met.*, vol. 18, pp. 85–88, 1987, doi: 10.1016/0379-6779(87)90858-7.

[61] A. Watanabe, M. Tanaka, and J. Tanaka, "Electrical and Optical Properties of a Stable Synthetic Metallic Polymer: Polypyrrole.," *Bulletin of the Chemical Society of Japan*, vol. 54, no. 8. pp. 2278–2281, 1981, doi: 10.1246/bcsj.54.2278.

[62] D. S. Maddison, J. Unsworth, and R. B. Roberts, "Electrical conductivity and thermoelectric power of polypyrrole with different doping levels," *Synth. Met.*, vol. 26, no. 1, pp. 99–108, Oct. 1988, doi: 10.1016/0379-6779(88)90339-6.

[63] W. P. Lee, Y. W. Park, and Y. S. Choi, "Metallic electrical transport of PF6-doped polypyrrole: dc conductivity and thermoelectric power," *Synth. Met.*, vol. 84, no. 1–3, pp. 841–842, 1997, doi: 10.1016/s0379-6779(96)04174-4.

[64] M. Bharti *et al.*, "Scalable free-standing polypyrrole films for wrist-band type flexible thermoelectric power generator," *Energy*, vol. 176, pp. 853–860, 2019, doi: 10.1016/j.energy.2019.04.013.

[65] H. Yao *et al.*, "Recent Development of Thermoelectric Polymers and Composites," *Macromol. Rapid Commun.*, vol. 1700727, p. 1700727, 2018, doi: 10.1002/marc.201700727.

[66] E. Lim, K. A. Peterson, G. M. Su, and M. L. Chabinyc, "Thermoelectric Properties of Poly(3-hexylthiophene) (P3HT) Doped with 2,3,5,6-Tetrafluoro-7,7,8,8-

tetracyanoquinodimethane (F4TCNQ) by Vapor-Phase Infiltration," *Chem. Mater.*, vol. 30, no. 3, pp. 998–1010, 2018, doi: 10.1021/acs.chemmater.7b04849.

[67] J. Hynynen, D. Kiefer, and C. Müller, "Influence of crystallinity on the thermoelectric power factor of P3HT vapour-doped with F4TCNQ," *RSC Adv.*, vol. 8, no. 3, pp. 1593–1599, 2018, doi: 10.1039/c7ra11912g.

[68] I. E. Jacobs *et al.*, "Comparison of solution-mixed and sequentially processed P3HT:F4TCNQ films: Effect of doping-induced aggregation on film morphology," *J. Mater. Chem. C*, vol. 4, no. 16, pp. 3454–3466, 2016, doi: 10.1039/c5tc04207k.

[69] B. Lüssem, C. M. Keum, D. Kasemann, B. Naab, Z. Bao, and K. Leo, "Doped Organic Transistors," *Chem. Rev.*, vol. 116, no. 22, pp. 13714–13751, 2016, doi: 10.1021/acs.chemrev.6b00329.

[70] Y. Qi, S. K. Mohapatra, S. Bok Kim, S. Barlow, S. R. Marder, and A. Kahn, "Solution doping of organic semiconductors using air-stable n-dopants," *Appl. Phys. Lett.*, vol. 100, no. 8, 2012, doi: 10.1063/1.3689760.

[71] J. Liu *et al.*, "N-Type Organic Thermoelectrics of Donor–Acceptor Copolymers: Improved Power Factor by Molecular Tailoring of the Density of States," *Adv. Mater.*, vol. 30, no. 44, 2018, doi: 10.1002/adma.201804290.

[72] T. Lei, J. H. Dou, X. Y. Cao, J. Y. Wang, and J. Pei, "Electron-Deficient Poly(p-phenylene vinylene) Provides Electron Mobility over 1 cm2 V-1 s-1 under Ambient Conditions," *J. Am. Chem. Soc.*, vol. 135, no. 33, pp. 12168–12171, 2013, doi: 10.1021/ja403624a.

[73] K. Shi *et al.*, "Toward High Performance n-Type Thermoelectric Materials by Rational Modification of BDPPV Backbones," *J. Am. Chem. Soc.*, vol. 137, no. 22, pp. 6979–6982, 2015, doi: 10.1021/jacs.5b00945.

[74] J. R. Reynolds, C. P. Lillya, and J. C. W. Chien, "Intrinsically Electrically Conducting Poly(metal tetrathiooxalates)," *Macromolecules*, vol. 20, no. 6, pp. 1184–1191, 1987, doi: 10.1021/ma00172a003.

[75] J. R. Reynolds, F. E. Karasz, C. P. Lillya, and J. C. W. Chien, "Electrically conducting transition metal complexes of tetrathio-oxalate," *J. Chem. Soc. Chem. Commun.*, no. 5, pp. 268–269, 1985, doi: 10.1039/c39850000268.

[76] C. Faulmann, J. Chahine, K. Jacob, Y. Coppel, L. Valade, and D. De Caro, "Nickel ethylene tetrathiolate polymers as nanoparticles: A new synthesis for future

applications?," *J. Nanoparticle Res.*, vol. 15, no. 4, 2013, doi: 10.1007/s11051-013-1586-5.

[77] K. Oshima, Y. Shiraishi, and N. Toshima, "Novel nanodispersed polymer complex, poly(nickel 1,1,2,2-ethenetetrathiolate): Preparation and hybridization for n-type of organic thermoelectric materials," *Chem. Lett.*, vol. 44, no. 9, pp. 1185–1187, 2015, doi: 10.1246/cl.150328.

[78] Y. Sun *et al.*, "Optimization of the thermoelectric properties of poly(nickel-ethylenetetrathiolate) synthesized via potentiostatic deposition," *Sci. China Chem.*, vol. 59, no. 10, pp. 1323–1329, 2016, doi: 10.1007/s11426-016-0175-9.

[79] H. Yao, Z. Fan, H. Cheng, X. Guan, C. Wang, and K. Sun, "Recent Development of Thermoelectric Polymers and Composites," vol. 1700727, pp. 1–22, 2018, doi: 10.1002/marc.201700727.

[80] K. Zhang, J. Qiu, and S. Wang, "Thermoelectric properties of PEDOT nanowire/PEDOT hybrids," *Nanoscale*, vol. 8, no. 15, pp. 8033–8041, 2016, doi: 10.1039/c5nr08421k.

[81] Q. Yao, L. Chen, W. Zhang, S. Liufu, and X. Chen, "Enhanced thermoelectric performance of single-walled carbon nanotubes/polyaniline hybrid nanocomposites," *ACS Nano*, vol. 4, no. 4, pp. 2445–2451, 2010, doi: 10.1021/nn1002562.

[82] C. Meng, C. Liu, and S. Fan, "A promising approach to enhanced thermoelectric properties using carbon nanotube networks," *Adv. Mater.*, vol. 22, no. 4, pp. 535–539, 2010, doi: 10.1002/adma.200902221.

[83] C. K. Mai *et al.*, "Varying the ionic functionalities of conjugated polyelectrolytes leads to both p- and n-type carbon nanotube composites for flexible thermoelectrics," *Energy Environ. Sci.*, vol. 8, no. 8, pp. 2341–2346, 2015, doi: 10.1039/c5ee00938c.

[84] B. Kumanek, G. Stando, P. S. Wróbel, M. Krzywiecki, and D. Janas, "Thermoelectric properties of composite films from multi-walled carbon nanotubes and ethyl cellulose doped with heteroatoms," *Synth. Met.*, vol. 257, no. July, p. 116190, 2019, doi: 10.1016/j.synthmet.2019.116190.

[85] G. P. Moriarty *et al.*, "Thermoelectric behavior of organic thin film nanocomposites," *J. Polym. Sci. Part B Polym. Phys.*, vol. 51, no. 2, pp. 119–123,

2013, doi: 10.1002/polb.23186.

[86] J. H. Hsu, W. Choi, G. Yang, and C. Yu, "Origin of unusual thermoelectric transport behaviors in carbon nanotube filled polymer composites after solvent/acid treatments," *Org. Electron.*, vol. 45, pp. 182–189, 2017, doi: 10.1016/j.orgel.2017.03.007.

[87] W. Lee, Y. H. Kang, J. Y. Lee, K. S. Jang, and S. Y. Cho, "Improving the thermoelectric power factor of CNT/PEDOT:PSS nanocomposite films by ethylene glycol treatment," *RSC Adv.*, vol. 6, no. 58, pp. 53339–53344, 2016, doi: 10.1039/c6ra08599g.

[88] X. Hu, G. Chen, and X. Wang, "An unusual coral-like morphology for composites of poly(3,4-ethylenedioxythiophene)/carbon nanotube and the enhanced thermoelectric performance," *Compos. Sci. Technol.*, vol. 144, pp. 43–50, 2017, doi: 10.1016/j.compscitech.2017.03.018.

[89] Q. Yao, Q. Wang, L. Wang, and L. Chen, "Abnormally enhanced thermoelectric transport properties of SWNT/PANI hybrid films by the strengthened PANI molecular ordering," *Energy Environ. Sci.*, vol. 7, no. 11, pp. 3801–3807, 2014, doi: 10.1039/c4ee01905a.

[90] L. Wang *et al.*, "Engineered Molecular Chain Ordering in Single-Walled Carbon Nanotubes/Polyaniline Composite Films for High-Performance Organic Thermoelectric Materials," *Chem. - An Asian J.*, vol. 11, no. 12, pp. 1804–1810, 2016, doi: 10.1002/asia.201600212.

[91] C. T. Hong *et al.*, "Effective doping by spin-coating and enhanced thermoelectric power factors in SWCNT/P3HT hybrid films," *J. Mater. Chem. A*, vol. 3, no. 23, pp. 12314–12319, 2015, doi: 10.1039/c5ta02443a.

[92] L. Liang, C. Gao, G. Chen, and C. Y. Guo, "Large-area, stretchable, super flexible and mechanically stable thermoelectric films of polymer/carbon nanotube composites," *J. Mater. Chem. C*, vol. 4, no. 3, pp. 526–532, 2016, doi: 10.1039/c5tc03768a.

[93] C. Pan *et al.*, "Preparation and thermoelectric properties study of bipyridine-containing polyfluorene derivative/SWCNT composites," *Polymers (Basel).*, vol. 11, no. 2, 2019, doi: 10.3390/polym11020278.

[94] N. E. Coates *et al.*, "Effect of interfacial properties on polymer-nanocrystal

thermoelectric transport," *Adv. Mater.*, vol. 25, no. 11, pp. 1629–1633, 2013, doi: 10.1002/adma.201203915.

[95] Y. Wang, S. M. Zhang, and Y. Deng, "Flexible low-grade energy utilization devices based on high-performance thermoelectric polyaniline/tellurium nanorod hybrid films," *J. Mater. Chem. A*, vol. 4, no. 9, pp. 3554–3559, 2016, doi: 10.1039/c6ta01140c.

[96] M. Longhin, M. Khalil, L. Abbassi, M. Beaudhuin, P. Papet, and R. Viennois, "Enhanced thermoelectric properties in Polypyrrole composites with silicide fillers," *Mater. Lett.*, vol. 264, p. 127373, 2020, doi: 10.1016/j.matlet.2020.127373.

[97] H. J. Lee *et al.*, "Enhanced thermoelectric performance of PEDOT:PSS/PANI-CSA polymer multilayer structures," *Energy Environ. Sci.*, vol. 9, no. 9, pp. 2806–2811, 2016, doi: 10.1039/c5ee03063c.

[98] F.-X. JIANG, J.-K. XU, B.-Y. LU, Y. XIE, R.-J. HUANG, and L.-F. Li, "Thermoelectric Performance of Poly(3,4- ethylenedioxythiophene): Poly(styrenesulfonate)," *Chinese Phys. Lett.*, vol. 25, no. 6, pp. 2202–2205, 2008.

[99] S. Kirchmeyer and K. Reuter, "Scientific importance, properties and growing applications of poly(3,4-ethylenedioxythiophene)," *J. Mater. Chem.*, vol. 15, no. 21, pp. 2077–2088, 2005, doi: 10.1039/b417803n.

[100] O. Bubnova *et al.*, "Optimization of the thermoelectric figure of merit in the conducting polymer poly(3,4-ethylenedioxythiophene)," *Nat. Mater.*, vol. 10, no. 6, pp. 429–433, 2011, doi: 10.1038/nmat3012.

[101] K. E. Aasmundtveit, E. J. Samuelsen, L. A. A. Pettersson, O. Inganäs, T. Johansson, and R. Feidenhans'l, "Structure of thin films of poly(3,4-ethylenedioxythiophene)," *Synth. Met.*, vol. 101, no. 1, pp. 561–564, 1999, doi: 10.1016/S0379-6779(98)00315-4.

[102] D. Evans, M. Fabretto, M. Mueller, K. Zuber, R. Short, and P. Murphy, "Structure-directed growth of high conductivity PEDOT from liquid-like oxidant layers during vacuum vapor phase polymerization," *J. Mater. Chem.*, vol. 22, no. 30, p. 14889, 2012, doi: 10.1039/c2jm32281a.

[103] M. Culebras, C. M. Gómez, and A. Cantarero, "Enhanced thermoelectric performance of PEDOT with different counter-ions optimized by chemical reduction," *J. Mater. Chem. A*, vol. 2, no. 26, pp. 10109–10115, 2014, doi:

10.1039/c4ta01012d.

[104] X. Wang *et al.*, "High electrical conductivity and carrier mobility in oCVD PEDOT thin films by engineered crystallization and acid treatment," *Sci. Adv.*, vol. 4, no. 9, pp. 1–10, 2018, doi: 10.1126/sciadv.aat5780.

[105] S. G. Im, K. K. Gleason, and E. A. Olivetti, "Doping level and work function control in oxidative chemical vapor deposited poly (3,4-ethylenedioxythiophene)," *Appl. Phys. Lett.*, vol. 90, no. 15, pp. 88–91, 2007, doi: 10.1063/1.2721376.

[106] J. Lu, N. J. Pinto, and A. G. MacDiarmid, "Apparent dependence of conductivity of a conducting polymer on an electric field in a field effect transistor configuration," *J. Appl. Phys.*, vol. 92, no. 10, pp. 6033–6038, 2002, doi: 10.1063/1.1511291.

[107] M. Fabretto, C. Jariego-moncunill, J. Autere, A. Michelmore, R. D. Short, and P. Murphy, "High conductivity PEDOT resulting from glycol / oxidant complex and glycol / polymer intercalation during vacuum vapour phase polymerisation," *Polymer (Guildf).*, vol. 52, no. 8, pp. 1725–1730, 2011, doi: 10.1016/j.polymer.2011.02.028.

[108] M. Mueller, M. Fabretto, D. Evans, P. Hojati-Talemi, C. Gruber, and P. Murphy, "Vacuum vapour phase polymerization of high conductivity PEDOT: Role of PEG-PPG-PEG, the origin of water, and choice of oxidant," *Polymer (Guildf).*, vol. 53, no. 11, pp. 2146–2151, 2012, doi: 10.1016/j.polymer.2012.03.028.

[109] I. Petsagkourakis *et al.*, "Correlating the Seebeck coefficient of thermoelectric polymer thin films to their charge transport mechanism," *Org. Electron. physics, Mater. Appl.*, vol. 52, no. November 2017, pp. 335–341, 2018, doi: 10.1016/j.orgel.2017.11.018.

[110] O. Bubnova *et al.*, "Optimization of the thermoelectric figure of merit in the conducting polymer poly(3,4-ethylenedioxythiophene)," *Nat. Mater.*, vol. 10, no. 6, pp. 429–433, 2011, doi: 10.1038/nmat3012.

[111] R. Noriega *et al.*, "A general relationship between disorder, aggregation and charge transport in conjugated polymers," *Nat. Mater.*, vol. 12, no. 11, pp. 1038–1044, 2013, doi: 10.1038/nmat3722.

[112] G.-H. Kim, L. Shao, K. Zhang, and K. P. Pipe, "Engineered doping of organic semiconductors for enhanced thermoelectric efficiency," *Nat. Mater.*, vol. 12, no.

8, pp. 719–723, 2013, doi: 10.1038/nmat3635.

[113] O. Bubnova *et al.*, "Semi-metallic polymers," *Nat. Mater.*, vol. 13, no. 2, pp. 190–194, 2013, doi: 10.1038/nmat3824.

[114] J. H. Huang and C. W. Chu, "Achieving efficient poly(3,4-ethylenedioxythiophene)-based supercapacitors by controlling the polymerization kinetics," *Electrochim. Acta*, vol. 56, no. 20, pp. 7228–7234, 2011, doi: 10.1016/j.electacta.2011.03.044.

[115] Y. H. Ha, N. Nikolov, S. K. Pollack, J. Mastrangelo, B. D. Martin, and R. Shashidhar, "Towards a transparent, highly conductive poly (3,4-ethylenedioxythiophene)," *Adv. Funct. Mater.*, vol. 14, no. 6, pp. 615–622, 2004, doi: 10.1002/adfm.200305059.

[116] M. Fabretto, M. Müller, K. Zuber, and P. Murphy, "Influence of peg-ran-ppg surfactant on vapour phase polymerised PEDOT thin films," *Macromol. Rapid Commun.*, vol. 30, no. 21, pp. 1846–1851, 2009, doi: 10.1002/marc.200900371.

[117] M. Fabretto, M. Müller, C. Hall, P. Murphy, R. D. Short, and H. J. Griesser, "In-situ QCM-D analysis reveals four distinct stages during vapour phase polymerisation of PEDOT thin films," *Polymer (Guildf).*, vol. 51, no. 8, pp. 1737–1743, 2010, doi: 10.1016/j.polymer.2010.02.019.

[118] M. Fabretto, K. Zuber, C. Hall, and H. J. Griesser, "The role of water in the synthesis and performance of vapour phase polymerised PEDOT electrochromic devices," pp. 7871–7878, 2009, doi: 10.1039/b912324e.

[119] S. H. Lee, H. Park, W. Son, H. H. Choi, and J. H. Kim, "Novel solution-processable, dedoped semiconductors for application in thermoelectric devices," *J. Mater. Chem. A*, vol. 2, no. 33, pp. 13380–13387, 2014, doi: 10.1039/c4ta01839g.

[120] K. Zuber, M. Fabretto, C. Hall, and P. Murphy, "Improved PEDOT conductivity via suppression of crystallite formation in Fe(III) tosylate during vapor phase polymerization," *Macromol. Rapid Commun.*, vol. 29, no. 18, pp. 1503–1508, 2008, doi: 10.1002/marc.200800325.

[121] T. Park, C. Park, B. Kim, H. Shin, and E. Kim, "Flexible PEDOT electrodes with large thermoelectric power factors to generate electricity by the touch of fingertips," *Energy Environ. Sci.*, vol. 6, no. 3, p. 788, 2013, doi: 10.1039/c3ee23729j.

[122] D. Wu *et al.*, "Temperature dependent conductivity of vapor-phase polymerized

PEDOT films," *Synth. Met.*, vol. 176, pp. 86–91, 2013, doi: 10.1016/j.synthmet.2013.05.033.

[123] J. Wang, K. Cai, and S. Shen, "Enhanced thermoelectric properties of poly(3,4-ethylenedioxythiophene) thin films treated with H2SO4," *Org. Electron.*, vol. 15, no. 11, pp. 3087–3095, 2014, doi: 10.1016/j.orgel.2014.09.012.

[124] Z. U. Khan *et al.*, "Acido-basic control of the thermoelectric properties of poly(3,4-ethylenedioxythiophene)tosylate (PEDOT-Tos) thin films," *J. Mater. Chem. C*, vol. 3, no. 40, pp. 10616–10623, 2015, doi: 10.1039/c5tc01952d.

[125] H. Wang, U. Ail, R. Gabrielsson, M. Berggren, and X. Crispin, "Ionic Seebeck effect in conducting polymers," *Adv. Energy Mater.*, vol. 5, no. 11, 2015, doi: 10.1002/aenm.201500044.

[126] A. Weathers *et al.*, "Significant Electronic Thermal Transport in the Conducting Polymer Poly(3,4-ethylenedioxythiophene)," *Adv. Mater.*, vol. 27, no. 12, pp. 2101–2106, Mar. 2015, doi: 10.1002/adma.201404738.

[127] I. Petsagkourakis *et al.*, "Structurally-driven Enhancement of Thermoelectric Properties within thin Films," *Nat. Publ. Gr.*, no. July, pp. 1–8, 2016, doi: 10.1038/srep30501.

[128] J. Wang, K. Cai, H. Song, and S. Shen, "Simultaneously enhanced electrical conductivity and Seebeck coefficient in Poly (3,4-ethylenedioxythiophene) films treated with hydroiodic acid," *Synth. Met.*, vol. 220, pp. 585–590, 2016, doi: 10.1016/j.synthmet.2016.07.023.

[129] D. Mayevsky, E. Gann, C. J. Garvey, C. R. McNeill, and B. Winther-Jensen, "Decoupling order and conductivity in doped conducting polymers," *Phys. Chem. Chem. Phys.*, vol. 18, no. 28, pp. 19397–19404, 2016, doi: 10.1039/C6CP03307E.

[130] G. Rosati, L. Sappia, R. Madrid, and N. Rozlòsnik, "Iron (III) -Tosylate Doped PEDOT and PEG : A Nanoscale Conductivity Study of an Electrochemical System with Biosensing Applications," *Int. J. Biomed. Biol. Eng.*, vol. 11, no. 11, pp. 597–605, 2017.

[131] K. Wijeratne, M. Vagin, R. Brooke, and X. Crispin, "Poly(3,4-ethylenedioxythiophene)-tosylate (PEDOT-Tos) electrodes in thermogalvanic cells," *J. Mater. Chem. A*, vol. 5, no. 2, pp. 19619–19625, 2017, doi: 10.1039/C7TA04891B.

[132] L. Ouyang *et al.*, "The contraction of PEDOT films formed on a macromolecular liquid-like surface," *J. Mater. Chem. C*, vol. 6, no. 3, pp. 654–660, 2018, doi: 10.1039/C7TC04661H.

[133] E. H. Khan *et al.*, "Environment-Friendly Post-Treatment of PEDOT-Tos Films by Aqueous Vitamin C Solutions for Tuning of Thermoelectric Properties," vol. 47, no. 7, 2018, doi: 10.1007/s11664-018-6279-5.

[134] J. Wang, K. Cai, and S. Shen, "A facile chemical reduction approach for effectively tuning thermoelectric properties of PEDOT films," *Org. Electron.*, vol. 17, pp. 151–158, 2015, doi: 10.1016/j.orgel.2014.12.007.

[135] Z. U. Khan *et al.*, "Acido-basic control of the thermoelectric properties of poly(3,4-ethylenedioxythiophene)tosylate (PEDOT-Tos) thin films," *J. Mater. Chem. C*, vol. 3, no. 40, pp. 10616–10623, 2015, doi: 10.1039/C5TC01952D.

[136] J. Y. Kim, M. H. Kwon, Y. K. Min, S. Kwon, and D. W. Ihm, "Self-assembly and crystalline growth of poly(3,4-ethylenedioxythiophene) nanofilms," *Adv. Mater.*, vol. 19, no. 21, pp. 3501–3506, 2007, doi: 10.1002/adma.200602163.

[137] C. D. O'Connell, M. J. Higgins, H. Nakashima, S. E. Moulton, and G. G. Wallace, "Vapor phase polymerization of EDOT from submicrometer scale oxidant patterned by dip-pen nanolithography," *Langmuir*, vol. 28, no. 26, pp. 9953–9960, 2012, doi: 10.1021/la301724v.

[138] Y. H. Lee, J. Oh, S. S. Lee, H. Kim, and J. G. Son, "Highly Ordered Nanoconfinement Effect from Evaporation-Induced Self-Assembly of Block Copolymers on In Situ Polymerized PEDOT:Tos," *ACS Macro Lett.*, vol. 6, no. 4, pp. 386–392, 2017, doi: 10.1021/acsmacrolett.7b00137.

II. THIN FILMS PREPARATION AND ANALYSIS

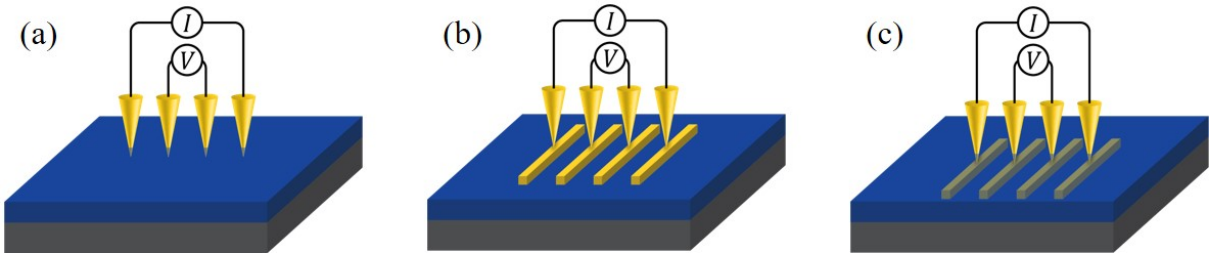

In this second chapter, the experimental processes used for the formation and characterization of PEDOT:Tos thin films will be described. In a first part, we focused on the preparation of PEDOT:Tos thin film by in-situ polymerization and vapor phase polymerization. In a second part, details on the characterization techniques used during this work are given with an emphasis on the spectroscopic characterization techniques. Finally, a study on how to measure accurately the electrical conductivity of PEDOT:Tos thin films is presented as several protocols are reported in the literature.

I- INTRODUCTION

The aim of this chapter is to present the experimental details carried during this Ph.D. The first part is dedicated to the preparation of PEDOT:Tos thin films using two synthetic pathways: in-situ polymerization (ISP) and vapor phase polymerization (VPP).

In the second part, we will focus on the methods to characterize the electronic transport and spectroscopic properties of PEDOT:Tos thin films. The electronic transport characterizations combine both the determination of the electrical conductivity and Seebeck coefficient. Concerning the spectroscopic characterizations, both X-ray photoelectron (XPS) and ultraviolet photoelectron (UPS) spectroscopies will be explained in order to relate the results of such measurements to the PEDOT:Tos electronic band structure.

In the third part, a study on electrical conductivity measurements is presented pointing out the effect of the substrate on the sheet resistance measurements while considering the effects of the probe configuration on the final result.

II- FORMATION OF PEDOT:TOS THIN FILMS

II-1- SUBSTRATE PREPARATION

Depending on the characterization techniques, different types of substrates were used in order to obtain consolidated results. For structural characterizations including atomic force microscopy (AFM), optical microscopy or X-ray diffraction (XRD), the substrates can be either glass or silicon as the nature of the substrate has no effect on the measurements. However, in order to study the thermoelectric properties, *i.e.* the Seebeck coefficient and the electrical conductivity, only the properties of the PEDOT:Tos film have to be probed, and glass substrates were chosen in order to avoid contributions arising from silicon substrates. Finally, for spectroscopic measurements, silicon permits to avoid charge accumulation on the surface of the film due to its intrinsic electronic transport properties.

The glass substrates used in this study are cover glasses (15×15 mm^2) commonly used for observations by optical microscopy. Silicon wafers, purchased from Sil'tronix, with different conductivity (intrinsic, n-doped and p-doped), have been also used through this study in order to probe the effect of Si-doping on the electronic properties of PEDOT:Tos films.

Metallic contacts were deposited with a metal evaporator, Lesker Mini Spectros, allowing us to deposit gold, silver, chromium or aluminum contacts by thermal evaporation. The crucible containing the metal is heated in order to evaporate the metal and it is noteworthy that the substrate temperature can reach more than 100°C using this technique. As a standard procedure, 10 nm of chromium and 100 nm of gold were sequentially deposited on clean glass or silicon substrates. It is noteworthy that all glass and silicon substrates used in this study were washed in ultrasonic baths of ethanol, isopropanol and acetone for 10 min per washing step.

II-2- PREPARATION OF THE FILMS

II-2-A- PREPARATION OF THE OXIDANT SOLUTION

The $Fe(Tos)_3$ oxidant solution at 40 wt% or 54 wt% in butanol was purchased from Heraus (Clevios CB40-V2 and CB54-V2). EDOT was purchased from TCI chemicals while butanol, pyridine and DMSO were purchased from Sigma Aldrich. All the chemicals were used as received without further purification. The oxidant solution was most frequently used at a concentration of 40 wt% [1]–[3]. The stock solution of 54 wt% was accordingly diluted in butanol in order to reach a concentration of 40 wt%. A high boiling point solvent, DMSO, and a weak base, pyridine, were commonly added to the oxidant solution at a volume fraction of 3 vt%. The formulations were then stirred for a minimum of 12 hours at room temperature and then store at 4°C until further use. It is noteworthy that the solution had to be used in the week after preparation because of a loss of properties due to the evaporation of pyridine [4].

N.B. In the following chapters, tosylate will refer to the Iron(III)Tosylate

II-2-B- PEDOT:TOS SYNTHESIS

All synthetic procedures PEDOT:Tos films were performed in a cleanroom environment at 22 ± 2°C.

- *In-situ polymerization*

In order to prepare PEDOT:Tos films using in-situ polymerization, the solutions of monomers and oxidants with additives were mixed and immediately deposited due to the fast kinetics of the polymerization. Indeed, after only ten minutes, the formation of PEDOT particles is visible inside the solution [5]. The EDOT and oxidant solutions were prepared taking into account that 2 moles of oxidants are needed to polymerize the system and 0.3 mole to dope it. This solution was then stirred for few seconds and then filtered through a 0.22 µm PTFE filter in order to remove all solid impurities. The filtered solution was deposited by spin-coating on a clean substrate (glass or silicon)

at a speed of 1500 RPM during 30 s. The as-prepared films were then placed on a hot plate during 15 min in order to accelerate the polymerization and to allow the formation of the PEDOT:Tos films. Such treatment is needed as $Fe(Tos)_3$ has a tendency to crystallize at room temperature. The last step is a rinsing step, in which the films are dipped during 5 min into three different baths, two of butanol and one of ethanol in order to remove excess of oxidants, EDOT and additives. Finally, the films are dried under an air flow. This process, depicted in Figure II 2, is based on previous processes developed in the laboratory [6].

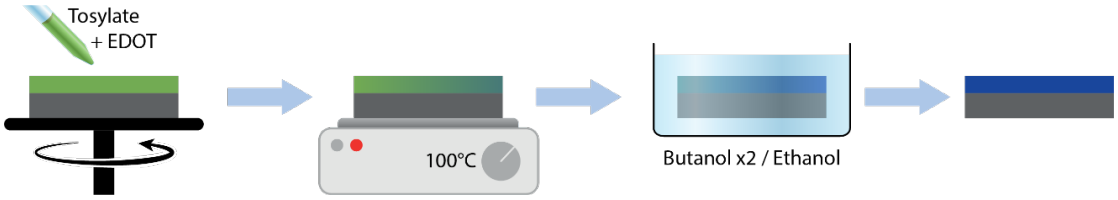

Figure II-1 Scheme of in-situ polymerization. Deposition of the solution of monomers with oxidants and additives, thermal activation of the polymerization, removing of the excess of products by rinsing steps.

- *Vapor phase polymerization*

The oxidant solution used in this case is the same than the one used previously. The various steps of the process are displayed Figure II 13 (a). The oxidant solutions containing the additives were filtrated with 0.22 µm PTFE filter and some drops of solution were then spin-coated on a substrate at 1500 RPM. The oxidant films were then deposited on a hot plate until the start of the VPP process, in order to avoid tosylate crystallization. The films were then suspended above EDOT droplets inside a homemade chamber as displayed in Figure II 13 (b). This container was placed on a hotplate and connected to a vacuum pump. All the temperatures discussed for the VPP processes are the temperature of the hotplate. It is noteworthy that, as the chamber is composed of thick glass, the temperature at the surface of the substrate is not the temperature displayed by the hotplate. Additionally, all VPP processes were performed under static vacuum. After the polymerization step, the films were placed on the hotplate during five minutes in order to evaporate remaining volatile species. The films were then rinsed in ethanol to remove any excess of oxidants, additives and EDOT, and dried with an air flow.

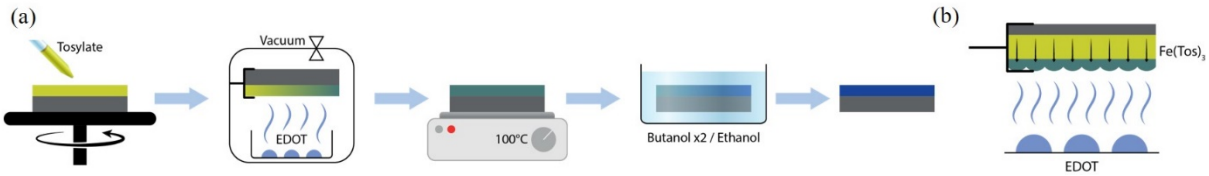

Figure II-2 (a) Steps of the VPP process (b) Growth of the film during VPP.

III- CHARACTERIZATIONS OF PEDOT:TOS FILMS

III-1- ELECTRONIC CHARACTERIZATIONS

III-1-A- ELECTRICAL CONDUCTIVITY

For in plane electrical conductivity measurements, films were made on 15×15 mm² glass substrates. The resistance of the films was measured by four-point probes measurement and by multiplying by the geometric factor, the sheet resistance was obtained. The parameters for the measurement of the resistance are described in Figure II-3.

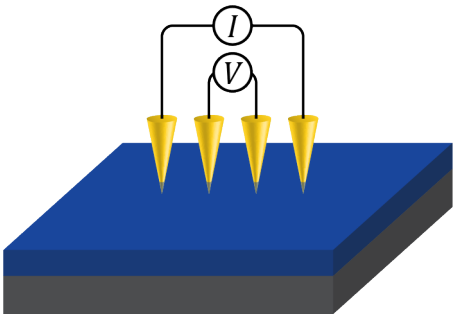

Probes gap	Material
1.6 mm	Tungsten
Radius	**Geometric factor**
40 µm	4.22

Figure II-3 Scheme of the 4-point probes techniques with characteristic parameters

The electrical conductivity is linked to the sheet resistance by the formula:

$$\sigma = \frac{1}{R_S \cdot t}$$ *Equation II-1*

where, R_S is the sheet resistance and t the thickness of the film. In order to calculate the conductivity, the thickness of the film was measured by scratching it and scanning through the scratch with a profilometer. For PEDOT:Tos thin films, the thickness varies between 30 and 300 nm depending on the deposition methods and conditions. The profile permits to deduce the thickness of the film. In order to have a better estimation of the electrical conductivity, three samples have been synthetized and three measurements were performed by sample. It allows us to deduce the standard deviations associated to the determination of the electrical conductivity.

III-1-B- SEEBECK COEFFICIENT

The configuration used for the Seebeck coefficient measurements is different than the one used for electrical conductivity. The PEDOT:Tos films were formed on rectangular glass substrates coated with gold contacts (100 nm thick) according with our homemade set-up configuration, as shown in Figure II-4. The gold contacts allow one to reduce the contact resistance between the probes and the sample while the glass substrate was chosen especially due to its insulator properties but also it allows a quick transfer of heat to the polymer leading to a fast thermal equilibration. The design of the sample is elongated in order to have larger contacts with the Peltier plates which control the temperature gradient but also in order to have longer current lines and thus a better estimation of the Seebeck coefficient [7].

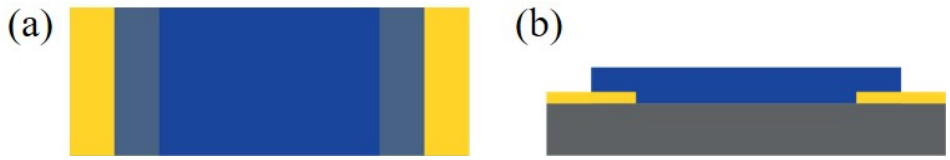

Figure II-4 Seebeck device, PEDOT:Tos is coated on top of gold electrodes (a) Top view (b) Side view.

The temperature gradient was induced with two Peltier plates, monitored by two temperature controllers and recorded by two Teflon-insulated copper/constantan thermocouples (OMEGA) attached to the gold contacts with a droplet of silver conductive paint (RS PRO). Thermal contacts between the sample and the Peltier plates were ensured using high thermal conductivity paste (OMEGATHERM 201). The thermoelectric voltage was measured at the same point, i.e. on the silver paint droplet, with two tungsten pins connected to a nano-voltmeter (Keithley) [8]. As PEDOT:Tos thermoelectric properties are highly interesting for room temperature applications; one side was kept at 22°C and the other one was slightly heated until it reaches 27°C. The Seebeck coefficient was calculated by measuring thermoelectric voltage ΔV for different temperature gradients and fitting with a straight-line $S = \Delta V/\Delta T$.

III-2- SPECTROSCOPIC CHARACTERIZATIONS

The spectroscopic characterizations have been performed on an ultra-high vacuum system build by SPECS. The apparatus, connected to glove boxes permits to transfer the samples for measurements under a controlled atmosphere. For our experiments, we used a load lock which allows to load the samples inside the vacuum line. The pressure inside the transfer line is about 10-10 mbar. The Phoibos hemispherical electron analyzer (100 mm diameter) is preceded by lenses which permit to sort the photoelectrons by energy and avoid damages of the analyzer. The size of the slit can be set up manually depending on the experiment. UPS measurements were performed before XPS ones because the energy applied to the sample is less important and do not lead to a modification of the surface properties.

III-2-A- XPS

Thin film samples for XPS experiments were prepared on n-doped silicon substrate (40 $S.cm^{-1}$) to avoid charge accumulation on the surface of the film which can disturb the XPS signal and alter the resulting spectrum. After preparation, the films were stored in a glove box until XPS measurements in order to avoid / reduce any surface modification like water absorption. XPS was performed under ultra-high vacuum (UHV) and X-rays were produced by a monochromatic aluminum anode (Al Kα) with an energy of 1486.6 eV. The X-ray source was set to deliver a power of 200 W (12 V at 16.5 A). During the experiment, the pressure inside the chamber was around 5×10^{-9} mbar. The data were fitted with the CasaXPS software.

As XPS is a surface technique, we probed only a few nanometers in depth from the sample surface. We then assumed that such penetration depth is representative of the overall sample composition. The energy scanning from 0 eV to 1300 eV, so-called survey scan, permits to attest the presence of elements in the sample. As displayed in Figure II-5, three characteristic peaks of PEDOT:Tos appear on a typical XPS spectrum. The first one corresponds to the 1s orbital of oxygen and appears around 531 eV. The second one is linked to the 1s orbital of carbon and appears at 285 eV. Finally, two sulfur orbitals appear around 229 eV and 165.5 eV for the 2s and 2p,

respectively. Oxygen, carbon and sulfur atoms are present in PEDOT but also in tosylate. In order to quantify the presence of each element, XPS scans targeted on each element have been performed. By this method, the contributions from PEDOT and tosylate can be separated. We focused here on the S2p orbital to quantify the number of tosylate per PEDOT repeating unit leading subsequently to the doping level as the sulfur signal takes into account the contributions from tosylate and PEDOT.

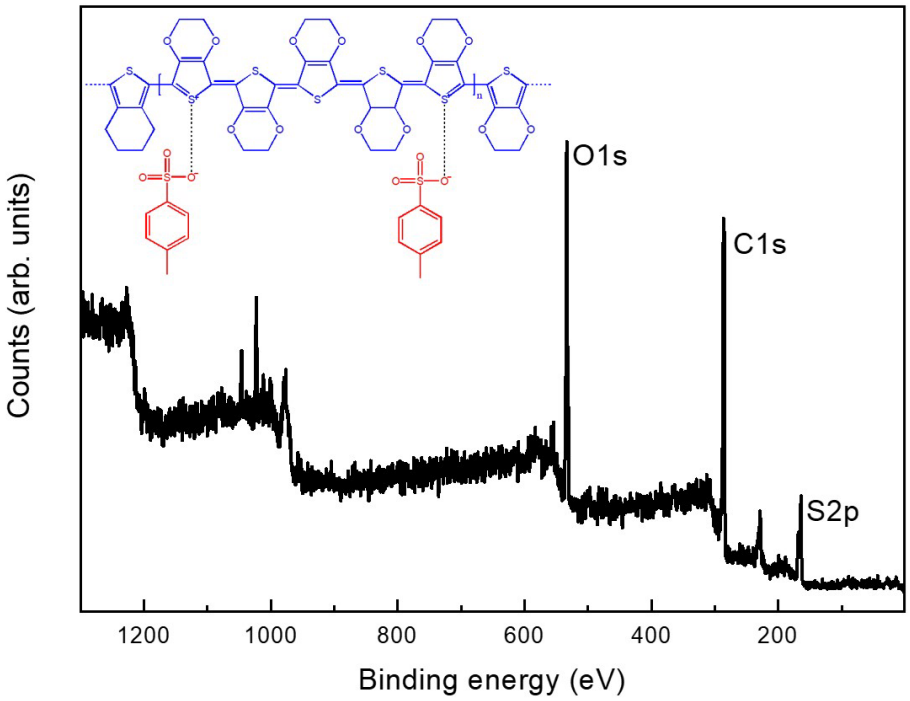

Figure II-5 Survey spectrum of in-situ polymerized PEDOT:Tos film. The characteristic peaks of PEDOT:Tos are labelled with in inset the chemical structure of the PEDOT:Tos complex.

XPS measurements allow one to have access to the oxidation level by calculating the ratio between the areas related to the contributions of tosylate and the total sulfur contributions [9]:

$$Oxidation\ level = \frac{\sum Areas_{reacted\ Tosylate}}{\sum Areas_{Thiophene}} \qquad \textit{Equation II-2}$$

This calculation leads to disagreements in the community because the fitting of S2p data are not performed in the same way. In the first case, researchers take into account one doublet corresponding to the binding of S with C in the thiophene unit

(PEDOT) and another doublet corresponding to the binding of S with O in tosylate. The fitting of the PEDOT contributions (thiophene unit) is done by an asymmetric tail which takes also into account the PEDOT+ sites, i.e. the localized charges on the PEDOT structure [10]. In our case, based on previous studies, we took into account these PEDOT+ sites and we deconvoluated the contributions of S-O bonds in the tosylate unit into two doublets, as some unreacted tosylate remains in the film, as shown in Figure II-6. To summarize, even if some researchers use two doublets to fit the S2p peak, we decided to use four doublets representing PEDOT, $PEDOT^+$, Tos and Tos^-. As polymers are considered as highly amorphous materials, Gaussian or Gaussian-Lorentzian (90:10) were used for the fitting of the various contributions [11]. The oxidation level can also be determined by taking into account the contributions of PEDOT and tosylate from O1s peak even if this methodology is less accurate [12].

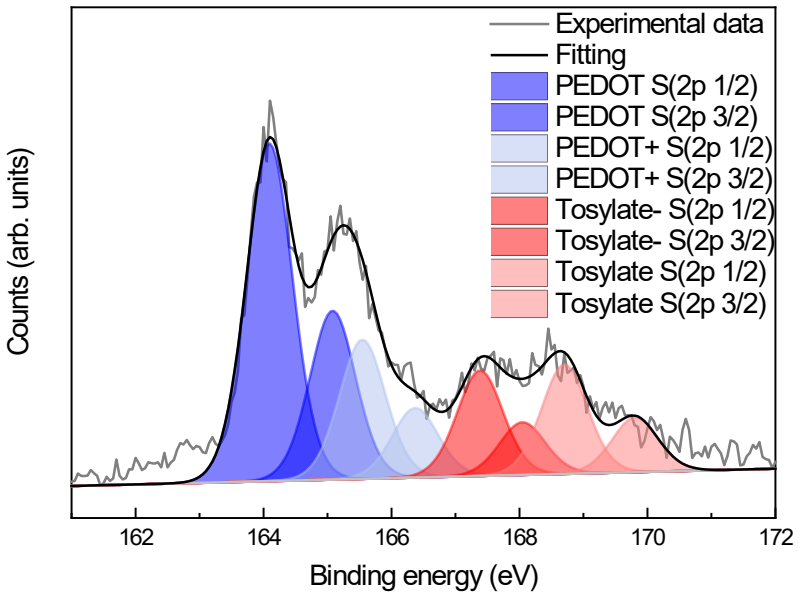

Figure II-6 XPS S2p spectrum of in-situ polymerizedPEDOT:Tos film. Blue and red areas represent the signals linked to S2p in PEDOT and tosylate, respectively.

III-2-B- UPS

UV photoelectron spectroscopy (UPS) can probe the occupied states of the valence band of thin film. The sample is irradiated with UV photons produced by a helium plasma discharge lamp. That source generated a mixture of He I and He II ions with respective energy of 21.22 eV and 40.81 eV. By tuning the pressure of the plasma, one

can modify the ratio of He I / He II. While the UV source works at a pressure level of 10^{-2} mbar, the analysis chamber is maintained to a lower pressure level of 10^{-7} mbar thanks to a dedicated 2 stages differential pumping.

Under irradiation, the sample ejects many photoelectrons in all directions and with all possible kinetic energies up to a maximum (equal to the energy source). A part of these photoelectrons are collected by a column lens system placed just above the sample (working distance of 4 mm) then enter into a hemispherical analyzer which selects (filter out) them in terms of kinetic energy. Finally, only the selected photoelectrons can reach the detector which counts the number of hits.

By scanning the kinetic energy with the analyzer and measuring the intensity in terms of counts for a certain period of time with the detector, we get a spectrum of counts versus kinetic energy.

Knowing the photons energy and measuring the kinetic energy of the photoelectrons allows one to obtain the binding energy (E_B) of the emitted photoelectrons from the following equation:

$$E_{kin} = h\nu - E_B \qquad \textit{Equation II-3}$$

where $h\nu$ is the energy source (21.22 eV in our case).

By convention, E_B = 0 eV corresponds to the energy at the Fermi level (E_F). An UPS spectrum gives an image of the density of states (DoS) of the valence band in the vicinity of the Fermi level and some relevant features can be assigned to the electronic structures of the material under study.

Moreover, the energy levels of the material are extracted from the spectrum as displayed in Figure II-6. The red curve corresponds to a typical UPS spectrum of a semiconductor. At the low kinetic energies (left part) the large background signal is due to inelastically scattered photoelectrons. In fact, the generated photoelectrons can lose energy through scattering processes on their way from their original depth up to the sample surface. The deeper is their origin, the more scattered they are, and the lower is their kinetic energy when they go out of the surface sample. The mean

free path length (λ) depends on the initial kinetic energy. With the initial incident energy of 21.22 eV, λ is about 10 Å. Hence, only photoelectrons travelling 3λ maximum (3 nm) can be emitted. This is why UPS is a very surface sensitive technic.

At the lowest kinetic energy, the abrupt drop is called the secondary electron cut-off. On the other side, close to E_F, at the higher kinetic energy (lower binding energy) is the HOMO level.
The ionization potential (IP) - the energy needed to extract an electron from the HOMO up to the vacuum level – is estimated by subtracting the spectrum width (HOMO – secondary electron cut-off) to the photon energy.

For metal, there is no band gap, then the Fermi level and HOMO are identical. In that case, IP is the same as the work function (usually abbreviated by WF or Φ).

For a semiconductor, WF and IP differ since the Fermi level is now located inside the band gap. The work function is then calculated as followed:

$$\Phi = IP - E_{HOMO} \qquad \textit{Equation II-4}$$

where E_{HOMO} is the energy of the HOMO level.

Practically a bias voltage of -4V was applied to improve photoelectrons extraction/emission. This in turn shifted all the spectrum to higher kinetic energies. Later - during data treatment - when spectra are shift corrected (as if the sample was not biased) the work function can be directly estimated from the plot of the spectrum in kinetic energy by reading the abscissa value after linearly fitting the secondary electron cut-off. This particular procedure has been chosen during this work and all the displayed UPS spectra are expressed versus kinetic energy in order to determine the work function.

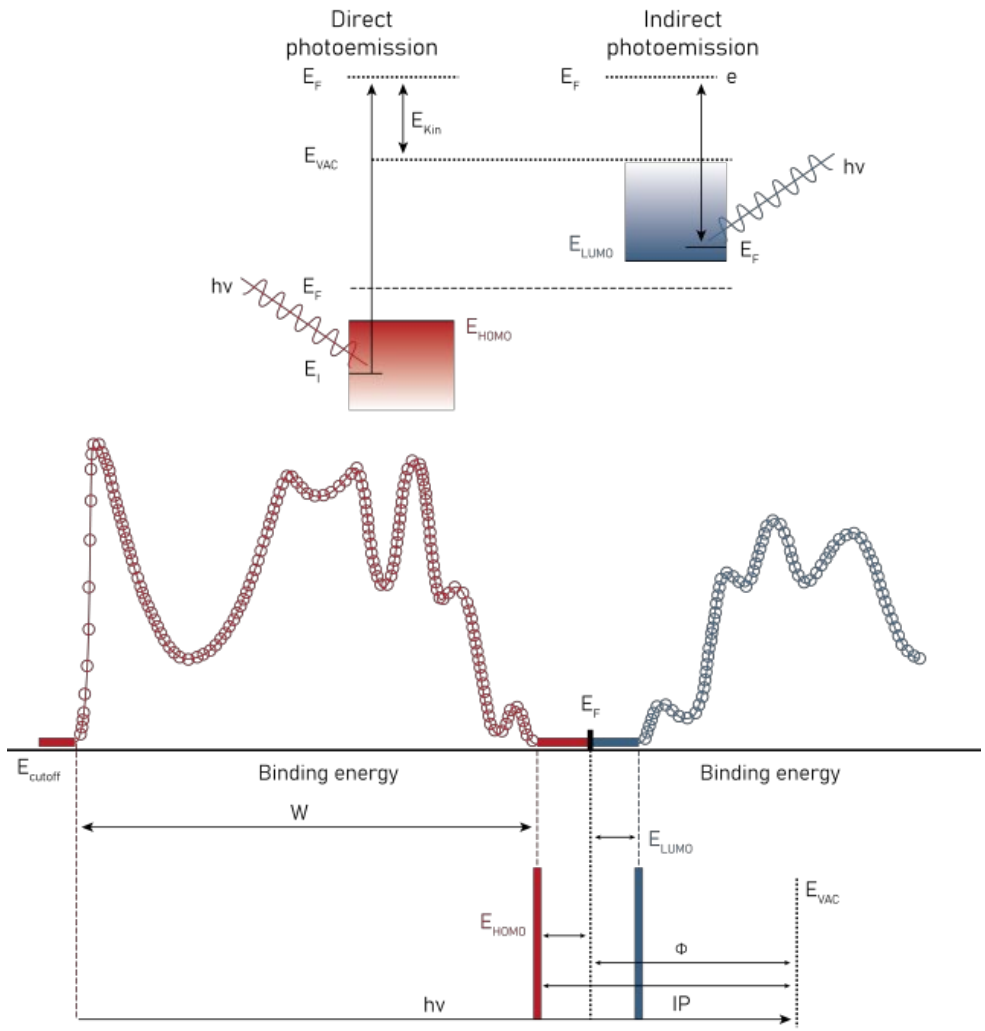

Figure II-7 Principles of direct (UPS) and indirect (IPES) photoemission spectroscopies, with the corresponding spectra in red and blue respectively. E_{VAC} corresponds to the energy of an electron outside the material, IP represents the ionization potential, $E_{cut-off}$ is the cut-off energy, hv the energy source and Φ the WF.

In the middle range of kinetic energies, the DoS of the sample appears. The shape of the DoS is a characteristic of the electronic arrangement within the material. At low-binding energy, the electron density contributes to the conduction within the material [13]. Moreover, the DoS around the Fermi level gives information about the electronic nature of the material (metal, semi-metal, semi-conductor, insulator). From this region, the HOMO level of the material can also be deduced by the intersection of two lines coming from the first peak near the Fermi level (π-band edge associated with HOMO level) and the base line of the spectrum. Moreover, to access to the LUMO and probe the unoccupied states, one can use the inverse photoelectron spectroscopy (IPES) as shown in Figure II-6 (blue curve) [14]. Finally, combining UPS and IPES gives access to the electronic band gap of the material.

III-3- STRUCTURAL CHARACTERIZATION

III-3-A- MICROSCOPIC ASPECT

In order to probe the surface morphology of PEDOT:Tos films, optical microscopy and atomic force microscopy were used. For optical microscopy, a Nikon Optiphot 88 was used equipped with a Nikon camera DS-Fi1 to record the images on the computer. For each sample, the images were recorded with magnification of 2.5 and 20.

Atomic force microscopy was performed using a Dimension FastScan AFM (Bruker) in tapping mode equipped with silicon cantilevers (Fastscan-A) of a typical tip radius of ≈ 5 nm. The resonance frequency of the cantilevers was ≈ 1.25 kHz. The root mean square roughness *Rq* were estimated on 4 µm² surfaces using Gwyddion software. The high resolution current mapping images were recorded simultaneously using Peak Force Tunneling AFM (PF-TUNA, Bruker) under 1 $nA.V^{-1}$ and a DC voltage bias of 2 V.

III-3-B- GIXRD

Grazing Incident X-ray Diffraction (GIXRD) data were recorded at room temperature in air on a Bruker D8 Discovery diffractometer with Cu Kα radiation equipped with a LynxEye detector in θ-2θ mode with a grazing incident angle of 0.6° and divergence slit of 0.05 mm. Diffraction profiles of films deposited on intrinsic silicon substrates were fitted with the help of X'Pert HighScore Plus software (PANalytical B. V.). Regarding the large width of diffraction peak of nanocrystals in amorphous matrix, the diffractometer sharp contribution was neglected during the analysis.

Silicon was used for GIXRD because it is a well-known material in crystallography and signals coming from the substrate can then be identified and not taken into account during the data treatment.

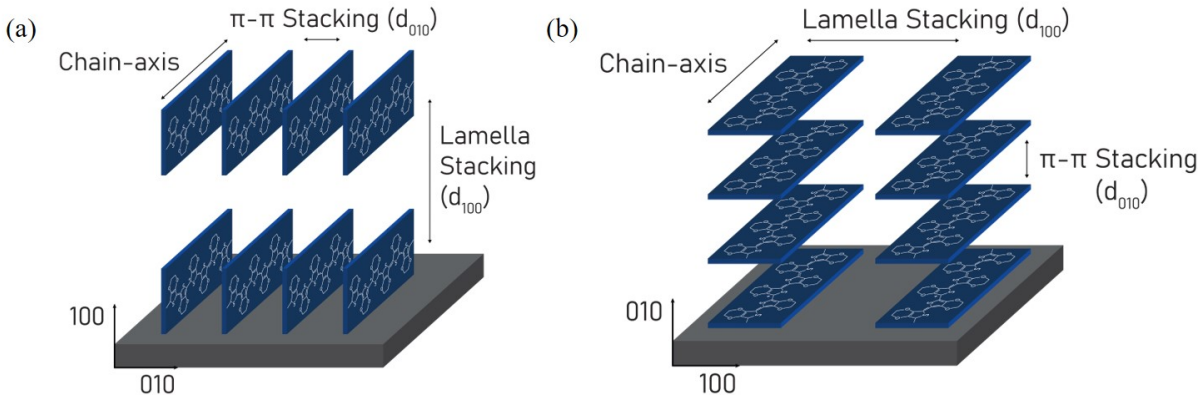

Figure II-8 (a) Edge-on orientation of PEDOT crystallites. (b) Face-on orientation of PEDOT crystallites. Characteristic distances which can be obtained by XRD measurements are labelled.

Based on the Bragg formula, it is possible to calculate the distance between crystallographic plans:

$$2d_{hkl} \cdot \sin(2\theta) = p \cdot \lambda \qquad \textit{Equation II-5}$$

where d_{hkl} is the interplanar distance, 2θ is the angle which can be read on the spectrum in radian, p is the diffraction order and λ the wavelength of X-rays (here copper anode: λ = 1.5406 Å).

According to Bragg's law, the peaks position is related to the inter-plan distances. Therefore, it is possible to estimate the lamellae ($d_{lamellae}$) and the π-π ($d_{\pi-\pi}$) stacking distances from the [h00] and [020] plan sets respectively.

IV- ELECTRICAL CONDUCTIVITY MEASUREMENTS: EFFECTS OF THE SUBSTRATE

IV-1- EFFECT OF THE NATURE OF THE SUBSTRATE

For electrical conductivity measurements, the substrate has to show insulating properties in order to exclude any contributions from it. In our case, we decided to use two types of substrates, glass and intrinsic silicon.

In order to verify that the substrate does not affect the measurement of the electrical conductivity in a thin film configuration, PEDOT:Tos films were deposited by in-situ polymerization. Three samples have been synthetized for each substrate (intrinsic silicon and glass), based on 40 wt% oxidant solution. For each sample, three measurements of the resistance have been done with a 4-point probes apparatus. In the same way, three thickness measurements have been done on each films in order to have a proper estimation. Based on the formula explained above, Equation II-1, the electrical conductivities have been calculated for each substrate and the results are displayed in Figure II-9.

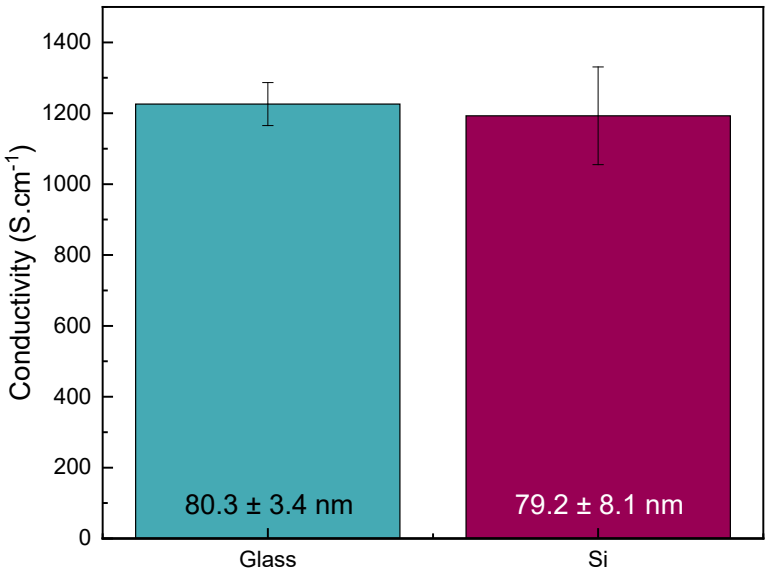

Figure II-9 Electrical conductivity of PEDOT:Tos films made by in-situ polymerization on glass (blue) and intrinsic silicon (purple). Thicknesses are given for each substrate.

The electrical conductivity is 1226 ± 60 and 1193 ± 138 $S.cm^{-1}$ for PEDOT:Tos films synthetized on glass and intrinsic silicon substrate, respectively. The value of the electrical conductivity is thus not affect by the substrate on which the film is deposited. Consequently, we assume that synthetize PEDOT:Tos films on glass or intrinsic silicon substrates leads to films with the same electrical properties.

IV-2- Effect of the configuration on electrical conductivity

For the previous measurements, the electrical conductivity was probed directly on PEDOT:Tos films. As polymers are soft matter, the probes are able to cross the film until the substrate. Besides, PEDOT:Tos shows an important surface roughness leading to a high contact resistance between the probes and the film. Accordingly, it is mandatory to question the resistance value extracted from 4-point probes measurements.

Accordingly, PEDOT:Tos films were made by VPP with three different samples configurations, as displayed in Figure II-10. The first measurement was performed by directly probing the resistance of the film. The second measurement consisted of depositing metallic contacts on top of PEDOT:Tos films, taking into account the configuration of the 4-points probes apparatus. In the last configuration, the metallic contacts were deposited prior to the PEDOT:Tos film deposition on top of the substrate.

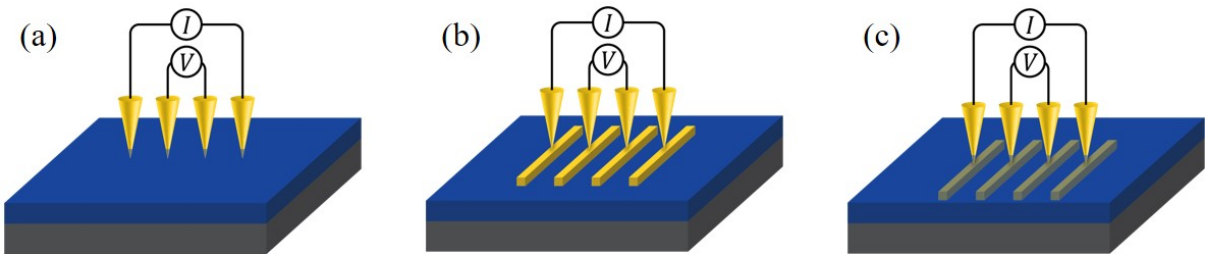

Figure II-10 (a) Measurement of film conductivity with 4-points probes (b) Measurement with contacts on top of the film (c) Measurement with contacts on top of the substrate.

Additionally, by depositing metallic contacts by thermal evaporation, PEDOT:Tos films are subjected to elevated temperatures. Indeed, temperature can sometimes reach more than 100°C during the process which is more than the temperature for the

polymerization. Besides, gold and silver have been deposited on two set of samples to compare the effect or not of the metal.

- *Contacts on top of the sample*

In order to analyze the effect of the sample configuration on the electrical conductivity, three samples were made and the thickness of each samples was measured using a profilometer. The electrical conductivity data (blue histogram) recorded directly on the PEDOT:Tos sample are displayed in Figure II-11. Afterwards, gold contacts were deposited via thermal evaporation following the configuration explained before. The sheet resistance of each film was once again measured by probing at three different positions on the contacts. The results are displayed in Figure II-11 (green histogram). Without contact, the electrical conductivity of PEDOT:Tos film made by VPP and based on 40 wt% oxidant solution is 665 ± 52 $S.cm^{-1}$, while this value is 3 times higher using gold contacts with an electrical conductivity of 1999 ± 89 $S.cm^{-1}$. The gold contacts permit to reduce the contact resistance between the polymer film and the probes of the apparatus [15] leading to a more accurate determination of the electrical conductivity of the film.

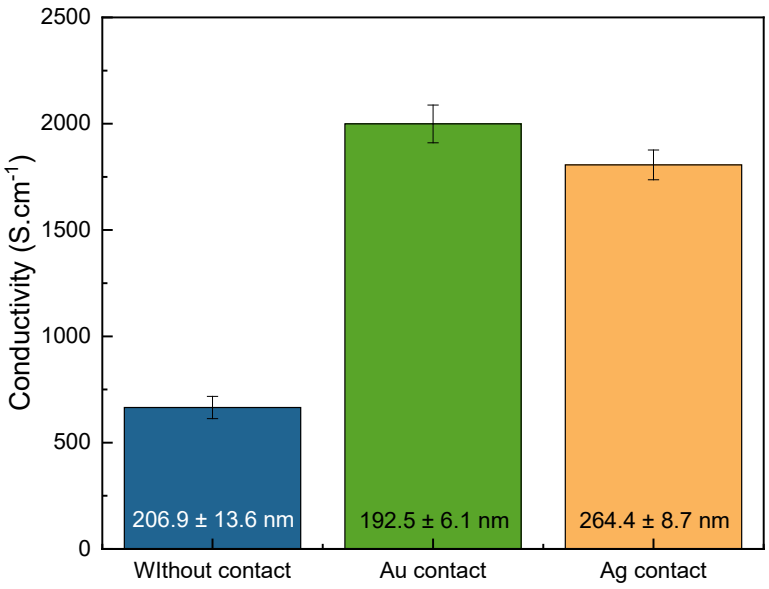

Figure II-11 Electrical conductivity of PEDOT:Tos films made by VPP without (blue), with gold contacts (green) and with silver contacts (yellow) on top of the film. Thicknesses are given for each type of metallic contacts.

In order to discriminate the effect of the contacts, the same procedure was performed replacing Au by Ag contacts. The choice of metals is due to the ease of deposition of these two compounds using our evaporator set-up but also because they do not have exactly the same electrical conductivity (4.11×10^5 S.cm^{-1} for Au against 6.30×10^5 S.cm^{-1} for Ag). The results are displayed in Figure II-11. The electrical conductivity probed using Ag contact is of the same order than the one obtained with Au contacts.
We had also to consider a modification of the electrical conductivity due to the thermal evaporation procedure which induces a thermal annealing of the PEDOT:Tos film. Moreover, the deposition of metallic contacts on top of the film can lead to a metallic diffusion inside the PEDOT:Tos film and thus alters the probed electrical conductivity.

- *Contacts on top of the substrate*

Even if it has been suggested that, PEDOT:Tos is not affected for temperatures below 100°C, we determined the electrical conductivity of PEDOT:Tos layer using contacts directly deposited on the substrate before the deposition of the PEDOT:Tos film. Accordingly, Au contacts were thermally deposited through the mask designed for 4-points probes directly on intrinsic silicon. PEDOT:Tos thin films were subsequently deposited on top of the substrate coated with the gold contacts. Three measurements have been done using this new configuration. The results were compared with the previous ones and are displayed in Figure II-12.

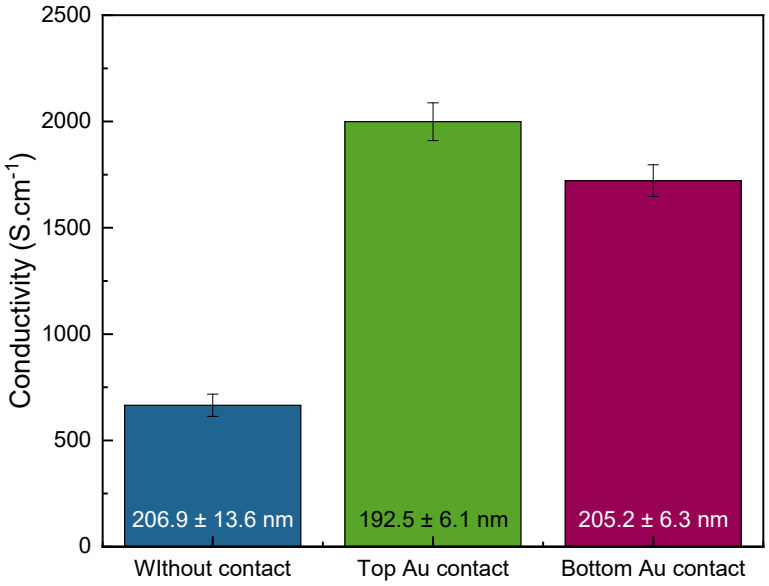

Figure II-12 Electrical conductivity of PEDOT:Tos films made by VPP without contact (blue), with gold contacts (green) on top of the film and with gold contacts on top of the substrate (purple). Thicknesses are given for each position of contacts.

The deposition of Au contacts directly on the substrate leads to an electrical conductivity of 1722 ± 75 $S.cm^{-1}$ which is of the same order than the one determined with Au contacts on top of the film. Thus, in this work, we decided to deposit the metallic contacts directly on the substrate in order to evaluate the electrical conductivity of the different samples.

In summary, the methodology to evaluate the electrical conductivity has to be taken into account in order to obtain consolidated results between the different polymerization processes. Besides, it was demonstrated that the deposition of metallic contacts is mandatory in order to properly evaluate the sheet resistance of PEDOT:Tos films due to a drastic decrease of the contact resistance between the probes of the apparatus and the polymer film.

[1] I. Petsagkourakis *et al.*, "Correlating the Seebeck coefficient of thermoelectric polymer thin films to their charge transport mechanism," *Org. Electron. physics, Mater. Appl.*, vol. 52, no. November 2017, pp. 335–341, 2018, doi: 10.1016/j.orgel.2017.11.018.

[2] T. Park, C. Park, B. Kim, H. Shin, and E. Kim, "Flexible PEDOT electrodes with large thermoelectric power factors to generate electricity by the touch of fingertips," *Energy Environ. Sci.*, vol. 6, no. 3, p. 788, 2013, doi: 10.1039/c3ee23729j.

[3] Z. U. Khan *et al.*, "Acido-basic control of the thermoelectric properties of poly(3,4-ethylenedioxythiophene)tosylate (PEDOT-Tos) thin films," *J. Mater. Chem. C*, vol. 3, no. 40, pp. 10616–10623, 2015, doi: 10.1039/c5tc01952d.

[4] B. Winther-Jensen, D. W. Breiby, and K. West, "Base inhibited oxidative polymerization of 3,4-ethylenedioxythiophene with iron(III)tosylate," *Synth. Met.*, vol. 152, no. 1–3, pp. 1–4, 2005, doi: 10.1016/j.synthmet.2005.07.085.

[5] B. Winther-Jensen and K. West, "Vapor-phase polymerization of 3,4-ethylenedioxythiophene: A route to highly conducting polymer surface layers," *Macromolecules*, vol. 37, no. 12, pp. 4538–4543, 2004, doi: 10.1021/ma049864l.

[6] I. Petsagkourakis *et al.*, "Structurally-driven enhancement of thermoelectric properties within poly(3,4-ethylenedioxythiophene) thin films," *Sci. Rep.*, vol. 6, no. March, pp. 1–8, 2016, doi: 10.1038/srep30501.

[7] S. Van Reenen and M. Kemerink, "Correcting for contact geometry in Seebeck coefficient measurements of thin film devices," *Org. Electron.*, vol. 15, no. 10, pp. 2250–2255, 2014, doi: 10.1016/j.orgel.2014.06.018.

[8] Q. Wei, M. Mukaida, K. Kirihara, Y. Naitoh, and T. Ishida, "Recent Progress on PEDOT-Based Thermoelectric Materials," vol. 8, pp. 732–750, 2015, doi: 10.3390/ma8020732.

[9] M. Fabretto, K. Zuber, C. Hall, and H. J. Griesser, "The role of water in the synthesis and performance of vapour phase polymerised PEDOT electrochromic devices," pp. 7871–7878, 2009, doi: 10.1039/b912324e.

[10] G. Greczynski, T. Kugler, and W. R. Salaneck, "Characterization of the PEDOT-PSS system by means of X-ray and ultraviolet photoelectron spectroscopy," *Thin Solid Films*, vol. 354, pp. 129–135, 1999.

[11] V. Jain, M. C. Biesinger, and M. R. Linford, "The Gaussian-Lorentzian Sum, Product, and Convolution (Voigt) functions in the context of peak fitting X-ray photoelectron spectroscopy (XPS) narrow scans," *Appl. Surf. Sci.*, vol. 447, pp. 548–553, 2018, doi: 10.1016/j.apsusc.2018.03.190.

[12] M. Fabretto, C. Jariego-moncunill, J. Autere, A. Michelmore, R. D. Short, and P. Murphy, "High conductivity PEDOT resulting from glycol / oxidant complex and glycol / polymer intercalation during vacuum vapour phase polymerisation," *Polymer (Guildf).*, vol. 52, no. 8, pp. 1725–1730, 2011, doi: 10.1016/j.polymer.2011.02.028.

[13] A. Sharma *et al.*, "Insights into the Oxidant / Polymer Interfacial Growth of Vapor Phase Polymerized PEDOT Thin Films," vol. 1800594, pp. 1–8, 2018, doi: 10.1002/admi.201800594.

[14] A. Kahn, "Fermi level, work function and vacuum level," *Mater. Horizons*, vol. 3, no. 1, pp. 7–10, 2016, doi: 10.1039/c5mh00160a.

[15] G.-H. Kim, L. Shao, K. Zhang, and K. P. Pipe, "Engineered doping of organic semiconductors for enhanced thermoelectric efficiency," *Nat. Mater.*, vol. 12, no. 8, pp. 719–723, 2013, doi: 10.1038/nmat3635.

III. INTERPLAY BETWEEN PEDOT:TOS POLYMERIZATION ROUTES AND ELECTRONIC CHARACTERISTICS

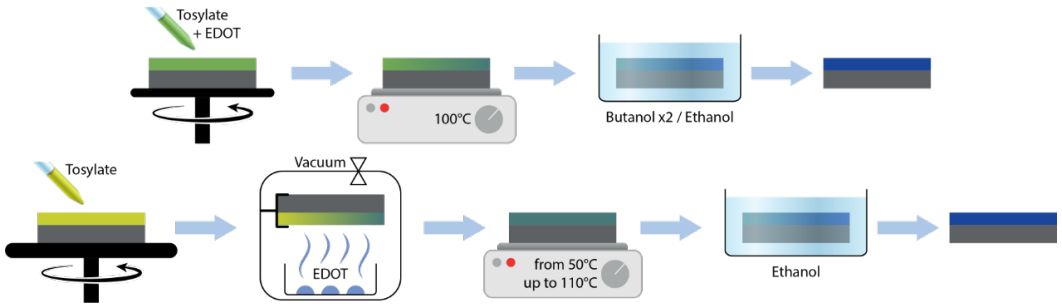

The polymerization of PEDOT:Tos can be performed by several methods but the most studied are in-situ and vapor phase polymerizations as they afford the formation of macroscopically homogenous films exhibiting high electrical conductivity. In this chapter, we will focus on the thermoelectric and morphological properties of PEDOT:Tos thin films synthetized through these two processes in order to decipher the relationships between the polymerization routes and their electronic properties.

I- INTRODUCTION

PEDOT has been studied for more than twenty years due to its exceptional electronic properties and especially in the form of PEDOT:PSS dispersions inherent to its good processability. Nevertheless, PEDOT can be doped with other small counter ions like $FeCl_3$, PF_6 or tosylate. We focused our attention on the tosylate form because PEDOT:Tos is highly interesting due to its high conductivity, around 1000 $S.cm^{-1}$, as regards to other organic materials. Accordingly, it appears as a promising material for thermoelectric applications as a high power factor could be expected.

PEDOT:Tos can be processed following three different routes which are in-situ chemical polymerization (ISP), Figure III-1 (a), vapor phase polymerization (VPP), Figure III-1 (b) and electropolymerization, Figure III-1 (c). In-situ polymerization is the oldest and simplest route to produce PEDOT:Tos films. The polymerization is initiated by the mixing and deposition of EDOT monomers and oxidant on a substrate. Leeuw *et al.* first developed this technique to generate PEDOT:Tos films with a conductivity of 300 $S.cm^{-1}$ [1]. In-situ polymerization has been subsequently used by a large number of research teams in order to enhance the electronic properties of the resulting materials with important applications in organic electronics. Focusing on thermoelectric applications, it has been shown that the formulation of the oxidant solution with additives can substantially increase the thermopower. For instance, using pyridine and PEG-*b*-PPG-*b*-PEG, Park *et al.* reached a conductivity of 1355 $S.cm^{-1}$ for PEDOT:Tos films [2]. At the best of our knowledge, this value is the highest reported for in-situ polymerized PEDOT:Tos films without further modifications or treatments.

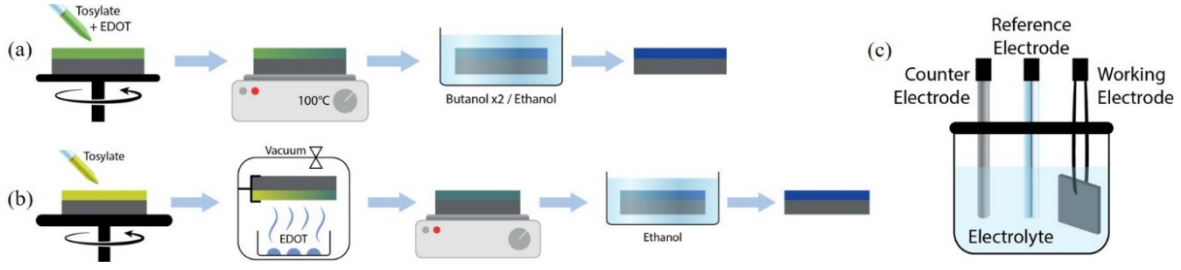

Figure III-1 Polymerization routes for the formation of PEDOT:Tos films(a) In-situ polymerization (b) Vapor phase polymerization (c) Electropolymerization.

In 2004, Winther-Jensen and coll. developed a novel route to synthetize PEDOT:Tos film: vapor phase polymerization, Figure III-1 (b) [3]. They based their study on the works of Mohammadi *et al.* who polymerized polypyrrole using $FeCl_3$ or H_2O_2 as oxidants with a chemical vapor deposition (CVD) process [4]. This technique consists of exposing $Fe(Tos)_3$ oxidant to EDOT vapors which induces a polymerization reaction. In practice, the oxidant is deposited by spin-coating on a substrate and then the sample is placed in a closed container with a jar containing EDOT monomers. Many parameters can then be tuned such as the temperature, the pressure, the oxidant concentration, and the additives. By optimizing all these parameters, VPP leads to highly conductive PEDOT:Tos films with conductivity as high as 3305 $S.cm^{-1}$ [5].

The last technique used to form PEDOT films is electropolymerization, as displayed in Figure III-1 (c). This technique was developed in 1988 by BAYER AG [6]. The polymerization takes place on a conductive substrate which is used as a working electrode. Two other electrodes, i.e. the counter electrode and the reference electrode, help with the transfer of charges inside an electrolyte solution. The electrolyte contains either positive and negative charges and various electrolytes can be used for the electropolymerization of PEDOT such as tetrabutylammonium perchlorate ($TBAClO_4$) [7], [8], tetra-n-butylammonium tetrafluoroborate ($TBABF_4$), lithium perchlorate ($LiClO_4$), and lithium tetrafluoroborate ($LiBF_4$) [8]. Yamato *et al.* further refined PEDOT electropolymerization in order to obtain free standing films which can be electrically characterized [9]. Tosylate can also be used to electropolymerize EDOT using Bu_4NTos as oxidant [10]. Electropolymerized PEDOT films can reach conductivity up to 2074 $S.cm^{-1}$ [11].
In the following parts, we will focus our attention on the two mains polymerization techniques: in-situ and VPP. These techniques are well-established to form PEDOT films but we still lack a deep understanding of the relationships between the experimental parameters and the resulting thermoelectric properties. The comparison between ISP and VPP will thus focused on the interdependence between the electrical, morphological and thermoelectric properties.

II- IN-SITU POLYMERIZATION

The in-situ polymerization or chemical polymerization is the most common route for the formation of PEDOT:Tos films [12]–[14]. In-situ polymerization consists of mixing EDOT monomers, $Fe(Tos)_3$ as oxidant and additives followed by their deposition to form conductive PEDOT films.

II-1- SYNTHESIS OF PEDOT:TOS AND STRUCTURAL PROPERTIES

II-1-A- PEDOT:TOS SYNTHESIS

- *Films preparation*

An oxidant solution of 40 wt% of tosylate in butanol with pyridine and DMSO was used for this study. A day after the preparation of the oxidant solution, PEDOT:Tos films were deposited by spin-coating using ISP process (explained in the previous chapter) on glass substrate (for electrical measurements) and silicon substrate (for spectroscopic and microscopic measurements). After preparation, the films were stored in a glove box until spectroscopic measurements in order to avoid any surface modification like water absorption.

- *Evaluation of the doping*

In order to evaluate the doping of PEDOT by tosylate, XPS measurements were performed. PEDOT:Tos films were prepared on conducting silicon to avoid charge accumulation on the surface of the film which can disturb the XPS signal and alter the resulting spectra. In order to quantify the presence of each element, XPS scans targeted on each element have been performed. By this method, contributions from PEDOT and tosylate can be separated. We focused here on the S2p orbital to quantify the number of tosylate per monomer unit leading subsequently to the doping level as the sulfur signal takes into account the contributions from tosylate (S=O binding) and PEDOT (S-C binding in thiophene configuration).

Figure II-6 shows a XPS fitting of the sulfur contributions of ISP PEDOT:Tos film. Both signals at 164.1 and 165.1 eV correspond to the doublet from the binding of C and S in the thiophene unit of PEDOT. By polymerizing and doping, the system creates delocalized charges and allows the formation of PEDOT cations visible with the doublet at 165.5 and 166.4 eV ($PEDOT^+$). The two other doublets are attributed to the tosylate as they correspond to the binding between S and O. One doublet at 167.4 and 168.0 eV, is attributed to the tosylate involved in the doping mechanism [10], and another one at 168.7 and 169.8 eV is attributed to unreacted tosylate which are still present inside the film. This result signifies that an amount of unreacted tosylate molecules is still present inside the film despite the three washing steps. XPS measurements further allows accessing to the oxidation level by calculating the ratio between the areas under the peak contributions of tosylate and the total contributions of sulfur [15]:

$$Oxidation\ level = \frac{\sum Areas_{reacted\ Tosylate}}{\sum Areas_{Thiophene}} \qquad \textit{Equation III-1}$$

The maximum oxidation of PEDOT by tosylate is 33% which significates that one tosylate can be found every three monomer units [16], [17]. This result is a theoretical result and without further treatment, it is not possible to reach this value. An oxidation level of 22 ± 2% was determined for all in-situ polymerized PEDOT:Tos films in accordance with literature [18], [19].

It is noteworthy that the oxidation level can also be determined by taking into account the contributions of PEDOT and tosylate from O1s peak even if it is more difficult since moisture can contributed to the oxygen signal [18].

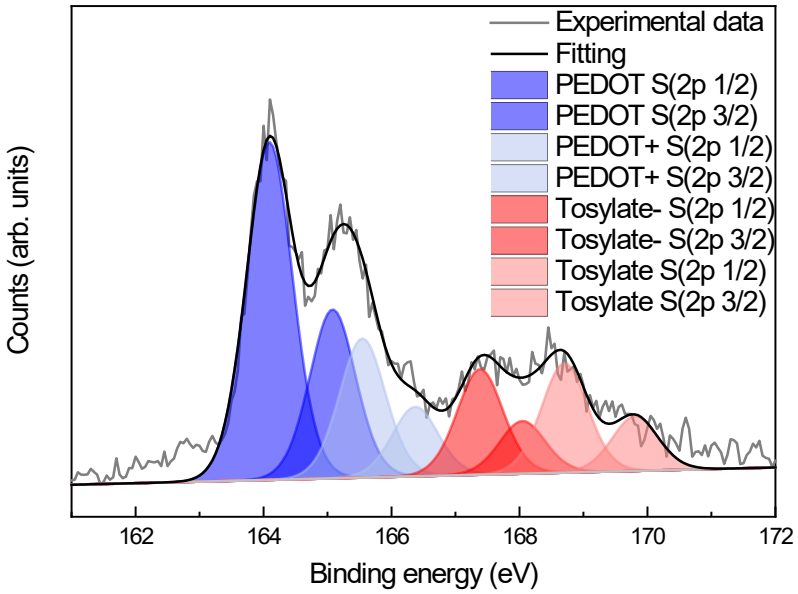

Figure III-2 XPS S2p spectrum of in-situ polymerized PEDOT:Tos film. Blue and red areas represent the signals linked to S2p in PEDOT and S2p in tosylate, respectively.

II-1-B- Structural characterization

In literature, the microstructure of PEDOT:Tos has been studied using different techniques like AFM, XRD, Grazing Incidence Wide Angle X-Rays Scattering (GIWAXS), Scanning Electron Microscopy (SEM) or Transmission Electron Microscopy (TEM). In this part, we will focus on microscopy and XRD characterizations.

PEDOT:Tos films, synthetized by in-situ chemical polymerization, are smooth and composed of small dots as it can be seen in Figure III-3. Those dots are arranged in lines, coming from the same point which is in the middle of the film. They are linked to the centrifugal force arising from spin-coating. They are explained by the fact that the solvent has a high evaporation rate and during the spin-coating there is an instability between all the components and the substrate [20]. This surface texture does not affect the electronic properties of the film which are comparable to those found in literature.

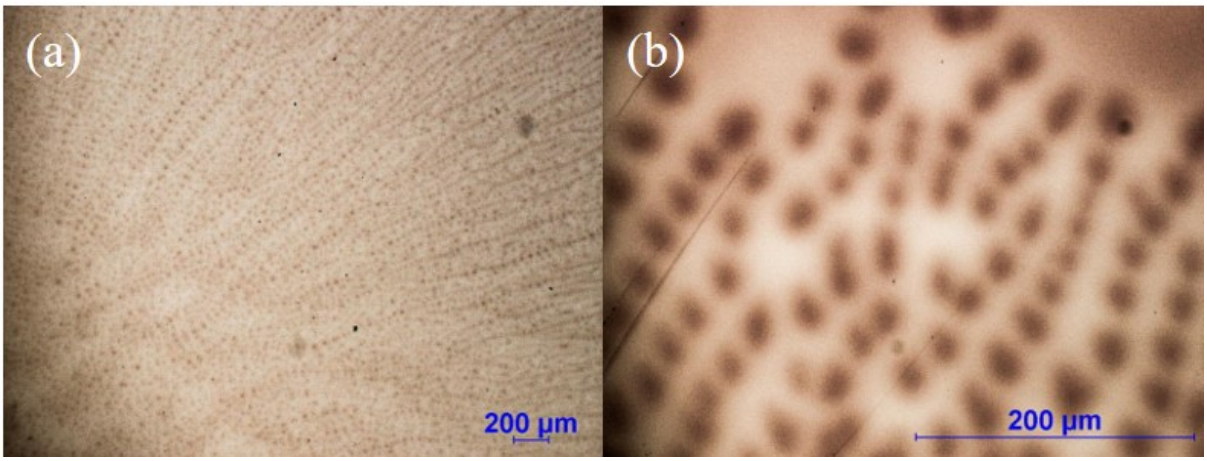

Figure III-3 Optical microscopy images of in-situ PEDOT:Tos film showing aligned dots due to the spin-coating effect (a) magnification ×2.5 (b) magnification ×20.

Despite these striations on the films, the PEDOT surfaces are homogeneous at the nanoscale with a low square roughness of 2.4 nm, determined by AFM. Figure III-4 shows a 2x2 µm² image of PEDOT:Tos topographical surface. This surface is smooth without any disparity and comparable with the one obtained by Ha *et al.* with another weak base [21].

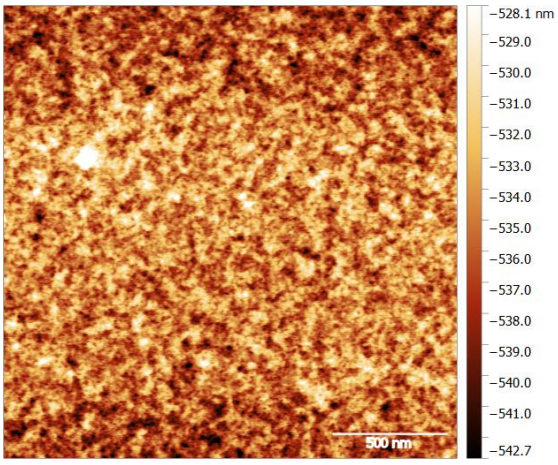

Figure III-4 Topographical AFM image 2×2 µm² of in-situ polymerized PEDOT:Tos film. The surface of the film is smooth with a low square roughness.

In order to better apprehend the electronic properties of the PEDOT:Tos films, it is mandatory to unveil the chain packing at the molecular level. PEDOT:Tos is a semi-crystalline polymer where four EDOT units and one tosylate ion are contained in an orthorhombic crystallographic cell [22]. This structure was unveiled by Aasmundtveit

with the assumption that PEDOT chains pack into a lamellar structure where the tosylate ions are positioned between the PEDOT layers [23]. It is interesting to note that a cell containing four EDOT units and one tosylate ion leads to an oxidation level of 25% which is in accordance with the oxidation level deduced from XPS. In order to probe the PEDOT:Tos film structure and compare our experimental results to the literature, XRD have been performed on selected PEDOT:Tos samples. XRD characterization permits to estimate crystallographic structure characteristics, i.e. the distance between plans depending of the stacking of the chains, crystallite size, relative crystallinity or the crystallization orientation. Two mains distance can be calculated from the XRD pattern analysis which are $d_{[010]}$, i.e. twice the π-π stacking distance, and $d_{[100]}$, i.e. the inter-lamellae stacking distance, as displayed Figure II-8 (a).

For the XRD analysis, PEDOT:Tos films were deposited on intrinsic silicon substrate. Silicon is a well-known material in crystallography and signal coming from the substrate can be identified and disregarded during the data treatment as the inherent diffraction peaks appear at well higher 2θ angles. The films were analyzed in a grazing incidence configuration (i.e., Grazing Incidence X-Rays Diffraction (GIXRD)), allowing us to probe thin PEDOT:Tos films. The GIXRD pattern corresponding to in-situ polymerized PEDOT:Tos film is displayed in Figure II-8 (b).

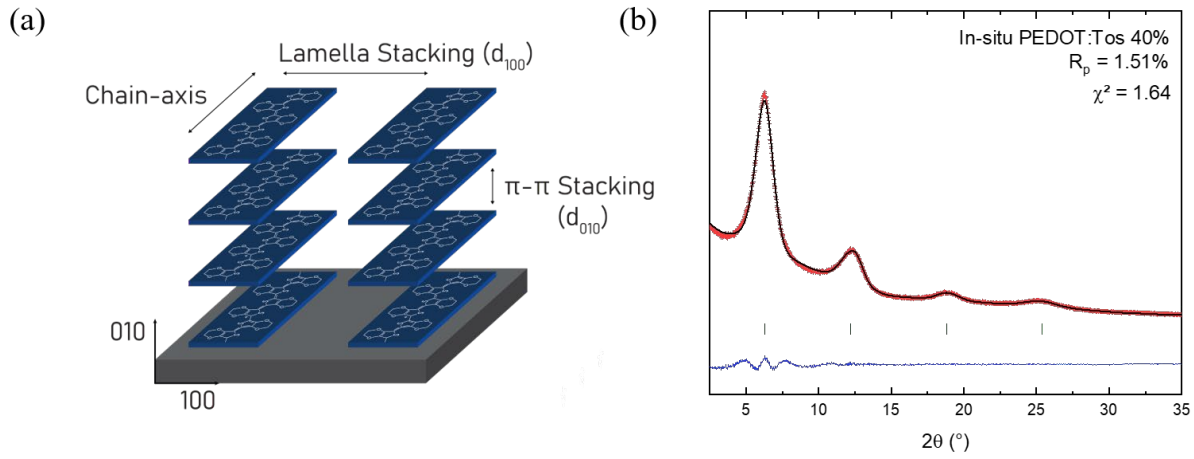

Figure III-5 (a) Characteristic distances which can be obtained by XRD measurements (b) GIXRD line profile fit with measured (red crosses) and fitted (black line) data and differences between them (blue line) of in-situ film. Vertical ticks are the Bragg peak positions [100], [200], [300] and [020] from right to left respectively, considering a primitive cell with a ~ 14.2 Å and b ~ 7 Å.

The pattern is composed of broad peaks, consistent with the paracrystalline nature of the films. Four peaks appear on the diffraction pattern, the first three, at 2θ equal to 6.3, 12.3 and 18.8°, are attributed to the first, second and third order of the [h00] series, respectively which correspond to an edge-on stacking orientation [24]. The last peak is attributed to [020] reflections and correspond to a face-on orientation. Based on the Bragg formula, it is possible to calculate the distance between plans:

$$2d_{hkl} \cdot \sin(\theta) = n \cdot \lambda \qquad \textit{Equation III-2}$$

where d_{hkl} is the interplanar distance, θ (rad) is half of the angle which can be read on the diffraction pattern, n is the diffraction order and λ the wavelength of X-rays (here a copper anode source: λ = 1.5406 Å).

The Bragg formula permitted to deduce $d_{[0k0]}$ = 7.06 ± 0.03 Å. As the π-π stacking distance is half of the characteristic distance along the *b*-axis, we deduced, $d_{\pi\text{-}\pi}$ = 3.53 ± 0.01 Å. Along the *a*-direction, we deduced a lamellae stacking distance $d_{[100]}$ = 14.17 ± 0.05 Å. These results are comparable to the ones reported by Aasmundtveit *et al.* [23].

II-2- THERMOELECTRIC PROPERTIES OF IN-SITU POLYMERIZED FILMS

II-2-A- ELECTRICAL CONDUCTIVITY

In-situ polymerized film properties were measured directly after deposition. For electrical conductivity measurements, films were made on 15×15 mm^2 glass substrates. The sheet resistance of the films was measured by four-point probes measurement, see previous chapter for more details. In most of the case, the thickness of in-situ polymerized films was included between 50 and 100 nm. This difference can be explained by the fact that over time, films were made using the two different stock solutions (40 wt% and 54 wt%). With time, the oldest solution (40 wt%) easily absorbs water from moist air which likely affects the concentration of oxidant. This difference results in the observed variation of thickness but the conductivity is only affected feebly. For each concentration, a minimum of three samples has been synthetized in order to have a panel of conductivity and so the error bars are the standard deviations. Figure III-6 displays the electrical conductivity of in-situ

polymerized PEDOT:Tos films made with a 40 wt.% oxidant concentration. Light blue shows data from the literature and darker blue data from this work. Here, we were able to reach conductivity of 995 ± 234 S.cm^{-1} without metallic contacts and 4398 ± 68 S.cm^{-1} with gold contacts. The large error bar can be explained by the fact that many samples were synthesized during the Ph.D. and so evidences the condition/process sensitivity. Nevertheless, this value is in accordance with state-of-the-art PEDOT:Tos films.

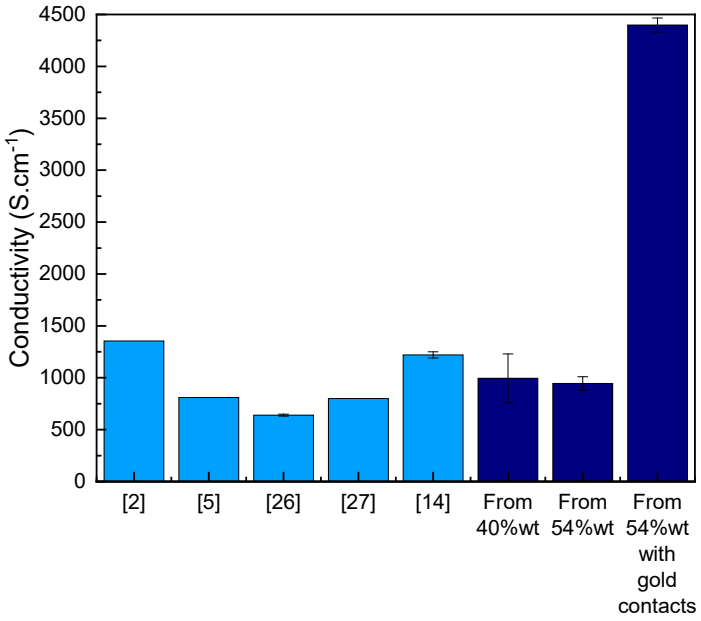

Figure III-6 Electrical conductivity for various PEDOT:Tos made by ISP. Light blue represents data from literature [2], [14], [25]–[27], darker blue concerns data from this work with films made based on 40 wt% and 54 wt% stock solution diluted to obtain a tosylate concentration of 40 wt%.

The best value for PEDOT:Tos based on 40% oxidant concentration has been reported by Park *et al.* with an electrical conductivity of 1355 S.cm^{-1} [2]. Their PEDOT:Tos was synthetized with the help of pyridine but also PEG-*b*-PPG-*b*-PEG which inhibits both the crystallization of $Fe(Tos)_3$ and the EDOT polymerization. Such treatment leads to a better packing of PEDOT chains and to highly crystalline materials. Note that, compared to literature, the high conductivity value observed here is most probably due to advanced chemical formulation and high quality measurements.

II-2-b- Seebeck coefficient

The Seebeck coefficient was measured by applying a temperature gradient between both sides of the sample. As PEDOT:Tos thermoelectric properties are highly interesting for room temperature applications; one side was kept at 22°C and the other one was slightly heated until it reaches 27°C. Accordingly, we obtained the thermovoltage versus temperature difference curve and deduced the Seebeck coefficient from the slope. In order to be more precise in the measurement of the Seebeck coefficient, both voltage and temperature are probed at the same time and at the same point on each side [28].

Three measurements were performed and a Seebeck coefficient of 19.8 ± 1 $\mu V.K^{-1}$ was found. Some studies show higher values of Seebeck coefficient (≈ 40 $\mu V.K^{-1}$) for in-situ polymerized films [12], [14], [29]. As the measure of the Seebeck coefficient depends on charge carrier concentration but also the sample configuration, the difference could be explained by the measurement itself [30].

II-3- Electronic properties

The electronic properties of PEDOT:Tos films can be also probed by UPS. The principle of this technique is to probe the valence band of a material to decipher the electronic behavior and energy levels of orbitals. As explained in the first chapter, according to the Mott's formula, the slope of the DoS at the Fermi level is proportional to the Seebeck coefficient. However, evaluating the slope at the Fermi level does not give the value of the Seebeck coefficient. Nevertheless, comparing two UPS spectrum permits to compare the Seebeck coefficient of two materials. For organic semiconductors material, the tail of the DoS (σ_{DoS}) of occupied states, around the Fermi level, is approximated by a Gaussian function [31]. It has been shown that for PEDOT, the value of σ_{DoS} given by UPS is higher than the real one. This difference was explained by the broadening induced by the spatially varying electrostatic potential due to the disordered distribution of the tosylate anions [32].

The films analyzed by UPS are exactly the same than those analyzed by XPS. UPS measurements have been done before XPS because the energy applied to the sample

is less important and do not lead to a modification of the surface. The resulting spectra are displayed Figure III-7. The work function of in-situ polymerized film is read by fitting the secondary electron cut-off and is equal to 4.3 ± 0.1 eV. This results is in accordance with previous study on in-situ polymerized PEDOT:Tos [19].

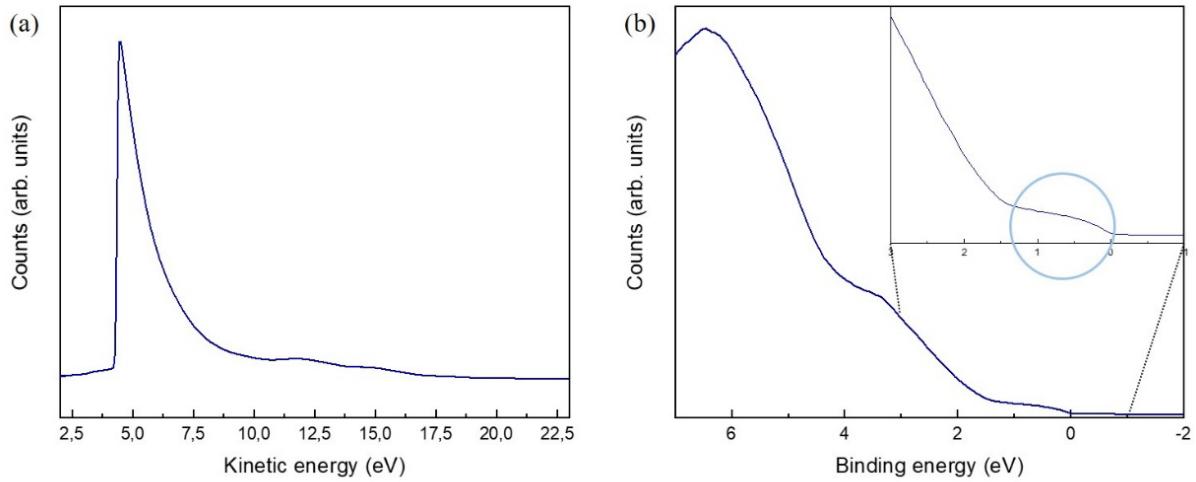

Figure III-7 UPS spectra of in-situ polymerized film (a) Secondary electron cut-off region (b) Valence band region. Binding energy equal to 0 represents Fermi level.

By having a look to the valence region, Figure III-7 (b), it is possible to visualize the spectral features which are characteristic of the DoS of the material, and by zooming on the region between 3 and -2 eV, we clearly see a small amount of electronic states near to the Fermi level (circle in Figure III-7 (b)). Such electronic states are characteristic of a semi-metallic behavior as it has been described by Bubnova *et al.* [33].

The HOMO value has been deduced from the spectrum to be -1.42 eV. Further details about the Seebeck coefficient and the disorder inside the material will be discussed when comparing ISP and VPP materials.

III- VAPOR PHASE POLYMERIZATION

Vapor phase polymerization (VPP) was developed by Winther-Jensen and his team in 2004 [34]. They wanted to develop a new route for the polymerization of PEDOT:Tos in order to control the formation of the film. By this technique, they were able to reach conductivity exceeding 1000 $S.cm^{-1}$. The procedure of VPP is to deposit an oxidant layer on a substrate followed by its exposure to EDOT vapors. VPP permits to control the atmosphere under which the PEDOT:Tos film grows. It is thus possible to carry the polymerization under N_2 flow, static inert atmosphere or vacuum while controlling the humidity in the polymerization chamber [35]–[38]. Additionally, quartz crystal microbalance (QCM) can be used to follow the thickness increase with polymerization time [39]. With such type of dedicated set-up, Metsik *et al.* measured the resistivity of their samples during the growth of the film allowing them to follow the change of electronic properties along the polymerization [40]. They observed that, with time, the electrical conductivity of their films decreases. This result was explained by the fact that the sheet resistance decreases while the thickness increases. The advantages of VPP are its easy way to setup and the huge number of tunable parameters (temperature, oxidant, monomer, additives…) [41].

These different studies point out the versatility of this technique, i.e. the fact that all the set-ups are different and do not allow to play on the same parameters. In the following parts, we will explain in details the set-up used and which parameters can be tuned in order to tailor the thermoelectric properties of vapor phase polymerized PEDOT:Tos films.

III-1- SYNTHESIS OF PEDOT:TOS AND STRUCTURAL PROPERTIES

III-1-A- PRINCIPLE OF VPP

The growth process of VPP films is still discussed in the community. Some researchers described this process as a top-down approach where the polymerization occurs at the surface or in the bulk of oxidant by the diffusion of the monomer through the oxidant [42], [43]. Nair *et al.* demonstrated this effect by following with a Quartz Crystal Microbalance (QCM) the polymerization of polypyrrole

inside PEO fiber. After 20h of polymerization, the frequency decreased showing that the fibers became hard and limited the diffusion of the monomer.

Others as Evans *et al.* described the film formation as a bottom up approach [44]. In this case, oxidant mixture diffuses by capillarity into a EDOT condensed layer at the surface and polymerizes this one. To conclude that, they studied the ratio between Iron ions Fe^{3+} (present in the tosylate layer) and Fe^{2+} (present after the formation of EDOT cation) by XPS. The high presence of Fe^{3+} at the top surface after polymerization process point out the fact that oxidant diffuses through the as-formed PEDOT:Tos layer.

III-1-B- Optimization of VPP parameters

It is possible to tune on a large number of parameters during the VPP process. In our case, we decided to analyze the effect of temperature on the resulting electrical conductivity. To do that, three samples were made for each VPP, with a concentration of 20% of Tosylate for the oxidant solution, and we varied the temperature from 50 to 110°C. VPP were carried out during 5 min in order to obtain thin films. For each sample, the sheet resistance was measured by 4-point probes and the thickness by profilometer. The results are displayed in Figure III-8. As the polymerization time is short and the oxidant solution has a low concentration, the thickness of the samples is quite low with a maximum value around 16 nm.

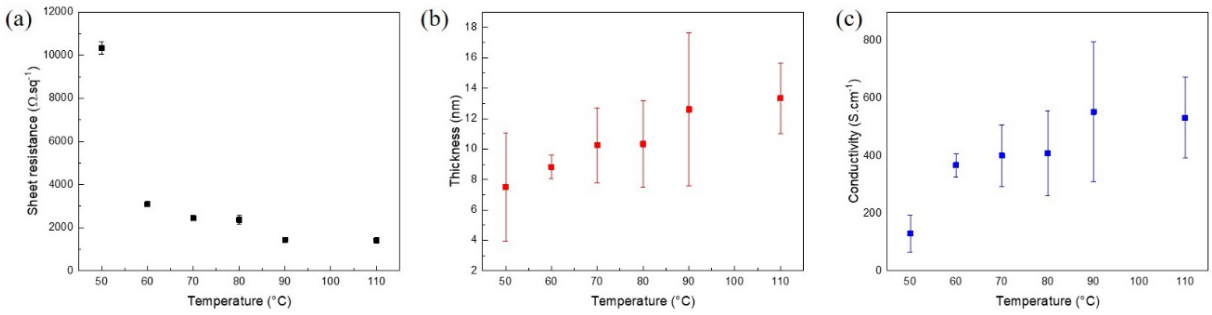

Figure III-8 (a)Sheet resistance, (b) thickness and (c) electrical conductivity against temperature of the hotplate during VPP process.

Regarding the sheet resistance, 50°C is not an appropriate temperature to run the VPP process. As it was explained before, the temperature of the substrate is too low and does not exceed the crystallization temperature of the tosylate molecules. Thus, tosylate molecules can crystallize on the substrate and disrupt the PEDOT:Tos layer growth which leads to inhomogeneous films.

In another hand, from 70°C, we noticed that the sheet resistance is almost constant and the resulting conductivity does not vary so much. Based on this study, we decided to run VPP between 70 and 100°C.

III-1-c- Validation of the doping

In order to verify the formation of PEDOT:Tos films after VPP, the films were analyzed by XPS. The XPS conditions were the same than the ones used for in-situ film measurements. First a survey spectrum was registered and showed the presence of carbon, oxygen and sulfur. After that, S2p spectra of PEDOT:Tos films were recorded in order to calculate the oxidation level and the results are displayed Figure III-9. The four different contributions of sulfur from PEDOT and tosylate can be identified in blue and red region, respectively. For vapor phase polymerized films, we managed to reach an oxidation level of 22 ± 2%.

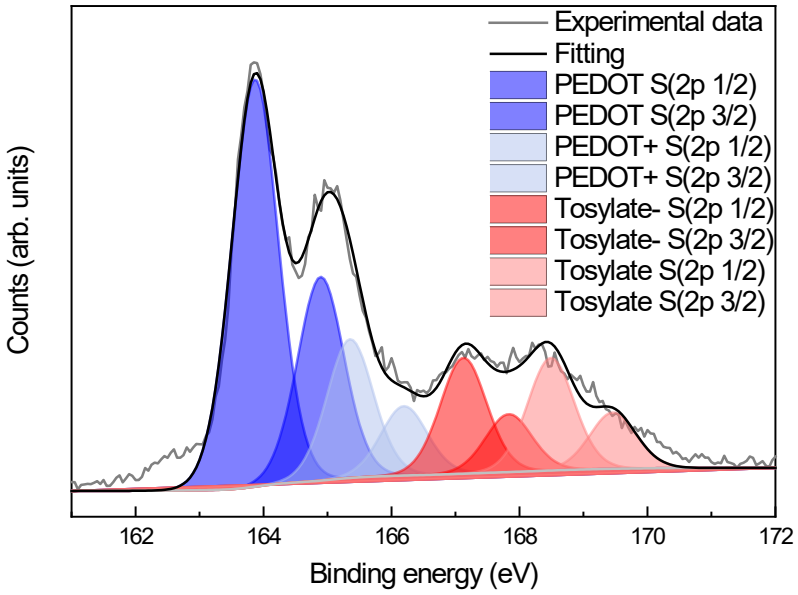

Figure III-9 S2p spectrum of PEDOT:Tos film vapor phase polymerized. Blue area represents signal link to S2p in PEDOT and red area S2p in tosylate.

III-1-D- STRUCTURAL CHARACTERIZATION

After VPP, the resulting samples are light blue hinting conjugation in the materials. At first glance, films looked homogenous but we analyzed by AFM and GIXRD in order to better apprehend the texture and crystallographic structure.

The top surface of VPP films is highly irregular and seems to be an assembly of small dots, as displayed Figure III-10 suggesting a nucleation and growth process. VPP leads to films with granular structure, explained by the formation of particles at the top surface of tosylate layer during the process [44]. Despite this granular structure, the roughness of the film is quite low, with an average roughness of 7.2 nm. The roughness of the film is associated with the redox activity of the oxidant, here $Fe(Tos)_3$ [47].

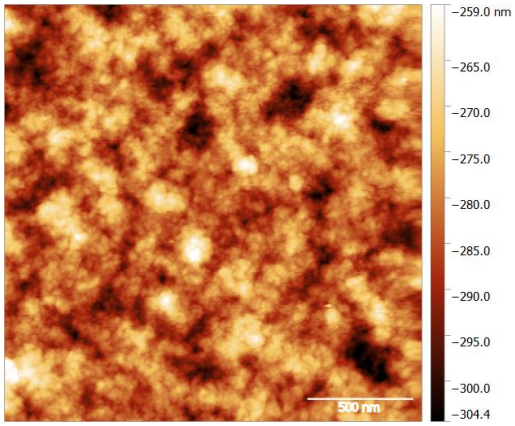

Figure III-10 Topological AFM image 2×2 µm² of vapor phase polymerized PEDOT:Tos film. The surface of the film is granular with a low square roughness.

As the growth of the film depends on the kinetic of the redox process, bulk of the film can be different than the surface. To probe that, we performed GIXRD on films vapor phase polymerized on silicon substrate. The peaks are relatively broad which is consistent with the paracrystalline nature of the films. Four peaks appear at 6.3, 12.3, 18.8 and 25.7° on GIXRD pattern, corresponding to [100], [200], [300] and [020] reflexions, respectively, as displayed Figure III-11. We can deduct from these values $d_{[0k0]}$ of 6.99 ± 0.01 Å which lead to a π-π stacking distance $d_{\pi-\pi}$ of 3.50 ± 0.01 Å and a lamellae stacking distance of 14.2 ± 0.2 Å. These results are in accordance which

others found in literature [35], [40], e.g. Wu *et al.* found a π-π stacking distance of 3.4 Å which is in the same range that what we obtained in this study.

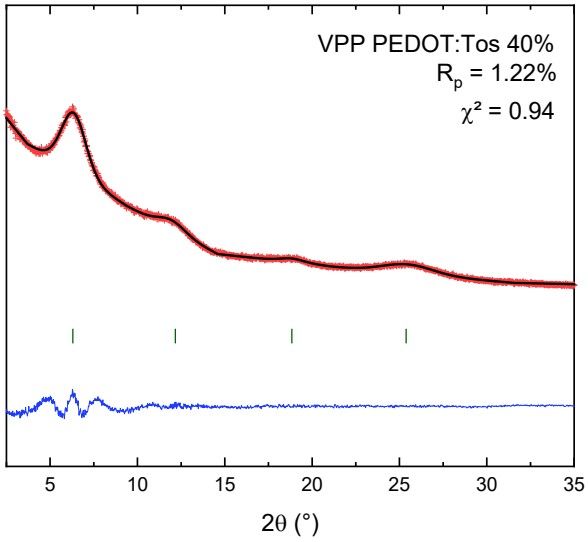

Figure III-11 GIXRD line profile fit with measured (red crosses) and fitted (black line) data and differences between them (blue line). Vertical ticks are the Bragg peak positions [100], [200], [300] and [020] from right to left respectively, considering a primitive cell with a ~ 14.2 Å and b ~ 7 Å.

III-2- THERMOELECTRIC PROPERTIES OF VAPOR PHASE POLYMERIZED FILMS

In order to probe the thermoelectric properties (electrical conductivity and Seebeck coefficient), vapor phase polymerized films were synthetized at 70°C during 5 minutes. In order to have a good sampling, 3 samples have been made per VPP procedure. Figure III-12 displays the electrical conductivity of some PEDOT:Tos films made of the basis of 40% oxidant concentration. Light blue shows data from literature and darker blue data from this work. Here, we were able to reach conductivity of 963 ± 169 and 3025 ± 67 $S.cm^{-1}$ for VPP films without and with gold contacts, respectively. The large error bar is explained by the fact that a lot of samples have been made, based on different solutions (but always with the same amount of components) and synthetized at different period of this work. Depositing gold contacts on the substrate permits to properly measure the electrical conductivity and so obtain the best value for VPP PEDOT:Tos.

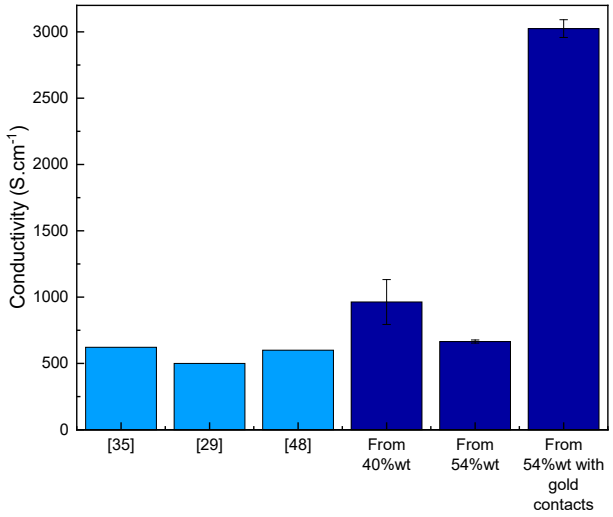

Figure III-12 Electrical conductivity for various vapor phase polymerized PEDOT:Tos films. Light blue represents data from literature [29], [35], [48], darker blue concerns data from this work with films made based on 40 %wt and 54 %wt.

For Seebeck coefficient measurements, PEDOT:Tos was polymerized on 30×15 mm^2 glass substrates previously coated with gold contacts. The deposition conditions were the same that previously. In order to obtain the thermoelectric properties of a same sampling, substrates for Seebeck and conductivity measurement were put at the same time in the VPP chamber.

After polymerization, the films were rinsed and half of the polymer on the top of contacts was removed using a cotton bud. Seebeck measurements were performed on a homemade set-up, varying the temperature of the "hot side" from 22 to 27°C. The temperature was measured at the same time in order to avoid mismeasurement. After fitting the values of the plateau obtained with a linear fit, PEDOT:Tos films prepared by VPP have a Seebeck coefficient of 19.6 ± 0.8 $\mu V.K^{-1}$. This value is in accordance with previous values found in literature [29], [36], [49], [50].

III-3- Electronic properties

As for ISP films, we performed UPS characterization on VPP films. Films were made with the same conditions that the previous ones (VPP 5 min at 70°C with an oxidant solution of 40%). The substrate used is a conducting silicon in order to avoid charge accumulation on the top surface. After UPS measurements, characteristic spectra, displayed Figure III-13, were obtained.

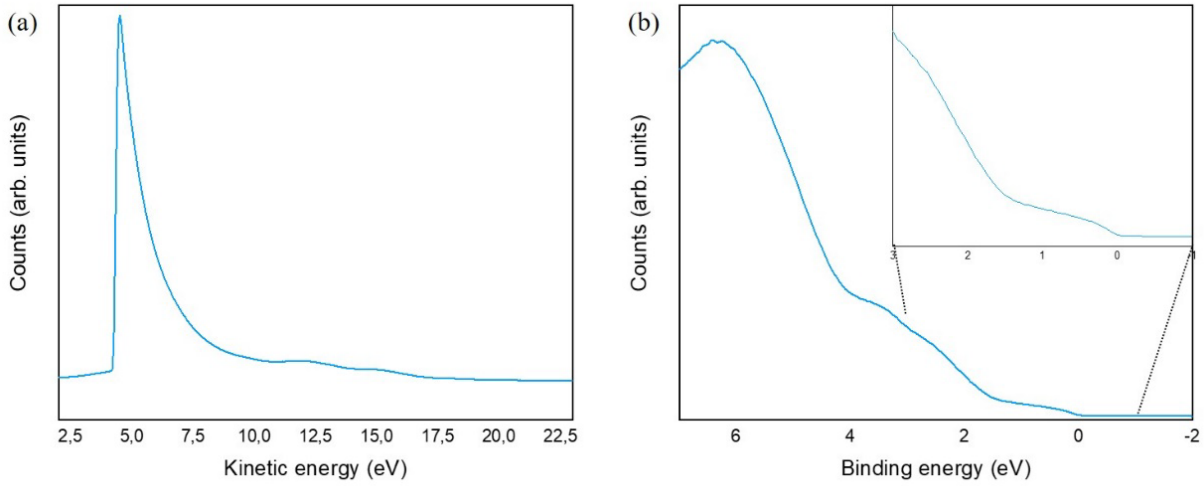

Figure III-13 UPS spectra of vapor phase polymerized film (a) Secondary electron cut-off region (b) Valence band region. Binding energy equal to 0 represents Fermi level.

Based on the fact that the fitting on the second electron cut-off gives the work function of our material, PEDOT:Tos made by VPP has a work function of 4.3 eV. This value is in accordance with the work or Sharma *et al.* who found a WF between 4 and 4.3 eV depending of the additives they put inside their solution [51]. Ouyang *et al.* found a value a bit higher, 4.62 eV [52]. In their work, they used PEG-*b*-PPG-*b*-PEG as additives that influences the properties of the film as regard to our additives. The WF is characteristic of the energy difference between Fermi level and vacuum level and depend on the oxidation level of the material [53]. They did not express their oxidation level and the difference between WF could be explained by a difference in oxidation level.

The valence region, displayed Figure III-13 (b), shows the DoS of the material. Especially in the region between 3 and -2 eV, we clearly see a small amount of electronic states near to the Fermi level. As said previously, this amount of electronic state near to the Fermi level is relevant of a semi-metallic behavior. The HOMO value has been deduced from the spectrum to be -1.25 eV.

IV-COMPARISON BETWEEN BOTH TECHNIQUES

ISP and VPP are the two most studied ways to polymerize PEDOT:Tos films. Researchers always tried to improve the Seebeck coefficient and the electrical conductivity of this polymer by playing on oxidation level or crystallinity.
In-situ polymerized PEDOT:Tos films conductivity can reach a conductivity of 1000 $S.cm^{-1}$ [14]. This value can be lightly improved by playing on additives put inside the oxidant solution (pyridine, block copolymer, imidazole…) but playing on polymerization parameters is limited. In another hand, VPP permits to increase the electrical conductivity because it is possible to play on a lot of parameters: oxidant or additives [37], [54], [55], temperature [35], [40], pressure and environment [38], time [40], [56]. These parameters point out the fact that it is easier to tune the electronic properties of vapor phase polymerized PEDOT:Tos thin films. By optimizing parameters, films made by VPP can reached electrical conductivity exceeding conductivity of in-situ polymerized films until 3305 $S.cm^{-1}$ [2], [5], [38], [44].

Few studies already aimed at the comparison between those two techniques. Madl *et al.* showed that VPP provides better films with regard to the electronic properties than in-situ polymerization [57]. First the electrical conductivity of VPP films is higher than in-situ one, 575 $S.cm^{-1}$ against a maximum of 126 $S.cm^{-1}$. Moreover, the VPP leads to thinner film and less rough than in-situ as shows the AFM study. They explained these differences by the fact that VPP permits to the polymer chains to organize themselves because of the polymerization time.

In the previous parts, we characterized films made by in-situ and vapor phase polymerization. In this following part we will compare these both techniques based on structure, thermoelectric and electronic properties and deduce their advantages and drawbacks.

IV-1- COMPARISON OF THE FORMATION OF PEDOT:TOS

PEDOT:Tos films have been made with the same oxidant concentration of 40%, the same additives, pyridine and DMSO, and the same kind of substrate depending of the characterization allowing us to investigate the influence of the polymerization technique on the crystallographic structure and the transport properties of the polymer.

IV-1-A- COMPOSITION OF THE SAMPLES

The composition of the samples was probed by XPS. Oxygen, carbon and sulfur signals appeared on the survey spectrum. These three elements were finely analyzed in order to deduce de composition of the samples. By calculating the area under each peak we were able to deduce a ratio of each element inside the first nanometers of PEDOT:Tos films:

Table III-1 Proportion of oxygen (O), carbon (C) and sulfur (S) in films versus the polymerization way

	Proportion of O	Proportion of C	Proportion of S
In-situ	0.20	0.57	0.22
VPP	0.19	0.59	0.22

The fittings of the peaks are presented in Figure III-14. O1s fitting shows the contribution of oxygen for PEDOT at 533.51 eV, $PEDOT^+$ at 534.93 eV, and also for tosylate at 531.95 eV and 531.01 eV. The last peak at 536.49 eV correspond to π to π* shake up peak due to the ejected core line electrons which collide with the shared electrons in the π orbital of the ring structure [18]. The S2p fitting was explained beforehand (*cf* II-2-b-). By calculating the ratio of areas under the peaks using Equation II-2, we found that the oxidation level for both films is the same and equal to 22 ± 2 %. This result shows that the oxidation of the PEDOT is not affect by the polymerization way used.

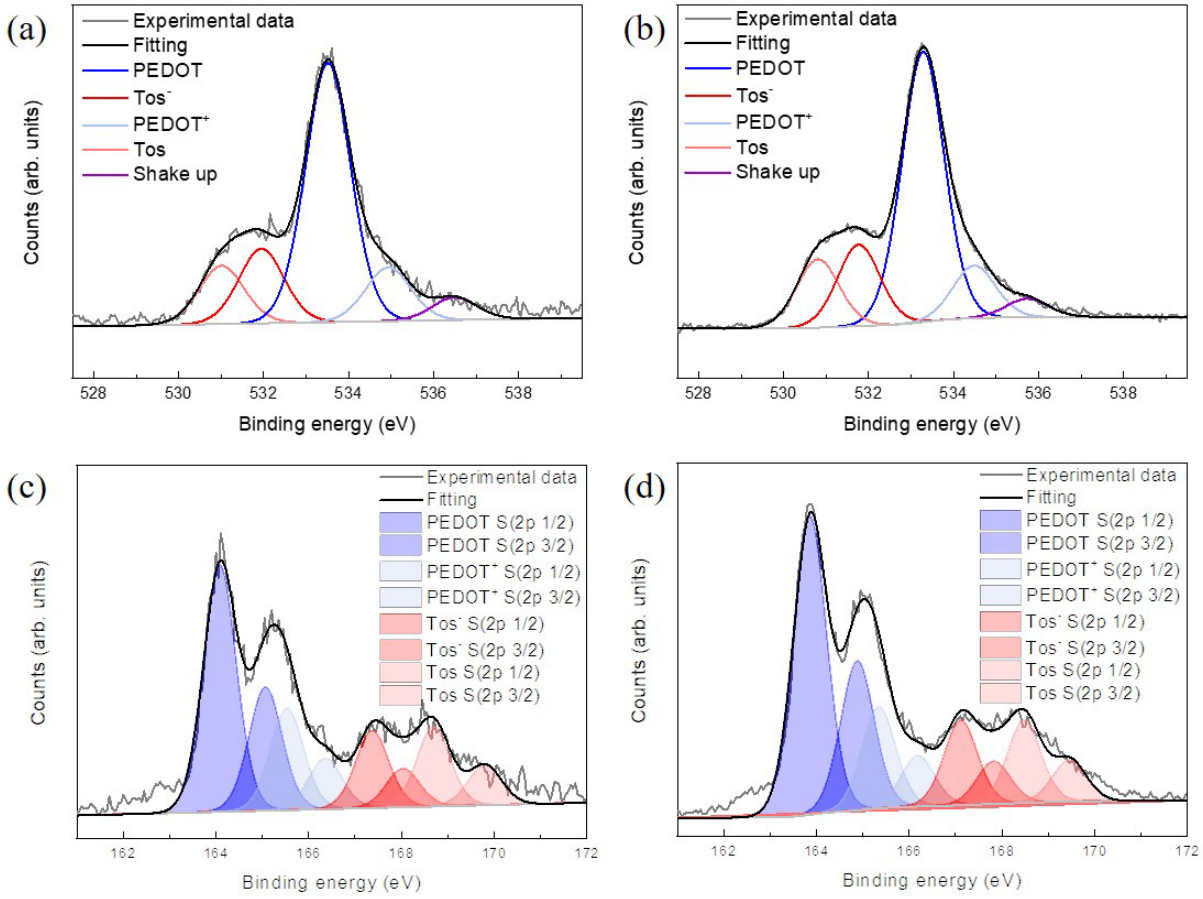

Figure III-14 XPS fitting of O1s and S2p peak of in-situ and VPP films. (a) O1s in-situ (b) O1s VPP (c) S2p in-situ (d) S2p VPP.

IV-1-B- CRYSTALLOGRAPHIC STRUCTURES: QUALITATIVE COMPARISON

- *Samples details and calculations*

Regarding the paracrystalline nature of PEDOT:Tos, a quantitative analysis of GIXRD pattern is hazardous because of the relatively wide diffraction peaks allowing several different elementary lattice structure to fit in and so avoiding a proper Lebail refinement. Hence, in order to investigate the influence of the polymerization technique on the crystallographic structure, we present a qualitative sample to sample comparison based on a line profile fit considering a literature-based elementary lattice, i.e. $a \sim 14.2$ Å and $b \sim 7$ Å and with the four diffraction peaks corresponding to the following Bragg plans [100], [200], [300] and [020]. For this purpose, all samples', i.e. 3 VPP-made and 3 in-situ-made on silicon substrates, diffraction patterns were recorded in the exact same conditions.

Analyzing XRD pattern gives insights of crystallite sizes of the polymer nanostructure. Based on these diffraction patterns and the broadening of a peaks, it is possible to calculate the coherence length, i.e. the average size of the crystallites inside the PEDOT:Tos by applying the Scherrer equation:

$$L_c = \frac{2\pi K}{\Delta_q} \qquad \textit{Equation III-3}$$

With L_c the coherence length, K the shape factor and Δ_q the peak width expressed as:

$$\Delta_q = \frac{4\pi \sin\beta}{\lambda} \qquad \textit{Equation III-4}$$

With β integral breadth.

That being said, in paracrystalline materials, finite grain size and cumulative disorder are common phenomena inducing cell parameters variations [58]. Therefore, within the same reflexion set, e.g. h00, the peaks widen with the increase of the diffraction order n and so, contrary to common interpretation based on the first peak width, one must plot the peak widths Δ_q vs. n^2 to compute the coherence length, i.e. taking into account cumulative disorder. The intercept of the linear fit is then equal to $^{2\pi}/_{L_c}$ Moreover, based on the assumption that a lamella is composed of one polymer chain, we can deduce the average chain number in a crystallite dividing L_c by the lamellae stacking distance $d_{lamellae}$. Finally, the relative crystallinity was estimated from the [100] peak height to background ratio normalized by the film thickness.

- *Results*

The polymerization of EDOT is faster in the case of ISP, because monomer and oxidant are mixed together prior to spin-coating. It is thus commonly accepted that such pathway leads to thin films with a lower crystallinity. Nevertheless, in our case, VPP kinetics can also be considered as fast, as VPP results in thick film in few minutes

due to an important PEDOT vapor pressure in the chamber. As displayed in Figure III-15, these polymerizations lead to films with slightly different crystallographic characteristics.

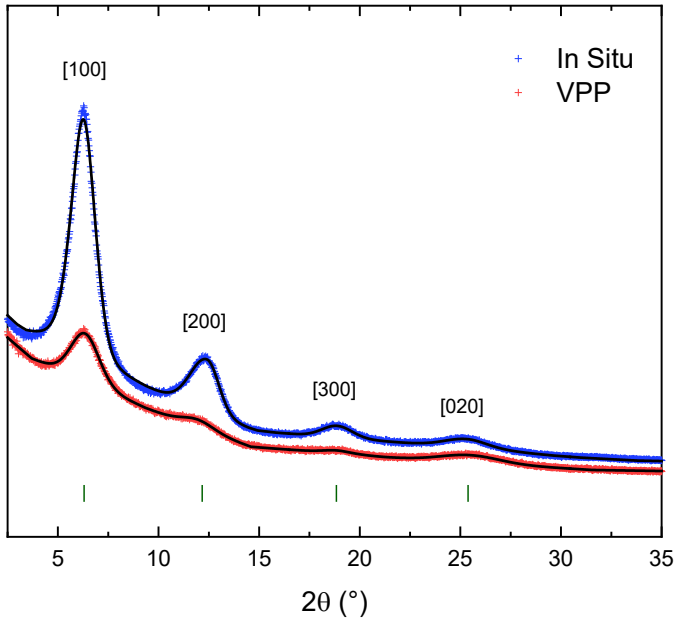

Figure III-15 GIXRD line profile fits with measured (crosses) and fitted (black lines) data. Vertical ticks are the Bragg peak positions.

First of all, ISP and VPP crystallographic data show four peaks, attributed to [100], [200], [300] and [020] reflexions. The ISP sample diffraction pattern is more intense than the VPP one which permits to firstly conclude that PEDOT:Tos made by ISP is more crystalline than sample made by VPP as highlighted by the relative crystallinity calculation (see later). The position and the shape of these peaks have been fitted in order to have access to the crystallography characteristic values which are plotted in Figure III-16 and mentioned in Table III-2.

The [0k0] reflexion, linked to π-π staking distance, is lower for VPP, Figure III-16 (b). By the application of Bragg law, we deduce a π-π staking distance of 3.50 ± 0.01 Å and 3.53 ± 0.01 Å for VPP and ISP, respectively. As previously mentioned, π-π staking distance is crucial in conjugated polymer and plays a role in the hopping mechanism of charge carriers. Lower is this distance, more the hopping is facilitated, higher the

conduction is. This result would suggest an enhanced "local" charge transport for samples made by VPP.

In another hand, the lamellae stacking distance, presented in Figure III-16 (a), is much higher for VPP samples with 14.28 ± 0.02 Å versus 14.17 ± 0.04 Å for ISP films, which suggests better conduction in the inter-lamellae direction [59].

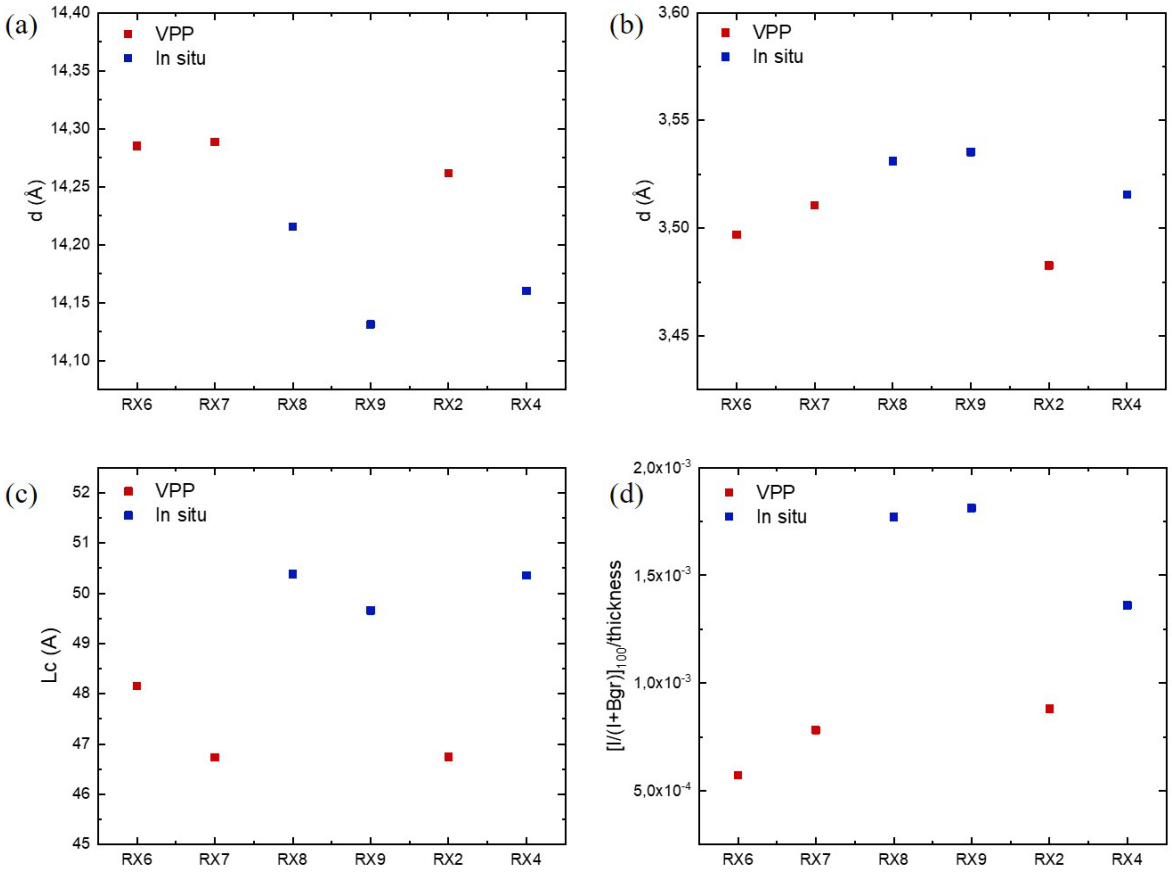

Figure III-16 Graphical representation of VPP (red) and in-situ (blue) crystallographic properties (a) π-π stacking distance (b) lamellae stacking distance (c) crystallites size and (d) relative crystallinity.

Table III-2 Crystallographic parameters extracted from the profile fit analysis of GIXRD pattern of PEDOT:Tos films made by VPP and ISP, with $d_{lamellae}$ ($d_{\pi-\pi}$) being the lamellae (π-π) stacking distance, L_c being the crystallite size, $L_c/d_{lamellae}$ being the average chain number in a crystallite, and rC being the relative crystallinity and Face-on Orientation being the crystallites face-on orientation proportion. Figures between parenthesis denote the standard deviation.

	$d_{lamellae}$	$d_{\pi-\pi}$	L_c	$L_c/d_{lamellae}$	rC	Face-on Orientation
	Å	Å	Å	-	arb. unit	%
VPP	14.28(2)	3.50(1)	47.2(8)	3.31(6)	$0.8(2)\times10^{-3}$	51(3)
ISP	14.17(4)	3.53(1)	50.1(4)	3.54(2)	$1.7(3)\times10^{-3}$	80(3)

By the fitting of the [100] peak, it is possible to estimate the relative crystallinity rC when compared from sample to sample based on diffraction patterns recorded in the exact same conditions. As can be seen in Table II-2, rC of ISP films is approximately twice higher than VPP films, confirming that ISP results in more crystalline films. This is supported by the coherence length analysis showing smaller crystallites in VPP samples, i.e. 47.2 ± 0.8 Å against 50.1 ± 0.4 Å for ISP samples, taking into account the cumulative disorder, i.e. considering the peaks widening at higher diffraction order. Concomitantly a smaller average chain number in one crystallite ($L_c/d_{lamellae}$) is observed in VPP films than in ISP films, i.e. 3.31 ± 0.06 against 3.54 ± 0.02. To sum up, by comparing XRD pattern of samples made by both techniques, PEDOT:Tos films are more crystalline when they are in-situ polymerized demonstrating a much lower lamellae stacking distance, a slightly lower π-π staking distance, a higher crystallite size together with a higher average chain number and a twice higher relative crystallinity. Hence, this result suggests a better charge carrier transport for ISP PEDOT:Tos films.

Despite the relative crystallinity which influences the charge carrier mobility in polymer films, the orientation of crystallites plays a role in the transport mechanism through the hopping between conjugated chains. Petsagkourakis *et al.* demonstrated the influence of additives on the orientation of crystallites and particularly on the amount of edge-on oriented crystallites in ISP films [26] while Chen et al. investigated VPP films [60] both on glass substrate. For ISP films, it was shown that the crystallites are mostly edge-on oriented from GIWAXS analysis. For VPP PEDOT:Tos, the edge-on crystallites orientation is the preferential orientation as demonstrated by Chen et al. [60]. As in both cases the preferential orientation is edge-on, the polymerization method does not seem to affect the crystallites orientation. This could have been being confirmed here by the similar ratio values of the [001] and [020] intensity peaks, i.e. thought as same edge-on to face-on crystallites ratio. But one has to consider the angular dependency of the X-ray intensity and the thickness-normalized integrated intensity. The angular dependency has to be corrected with the Lorentz-Polarization (LP) factor:

$$LP(\theta) = \frac{1 + cos^2(2\theta)}{sin^2(2\theta)\cos(\theta)}$$ *Equation III-5*

By using the angular dependency correction, , and by converting the normalized [020] (face-on) integrated intensity into equivalent normalized [100] (edge-on) integrated intensity, the face-on proportion can be accurately estimated (and vice-versa). As displayed in Table 1, the face-on orientation proportion is much higher in ISP films compared to the VPP films one, i.e. 80 ± 3% and 51 ± 6% respectively, which is consistent with a higher conductivity for ISP samples [24]. At first this result is surprising as it is commonly found in literature that face-on orientation is preferred in PEDOT films with small counterions like Cl^-, Br^- and $HSO4^-$ [61], in contrast to bigger counterions like PSS, Tos and OTf leading to a preferred edge-on orientation [62]. That being said, polymerization conditions, dopant's precursor nature can totally modify the crystallites orientation as reported for oCVD PEDOT:Cl [24]. The substrate nature is also highly influential as shown by Franco-Gonzalez *et al.* [63], i.e. PEDOT:Tos crystallites were found to preferentially orient face-on (edge-on, respectively) on ordered (amorphous, respectively) substrates.

IV-2- THERMOELECTRIC COMPARISON

As a reminder, the films for thermoelectric measurements were made on glass substrate with metallic contacts in order to avoid the contributions from the substrate and decrease the contacts resistance during the measurement. The oxidant solution used was tosylate diluted at 40 w% in butanol. The electrical conductivity was measured the same way for both polymerization routes. For ISP and VPP films, the thermoelectric properties of the films are displayed Figure III-17.

The electrical conductivity is higher for ISP film, 4398 ± 68 $S.cm^{-1}$, than vapor phase polymerized films, 3025 ± 67 $S.cm^{-1}$. However, the sheet resistance of films made by VPP is lower than these made by in-situ polymerization (21.7 against 29 $\Omega.sq^{-1}$). The parameter which induces a lower electrical conductivity is the thickness. PEDOT:Tos films made by VPP are two times thicker than the ISP ones, 156 ± 19 nm compared to 78 ± 8 nm. VPP has been developed by the community to obtain PEDOT:Tos films with lower thickness and higher electrical conductivity. In this study, the amount of EDOT

and the way that the monomer comes inside the jar were not optimized which lead to a high speed of polymerization. The thickness of the films was 200 nm. In order to obtain thinner films for the same time of polymerization, the introduction of EDOT monomer should be controlled.

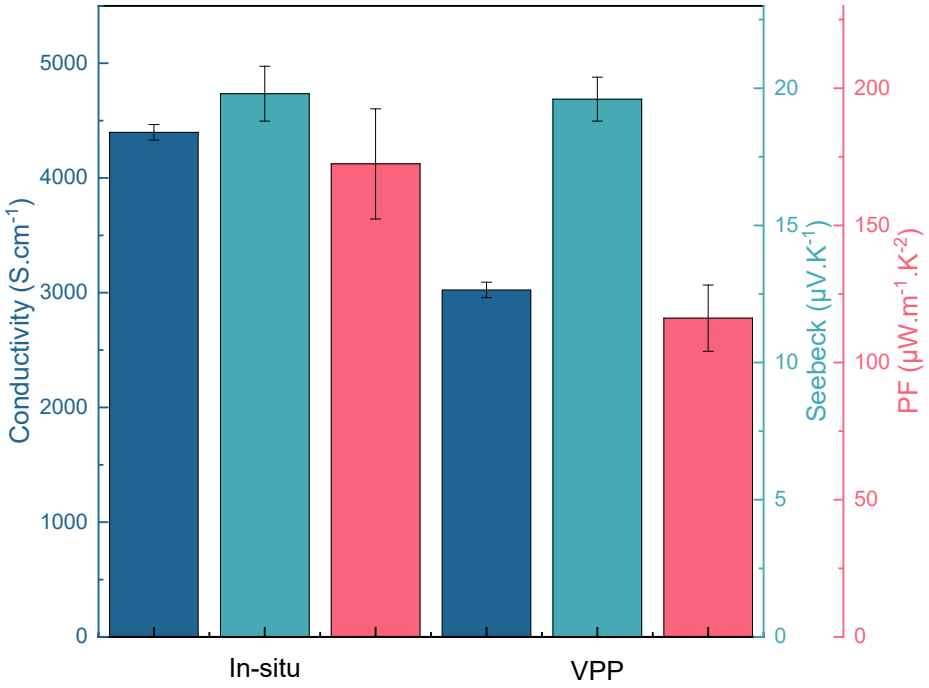

Figure III-17 Thermoelectric properties of PEDOT:Tos films made by In-situ and VPP. Dark blue is referred to electrical conductivity, light blue to Seebeck coefficient and pink to power factor.

The Seebeck coefficient does not vary depending on the polymerization route. The measured values are almost the same with 19.8 ± 1 and 19.6 ± 0.8 $\mu V.K^{-1}$ for ISP and VPP films respectively. As the Seebeck coefficient is dependent of the charge carrier concentration and the carrier mobility, the similar oxidation level, as mentioned above, suggests the same electronic structure for both polymerization techniques. In the hypothesis of a valid Mott formula, the slope at the Fermi level should be the same for ISP and VPP.

The PF is logically higher for the ISP PEDOT:Tos films than VPP one, as the electrical conductivity is higher for the first ones, 172.4 ± 20 $\mu W.m^{-1}.K^{-2}$ and 116.2 ± 12 $\mu W.m^{-1}.K^{-2}$ respectively. From a thermoelectric point of view, this result demonstrates that those ISP films are much more efficient than VPP ones.

IV-3- DENSITY OF STATES COMPARISON

PEDOT doped with tosylate is p-type polymer with a bipolaron network. The transport in the material occurs with the thermally assisted hopping of the bipolarons and will be modified depending on the doping. The doping of PEDOT by tosylate and so the creation of a bipolaron network leads to the semi-metallicity of PEDOT:Tos with the reduction of the band gap from 1.7 eV [64], [65] for a single neutral chain to 0.5 eV [32] for a p-doped PEDOT. UPS measurements permit to decipher the occupied states in the valence band of a material. The density of states is then proportional to the intensity count. As the conditions of experiment are the same for the two different samples (VPP and ISP films), it is possible to compare the effect of the polymerization on the electronic structure of PEDOT:Tos. Through doping, the tosylate counterions are randomly distributed in the sample, inducing a spatially varying electrostatic potential and so, charge carriers experience heterogeneous binding energies, concomitantly with heterogeneous vacuum levels at the surface (ε_{vac}^{S}). Therefore, as the ultraviolet photoelectron spectroscopy (UPS) measures the energy difference between ε_{vac}^{S} and the irradiating energy $h\upsilon$, this technique provides useful information on the spatially varying electrostatic potential, i.e. a disorder character, which is directly related to the randomly distributed tosylate anions. As demonstrated for PEDOT:Tos with a multiscale realistic morphological model [32], the broad range of ε_{vac}^{S} is the origin of the observed Gaussian tail broadening of ~ 1 eV in UPS spectra, in contrast to the commonly DOS broadening of ~ 0.1 eV observed with other techniques. Hence, this suggests, the broader, the more disordered the anions distribution in the sample. In Figure III-18, we present the UPS spectra for PEDOT:Tos made by in-situ and VPP.

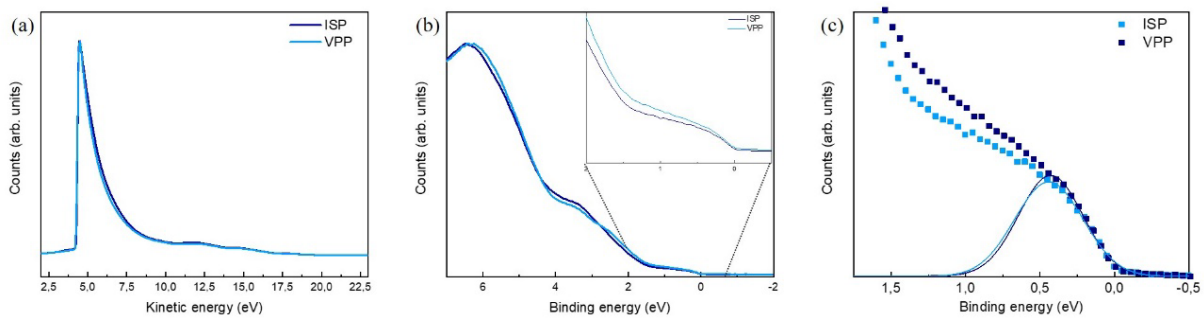

Figure III-18 UPS spectra of films made by in-situ polymerization and VPP (a) Cut-off region showing the work function (b) Valence band of the material showing the semi-metallic behavior (c) Gaussian fits of the valence tail.

Regarding the cut-off region, at low kinetic energy in Figure III-18 (a), ISP and VPP PEDOT:Tos have the same work function 4.3 eV. As the work function is characteristic of the top surface of the film, these results demonstrate that the VPP and in-situ polymerization of PEDOT:Tos provide similar film surfaces with regards to the electronic properties. The valence band shows small differences between the two films, Figure III-18 (b), but the curves are similar when the binding energy tends to 0 eV and reveal the semi-metallic behavior with the small amount of electronic states near the Fermi level [33]. According to the Mott's formula, the slope of the density of states at the Fermi level is proportional to the Seebeck coefficient. As the slopes at 0 eV of both sample types are rather similar, this confirms quasi equal Seebeck coefficient for both polymerization methods as it has been measured previously. But, here, the inherent disorder of the randomly distributed Tos^- prevent such an analysis since, as previously mentioned, the Gaussian broadening induced by the heterogeneous electrostatic potential hide the DOS tail broadening. (Also, despite that here, ISP and VPP samples possess the same doping level, it is noteworthy that its influence on the DOS broadening has been calculated and revealed itself to be barely insensitive [32]). That being said, the valence band tail can be roughly approximated by a Gaussian function, revealing the disorder character of the counterions distribution in the films. As can be seen Figure III-18 (c) Gaussian fits have been performed in the same energy range, close to the Fermi energy. Analyzing the fits, with quality criteria $R > 0.994$, leads to full width at half maximum values (FWHM) of 0.54 ± 0.04 eV and 0.51 ± 0.02 eV for ISP and VPP films respectively, which is almost twice lower than the expected broadening and 5 times higher than the DOS

broadening, consistent with the expected DOS hidden signature. Such close and slightly overlapping values with respect to the uncertainties suggest very similar disorder characters of the Tos^- distribution with a tiny higher trend to disorder in the ISP film.

Besides, the HOMO value is different for both types of PEDOT:Tos films, as it is displayed in Figure III-19. The HOMO value is linked to the ionization potential (IP) by the fact that IP is the energy needed to ionize the material. To summarize, more the energy of the HOMO is high, more the energy needed to extract an electron from the HOMO is high. In this case, IP is higher for the in-situ film that VPP film.

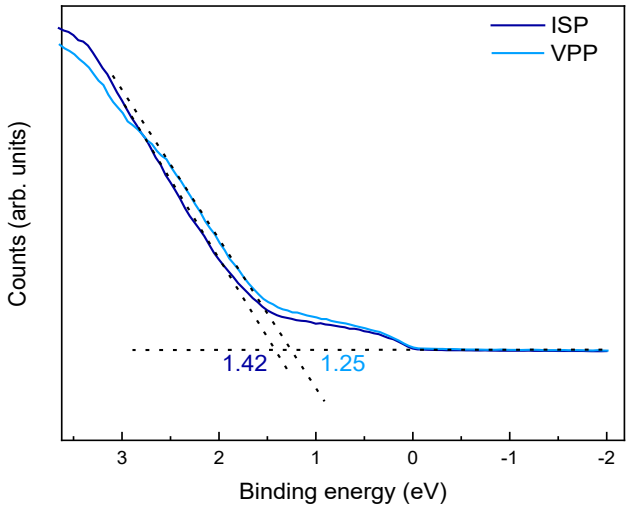

Figure III-19 Calculation of the value of the HOMO level. These values represent the energy gap between HOMO and Fermi level.

The doping level is the first parameter which can influence the IP. In the case of this study, we demonstrated by XPS that the oxidation level is the same for both films, so we cannot take into account this element. Another parameter is the orientation of the crystallites inside the film. Indeed, it was demonstrated by Duhm *et al.* that the IP value changes with the modification of the crystallites orientation. [66]. In the case of PEDOT:Tos, GIXRD showed slightly different structures regarding the polymerization way. Films made by VPP are less crystalline but showed a smaller π-π stacking distance. However, UPS spectra do not show the appearance of a signal related to a change in the orientation of the PEDOT:Tos crystallites, as explained by Sehati *et al.* with the perylene-derivative, PTCDA [59].

V- Conclusion

In this chapter, we focused our study on the two different pathways to polymerize PEDOT:Tos. In-situ chemical polymerization and vapor phase polymerization are the two main routes to obtain PEDOT:Tos films. These syntheses produced films with slightly different structures as it has been demonstrated by AFM and GIXRD. However, analyzing the two types of sample by spectroscopy permits to calculate the same oxidation level of 22 %. The XPS results demonstrated that samples are chemically identical and the polymerization way does not play a role on the chemical structure and the doping.

From a thermoelectric point of view, we observed some differences in the electrical conductivity explained by the fact that π-π stacking distance is smaller for in-situ polymerized films leading to a better hopping and so a better electrical conductivity inside the film. The Seebeck coefficient is not affected by the polymerization as the Seebeck coefficient is relative to the entropy per charge carrier and depends on the oxidation level.

The shape of the density of electronic state of the films has been probed by UPS and are similar. The work functions remain the same with the different polymerization techniques. The transport properties of those PEDOT:Tos thin films does partially depend on the polymerization technique as only the charge carrier mobility and the HOMO level is influenced, resulting in an approximately 34% improvement of the power factor for in-situ-polymerized films.

We can conclude that the properties of PEDOT:Tos thin films does not strongly depend of the polymerization way in contrary to the products used like additives or post treatments as it has been shown in the literature.

To follow up on this chapter, we opted to further study the vapor phase polymerization technique as there is a lack in the literature of deep understanding of the processes inherent to the optimization of the thermoelectric properties for materails produced

by this synthetic route. Accordingly, the following chapter will focus on the modification of the synthetic parameters during the VPP process with a focus on the role of additives and oxidant concentration.

[1] D. M. de Leeuw, P. a. Kraakman, P. F. G. Bongaerts, C. M. J. Mutsaers, and D. B. M. Klaassen, "Electroplating of conductive polymers for the metallization of insulators," *Synth. Met.*, vol. 66, no. 3, pp. 263–273, 1994.

[2] T. Park, C. Park, B. Kim, H. Shin, and E. Kim, "Flexible PEDOT electrodes with large thermoelectric power factors to generate electricity by the touch of fingertips," *Energy Environ. Sci.*, vol. 6, no. 3, p. 788, 2013, doi: 10.1039/c3ee23729j.

[3] B. Winther-Jensen and K. West, "Vapor-phase polymerization of 3,4-ethylenedioxythiophene: A route to highly conducting polymer surface layers," *Macromolecules*, vol. 37, no. 12, pp. 4538–4543, 2004, doi: 10.1021/ma049864l.

[4] A. Mohammadi, M. A. Hasan, B. Liedberg, I. Lundström, and W. R. Salaneck, "Chemical vapour deposition (CVD) of conducting polymers: Polypyrrole," *Synth. Met.*, vol. 14, no. 3, pp. 189–197, 1986, doi: 10.1016/0379-6779(86)90183-9.

[5] P. Hojati-Talemi, C. Bächler, M. Fabretto, P. Murphy, and D. Evans, "Ultrathin polymer films for transparent electrode applications prepared by controlled nucleation," *ACS Appl. Mater. Interfaces*, vol. 5, no. 22, pp. 11654–11660, 2013, doi: 10.1021/am403135p.

[6] H. Gerhard and J. Friedrich, "Poly(alkylenedioxythiophene)s - new, very stable conducting polymers," *Adv. Mater.*, vol. 4, no. 2, pp. 116–118, 1992.

[7] M. Eickenscheidt, E. Singler, and T. Stieglitz, "Pulsed electropolymerization of PEDOT enabling controlled branching," *Polym. J.*, vol. 51, no. 10, pp. 1029–1036, 2019, doi: 10.1038/s41428-019-0213-4.

[8] E. Poverenov, M. Li, A. Bitler, and M. Bendikov, "Major effect of electropolymerization solvent on morphology and electrochromic properties of PEDOT films," *Chem. Mater.*, vol. 22, no. 13, pp. 4019–4025, 2010, doi: 10.1021/cm100561d.

[9] H. Yamato, K. I. Kai, M. Ohwa, T. Asakura, T. Koshiba, and W. Wernet, "Synthesis of free-standing poly(3,4-ethylenedioxythiophene) conducting polymer films on a pilot scale," *Synth. Met.*, vol. 83, no. 2, pp. 125–130, 1996, doi: 10.1016/S0379-6779(97)80065-3.

[10] G. Zotti *et al.*, "Electrochemical and XPS studies toward the role of monomeric and polymeric sulfonate counterions in the synthesis, composition, and

properties of poly(3,4-ethylenedioxythiophene)," *Macromolecules*, vol. 36, no. 9, pp. 3337–3344, 2003, doi: 10.1021/ma021715k.

[11] M. Culebras, C. M. Gómez, and A. Cantarero, "Enhanced thermoelectric performance of PEDOT with different counter-ions optimized by chemical reduction," *J. Mater. Chem. A*, vol. 2, no. 26, pp. 10109–10115, 2014, doi: 10.1039/c4ta01012d.

[12] O. Bubnova *et al.*, "Optimization of the thermoelectric figure of merit in the conducting polymer poly(3,4-ethylenedioxythiophene)," *Nat. Mater.*, vol. 10, no. 6, pp. 429–433, 2011, doi: 10.1038/nmat3012.

[13] H. Wang, U. Ail, R. Gabrielsson, M. Berggren, and X. Crispin, "Ionic Seebeck effect in conducting polymers," *Adv. Energy Mater.*, vol. 5, no. 11, 2015, doi: 10.1002/aenm.201500044.

[14] I. Petsagkourakis *et al.*, "Correlating the Seebeck coefficient of thermoelectric polymer thin films to their charge transport mechanism," *Org. Electron. physics, Mater. Appl.*, vol. 52, no. November 2017, pp. 335–341, 2018, doi: 10.1016/j.orgel.2017.11.018.

[15] M. Fabretto, K. Zuber, C. Hall, and H. J. Griesser, "The role of water in the synthesis and performance of vapour phase polymerised PEDOT electrochromic devices," pp. 7871–7878, 2009, doi: 10.1039/b912324e.

[16] S. G. Im, K. K. Gleason, and E. A. Olivetti, "Doping level and work function control in oxidative chemical vapor deposited poly (3,4-ethylenedioxythiophene)," *Appl. Phys. Lett.*, vol. 90, no. 15, pp. 88–91, 2007, doi: 10.1063/1.2721376.

[17] J. Lu, N. J. Pinto, and A. G. MacDiarmid, "Apparent dependence of conductivity of a conducting polymer on an electric field in a field effect transistor configuration," *J. Appl. Phys.*, vol. 92, no. 10, pp. 6033–6038, 2002, doi: 10.1063/1.1511291.

[18] M. Fabretto, C. Jariego-moncunill, J. Autere, A. Michelmore, R. D. Short, and P. Murphy, "High conductivity PEDOT resulting from glycol / oxidant complex and glycol / polymer intercalation during vacuum vapour phase polymerisation," *Polymer (Guildf).*, vol. 52, no. 8, pp. 1725–1730, 2011, doi: 10.1016/j.polymer.2011.02.028.

[19] K. Z. Xing, M. Fahlman, X. W. Chen, O. Inganäs, and W. R. Salaneck, "The

electronic structure of poly(3,4-ethylene-dioxythiophene): studied by XPS and UPS," *Synth. Met.*, vol. 89, no. 3, pp. 161–165, 1997, doi: 10.1016/S0379-6779(97)81212-X.

[20] P. Mokarian-Tabari, M. Geoghegan, J. R. Howse, S. Y. Heriot, R. L. Thompson, and R. A. L. Jones, "Quantitative evaluation of evaporation rate during spin-coating of polymer blend films: Control of film structure through defined-atmosphere solvent-casting," *Eur. Phys. J. E*, vol. 33, no. 4, pp. 283–289, 2010, doi: 10.1140/epje/i2010-10670-7.

[21] Y. H. Ha, N. Nikolov, S. K. Pollack, J. Mastrangelo, B. D. Martin, and R. Shashidhar, "Towards a transparent, highly conductive poly (3,4-ethylenedioxythiophene)," *Adv. Funct. Mater.*, vol. 14, no. 6, pp. 615–622, 2004, doi: 10.1002/adfm.200305059.

[22] E. G. Kim and J. L. Brédas, "Electronic evolution of poly(3,4-ethylenedioxythiophene) (PEDOT): From the isolated chain to the pristine and heavily doped crystals," *J. Am. Chem. Soc.*, vol. 130, no. 50, pp. 16880–16889, 2008, doi: 10.1021/ja806389b.

[23] K. E. Aasmundtveit, E. J. Samuelsen, L. A. A. Pettersson, O. Inganäs, T. Johansson, and R. Feidenhans'l, "Structure of thin films of poly(3,4-ethylenedioxythiophene)," *Synth. Met.*, vol. 101, no. 1, pp. 561–564, 1999, doi: 10.1016/S0379-6779(98)00315-4.

[24] M. H. Gharahcheshmeh, M. M. Tavakoli, E. F. Gleason, M. T. Robinson, J. Kong, and K. K. Gleason, "Tuning, optimization, and perovskite solar cell device integration of ultrathin poly(3,4-ethylene dioxythiophene) films via a single-step all-dry process," *Sci. Adv.*, vol. 5, no. 11, pp. 1–13, 2019, doi: 10.1126/sciadv.aay0414.

[25] Z. U. Khan *et al.*, "Acido-basic control of the thermoelectric properties of poly(3,4-ethylenedioxythiophene)tosylate (PEDOT-Tos) thin films," *J. Mater. Chem. C*, vol. 3, no. 40, pp. 10616–10623, 2015, doi: 10.1039/c5tc01952d.

[26] I. Petsagkourakis *et al.*, "Structurally-driven enhancement of thermoelectric properties within poly(3,4-ethylenedioxythiophene) thin films," *Sci. Rep.*, vol. 6, no. March, pp. 1–8, 2016, doi: 10.1038/srep30501.

[27] K. Wijeratne, M. Vagin, R. Brooke, and X. Crispin, "Poly(3,4-ethylenedioxythiophene)-tosylate (PEDOT-Tos) electrodes in thermogalvanic

cells," *J. Mater. Chem. A*, vol. 5, no. 2, pp. 19619–19625, 2017, doi: 10.1039/C7TA04891B.

[28] Q. Wei, M. Mukaida, K. Kirihara, Y. Naitoh, and T. Ishida, "Recent Progress on PEDOT-Based Thermoelectric Materials," vol. 8, pp. 732–750, 2015, doi: 10.3390/ma8020732.

[29] A. Weathers *et al.*, "Significant Electronic Thermal Transport in the Conducting Polymer Poly(3,4-ethylenedioxythiophene)," *Adv. Mater.*, vol. 27, no. 12, pp. 2101–2106, Mar. 2015, doi: 10.1002/adma.201404738.

[30] S. Van Reenen and M. Kemerink, "Correcting for contact geometry in Seebeck coefficient measurements of thin film devices," *Org. Electron.*, vol. 15, no. 10, pp. 2250–2255, 2014, doi: 10.1016/j.orgel.2014.06.018.

[31] W. A. Muñoz, S. K. Singh, J. F. Franco-Gonzalez, M. Linares, X. Crispin, and I. V. Zozoulenko, "Insulator to semimetallic transition in conducting polymers," *Phys. Rev. B*, vol. 94, no. 20, pp. 1–8, 2016, doi: 10.1103/PhysRevB.94.205202.

[32] W. A. Muñoz, X. Crispin, M. Fahlman, and I. V. Zozoulenko, "Understanding the Impact of Film Disorder and Local Surface Potential in Ultraviolet Photoelectron Spectroscopy of PEDOT," *Macromol. Rapid Commun.*, vol. 1700533, pp. 1–8, 2017, doi: 10.1002/marc.201700533.

[33] O. Bubnova *et al.*, "Semi-metallic polymers," *Nat. Mater.*, vol. 13, no. 2, pp. 190–194, 2013, doi: 10.1038/nmat3824.

[34] B. Winther-Jensen and K. West, "Vapor-phase polymerization of 3,4-ethylenedioxythiophene: A route to highly conducting polymer surface layers," *Macromolecules*, vol. 37, no. 12, pp. 4538–4543, 2004, doi: 10.1021/ma049864l.

[35] D. Wu *et al.*, "Temperature dependent conductivity of vapor-phase polymerized PEDOT films," *Synth. Met.*, vol. 176, pp. 86–91, 2013, doi: 10.1016/j.synthmet.2013.05.033.

[36] J. Wang, K. Cai, and S. Shen, "Enhanced thermoelectric properties of poly(3,4-ethylenedioxythiophene) thin films treated with H2SO4," *Org. Electron.*, vol. 15, no. 11, pp. 3087–3095, 2014, doi: 10.1016/j.orgel.2014.09.012.

[37] R. Brooke *et al.*, "Effect of oxidant on the performance of conductive polymer films prepared by vacuum vapor phase polymerization for smart window applications," *Smart Mater. Struct.*, vol. 24, no. 3, 2015, doi: 10.1088/0964-

1726/24/3/035016.

[38] H. Goktas, X. Wang, A. Ugur, and K. K. Gleason, "Water-Assisted Vapor Deposition of PEDOT Thin Film," *Macromol. Rapid Commun.*, vol. 36, no. 13, pp. 1283–1289, 2015, doi: 10.1002/marc.201500069.

[39] M. Fabretto, M. Müller, C. Hall, P. Murphy, R. D. Short, and H. J. Griesser, "In-situ QCM-D analysis reveals four distinct stages during vapour phase polymerisation of PEDOT thin films," *Polymer (Guildf).*, vol. 51, no. 8, pp. 1737–1743, 2010, doi: 10.1016/j.polymer.2010.02.019.

[40] J. Metsik *et al.*, "Growth of Poly (3 , 4-ethylenedioxythiophene) Films Prepared by Base-Inhibited Vapor Phase Polymerization," *J. Polym. Sci. Part B Polym. Phys.*, vol. 52, pp. 561–571, 2014, doi: 10.1002/polb.23450.

[41] R. Brooke, P. Cottis, P. Talemi, M. Fabretto, P. Murphy, and D. Evans, "Recent advances in the synthesis of conducting polymers from the vapour phase," *Prog. Mater. Sci.*, vol. 86, pp. 127–146, 2017, doi: 10.1016/j.pmatsci.2017.01.004.

[42] S. Nair, S. Natarajan, and S. H. Kim, "Fabrication of electrically conducting polypyrrole-poly(ethylene oxide) composite nanofibers," *Macromol. Rapid Commun.*, vol. 26, no. 20, pp. 1599–1603, 2005, doi: 10.1002/marc.200500457.

[43] Y. Fu, R. A. Weiss, P. P. Gan, and M. D. Bessette, "Conductive elastomeric foams prepared byin situ vapor phase polymerization of pyrrole and copolymerization of pyrrole and N-methylpyrrole," *Polym. Eng. Sci.*, vol. 38, no. 5, pp. 857–862, 1998, doi: 10.1002/pen.10251.

[44] D. Evans, M. Fabretto, M. Mueller, K. Zuber, R. Short, and P. Murphy, "Structure-directed growth of high conductivity PEDOT from liquid-like oxidant layers during vacuum vapor phase polymerization," *J. Mater. Chem.*, vol. 22, no. 30, p. 14889, 2012, doi: 10.1039/c2jm32281a.

[45] T. Giffney, M. Xie, M. Sartelet, and K. C. Aw, "Vapor phase polymerization of PEDOT on silicone rubber as flexible large strain sensor," *AIMS Mater. Sci.*, vol. 2, no. 4, pp. 414–424, 2015, doi: 10.3934/matersci.2015.4.414.

[46] B. Winther-Jensen *et al.*, "Order-disorder transitions in poly(3,4-ethylenedioxythiophene)," *Polymer (Guildf).*, vol. 49, no. 2, pp. 481–487, 2008, doi: 10.1016/j.polymer.2007.11.055.

[47] T. Le Truong *et al.*, "Poly(3,4-ethylenedioxythiophene) vapor-phase

polymerization on glass substrate for enhanced surface smoothness and electrical conductivity," *Macromol. Res.*, vol. 15, no. 5, pp. 465–468, 2007, doi: 10.1007/bf03218815.

[48] D. Mayevsky, E. Gann, C. J. Garvey, C. R. McNeill, and B. Winther-Jensen, "Decoupling order and conductivity in doped conducting polymers," *Phys. Chem. Chem. Phys.*, vol. 18, no. 28, pp. 19397–19404, 2016, doi: 10.1039/C6CP03307E.

[49] Z. U. Khan *et al.*, "Acido-basic control of the thermoelectric properties of poly(3,4-ethylenedioxythiophene)tosylate (PEDOT-Tos) thin films," *J. Mater. Chem. C*, vol. 3, no. 40, pp. 10616–10623, 2015, doi: 10.1039/C5TC01952D.

[50] J. Wang, K. Cai, H. Song, and S. Shen, "Simultaneously enhanced electrical conductivity and Seebeck coefficient in Poly (3,4-ethylenedioxythiophene) films treated with hydroiodic acid," *Synth. Met.*, vol. 220, pp. 585–590, 2016, doi: 10.1016/j.synthmet.2016.07.023.

[51] A. Sharma *et al.*, "Insights into the Oxidant / Polymer Interfacial Growth of Vapor Phase Polymerized PEDOT Thin Films," vol. 1800594, pp. 1–8, 2018, doi: 10.1002/admi.201800594.

[52] L. Ouyang *et al.*, "The contraction of PEDOT films formed on a macromolecular liquid-like surface," *J. Mater. Chem. C*, vol. 6, no. 3, pp. 654–660, 2018, doi: 10.1039/C7TC04661H.

[53] A. Kahn, "Fermi level, work function and vacuum level," *Mater. Horizons*, vol. 3, no. 1, pp. 7–10, 2016, doi: 10.1039/c5mh00160a.

[54] J. S. Kim, W. Jang, and D. H. Wang, "The investigation of the seebeck effect of the poly(3,4-ethylenedioxythiophene)-tosylate with the various concentrations of an oxidant," *Polymers (Basel).*, vol. 11, no. 1, 2018, doi: 10.3390/polym11010021.

[55] M. Mueller, M. Fabretto, D. Evans, P. Hojati-Talemi, C. Gruber, and P. Murphy, "Vacuum vapour phase polymerization of high conductivity PEDOT: Role of PEG-PPG-PEG, the origin of water, and choice of oxidant," *Polymer (Guildf).*, vol. 53, no. 11, pp. 2146–2151, 2012, doi: 10.1016/j.polymer.2012.03.028.

[56] J. Kim, E. Kim, Y. Won, H. Lee, and K. Suh, "The preparation and characteristics of conductive poly (3 , 4-ethylenedioxythiophene) thin film by vapor-phase polymerization," vol. 139, pp. 485–489, 2003, doi: 10.1016/S0379-6779(03)00202-9.

[57] C. M. Madl, P. N. Kariuki, J. Gendron, L. F. J. Piper, and W. E. Jones, "Vapor phase polymerization of poly (3,4-ethylenedioxythiophene) on flexible substrates for enhanced transparent electrodes," *Synth. Met.*, vol. 161, no. 13–14, pp. 1159–1165, 2011, doi: 10.1016/j.synthmet.2011.03.024.

[58] J. Rivnay, S. C. B. Mannsfeld, C. E. Miller, A. Salleo, and M. F. Toney, "Quantitative determination of organic semiconductor microstructure from the molecular to device scale," *Chem. Rev.*, vol. 112, no. 10, pp. 5488–5519, 2012, doi: 10.1021/cr3001109.

[59] P. Sehati, S. Braun, and M. Fahlman, "Energy level alignment in Au/pentacene/PTCDA trilayer stacks," *Chem. Phys. Lett.*, vol. 583, pp. 38–41, 2013, doi: 10.1016/j.cplett.2013.07.035.

[60] S. Chen, I. Petsagkourakis, N. Spampinato, X. Crispin, and M. P. Jonsson, "Unraveling vertical inhomogeneity in vapour phase polymerized PEDOT:Tos film," *J. Mater. Chem. A*, 2020, doi: 10.1039/d0ta06031c.

[61] M. H. Gharahcheshmeh and K. K. Gleason, "Texture and nanostructural engineering of conjugated conducting and semiconducting polymers," *Mater. Today Adv.*, vol. 8, p. 100086, 2020, doi: 10.1016/j.mtadv.2020.100086.

[62] X. Wang *et al.*, "High electrical conductivity and carrier mobility in oCVD PEDOT thin films by engineered crystallization and acid treatment," *Sci. Adv.*, vol. 4, no. 9, pp. 1–10, 2018, doi: 10.1126/sciadv.aat5780.

[63] J. F. Franco-Gonzalez, N. Rolland, and I. V. Zozoulenko, "Substrate-Dependent Morphology and Its Effect on Electrical Mobility of Doped Poly(3,4-ethylenedioxythiophene) (PEDOT) Thin Films," *ACS Appl. Mater. Interfaces*, vol. 10, no. 34, pp. 29115–29126, 2018, doi: 10.1021/acsami.8b08774.

[64] H. J. Ahonen, J. Lukkari, and J. Kankare, "n- and p-doped poly(3,4-ethylenedioxythiophene): Two electronically conducting states of the polymer," *Macromolecules*, vol. 33, no. 18, pp. 6787–6793, 2000, doi: 10.1021/ma0004312.

[65] E. E. Havinga, C. M. J. Mutsaers, and L. W. Jenneskens, "Absorption properties of alkoxy-substituted thienylene-vinylene oligomers as a function of the doping level," *Chem. Mater.*, vol. 8, no. 3, pp. 769–776, 1996, doi: 10.1021/cm9504551.

[66] S. Duhm *et al.*, "Orientation-dependent ionization energies and interface dipoles in ordered molecular assemblies," *Nat. Mater.*, vol. 7, no. 4, pp. 326–332, 2008,

doi: 10.1038/nmat2119.

IV. TAILORING THE ELECTRONIC PROPERTIES OF VAPOR PHASE POLYMERIZED PEDOT:TOS

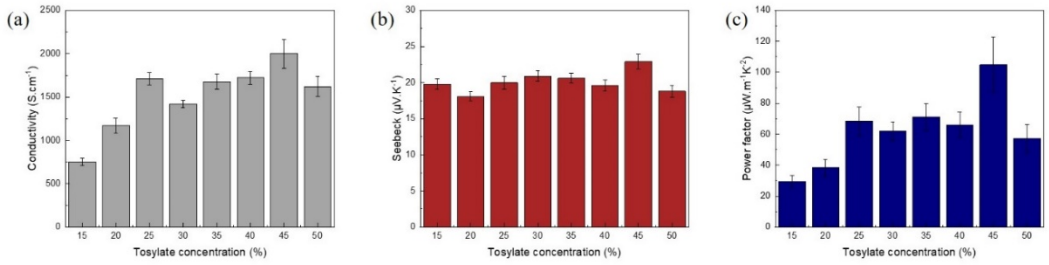

The vapor phase polymerization of PEDOT:Tos is the focus of this particular chapter as the tailoring of the polymerization parameters can afford a fine tuning of the electronic properties of such films. In particular, optimized thermoelectric properties can be obtained by modifying the synthetic parameters such as the oxidant concentration or the additives used during the polymerization. Accordingly, we analyzed the structural and thermoelectric properties depending of these parameters. Besides we also probed the vertical structural and electronic stratification of the PEDOT:Tos films obtained by VPP in order to probe the homogeneity of the film over the film thickness.

I- INTRODUCTION

Vapor phase polymerization (VPP) was developed by Winther-Jensen and his team in 2004 to develop a new route for the polymerization of EDOT in order to control the growth of PEDOT:Tos films [1]. They based their study on the pioneering work of Mohammadi *et al.* who polymerized polypyrrole using $FeCl_3$ or H_2O_2 as oxidants with a Chemical Vapor Deposition (CVD) process [2]. By this technique, they were able to reach conductivity exceeding 1000 S/cm. As mentioned in the previous chapters, it is possible to play on several extrinsic (temperature, pressure, etc.) and intrinsic (concentration, additives, oxidant, etc.) parameters to polymerize EDOT in vapor phase. All these parameters can be tuned using the appropriate set-up and we have developed a VPP set-up allowing us to play mainly on the temperature and the concentration of reactants.

Indeed, the addition of additives, and especially pyridine, has been shown to enhance the electrical conductivity of PEDOT by decreasing the pH of the oxidant solution. Pyridine inhibits undesirable acidic side reactions leading to an increase of the molecular weight of PEDOT [1]. Le Truong *et al.* have subsequently showed that the electrical conductivity of PEDOT:Tos films can be tuned with varying the amount of pyridine. [3]. But pyridine is not the only one additive used in the literature. Block copolymers can also be used in order to guide the crystallization of the PEDOT.

VPP dedicated to the formation of PEDOT:Tos films is rather a novel methodology and it is thus mandatory to gain further insight into its mechanisms in order to produce films with the optimal thermoelectric properties. One of the point is to understand the growth mechanism of the film which is still under discussion in the community. Probing the film during its formation will allow us to better understand the structure/property relationships leading to enhanced thermoelectric properties.

In order to increase the thermoelectric properties of PEDOT films, some studies played on the quantity of oxidant in the VPP chamber [4]–[6]. Adding more counterions permits to polymerize a higher amount of EDOT leading to thicker PEDOT films. In another hand, adding more oxidant permits to decrease the sheet resistance of the films which are smoother. Nevertheless, the increase of the thickness and the decrease of the sheet resistance do not allow to obtain a better electrical conductivity

in every case as the electrical conductivity is conversely proportional to the product between the thickness and the sheet resistance.

In this chapter, we will keep constant the extrinsic parameters of the VPP and only play on the properties of PEDOT:Tos thin films by tuning the additives and oxidant concentration.

II- PROPERTIES OF VAPOR PHASE POLYMERIZED FILMS, ROLE OF ADDITIVES

Vapor phase polymerized films are synthetized when an oxidant solution is exposed to EDOT vapors. The composition of the oxidant solution plays a major role in the formation of PEDOT films and several studies revealed that additives can be used in order to obtain smooth films with good electrical conductivity and Seebeck coefficient. Among the additives used in the literature, copolymers containing PEG and PPG are the most common [7]–[10]. Zuber *et al.* vapor phase polymerized EDOT with PEG-*stat*-PPG in order to decrease the number of tosylate crystallites inside their films [11]. By drastically reducing the number of crystallites, smoother PEDOT films could be obtained, and an electrical conductivity of 761 $S.cm^{-1}$ was reached by adding 5 wt% of copolymer inside the oxidant solution.

Pyridine can also be used as additive for the formation of PEDOT films by VPP. Adding pyridine allows one to slow down the polymerization of EDOT leading to an increase of the chain molecular weight due to a better control of the polymerization process (less transfer reactions). Such increase of the PEDOT molecular weight with fewer sequence defects facilitates chain packing and charge transport leading to a macroscopic increase of the electrical conductivity.

Alternatively, high boiling point solvents can be added to further increase the crystallinity of PEDOT:Tos films by decreasing the evaporation rate of the solvent acting thus as a plasticizer. [12]. Petsagkourakis *et al.* studied the effect of high boiling point solvent on the properties of in-situ polymerized PEDOT:Tos films. They demonstrated that the addition of DMF or DMSO in the oxidant solution permits to increase the electrical conductivity up to 640 ± 10 $S.cm^{-1}$. Later, they mixed pyridine and DMSO to take advantage of the both effects in order to reach conductivity of 1220 ± 30 $S.cm^{-1}$ [13].

In our study, we choose to evaluate the effect of the addition of DMSO and pyridine during the VPP process. To the best of our knowledge, the use of both additives have not been reported in the literature and could be highly beneficial to the electronic properties as regards to the results obtained for ISP PEDOT:Tos films.

II-1- Formation of PEDOT:Tos films and structural properties

II-1-a- PEDOT:Tos synthesis

- *Films preparation*

In order to compare the effect of additives, two oxidant solutions containing 40% of tosylate were made, one without additives and another one with the addition of pyridine and DMSO. Indeed, as suggested by Le Truong *et al.*, pyridine coordinates with the $Fe(Tos)_3$ substituting the alcohol ligands via the unbounded nitrogen electrons, as presented in Figure IV-1 (a) (2 and 3). This leads to a better control of the polymerization kinetics. The unbounded electrons of pyridine could also interact with the radical cation of EDOT during the VPP reaction, Figure IV-1 (a) (4), further stabilizing the active center. In another hand, DMSO permits to plasticize the PEDOT:Tos film leading to improved crystallinity [12]. Such effect is displayed in Figure IV-1 (b). VPP were carried out for 5 minutes at 70°C on silicon substrate coated with chromium and gold for further 4-points electrical characterization (see chapter 2 for details).

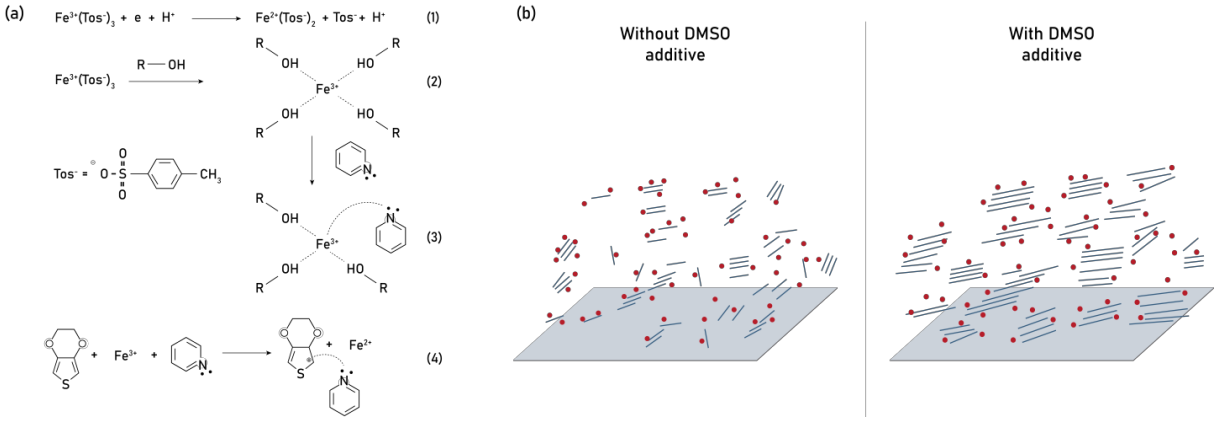

Figure IV-1 (a) Mechanism of effect of the of pyridine on PEDOT polymerization proposed by Le Truong et al. (b) Effect of the DMSO on the PEDOT polymerization. Blue lines and red dots represent PEDOT and tosylate respectively.

- *Comparison of the composition*

Immediately after the VPP process, we observed films with different colors which means that the thickness of samples with or without additives are not the same. The

films without additive are dark blue with macroscopic irregularities while films processed with additives are light blue. Such observation means that the PEDOT:Tos film growth did not happen following the same kinetics and potential modifications in the film composition should be accordingly probed. XPS measurements were thus performed and it is evident from Figure IV-2 that the contribution of tosylate with regard to PEDOT is less important in the case of the films without additives. An oxidation degree of 14.9% was determined for films without additives while it is 22 % for PEDOT:Tos films processed with pyridine and DMSO. The additives play thus a key-role in the doping of PEDOT through their ability to slow down the EDOT polymerization (resulting in macroscopically thinner film) while inhibiting the oxidant crystallization. Both effects allowed an improved doping of the PEDOT chains.

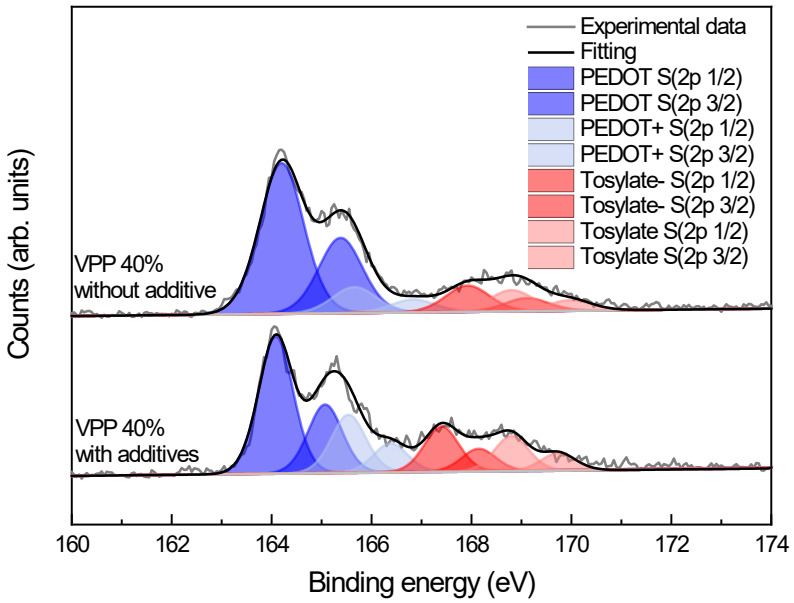

Figure IV-2 XPS S2p spectra of PEDOT:Tos films with and without additives made by VPP. Blue and red areas represent the signals linked to S2p in PEDOT and S2p in tosylate, respectively.

II-1-B- Morphological characterization

As previously shown, the use of additives permits to inhibit the crystallization of tosylate, which is detrimental to the PEDOT crystallization and doping. Macroscopically, this effect is already observed since the films without additives are not homogeneous with some cracks due to the fast polymerization. The films were analyzed by AFM and the AFM images are displayed Figure IV-3. These three images

have been taken on three different films. The differences between these AFM images are quite important and attributed to the non-homogeneity of PEDOT:Tos polymerized without additives. The square roughness varies from 4.2 to 28.9 nm depending of the observed area

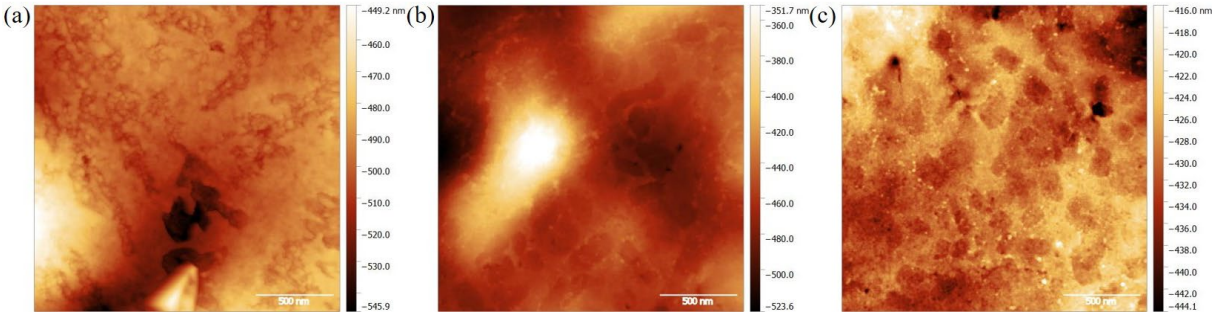

Figure IV-3 Topological AFM images 2×2 µm² of three samples of VPP PEDOT:Tos films made without additives with square roughness of (a) 14.2 nm (b) 28.9 nm (c) 4.2 nm.

Figure IV-4 further compares films with and without additives. The characteristic dot-like structure of PEDOT:Tos is clearly distinguishable in the image of PEDOT:Tos with additives and is in accordance with the structure observed for PEDOT:Tos films processed by ISP [14]. These structural discrepancies are foreseen to affect the microscopic structure of the PEDOT:Tos and the conformation of polymer chains. As the electrical conductivity is inherent to the ordering of polymer chains, a microscopic and macroscopic disruptive structure is expected to lead a worse electrical conductivity for films without additives.

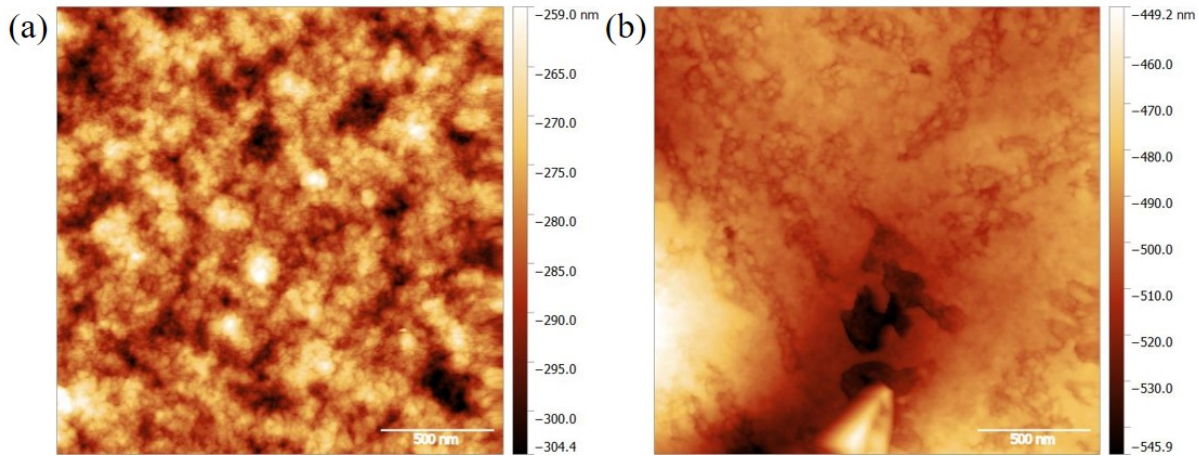

Figure IV-4 Topological AFM images 2×2 µm² of VPP PEDOT:Tos films made (a) with additives and (b) without additives.

II-2 THERMOELECTRIC PROPERTIES

The PEDOT:Tos films were made on intrinsic silicon coated with gold contacts in order to measure the resistance with 4-points probes apparatus. Without such contacts, it was not possible to measure a proper resistive behavior for films prepared without additives (i.e. a linear I-V curve) due to the roughness of the PEDOT:Tos films leading to high contact resistances. The electrical conductivity was subsequently obtained by measuring the sheet resistance and the thickness of at least three films. It is noteworthy that the films without additives are almost ten times thicker than the films with additives. This difference is linked to the reactivity of $Fe(Tos)_3$ without inhibitor which is highly inhibited by the addition of pyridine [3]. Indeed the pH of the oxidant solution with pyridine is drastically increased, thus decreasing the redox activity of $Fe(Tos)_3$ during the EDOT polymerization [1]. The Seebeck coefficient was measured on our home-made Seebeck set-up, as presented in the previous chapter, on PEDOT:Tos films deposited on glass substrate with gold contacts. The thermoelectric results are displayed in Figure IV-5 for PEDOT:Tos films with and without additives.

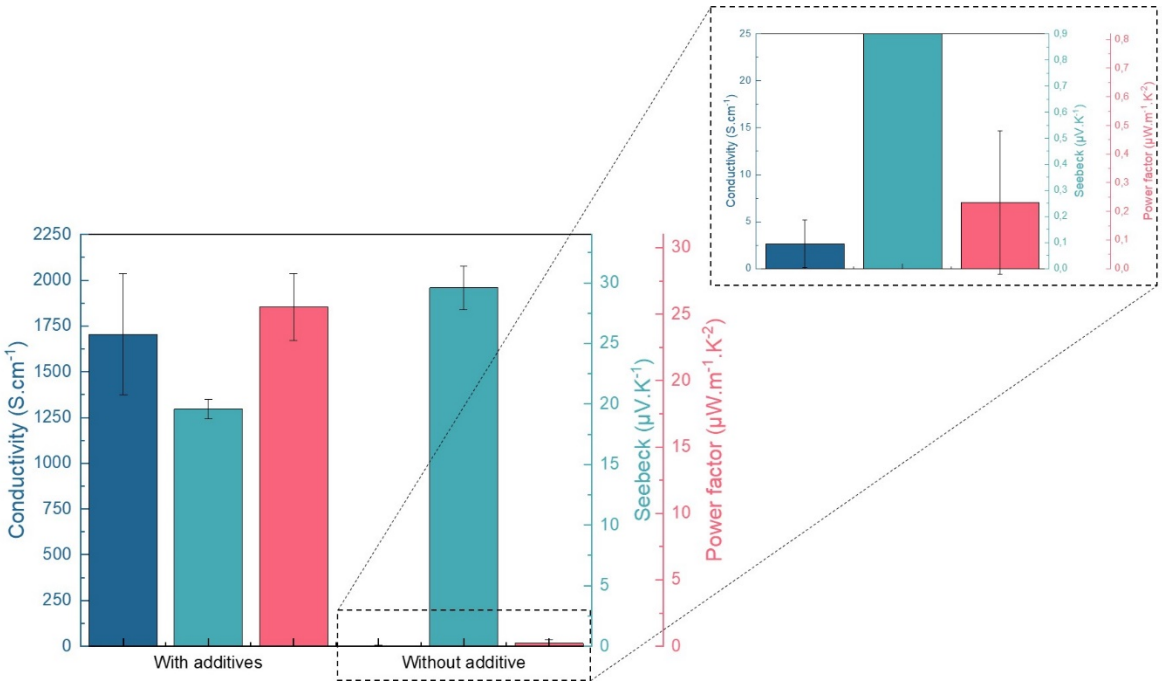

Figure IV-5 Thermoelectric properties of PEDOT:Tos films made by VPP with and without additives. The electrical conductivity, the Seebeck coefficient and the power factor are represented in dark blue, light blue and pink respectively.

The electrical conductivity of PEDOT:Tos films with additives is relatively high, 1705 ± 331.6 $S.cm^{-1}$ with regard to the one without additives, 2.6 ± 2.5 $S.cm^{-1}$. The large uncertainties are linked to the corrugated surface of the films. Contrary to electrical conductivity, the Seebeck coefficient is higher in the case of PEDOT:Tos without additives. As electrical conductivity and Seebeck coefficient have an antagonist behavior, decreasing the electrical conductivity leads to an increase of the Seebeck coefficient. These results lead to a power factor hundred time higher when additives are added inside the solution of oxidant. Pyridine and DMSO are thus highly beneficial in order to obtain a better PEDOT:Tos thermoelectric material.

II-3- ELECTRONIC PROPERTIES

The electronic properties of the films were subsequently probed by UPS measurements. A WF of 4.2 eV was determined for both types of PEDOT:Tos films disregarding the addition or not of additives, as shown in Figure IV-6 (a). However, despite the same WF, the spectra are different. First the "bumping" region linked to spectral feature of the DoS is different meaning that electronic states are not distributed in the same way. This result is directly linked to the charge localization on the PEDOT:Tos chains. Moreover, the characteristic semi-metallic behavior is not clearly observed for films without additives with little or no electronic states near to the Fermi level, as shown in Figure IV-6 (b).

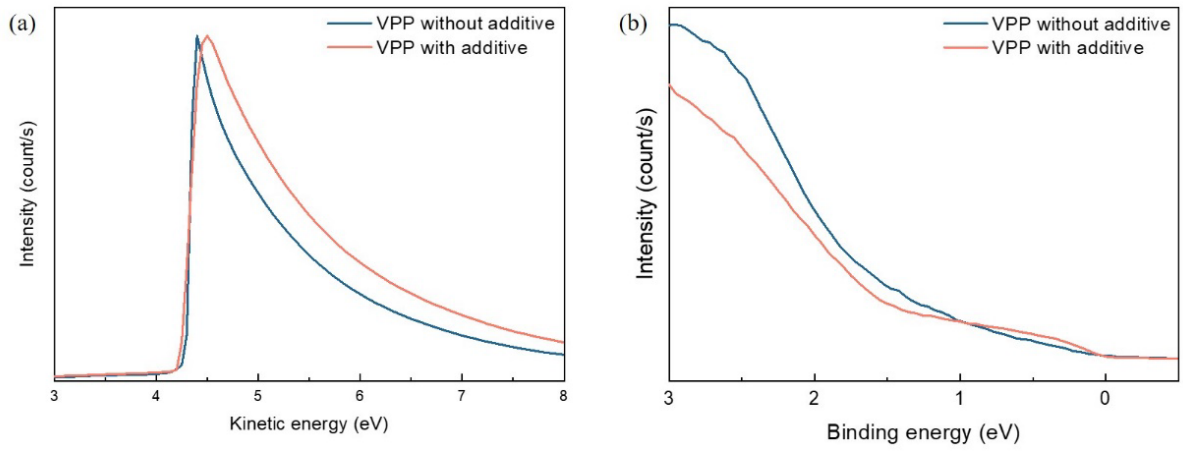

Figure IV-6 UPS spectra of the PEDOT:Tos films made by VPP with and without additives. (a) Second electron cut-off (b) Valence band.

According to the Mott's formula, the slope of the density of states at the Fermi level should be proportional to the Seebeck coefficient. However, the orientation of PEDOT:Tos crystallites influences the DoS at Fermi level [15] and as it has been shown previously, the distribution of the tosylate participates to the broadening of the tail at E_F. As the film without additive is non-homogeneous and less doped than the film with additives, DoS features are not similar to a "normal doped" PEDOT:Tos.

The valence band tail can be roughly approximated by a Gaussian function, revealing the disorder character of the counterions distribution along the polymer chains As presented in Figure IV-7, Gaussian fits have been performed close to the Fermi energy. Analyzing the fits, with quality criteria R > 0.994, leads to FWHM values of 0.48 ± 0.02 eV and 0.85 ± 0.09 eV for VPP films with and without additives, respectively. This is lower than the expected broadening (1 eV) and higher than the DoS broadening (0.1 eV) deduced by other transport analysis, consistent with the expected DoS hidden signature [15]. Such close and slightly overlapping values with respect to the uncertainties suggest different disorder characters of the Tos^- distribution with a higher trend to disorder in the film without additives. Nevertheless, the behavior around the Fermi level is also dependent of the oxidation level which is different for films with and without additives. Thus, the observed differences between the DoS signature could also be related to the oxidation level.

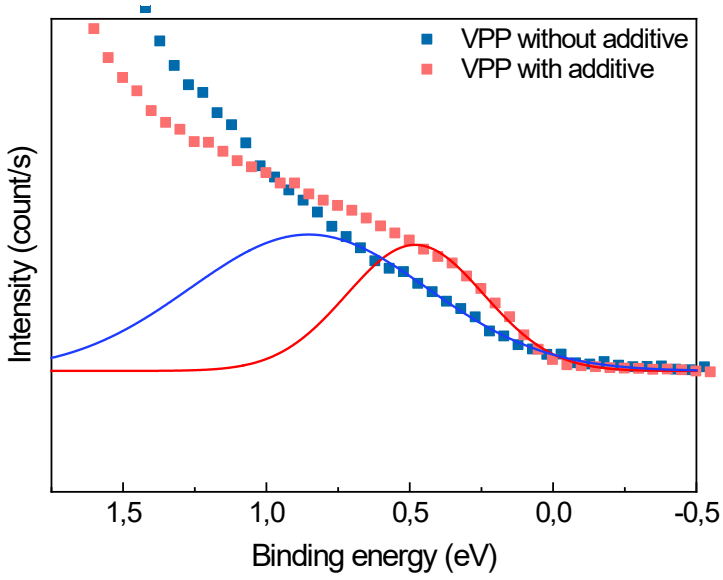

Figure IV-7 Gaussian fits of the valence band tail showing the broadening of the DoS tail around the Fermi level.

III- EFFECT OF OXIDANT CONCENTRATION

Vapor phase polymerization allows to play on various parameters to obtain PEDOT:Tos films. As it has been shown in the previous chapter, the conditions of VPP and particularly the polymerization temperature have a strong influence on the electrical conductivity of polymerized films and can be optimized in order to reach the best electrical conductivity. As shown in the first part of this chapter, another important parameter is the presence or not of additives. When pyridine and DMSO are added to the oxidant solution, PEDOT:Tos electrical conductivity can reach thousands of $S.cm^{-1}$. The role of additives is to allow a better chain packing of the crystalline PEDOT:Tos phase which subsequently facilitates the conduction. Another important parameter is the concentration of oxidant. Kim *et al.* studied the effect of oxidant solution concentration on the properties of PEDOT:Tos films [16]. Oxidant solution concentrations from 1 to 80 wt% were studied. They concluded that increasing the amount of tosylate leads to an increase of both the electrical conductivity (from 2.7×10^{-5} to 0.96 $S.cm^{-1}$) and the oxidation degree. In their study, no pyridine was added which explains the low electrical conductivity obtained.

In our work, we decided to evaluate the impact of the concentration of tosylate on vapor phase polymerized PEDOT:Tos films. As the oxidant used is the commercially available Clevios from Heraeus with a concentration of 54 wt.%, we decided to vary the concentration from 15 to 50 wt.%.

III-1- PEDOT:TOS FILMS MADE WITH VARIOUS OXIDANT SOLUTION CONCENTRATION

III-1-A- FORMATION OF PEDOT:TOS THIN FILMS

Clevios C-B 54 was bought from Heraeus and consists of a solution of 54 wt.% of Iron tosylate in butanol. 8 solutions with concentrations from 15 to 50 wt.% were prepared from the stock Clevios solution with the addition of pyridine and DMSO. The VPP conditions were kept constant for all samples: the tosylate solutions were deposited on glass or silicon substrates coated with gold contacts and VPP was carried out during 5 min at 70°C under vacuum.

XPS measurements were performed in an ultra-high vacuum chamber with a monochromatic X-rays Al source. Highly resolved scans of carbon, oxygen and sulfur atoms were carried out. Sulfur scans were analyzed to determine the oxidation level of PEDOT:Tos for each concentration. As the experiments were not done the same day, the vacuum conditions can slightly change which can affect the average intensity of the spectra. XPS spectra of these samples are displayed in Figure IV-8 and the doping level was evaluated following the procedure already described. Interestingly, an doping level of 22.3 ± 0.6 % was retrieved for all the PEDOT:Tos films which decoupled clearly the oxidant concentration from the resulting oxidation degree of the PEDOT:Tos.

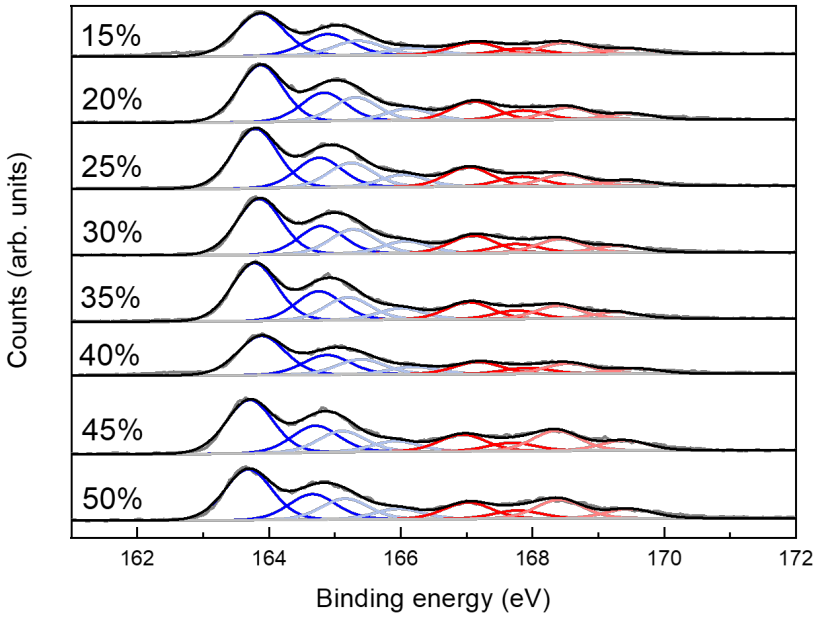

Figure IV-8 XPS S2p spectra of PEDOT:Tos film vapor phase polymerized with a concentration of oxidant from 15 to 40%. Blue and red curves represent the signals linked to S2p in PEDOT and S2p in tosylate, respectively.

The oxidation level is thus not affected by the amount of oxidant meaning that the tosylate is always in excess as compared to EDOT during the film formation. Finally, the concentration of tosylate will only play on the thickness of the film by allowing further growth of PEDOT material.

III-1-b- Thermoelectric and electronic properties of PEDOT:Tos thin films

While several studies focused on increasing electrical conductivity and Seebeck coefficient by adding additives or post-treating the films, the role of the oxidant concentration on the electronic properties has not been studied into details. Brooke *et al.* vapor phase polymerized EDOT with multiple concentration of iron trifluoromethane sulfonate counter-ion ($Fe(OTf)_3$) [17]. They varied the amount of $Fe(OTf)_3$ from 3 to 11.5 wt.% and noticed a decrease of electrical conductivity with the increase of the oxidant concentration. This result was explained by the increase of the sample thickness with the increase of oxidant concentration. As conductivity is inversely proportional to the thickness, thicker the films are, lower the electrical conductivity is.

Increasing the amount of oxidant for PEDOT:Tos obtained by VPP leads to the same conclusion concerning the evolution of the thickness. The thickness varies from 63 ± 3 nm, for 15% oxidant concentration, to 443 ± 6 nm, for 50% oxidant concentration. Adding more tosylate permits to faster polymerize EDOT and so create more and more PEDOT layers. The electrical conductivity and Seebeck coefficient have been measured for each film and the power factor was deduced from these values. As displayed in Figure IV-9 (a), the electrical conductivity increases with the increase of tosylate concentration to reach a maximum for 45% of oxidant concentration with a conductivity of 2001 ± 166 $S.cm^{-1}$. This value is higher than the ones reported for PEDOT:Tos films made by vapor phase polymerization by Winther-Jensen *et al* [1], [18] but still lower than the best reported value obtained by Hojati-Talemi *et al.* who reached 3305 $S.cm^{-1}$ [9]. As far as we know, no studies on VPP PEDOT:Tos reports the use of pyridine and DMSO together. The minimum electrical conductivity value was found for PEDOT:Tos with 15% of tosylate, 752 ± 42 $S.cm^{-1}$. At this concentration, the final thickness of the film is low which, combined with a short polymerization time, induces a higher sheet resistance probably linked to a lower crystallinity of the film. The Seebeck coefficient does not vary with the increase of oxidant concentration with an average value of 20.1 ± 0.8 $\mu V.K^{-1}$ which is in the order of magnitude of PEDOT:Tos material [8], [19].

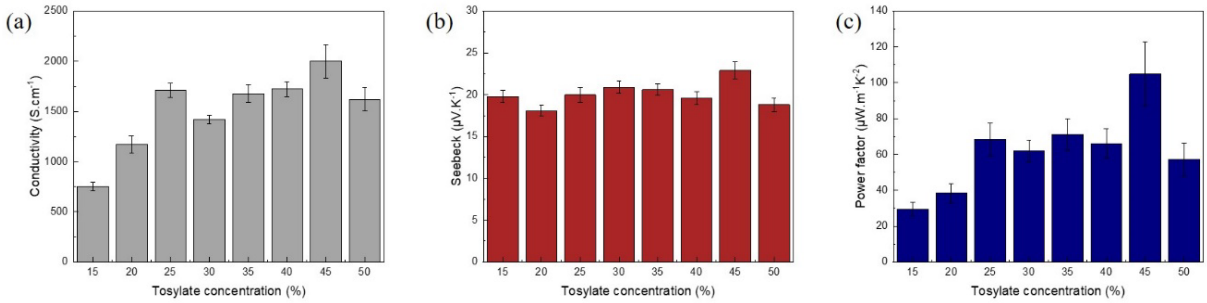

Figure IV-9 Thermoelectric properties of PEDOT:Tos thin films dependent of the tosylate concentration (a) electrical conductivity (b) Seebeck coefficient (c) power factor

As the power factor is the product between the square of the Seebeck coefficient and the electrical conductivity, the variations are mostly due to the variation of the Seebeck coefficient. The maximum power factor has been found to be 105 ± 18 $\mu W.m^{-1}K^{-2}$ for 45% of oxidant concentration, higher than other PEDOT:Tos films made by VPP [20]. To the best of our knowledge, this value is the highest reported in the literature for PEDOT:Tos thin film directly after polymerization. Nevertheless, higher values have been reported for PEDOT:Tos films post-treated by strong acids [8], [21].

III-2- ELECTRONIC PROPERTIES VERSUS OXIDANT CONCENTRATION

The concentration of oxidant has an effect on the electrical conductivity of PEDOT:Tos without influencing the Seebeck coefficient. These results were further confirmed by UPS measurements. The work function of the material is linked to the interface between the substrate and the film, remain the same for 20 to 50% of oxidant, as shown in Figure IV-10 (a). The spectra for a concentration of 15% is nevertheless different. This difference can be attributed to the low thickness of the film which allows to probe the dipole formation at the silicon-film interface. In this last case, the signal from the substrate contributes to the signal of PEDOT:Tos. As the WF of silicon is in the same range than PEDOT ones, a small shift can be observed.

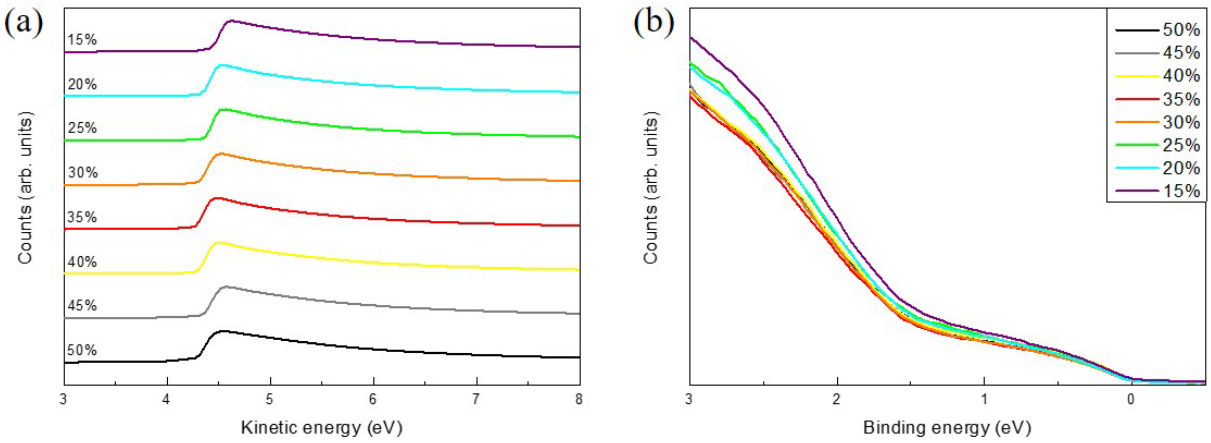

Figure IV-10 UPS spectra of PEDOT:Tos films made by VPP with different oxidant concentration. (a) Second electron cut-off (b) Valence band.

The HOMO level has been calculated for each concentration and was determined to be constant for all samples, i.e. -1.23 eV. This result indicates that despite the differences in conductivity and thickness, the electronic structure seems to be the same for each oxidant concentration. According to the Mott's formula, the slope at Fermi level is proportional to the Seebeck coefficient but according to Muñoz *et al.*, for PEDOT:Tos, the broadening of the tail at Fermi level is influenced by the irregular distribution of the anions on the PEDOT chains [15]. If we compare this slope for each oxidant concentration, we observe that the slope is comparable for each samples which confirms the results obtained from the direct measurement of the Seebeck coefficient: the Seebeck coefficient does not vary with the oxidant concentration. However, the broadening of the tail is not exactly the same with a slight difference for samples made from a low concentration of tosylate. Based on the lower electrical conductivity and the broadening of the tail, we can make the hypothesis that at low concentration of tosylate, PEDOT:Tos films are more disordered. Regarding to UPS measurements, we can conclude that PEDOT:Tos films made by VPP with various oxidant concentration have the same electronic properties.

IV- Through the thickness of PEDOT:Tos

After analyzing the effects of additives and oxidant concentration in the previous parts, we concluded that additives are important to obtain homogeneous films with high electrical conductivity. In this following part, we will focus on the homogeneity along the thickness of PEDOT:Tos films. Some studies have been performed to understand how PEDOT:Tos film grows during the VPP, with two proposed mechanisms (top-down or bottom-up approaches) [22]–[24]. A method to understand the growth of PEDOT:Tos films by VPP is to probe the thermoelectric properties during the polymerization. Metsik *et al.* measured the sheet resistance during the VPP with an home-made VPP set-up connected to electrical probers [25]. They concluded that while the sheet resistance of the film decreases with the advance of the polymerization process, this effect is counterbalanced by the rapid increase of the film thickness. Accordingly, lower electrical conductivities were recorded with the advance of the polymerization process. Besides, they also noticed that higher temperatures of VPP were detrimental to the electrical conductivity. More recently, Chen *et al.* investigated the properties of PEDOT:Tos films by studying the top surface (PEDOT:Tos in contact with air) and the bottom surface (PEDOT:Tos in contact with the substrate). By using a combination of XPS, GIWAXS, AFM and UPS, they concluded that PEDOT:Tos films with PEG–*b*-PPG–*b*-PEG as additives are not homogeneous during the growth process [26]. They found that the films are constituted of several layers of PEDOT:Tos with different degrees of arrangement. In this part, we will focus on the morphological and electronic properties of the bottom and top surfaces to probe the homogeneity of PEDOT:Tos films along the thickness.

IV-1- Method

As discussed in the chapter 2, contradictory reports about PEDOT:Tos film growth by VPP are found in the literature. VPP is described as either a top-down or a bottom-up process; i.e. the vapor phase polymerized film was reported to growth either inside the oxidant layer or at the oxidant/air interface. In order to probe the properties of PEDOT:Tos films over its thickness, we decided to implement a methodology allowing

us to recover free-standing PEDOT:Tos films in order to study both interfaces. Taking into account that a thin residual oxidant layer is still present at the bottom interface of the PEDOT:Tos film, the films were immerged in an ethanol bath leading to the dissolution of this thin layer. Two methods were further used to recover the free-standing films and are displayed in Figure IV-11. The first method consists of recovering a "flipped" film on a microscope slide to probe the conductivity and the surface morphology, as shown in Figure IV-11 (a). The second one consists of peeling the film from the substrate with a tweezer, flipping it and depositing it on another substrate, as shown in Figure IV-11 (b). After such process, the films were removed from the ethanol bath and dried with a nitrogen gun.

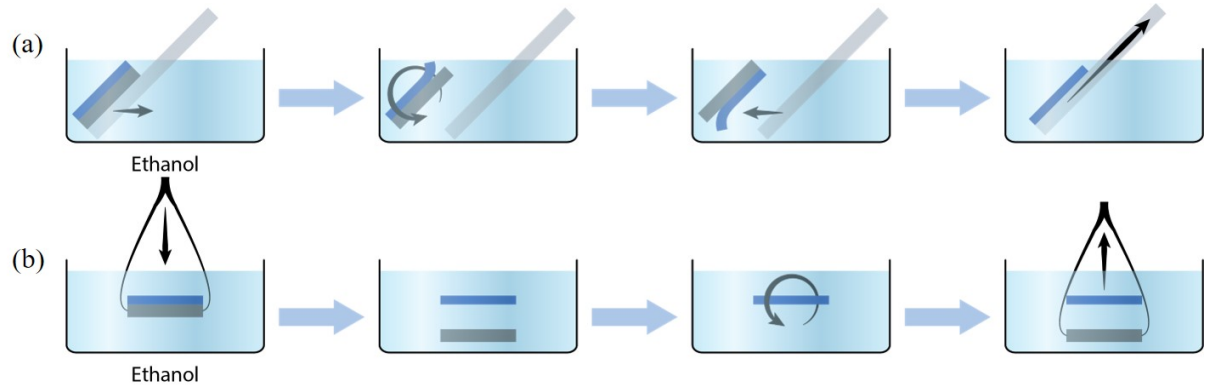

Figure IV-11 Methods to get back PEDOT:Tos film after VPP (a) the first method consists of flipping the film with the substrate on a microscope slide and wait for the substrate to fall (b) the second method consists of detaching the film from the substrate, flipping it and put it in another substrate.

IV-2- Structural and electronic properties

In the following parts, top surface and bottom surface will refer to the surface of the film in contact with air and in contact with the substrate, respectively.

IV-2-a- Structural properties

The PEDOT:Tos morphology is known to be composed of small spherical dots [20]. The structural properties of the top and bottom surfaces were analyzed by AFM in order to better apprehend morphological changes during the film growth. The top surface, displayed in Figure IV-12 (a), is composed of a rather homogeneous layer of sintered dots as seen in previous chapters. Notwithstanding possible damages from the

flipping procedure, the bottom surface is drastically different with a sponge-like structure which can be attributed to the specific growth mechanism of the film from the top interface to the bottom one.

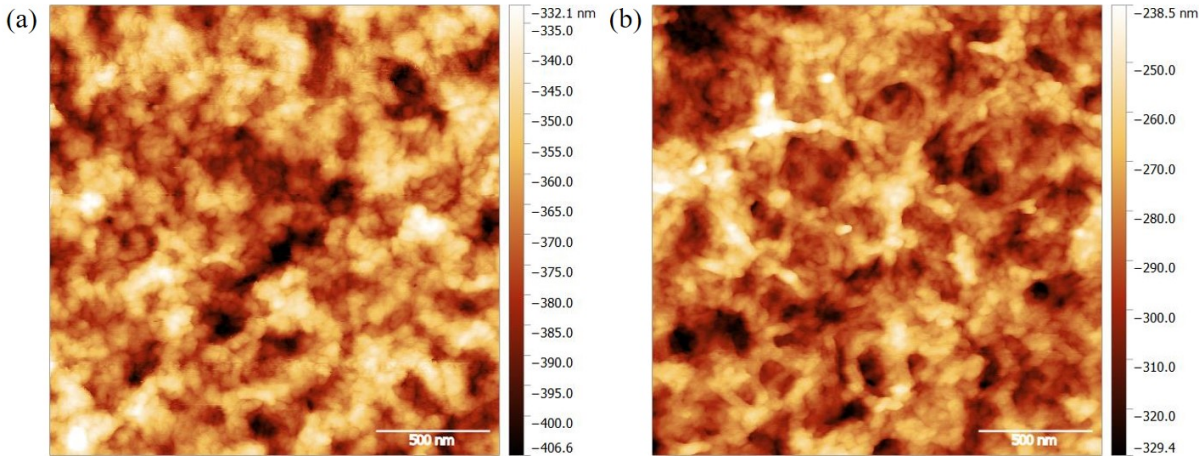

Figure IV-12 AFM topographical images 2×2 µm² of PEDOT:Tos (a) top surface (b) bottom surface.

In order to definitely discard that the visualized structure is linked to the flipping procedure, the substrate where the film where pilled-off was analyzed by AFM. The resulting image is displayed in Figure IV-13. Some dots of 60 nm were found on the silicon which can correspond to the holes found in the bottom surface.

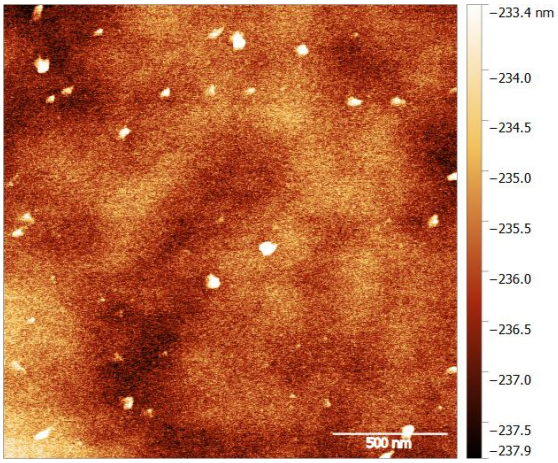

Figure IV-13 AFM topographical images 2×2 µm² of silicon after the removal of PEDOT:Tos film. The small dots can correspond to PEDOT:Tos particles.

The dots on the surface can correspond to pieces of PEDOT:Tos film but also to silicon dust. In order to confirm that, XPS measurements were performed on a clean silicon

substrate and on the substrate after the removal of PEDOT:Tos film. The survey spectra were recorded to check the presence or absence of any compound of PEDOT:Tos (Sulfur, Carbon or Oxygen). In Figure IV-14 (a), the signal from oxygen appears, around 528 eV, in both cases coming from the native SiO_2 layer on the top of silicon substrate. In the case of carbon, a signal appears but only for the silicon after removal, around 585 eV. The last compound of PEDOT:Tos is sulfur. Having a closer look to the region where the signal can appear, in Figure IV-14 (b), we can see that there is no difference between the two substrates.

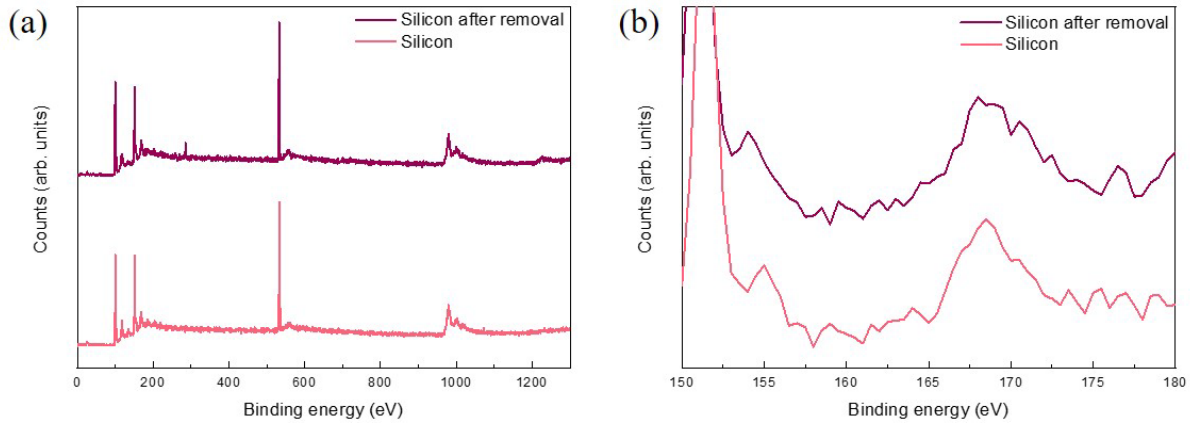

Figure IV-14 XPS measurements of clean silicon (pink) and silicon after removal (purple). (a) Survey spectrum. (b) Zoom on the region corresponding to the sulfur signal.

Sulfur is the element which can permit to confirm the presence of PEDOT:Tos. In Figure IV-14 (b), the region of sulfur signal has been scanned and shows a small peak which is present for both silicon substrates. This peak is then attributed to background noise. These spectra permit to deduce that no PEDOT:Tos is present on the surface of silicon after the removal of the film and the small dots on the surface are not related to PEDOT:Tos materials.

Based on the previous results, the sponge like structure could be attributed on the growth mechanism of VPP PEDOT:Tos film. Indeed, as the EDOT vapors reach the oxidant layer, the growth of the film appears to be an island growth mechanism. EDOT vapors polymerized at many nucleation points on the tosylate layer, leading to the formation of PEDOT:Tos islands during the growth process. Later on, the islands

started to connect between each other leading to a homogenous film at the top surface. As the VPP process is fast, the first complete layer is on top of an incomplete layer which can explain the resulting morphology of the bottom interface.

XPS measurements were also used to probe the oxidation level at the top and bottom interfaces. Highly resolved scans of sulfur are shown in Figure IV-15. The oxidation level was calculated taking into account the signals from PEDOT (blue areas) and the signal of reacted tosylate (darker red areas). The oxidation levels for the top surface and the bottom surface are 25 % and 25.8 %, respectively. The calculation permits to say that 1 EDOT unit over 4 is doped by the tosylate as it has been seen in the previous chapter for VPP films. Interestingly, this result confirms that PEDOT doping appears to be constant over the film thickness.

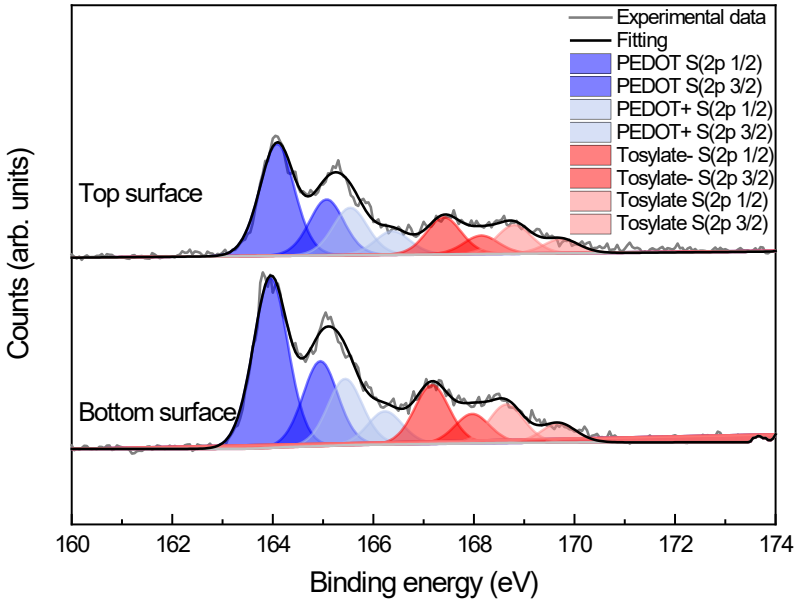

Figure IV-15 XPS S2p spectra of top and bottom surfaces of PEDOT:Tos film vapor phase polymerized. Blue and red areas represent the signals linked to S2p in PEDOT and S2p in tosylate, respectively.

IV-2-B- Electronic properties

As the composition of the film appears homogeneous, the electronic structure should be homogeneous along the thickness. UPS measurements have been done in order to probe the WF and the valence band at the two interfaces. The WFs at the top surface and the bottom surface are the same (4.1 eV), as displayed in Figure IV-16 (a). This

result demonstrates that the contact with the substrate does not change the energy needed to extract an electron from the HOMO level and thus the surface electronic state is the same for both surfaces. Having a closer look to the valence band, as shown in Figure IV-16 (b), the HOMO level is the same at both interfaces. Besides a semi-metallic behavior can also be found at both interfaces as electronic states near the Fermi level are observable on both UPS spectra.

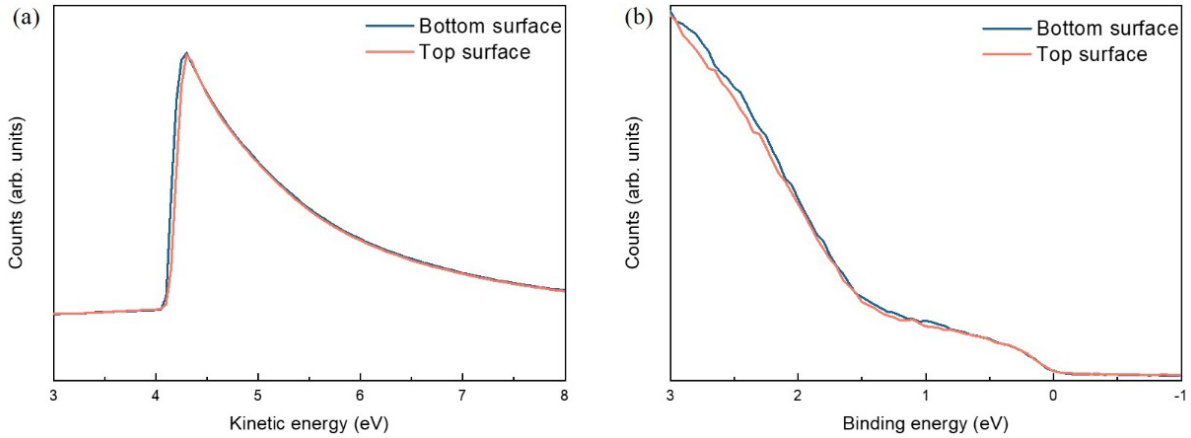

Figure IV-16 UPS spectra of the top surface and bottom surface of PEDOT:Tos films made by VPP. (a) Second electron cut-off (b) Valence band.

Finally, we can conclude that all the probed properties reveal that the PEDOT:Tos film is the same along its thickness. No difference was found in terms of composition or electronic structure as shown by XPS and UPS. The morphology is not the same at both interfaces as shown by AFM. We can make a hypothesis on the growth process of PEDOT:Tos by VPP according to a nucleation and growth process. Moreover, this study permits to understand that the formation of the film occurs between the oxidant layer and the surface of this layer and not at the interface oxidant-substrate.

V- Conclusion

In this chapter, we focused our study on the comprehension of the PEDOT:Tos films made by vapor phase polymerization. The main parameters we played on were the additives and the oxidant solution concentration. We also wanted to know if VPP produces homogeneous thin films.

Additives are known to enhance the properties of PEDOT:Tos films by playing on the crystallization and the molecular weight of the PEDOT chains. We demonstrated that without additives, the obtained films were black and inhomogeneous as regard to films with additives. This characteristic explains the very low electrical conductivity of this type of films. Moreover, the lack of additives leads to a fast polymerization preventing the doping of PEDOT by tosylate as it has been shown by XPS. The Seebeck coefficient is higher in the case of the film without additives explained by the antagonist behavior with the electrical conductivity.

The concentration of oxidant turns out to be an important parameter to play on in order to tune the thickness of the film but also the sheet resistance. The best thermoelectric properties were obtained with an oxidant concentration of 40 and 45%. As additives are present in the solution, the growth of the film is homogeneous and does not depend of the oxidant concentration, leading to films with the same doping level.

In the community, studies focused on the understanding of the formation of PEDOT:Tos during the polymerization process. By carefully analyzing the bottom and top surfaces of VPP PEDOT:Tos films, we concluded that the electronic properties of PEDOT:Tos films made by VPP are homogenous along the thickness of the film. However the AFM characterization clearly demonstrated that the first VPP generated layers of PEDOT:Tos are structurally different from the core of the film with a sponge-like structure.

To follow up on this chapter, we decided to use vapor phase polymerization to induce advanced structuration of PEDOT:Tos films using block-copolymer materials as guiding templates. Our aim was to probe the organization of PEDOT:Tos chains under a strong spatial confinement in order to probe the resulting electronic properties.

[1] B. Winther-Jensen and K. West, "Vapor-phase polymerization of 3,4-ethylenedioxythiophene: A route to highly conducting polymer surface layers," *Macromolecules*, vol. 37, no. 12, pp. 4538–4543, 2004, doi: 10.1021/ma049864l.

[2] A. Mohammadi, M. A. Hasan, B. Liedberg, I. Lundström, and W. R. Salaneck, "Chemical vapour deposition (CVD) of conducting polymers: Polypyrrole," *Synth. Met.*, vol. 14, no. 3, pp. 189–197, 1986, doi: 10.1016/0379-6779(86)90183-9.

[3] T. Le Truong *et al.*, "Poly(3,4-ethylenedioxythiophene) vapor-phase polymerization on glass substrate for enhanced surface smoothness and electrical conductivity," *Macromol. Res.*, vol. 15, no. 5, pp. 465–468, 2007, doi: 10.1007/bf03218815.

[4] Y. H. Han, J. Travas-Sejdic, B. Wright, and J. H. Yim, "Simultaneous vapor-phase polymerization of PEDOT and a siloxane into organic/inorganic hybrid thin films," *Macromol. Chem. Phys.*, vol. 212, no. 5, pp. 521–530, 2011, doi: 10.1002/macp.201000634.

[5] M. A. Ali, H. Kim, C. Lee, H. Nam, and J. Lee, "Effects of iron(III) p-toluenesulfonate hexahydrate oxidant on the growth of conductive poly(3,4-ethylenedioxythiophene) (PEDOT) nanofilms by vapor phase polymerization," *Synth. Met.*, vol. 161, no. 13–14, pp. 1347–1352, 2011, doi: 10.1016/j.synthmet.2011.04.036.

[6] J. H. Yim, "Mechanically robust poly(3,4-ethylenedioxythiophene)-SiO2 hybrid conductive film prepared by simultaneous vapor phase polymerization," *Compos. Sci. Technol.*, vol. 86, pp. 45–51, 2013, doi: 10.1016/j.compscitech.2013.06.023.

[7] M. Fabretto, M. Müller, C. Hall, P. Murphy, R. D. Short, and H. J. Griesser, "In-situ QCM-D analysis reveals four distinct stages during vapour phase polymerisation of PEDOT thin films," *Polymer (Guildf).*, vol. 51, no. 8, pp. 1737–1743, 2010, doi: 10.1016/j.polymer.2010.02.019.

[8] J. Wang, K. Cai, H. Song, and S. Shen, "Simultaneously enhanced electrical conductivity and Seebeck coefficient in Poly (3,4-ethylenedioxythiophene) films treated with hydroiodic acid," *Synth. Met.*, vol. 220, pp. 585–590, 2016, doi: 10.1016/j.synthmet.2016.07.023.

[9] P. Hojati-Talemi, C. Bächler, M. Fabretto, P. Murphy, and D. Evans, "Ultrathin

polymer films for transparent electrode applications prepared by controlled nucleation," *ACS Appl. Mater. Interfaces*, vol. 5, no. 22, pp. 11654–11660, 2013, doi: 10.1021/am403135p.

[10] R. Brooke *et al.*, "Effect of oxidant on the performance of conductive polymer films prepared by vacuum vapor phase polymerization for smart window applications," *Smart Mater. Struct.*, vol. 24, no. 3, 2015, doi: 10.1088/0964-1726/24/3/035016.

[11] K. Zuber, M. Fabretto, C. Hall, and P. Murphy, "Improved PEDOT conductivity via suppression of crystallite formation in Fe(III) tosylate during vapor phase polymerization," *Macromol. Rapid Commun.*, vol. 29, no. 18, pp. 1503–1508, 2008, doi: 10.1002/marc.200800325.

[12] I. Petsagkourakis *et al.*, "Structurally-driven enhancement of thermoelectric properties within poly(3,4-ethylenedioxythiophene) thin films," *Sci. Rep.*, vol. 6, no. March, pp. 1–8, 2016, doi: 10.1038/srep30501.

[13] I. Petsagkourakis *et al.*, "Correlating the Seebeck coefficient of thermoelectric polymer thin films to their charge transport mechanism," *Org. Electron. physics, Mater. Appl.*, vol. 52, no. November 2017, pp. 335–341, 2018, doi: 10.1016/j.orgel.2017.11.018.

[14] J. H. Huang and C. W. Chu, "Achieving efficient poly(3,4-ethylenedioxythiophene)-based supercapacitors by controlling the polymerization kinetics," *Electrochim. Acta*, vol. 56, no. 20, pp. 7228–7234, 2011, doi: 10.1016/j.electacta.2011.03.044.

[15] W. A. Muñoz, X. Crispin, M. Fahlman, and I. V. Zozoulenko, "Understanding the Impact of Film Disorder and Local Surface Potential in Ultraviolet Photoelectron Spectroscopy of PEDOT," *Macromol. Rapid Commun.*, vol. 1700533, pp. 1–8, 2017, doi: 10.1002/marc.201700533.

[16] J. S. Kim, W. Jang, and D. H. Wang, "The investigation of the seebeck effect of the poly(3,4-ethylenedioxythiophene)-tosylate with the various concentrations of an oxidant," *Polymers (Basel).*, vol. 11, no. 1, 2018, doi: 10.3390/polym11010021.

[17] R. Brooke *et al.*, "Vapor phase synthesized poly(3,4-ethylenedioxythiophene)-trifluoromethanesulfonate as a transparent conductor material," *J. Mater. Chem. A*, vol. 6, no. 43, pp. 21304–21312, 2018, doi: 10.1039/C8TA04744H.

[18] B. Winther-Jensen, D. W. Breiby, and K. West, "Base inhibited oxidative polymerization of 3,4-ethylenedioxythiophene with iron(III)tosylate," *Synth. Met.*, vol. 152, no. 1–3, pp. 1–4, 2005, doi: 10.1016/j.synthmet.2005.07.085.

[19] A. Weathers *et al.*, "Significant Electronic Thermal Transport in the Conducting Polymer Poly(3,4-ethylenedioxythiophene)," *Adv. Mater.*, vol. 27, no. 12, pp. 2101–2106, Mar. 2015, doi: 10.1002/adma.201404738.

[20] J. Wang, K. Cai, and S. Shen, "A facile chemical reduction approach for effectively tuning thermoelectric properties of PEDOT films," *Org. Electron.*, vol. 17, pp. 151–158, 2015, doi: 10.1016/j.orgel.2014.12.007.

[21] Y. Jia *et al.*, "Efficient enhancement of the thermoelectric performance of vapor phase polymerized poly(3,4-ethylenedioxythiophene) films with poly(ethyleneimine)," *J. Polym. Sci. Part B Polym. Phys.*, vol. 57, no. 5, pp. 257–265, 2019, doi: 10.1002/polb.24778.

[22] S. Nair, S. Natarajan, and S. H. Kim, "Fabrication of electrically conducting polypyrrole-poly(ethylene oxide) composite nanofibers," *Macromol. Rapid Commun.*, vol. 26, no. 20, pp. 1599–1603, 2005, doi: 10.1002/marc.200500457.

[23] Y. Fu, R. A. Weiss, P. P. Gan, and M. D. Bessette, "Conductive elastomeric foams prepared byin situ vapor phase polymerization of pyrrole and copolymerization of pyrrole and N-methylpyrrole," *Polym. Eng. Sci.*, vol. 38, no. 5, pp. 857–862, 1998, doi: 10.1002/pen.10251.

[24] D. Evans, M. Fabretto, M. Mueller, K. Zuber, R. Short, and P. Murphy, "Structure-directed growth of high conductivity PEDOT from liquid-like oxidant layers during vacuum vapor phase polymerization," *J. Mater. Chem.*, vol. 22, no. 30, p. 14889, 2012, doi: 10.1039/c2jm32281a.

[25] J. Metsik *et al.*, "Growth of Poly (3 , 4-ethylenedioxythiophene) Films Prepared by Base-Inhibited Vapor Phase Polymerization," *J. Polym. Sci. Part B Polym. Phys.*, vol. 52, pp. 561–571, 2014, doi: 10.1002/polb.23450.

[26] S. Chen, I. Petsagkourakis, N. Spampinato, X. Crispin, and M. P. Jonsson, "Unraveling vertical inhomogeneity in vapour phase polymerized PEDOT:Tos film," *J. Mater. Chem. A*, 2020, doi: 10.1039/d0ta06031c.

V. NANOSTRUCTURING PEDOT:TOS USING BLOCK-COPOLYMER TEMPLATES

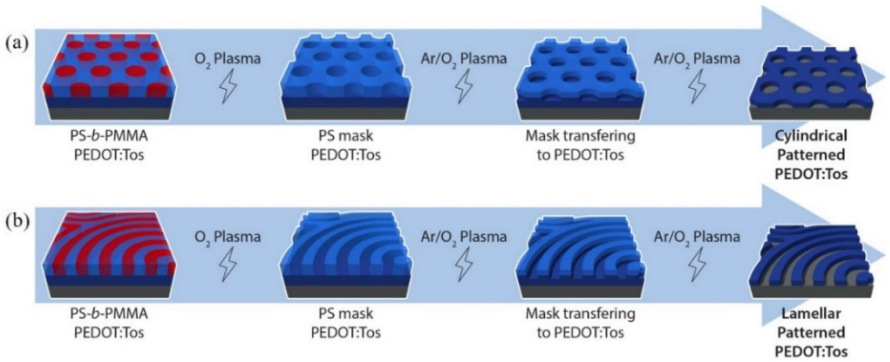

Improving PEDOT:Tos thermoelectric properties is of foremost importance for applications since the efficiency of thermoelectric modules comprising PEDOT materials is still low. A key point for this quest is inherent to the engineering of the PEDOT:Tos crystalline structure which could be achieved by a spatial confinement of the PEDOT:Tos crystallites. Here, we decided to use the self-assembling properties of block copolymers in order to template PEDOT:Tos. Two main approaches will be discussed in this chapter: *i.* a lithographic method in which the block copolymer acts as a mask to pattern a PEDOT:Tos layer, and *ii.* a confined growth of PEDOT:Tos inside a particular self-assembled block copolymer domain using a selective hybridization between PEDOT:Tos precursors and the block copolymer chemistry.

I- INTRODUCTION

We have demonstrated through this manuscript that PEDOT:Tos can be considered as one of the most promising polymers for thermoelectric applications with its low thermal conductivity, relatively good Seebeck coefficient and high electrical conductivity. In order to further enhance its thermoelectric efficiency, increasing the electrical conductivity appears as a potent pathway. Tuning electrical conductivity in PEDOT systems have been performed following two main processes. A chemical route by which PEDOT:Tos films are modified after deposition with an acidic treatment or other chemicals [1]–[3], leading to a modification of the PEDOT:Tos chemical structure by a de-doping process. In this case, removing tosylate leads to an increase of the Seebeck coefficient and a decrease of the electrical conductivity. Another route is related to the confinement or patterning of the PEDOT structure during or after the film formation [4]–[7]. For instance, Brooke *et al.* used an inkjet printing process to deposit a tosylate solution prior to the VPP of EDOT. With this method, they were able to reach a conductivity of 972 $S.cm^{-1}$ which is the value generally obtained for larger film [4]. O'Connell *et al.* used dip-pen lithography to deposit tosylate spots before polymerizing EDOT by VPP. They observed in this case an electrical conductivity comparable to PEDOT:PSS commercial solution (1 $S.cm^{-1}$) [7]. Cho *et al.* used a mold selectively covered by $FeCl_3$ inside trenches to vapor phase polymerize EDOT. They were able to obtain a single PEDOT crystal with high electrical conductivity of 8797 $S.cm^{-1}$ [5]. Lee *et al.* directly mixed PEO-*b*-PPO-*b*-PEO with tosylate salts in order to nano-confine tosylate moieties into the PEO domains prior to VPP. They obtained electrical conductivity over 2200 $S.cm^{-1}$ [6].

In this work, we decided to employ block copolymer self-assembly to direct the arrangement of PEDOT:Tos chains or to pattern PEDOT:Tos films. Such strategy allows one to either precisely define conduction pathways in a PEDOT:Tos layer or nano-confine PEDOT:Tos crystallites during the film formation process (and thus modulate the crystal arrangement with an influence on the charge transport).

A block copolymer is composed of two or more chemically distinct polymer chains that are covalently bonded together. In the simplest case of a diblock copolymer (BCPs), two blocks are covalently linked in a linear architecture. BCPs are of interest for nanostructuration because they can self-assemble into a variety of nanostructures depending of their macromolecular characteristics [8]. The self-assembly behavior of BCPs is determined by the incompatibility between the two blocks, χ (Flory-Huggins parameter), the overall degree of polymerization, *N*, and the BCP composition (volume fraction, f). For a particular system, synthetic manipulations of these parameters permit to navigate in a phase diagram showing different morphologies such as spheres, cylinders, gyroids or lamellae, as displayed in Figure V-1. Interestingly, as the two blocks are chemically different, they can exhibit drastically different chemical or bonding properties. For example, one block can be hydrophilic and the other hydrophobic which allows a selective coordination with specific chemical moieties.

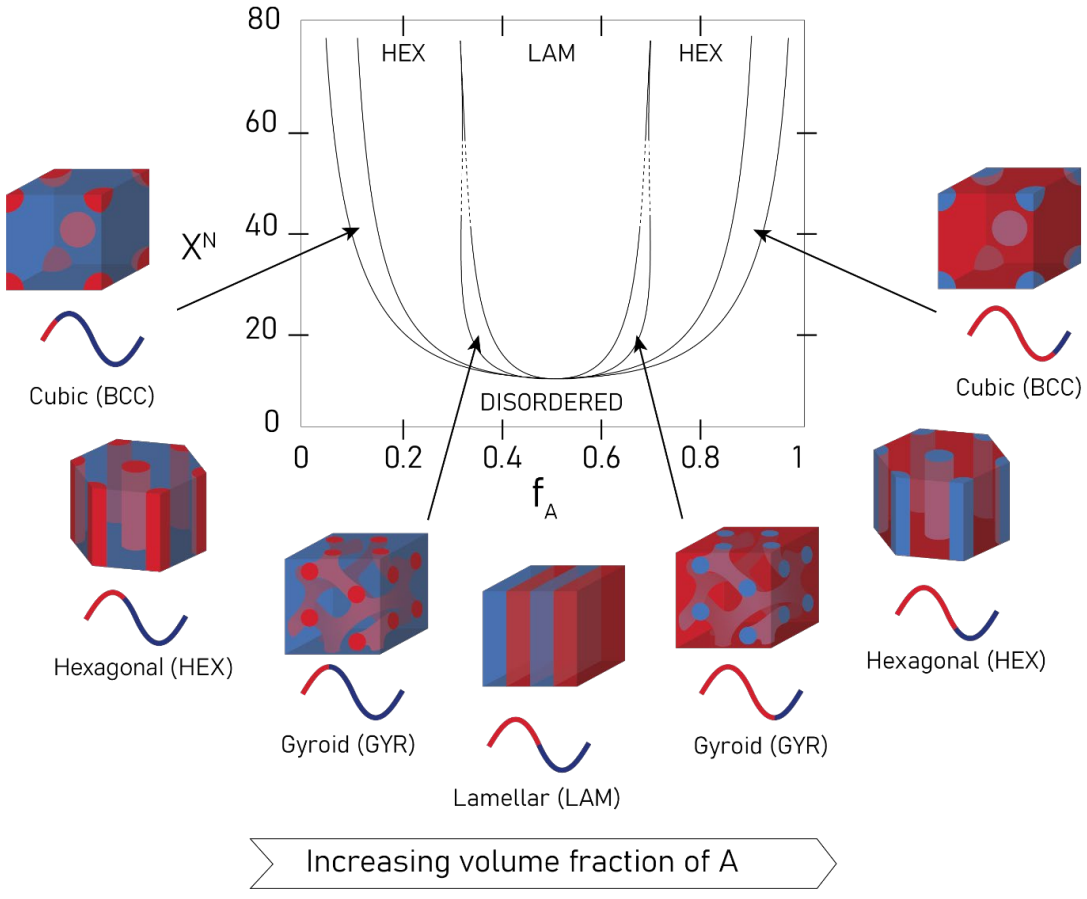

Figure V-1 Phase diagram of a BCP with the different configurations obtained by playing on f_A, N and χ. The block A is represented in red meanwhile the block B is in blue.

While the aforementioned structures are the thermodynamically stable ones in bulk, the self-assembly of BCPs in a thin film configuration requires more attention due to the presence of interfaces (air/BCP and BCP/substrate) which drastically modify the self-assembly behavior [9]. In particular, the controlled orientation of BCP structures (parallel or perpendicular to the substrate) will depend of the interfacial energies between the BCP domains and the air and substrate interfaces. The thickness of the BCP film (with respect to the intrinsic BCP period, L_0) has also an important influence on the final morphology, as displayed Figure V-2. Accordingly, surface modifications by polymer brushes or complex annealing treatments (solvent or anti-solvent annealing) are often used to direct the BCP structure towards the chosen orientation. Such methods are particularly developed for cylindrical and lamellar morphologies which can be further used as templates for nano-lithography.

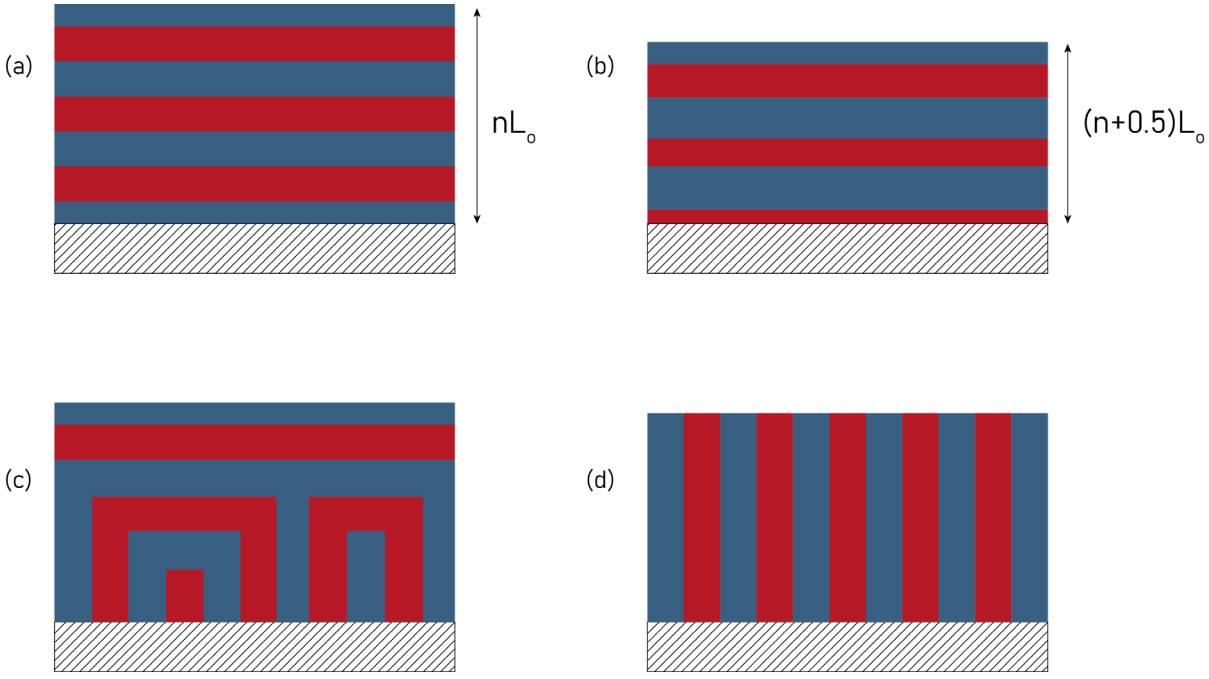

Figure V-2 Orientation of the BCP domains regarding the commensurability of L0 with the film thickness and the affinity of the blocks for the interfaces. (a) symmetric wetting, (b) asymmetric wetting, (c) neutral wetting with blue block preferentiality for the air surface, (d) neutral wetting.

II- PATTERNING PEDOT:TOS WITH A LITHOGRAPHIC PROCESS BASED ON BLOCK COPOLYMERS

Over the last years, BCPs have demonstrated their potential for miniaturization of components in microelectronics. In particular, BCPs are used as a mask in order to transfer a pattern into a functional material in a similar manner than photolithography. Considering a PEDOT:Tos layer as the functional material, UV light has been used to pattern PEDOT:Tos. In particular, Edberg *et al.* used masks obtained with a conventional printer to expose a tosylate layer to UV light. After this step, they used VPP to polymerize EDOT on the exposed and unexposed tosylate areas [10]. Through a rinsing step, they were able to selectively remove the exposed areas of the film. Moreover, this technique allows to modulate the electrical conductivity on the exposed and unexposed parts of the films over 6 orders of magnitude even if a low electrical conductivity was recorded on the exposed areas. Similar processes using UV exposure were also demonstrated on PEDOT:PSS films [11]–[13].

Our methodology aimed to take advantage of block copolymer self-assembly to nano-pattern PEDOT:Tos layer and PS-*b*-PMMA was chosen as structuring mask. PS-*b*-PMMA is the archetypical material in BCP lithography, as its self-assembly behavior is well known and understood [14]. Additionally, PS and PMMA have similar surface energy which allow to obtain a perpendicular orientation of the BCP structure as regards to the substrate by a feeble tuning of the interfacial energy between the BCP layer and the substrate. Moreover, PMMA can be selectively etched by plasma chemistry, concomitantly triggering the cross-linking of PS domains [15]. In particular, reactive ion etching (RIE) has been used by Asakawa and Hiraoka to selectively remove the PMMA domains in order to subsequently pattern a silicon substrate [16]. To the best of our knowledge, RIE etching has not been used for patterning PEDOT:Tos but micro-patterning of PEDOT:PSS by RIE process have been successfully reported [17], [18]. The aim of this study was thus to used PS-*b*-PMMA as a mask and RIE for etching in order to pattern a PEDOT:Tos layer at the nanometer scale.

II-1- SAMPLES PREPARATION

PEDOT:Tos films were first deposited on glass substrates by ISP using an oxidant tosylate solution at 40% in butanol. On top on this film, a block copolymer film was then deposited in order to be used as a mask for the lithographic process. The chosen BCP to act as a mask is PS-*b*-PMMA and two different BCP architectures were used in order to produce out-of-plane lamellae and cylinders. As the orientation of the BCP domains depends of the interfacial interactions, the wetting of the BCP domains on the PEDOT:Tos layer has to be taken into account. The formation of out-of-plane lamellae or cylinders requires no preferential wetting at the interfaces [19]. Accordingly, a statistical PS-*stat*-PMMA copolymer brush composed of 74% PS was grafted on top of the PEDOT:Tos layer in order to neutralize the surface. As the surface chemistry of PEDOT:Tos is different from the classical native oxide SiO_2 substrate, the grafting procedure has to be repeated three times in order to obtain a proper grafting density of the PS-*stat*-PMMA. The last step consists of the spin-coating of a PS-*b*-PMMA solution followed by a thermal annealing step to promote the self-assembly.

The resulting system is thus composed of two layers which are PEDOT:Tos and PS-*b*-PMMA located on top of the substrate. The BCP was then used as a mask to pattern the PEDOT:Tos layer. The mask was generated using O_2 plasma as PMMA shows a higher etching rate than PS. The transfer of the BCP pattern into the PEDOT:Tos layer was subsequently performed using either Ar or O_2 plasmas. Indeed an Ar plasma is defined as a physical plasma where etching is dominated by physical sputtering when an O_2 plasma is rather a chemical plasma where etching is dominated by ions collisions [20]. Both plasma chemistries were probed in order to evaluate their influence of the resulting patterned PEDOT:Tos chemical structure and electronic properties. The overall process flow is summarized in Figure V-3.

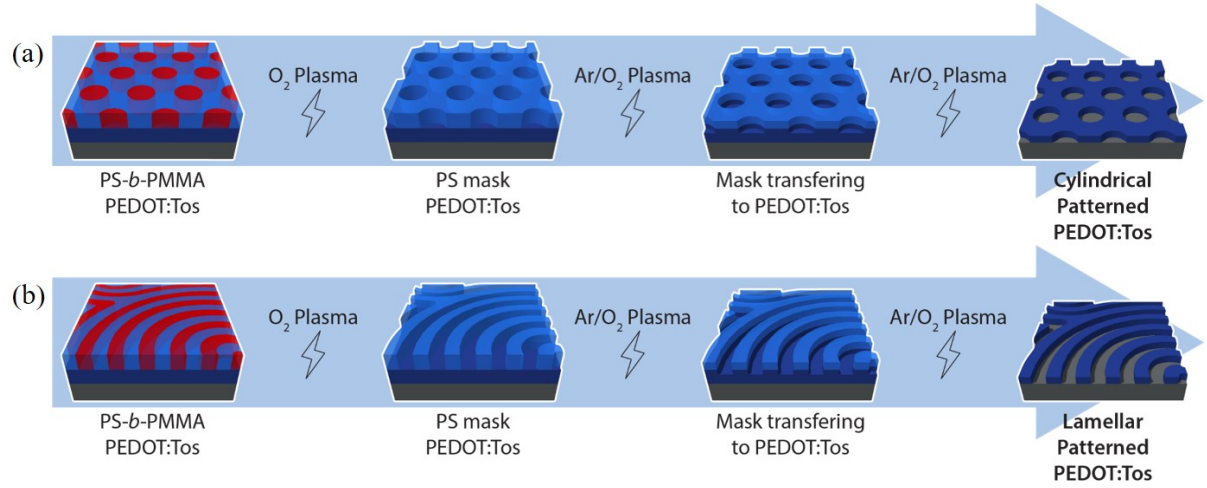

Figure V-3 Lithographic process used to patter PEDOT:Tos thin film (a) with a cylindrical configuration, (b) with a lamellar configuration.

For cylindrical system, a PS-*b*-PMMA BCP with 30% of PMMA and 70% of PS was used. Such chemical composition leads to the formation of hexagonally-packed PMMA cylinders in a PS matrix. Following the process previously described, bilayers composed of a PEDOT:Tos layer and out-of-plane cylindrical BCP layer were produced. The removal of the PMMA domains leads to a PS layer perforated by holes which was further employed as a mask to define an anti-dot lattice in the PEDOT:Tos layer. The bilayer thickness was evaluated to 89 ± 1 nm with a underlying PEDOT:Tos layer of 50-60 nm, as displayed in Figure V-4 (a).

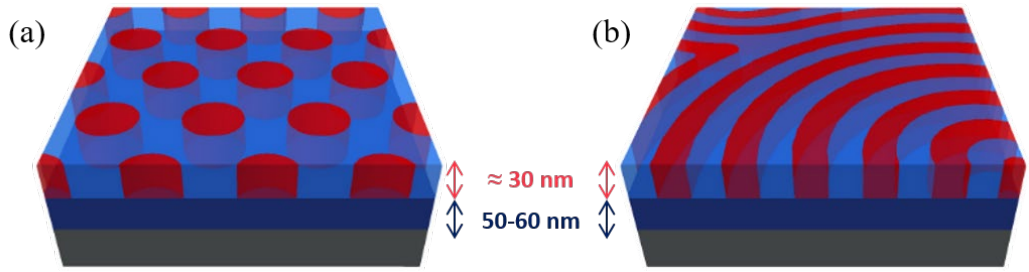

Figure V-4 Bilayer representation with a (a) cylindrical PS-b-PMMA structure on top of a PEDOT:Tos layer, (b) . The dark blue layer corresponds to PEDOT:Tos, while light blue and red domains are PS and PMMA, respectively.

We subsequently applied this methodology to a lamellar PS-*b*-PMMA block copolymer with 50% of PMMA and 50% of PS. Bilayers are composed of a PEDOT:Tos layer and out-of-plane lamellae of PS and PMMA on top of it. Removing the PMMA domains would lead to a line/space pattern which will be further transfer into the

PEDOT:Tos layer forming a nano-patterned conductive grid. The total film thickness is 85 ± 1 nm knowing that the PEDOT:Tos layer is around 50-60 nm and the PS-*b*-PMMA one is around 30 nm, as displayed in Figure V-4 (b).

II-2- PATTERNING WITH O_2 PLASMA

II-2-A- PROPERTIES OF PATTERNED PEDOT:TOS WITH O_2 PLASMA

An extended O_2 RIE treatment (20 sccm, 40W and 140 s) was used to sequentially remove the PMMA domains and etch the PS protecting and PEDOT:Tos. Topographical AFM image, displayed in Figure V-5, shows a perforated layer with hexagonally arranged holes which correspond to the cylindrical morphology of the PS-*b*-PMMA (a), and resulting line/space pattern which corresponds to the lamellar morphology of the PS-*b*-PMMA (b). The thickness of the resulting films is 24 and 26 nm for cylindrical and lamellar morphology, respectively. These thicknesses are lower than the initial PEDOT:Tos thickness, corroborating the elimination of the PS mask after the extended plasma treatment. It is noteworthy that we retrieved with this process a granular structure of the PEDOT:Tos anti-dot lattice patterned and lines with a cylindrical and lamellar BCP, respectively.

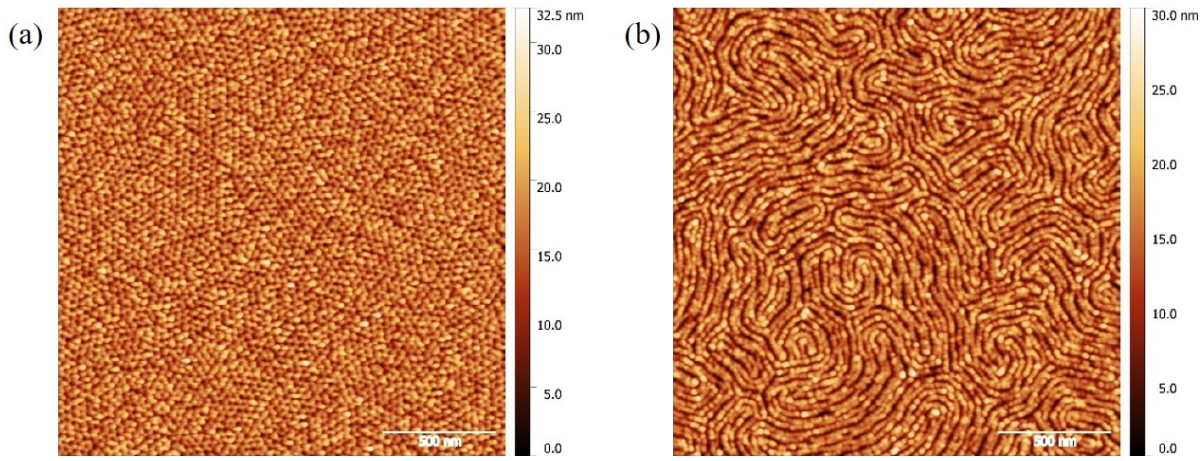

Figure V-5 Topographical AFM images 2×2 µm² of PEDOT:Tos film after lithography process with O2 plasma (a) with a cylindrical BCP, (b) with lamellar BCP.

In order to probe the chemical composition of the sample, XPS measurements have been performed on PEDOT:Tos films patterned with O_2 plasma. Signals corresponding

to contributions of sulfur atoms appear which hint that the PEDOT:Tos structure is preserved at the end of the plasma treatment. Precise scans of sulfur signals are displayed in Figure V-6, for both morphologies.

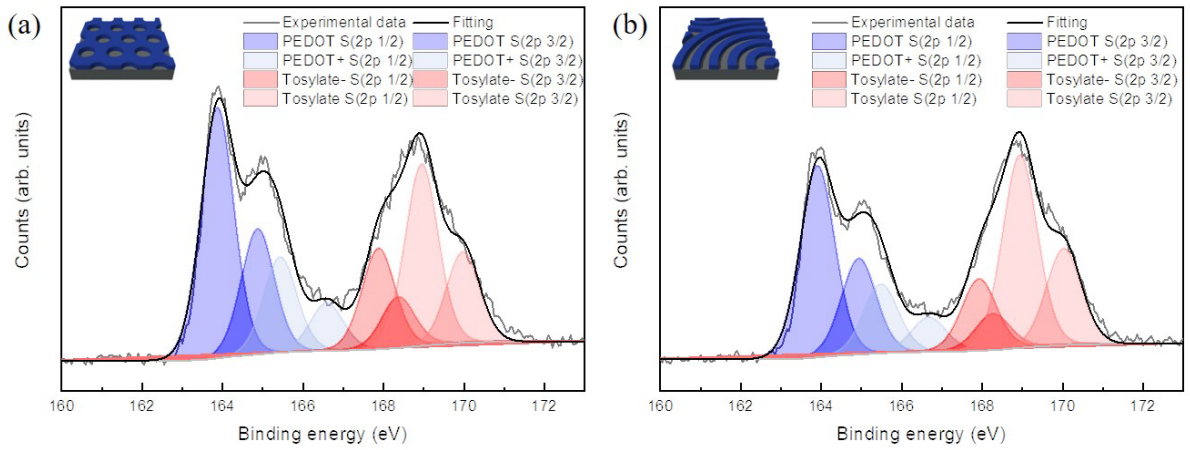

Figure V-6 XPS S2p spectra of patterned PEDOT:Tos film with (a) cylindrical BCP and (b) lamellar BCP, under O2 plasma. Blue and red areas represent the signals linked to S2p in PEDOT and S2p in tosylate, respectively.

More precisely, all 4 contributions (and their doublets) of PEDOT:Tos can be clearly observed meaning that the film is composed of PEDOT:Tos. However, the contributions of "tosylate" (the S=O bond) are more important than in the case of native PEDOT:Tos film (see previous chapters for details). The oxidation levels were determined to be 29 and 27% which are higher than the one retrieved for native PEDOT:Tos films [21], [22]. As the PEDOT:Tos film is the first deposited layer, the modification of the doping level is linked to the plasma procedure. In this particular case, O_2 plasma can alter the PEDOT structure as well as the interactions with tosylate, creating novel S=O bonds with oxygen species arising from the plasma treatment. Indeed O_2 plasma creates radicals and ions which can induce some recombinations [23].

Additionally, we also noticed a shift of the WF by 0.3 and 0.2 eV (4.3 *vs* 4.6 and 4.5 eV) for the nano-patterned PEDOT:Tos layer, with cylindrical and lamellar BCP respectively, as shown in Figure V-7 (a). Moreover the amount of electronic states near the Fermi level, characteristic of the semi-metallicity, is also drastically reduced (see Figure V-7 (b)).

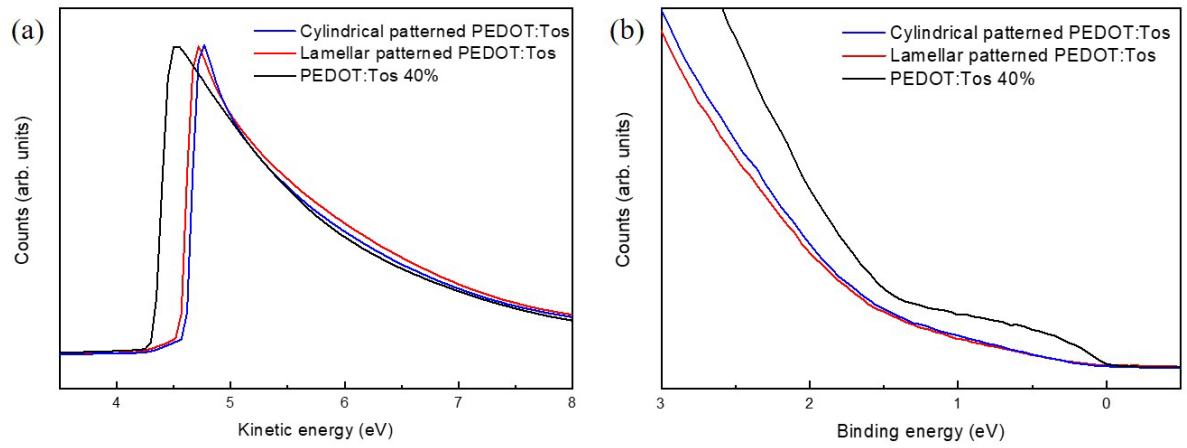

Figure V-7 UPS spectra of PEDOT:Tos film and lamellar patterned PEDOT:Tos film with O2 plasma (a) Secondary electron cut-off region (b) Valence band region. Binding energy equal to 0 represents Fermi level.

The change in the work function suggest a modification of the top surface of the film. In PEDOT:PSS system, the increase of the WF upon post-treatment is linked to the segregation of PSS on the top of the film [24], [25]. Beyond that, they observed an increase of the electrical conductivity with the decrease of the WF explained by the morphological aspect of PEDOT:PSS. It is possible to make an analogy with our system as the O_2 plasma modifies the structure of PEDOT:Tos by segregating the tosylate units on top of the film.

II-2-B- TRANSPORT PROPERTIES ALONG THE THICKNESS

The transport properties were subsequently evaluated along the nano-patterned PEDOT:Tos thickness by tuning the plasma duration allowing one to control the resulting PEDOT:Tos thickness. The sheet resistance and the thickness were measured stepwise after every 15 s of O_2 plasma starting from the top interface of PS-*b*-PMMA. As the copolymer layer is insulating, the resistivity probed through the 4-probes apparatus is related to the PEDOT:Tos layer. Accordingly, the electrical conductivity was calculated taking into account the sole thickness of the PEDOT:Tos layer until the PEDOT:Tos layer was reached. The decrease of the thickness during plasma exposure is not linear, as shown Figure V-8. From 75 s and 90 s of exposure for the cylindrical and lamellar morphologies, respectively, the PS-*b*-PMMA layer is totally removed and the plasma starts to etch the PEDOT:Tos layer.

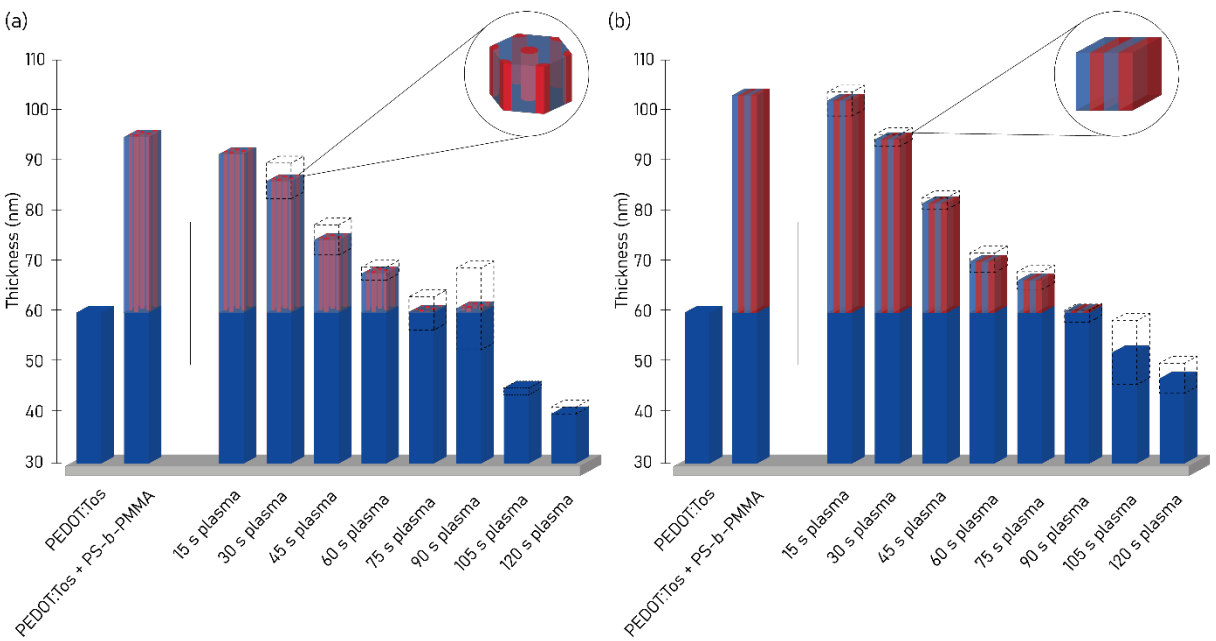

Figure V-8 Film thickness according to the duration of the plasma exposure. The dark blue box referred to PEDOT:Tos layer while red and light blue box referred to PS-b-PMMA. The dashed boxes represent the error bars. (a) cylindrical and (b) lamellar morphologies.

The structural and electrical properties of the BCP/PEDOT:Tos stack were probed after each plasma exposure step by a 4-point probes measurement, a thickness profile and an AFM scan. As shown in Figure V-10, the anti-dot morphology of the film is preserved during the plasma treatment until the last exposure step (t = 120 s) for which a more defective pattern is resolved by AFM. We related this modification to the fidelity loss induced by the loss of etching contrast inherent to the removal of the PS mask.

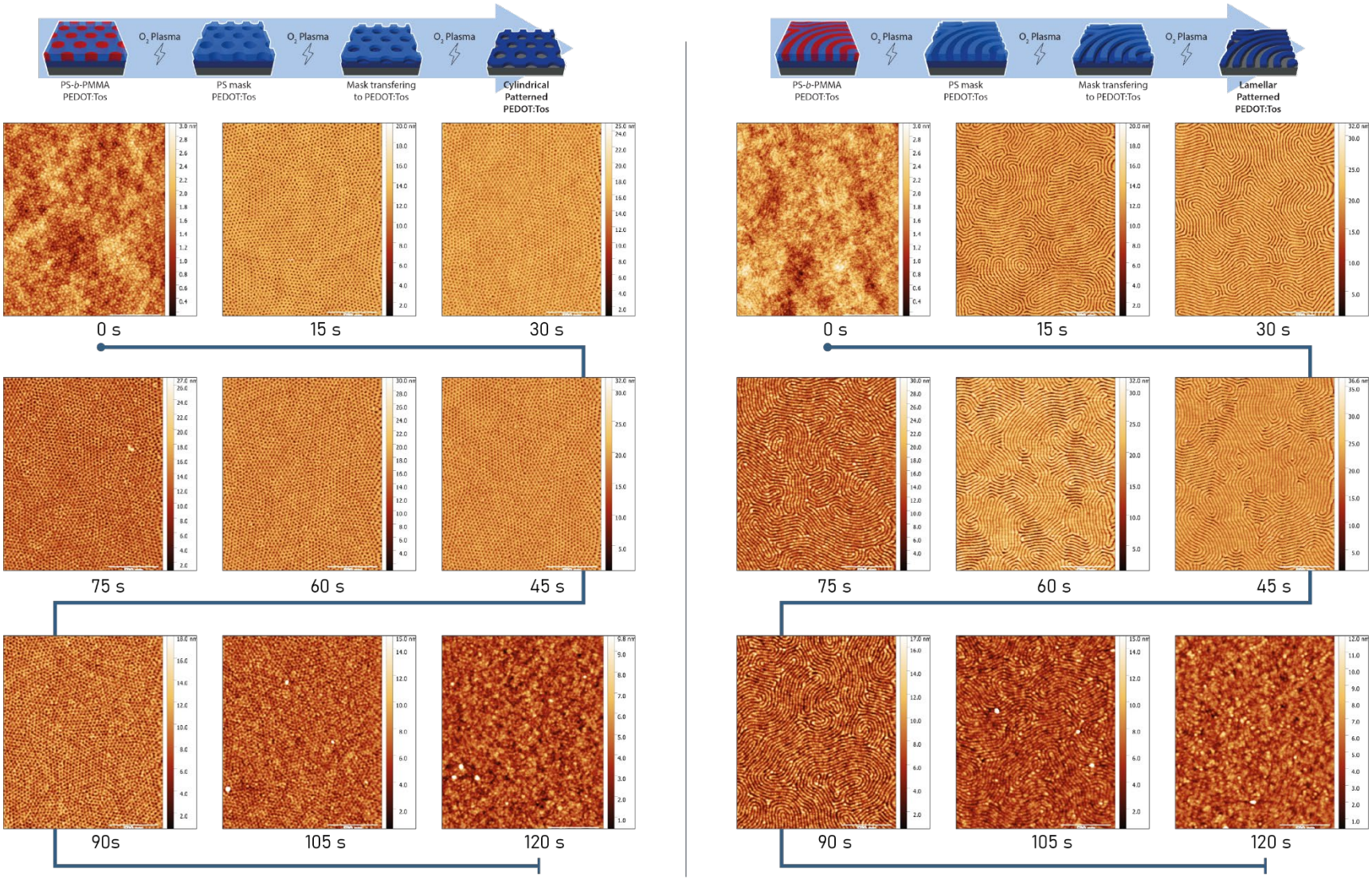

Figure V-9 Topographical AFM image 2×2 µm² of PEDOT:Tos /PS-b-PMMA films after several O_2 plasma exposure for cylindrical and lamellar morphologies.

The morphology of the sample plays a role in the electrical conductivity through the conduction pathways which can be created inside the film. As the films are, after 75 and 90 s of plasma exposure, composed of a performed layer or lines of PEDOT:Tos, the conduction pathways differ from a normal PEDOT:Tos layer.

The electrical conductivity of the initial PEDOT:Tos layer is 2142 ± 121 $S.cm^{-1}$. However, after depositing the PS-*b*-PMMA layer, the electrical conductivity heavily decreases to 63 ± 4 $S.cm^{-1}$ and 63 ± 4 $S.cm^{-1}$ as displayed in Figure V-10. This decrease could have several explanations. First, during the BCP annealing at high temperature, a migration of the tosylate moieties at the BCP/PEDOT interface can occur due to preferential interactions with the methacrylate units. Secondly, as the electrical conductivity is measured on a bilayer system, a contact resistance can be created between the apparatus probes and the BCP/PEDOT:Tos. Thirdly, as the probes of the apparatus have to penetrate an insulating layer, the pins can be coated with a thin insulating copolymer layer which would drastically decrease the measured value of the electrical conductivity. Finally, as the solvent used for the block copolymer is an acetate, the solvent could also swell the PEDOT layer inducing a modification of its crystalline structure which leads to a drastic decrease of the electrical conductivity.

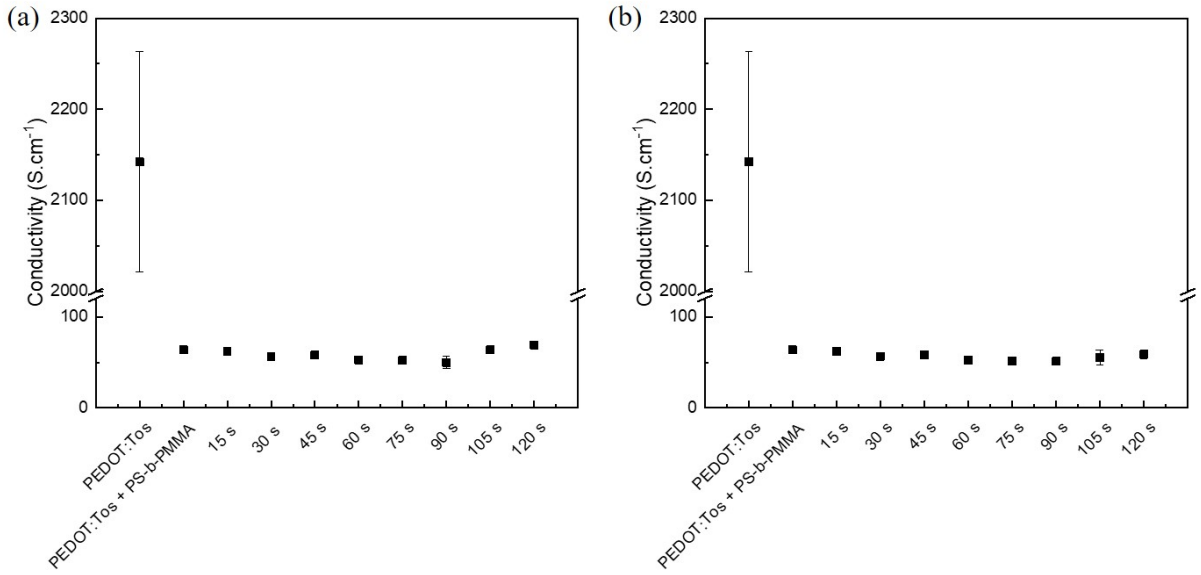

Figure V-10 Electrical conductivity of PEDOT:Tos /PS-b-PMMA bilayer films at different steps of the process. (a) cylindrical BCP, (b) lamellar BCP. The time in second represents the plasma exposure time.

Conducting AFM has been performed in order to locally probe the conducting domains of patterned PEDOT:Tos. Figure V-11 displays the resulting AFM measurements with the topographical and conductive images displayed on the left and right panels, respectively. Even if the conductive image is vaguely correlated with the topographical features, it is clear that the application of the plasma treatment drastically modifies the PEDOT electronic properties as a very low response (in the range of pA) is recorded.

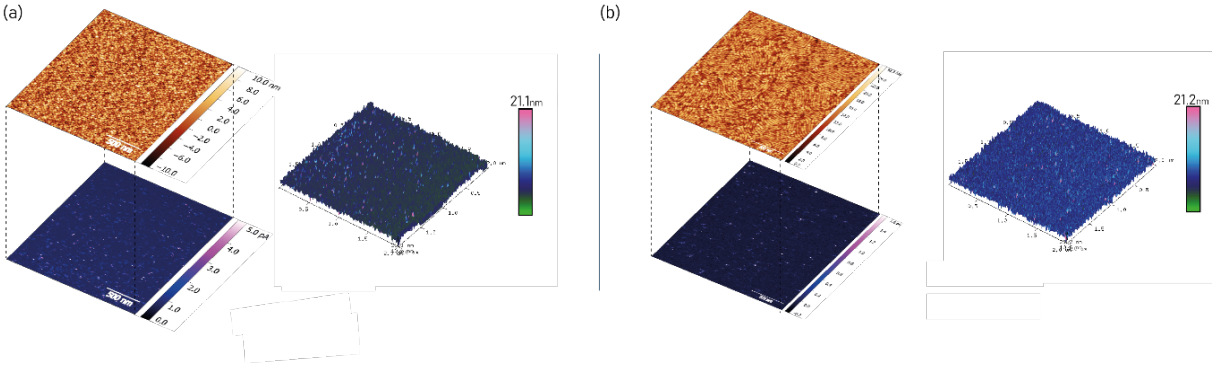

Figure V-11 Topographical AFM 2×2 µm² image, conducting AFM 2×2 µm² image and the resulting 3D image composed of the morphology and the conducting area. (a) cylindrical morphology, (b) lamellar morphology. White and pink dots correspond to the most conducting parts.

In summary, BCP lithography with a cylindrical and lamellar PS-*b*-PMMA enables the patterning of an anti-dot and a line/space PEDOT:Tos layer. Despite the increase of the oxidation level, the plasma treatment required to template the structure is highly detrimental to the electronic properties of the PEDOT:Tos layer with a resulting electrical conductivity of ≈ 70 $S.cm^{-1}$. The increase of the S=O signal shown previously can be linked to recombination of O species created by the plasma with PEDOT:Tos material. As the results obtained by O_2 plasma were not satisfying, we moved forward with a dual O_2 and Ar plasma treatment in order to avoid the degradation of the PEDOT:Tos layer characteristics.

II-3- Patterning with O_2 and Ar dual plasma

An O_2 (20 sccm, 40W and 30 s) RIE treatment was used to remove the PMMA domains leading to either a PS layer perforated with holes for the cylindrical BCP or a

line/space pattern for the lamellar BCP. The removing of the PMMA domains was confirmed by AFM, as shown in Figure V-12 which displays the result obtained for the lamellar BCP.

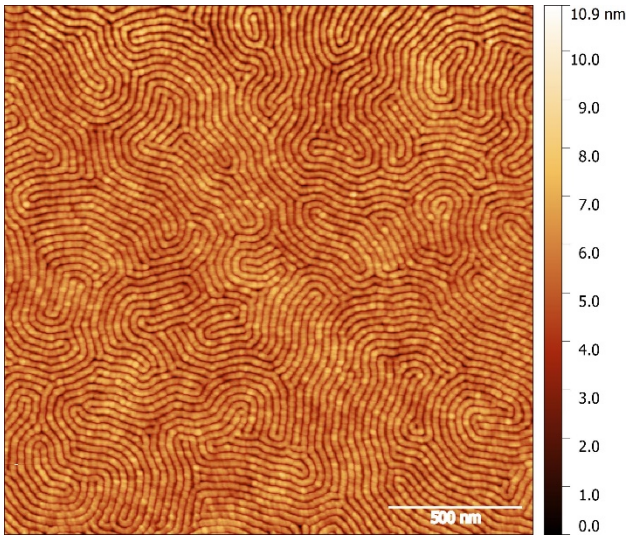

Figure V-12 Topographical AFM images 2×2 µm² of PEDOT:Tos/PS-b-PMMA bilayer film after 30 s of O_2 plasma,

Following this treatment, an Ar plasma (20 sccm, 40W and 110 s) was performed to concomitantly etch the PS domain and transfer the pattern into the PEDOT:Tos layer. Topographical AFM images of the two configurations, displayed in Figure V-13, show the anti-dot lattice with hexagonally arranged perforations corresponding to the PMMA domains and lines/space. It is noteworthy that the PEDOT:Tos perforated layer is composed by small sintered grains as evidenced on the topographic AFM image. The resulting film thickness is around 7 nm for the first configuration, which is 10 times lower than the initial PEDOT:Tos thickness, demonstrating the harshness of a physical Ar treatment. With lamellar BCP, the thickness is slightly higher, around 19 nm,

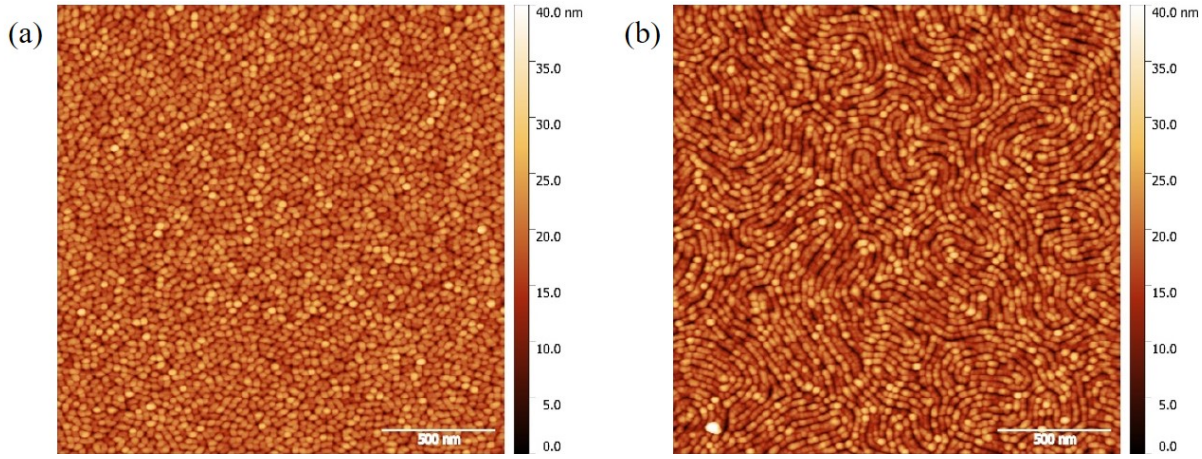

Figure V-13 Topographical AFM images 2×2 µm² of PEDOT:Tos/PS-b-PMMA bilayer film after 30 s of O_2 plasma and 110 s of Ar plasma (a) with cylindrical BCP, (b) with lamellar BCP,

It is noteworthy that the texture of the PEDOT:Tos layer observed on the topographical images appear less homogenous than the one observed using only O_2 plasma which can be explained by the different nature of plasmas.

As previously, XPS measurements were performed on PEDOT:Tos films patterned with the dual plasma treatment. As the film is very thin, Si signal appears on the survey spectrum. Similar conclusions than the ones obtained with the O_2 plasma treatment have been drawn as shown in Figure V-14, i.e. the "tosylate" contributions are more important than in pristine PEDOT:Tos films.

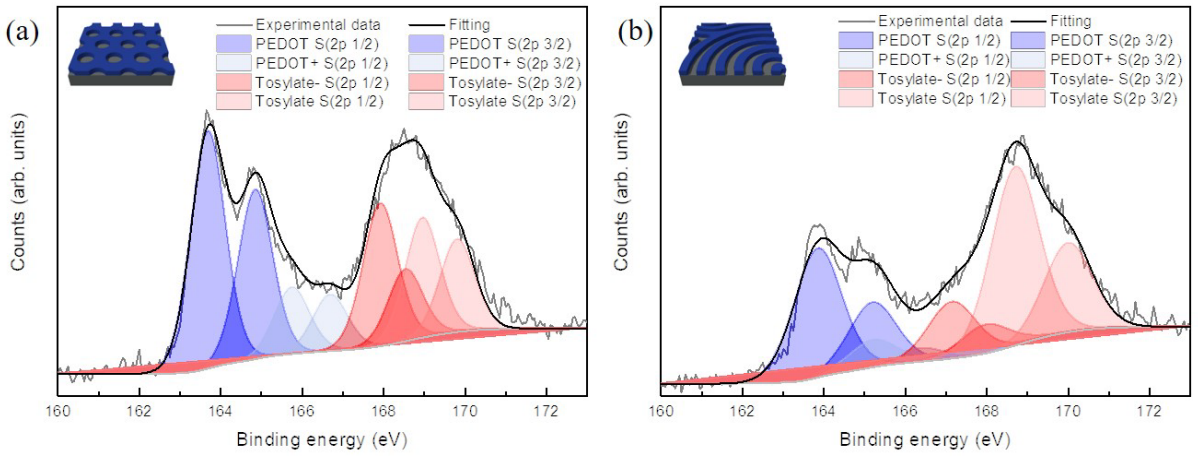

Figure V-14 XPS S2p spectra of patterned PEDOT:Tos film under Ar plasma with (a) cylindrical BCP, (b) lamellar BCP. Blue and red areas represent the signals linked to S2p in PEDOT and S2p in tosylate, respectively.

The oxidation levels were determined to be 37.9 and 36.3 % for the cylindrical and lamellar morphologies, respectively, which are higher than the one retrieved for native PEDOT:Tos films [21], [22]. The modification of the doping is clearly linked to the plasma treatment. Additionally, UPS spectroscopy reveals that the electronic properties of the patterned PEDOT:Tos layer is drastically influenced by the plasma treatment. Firstly, the work function, displayed in Figure V-15 (a), increases from 4.3 to 4.6 and 4.7 eV, meaning that the surface of the PEDOT:Tos layer is not in the same electronic state. It is then more difficult to extract an electron from the surface of patterned PEDOT:Tos than a conventional film. As explained previously, the surface of the film can have been altered by the formation of new species resulting from the reaction between the oxygen ions or radicals and tosylate units. In addition, the electronic states near the Fermi level are also modified by the patterning of the PEDOT:Tos as the electronic states related to the semi-metallic behavior vanished, as shown in Figure V-15 (b).

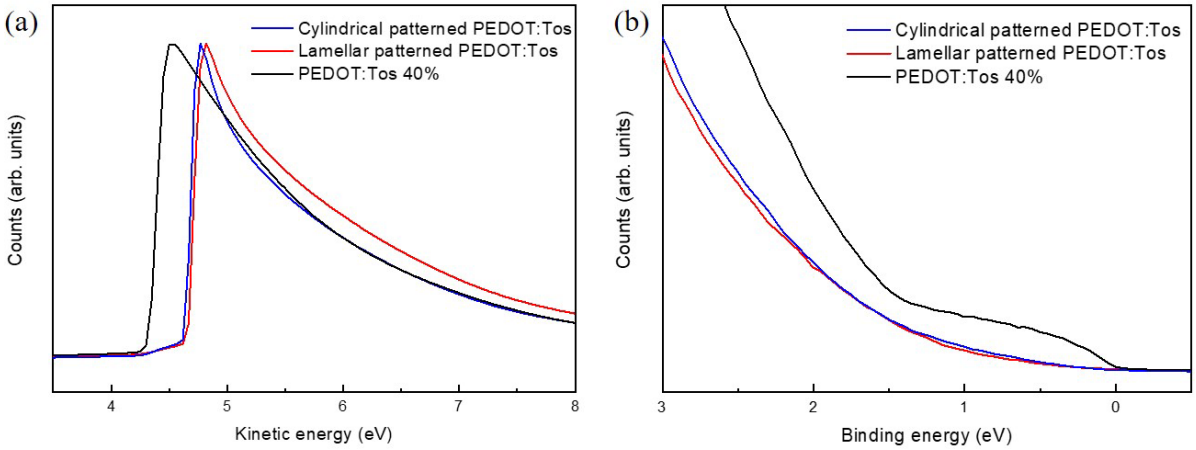

Figure V-15 UPS spectra of PEDOT:Tos film and cylindrical/lamellar patterned PEDOT:Tos film with dual plasma (a) Secondary electron cut-off region (b) Valence band region. Binding energy equal to 0 represents Fermi level.

As the Ar plasma is a physical plasma, we had supposed that it would not preferentially alter specific sites of the PEDOT:Tos structure. However, such treatment still activates the PEDOT:Tos layer as regards to subsequent reactions with environmental species which leads to a super oxidized PEDOT:Tos layer. As a consequence, the doping level is also modified as shown by the XPS spectrum. The contributions between 167.5 and 171 eV are linked to the S-O bonding which can

correspond to tosylate but also to newly formed S-O bonds. Moreover, UPS measurements showed that the patterned PEDOT:Tos surface have been drastically changed with modification of the WF and the loss of electronic states near to the Fermi level. As the states at low binding energy are linked to the electrical conductivity, the patterned PEDOT:Tos are not anymore conducting.

II-4- Conclusion

BCP lithography was demonstrated to enable the nano-patterning of PEDOT:Tos layer using a BCP mask. Both anti-dot and line/space patterns were obtained following this methodology. However both spectroscopic and electrical measurements allow us to conclude that the plasma treatments needed to transfer the BCP pattern are highly detrimental to the chemical and electronic structures of the nano-patterned PEDOT:Tos layer. Indeed the electrical conductivity measurements showed that the patterned PEDOT:Tos is still conducting but the electrical conductivity value are drastically reduced with respect to pristine PEDOT:Tos film. In particular, XPS and UPS demonstrated than the oxidation level was heavily modified leading to an over-doping of the PEDOT structure and the surface of the film has different energy level which should arise from an oxygen enrichment due to the plasma treatment and/or a diffusion of tosylate moieties to the surface of the film. In order to improve these results, a perspective would be to use lower energy plasma under controlled atmosphere (in particular without oxygen), and then re-expose the material to tosylate to re-dope it.

III- PEDOT:Tos INCLUSION IN PS-*b*-P2VP

Polystyrene-*block*-poly(2vinylpyridine) (PS-*b*-P2VP) is an amphiphilic block copolymer composed of a hydrophobic block (PS) and a hydrophilic block (P2VP) [27]. The pyridine unit in P2VP which is a Brønsted base is able to capture a proton which can be used to further bond various moieties onto the P2VP backbone [28]. Accordingly, PS-*b*-P2VP BCPs have been commonly used to self-assemble metallic or oxide nanoparticles from salt precursors due to the selective interactions with the P2VP domains [19], [28], [29]. In the case of tosylate, we assumed that the pyridine unit and the tosylate moieties can have a strong interaction due to the ionic nature of iron tosylate, as displayed in Figure V-16.

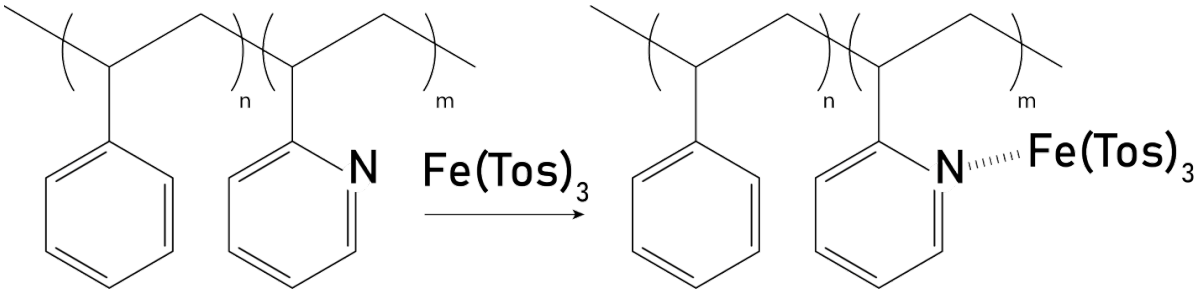

Figure V-16 PS-b-P2VP interaction with tosylate couterions.

III-1- PS-*b*-P2VP IMMERSION IN TOSYLATE

We initially choose to work with a lamellar PS-*b*-P2VP structure in order to demonstrate how a selective polymerization of EDOT could take place inside the self-assembled P2VP domains. By selectively introducing tosylate molecules through the swelling of the P2VP domains, EDOT could be subsequently polymerized by VPP using the swelled P2VP domains as a template. The schematic process flow is described in Figure V-17. First, a thin film of PS-*b*-P2VP is self-assembled to obtain a lamellar structure oriented perpendicularly to the substrate. The film is then dipped inside a tosylate bath during few minutes. As the tosylate solution is highly viscous, a sublayer subsists on top of the BCP film, that was removed by rinsing the film inside a butanol bath. A mild O_2 plasma treatment was then applied inducing the crosslinking of the BCP film in order to avoid a further dissolution due to the exposure to EDOT vapors.

The sample was then exposed to EDOT vapors in a VPP chamber for few minutes. A post thermal treatment of 5 minutes on a hotplate was further applied to promote the polymerization followed by a rinsing step in an ethanol bath. Reconstruction of the nanostructured PS-b-(P2VP/PEDOT:Tos) surface was finally accomplished by dipping in PGMEA in order to reveal the PEDOT:Tos lamellar structure.

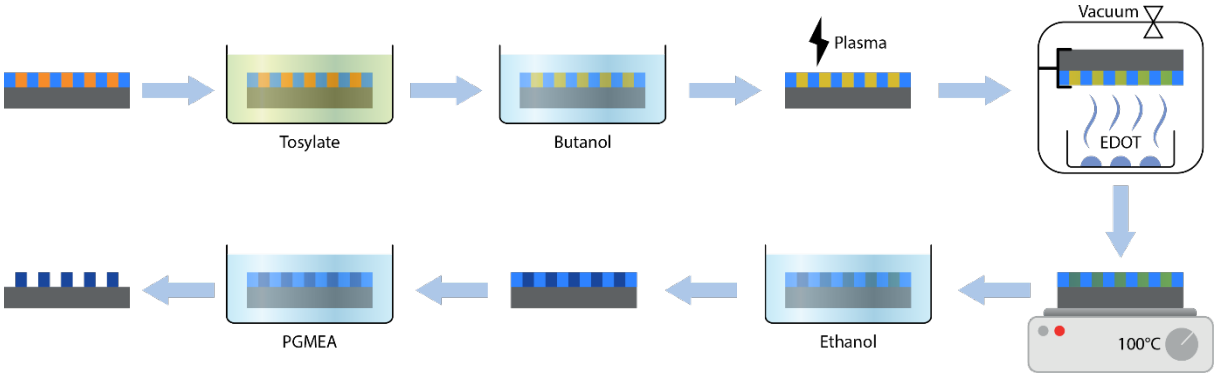

Figure V-17 Scheme of the process to polymerize EDOT in P2VP block by dipping block copolymer into tosylate.

III-1-a- P2VP RECONSTRUCTION

As tosylate in solution is dissolved in butanol, the effect of butanol on the PS-*b*-P2VP morphology has to be taken into account. Alcoholic solvents such as butanol or ethanol are characterized by hydroxyl groups able to interact with the electron lone pair of the nitrogen group of P2VP [30]. Electrostatic repulsion forces dominate during this step leading to a swelling of the P2VP domains. Chai *et al.* demonstrated a mushroom like structure with P2VP chains protuberating from the film surface due to the swelling of the P2VP domains [31], [32]. In particular for out-of-plane configuration of the P2VP domains, the P2VP swelling leads to a PS matrix with nanopores inherent to such surface reconstruction [33].

PS-*b*-P2VP films were accordingly dipped during 5 min either in a butanol bath or an ethanol bath and AFM images were recorded as displayed in Figure V-18. After dipping in butanol or ethanol, the P2VP domains (bright domains) swell and some P2VP chains are expelled from the initial domains (see topographical profile in insets) and partially cover the PS lamellae. The line profiles of BuOH and EtOH dipping samples show a twice higher height than pristine PS-*b*-P2VP.

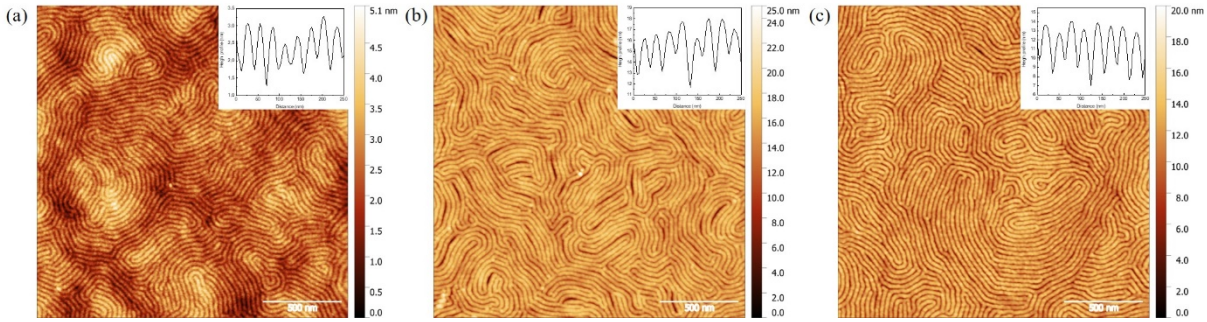

Figure V-18 Topographical AFM 2×2 µm² images (a) PS-b-P2VP lamellar morphology (b) PS-b-P2VP lamellar morphology after 5 min in BuOH bath (c) PS-b-P2VP lamellar morphology after 5 min in EtOH bath. Topographical profile is inserted in inset.

III-1-B- TOSYLATE CONCENTRATION

As previously demonstrated, butanol is able to swell P2VP domains, and tosylate anions in butanol are thus expected to infiltrate the P2VP domains. However, the concentration of tosylate in the initial butanol solution can play a role in the infiltration process. To gain further insights on the role of the tosylate concentration, PS-*b*-P2VP films were dipped into tosylate baths with different concentrations (0.5, 1, 2, 5, 10 and 15%) followed by a rinsing in a butanol bath to remove any excess at the surface. The AFM results are displayed in Figure V-19. At low concentration, from 0.5 to 2%, the PS-*b*-P2VP morphology is drastically modified and no lamellar structure is observed. From 5 to 15% of tosylate, the lamellar structure appears and it is clear that regions of the nanostructure have swelled. This swelling does not affect the overall period of the copolymer which remains at 31 nm highlighting the role of the rigid PS domains.

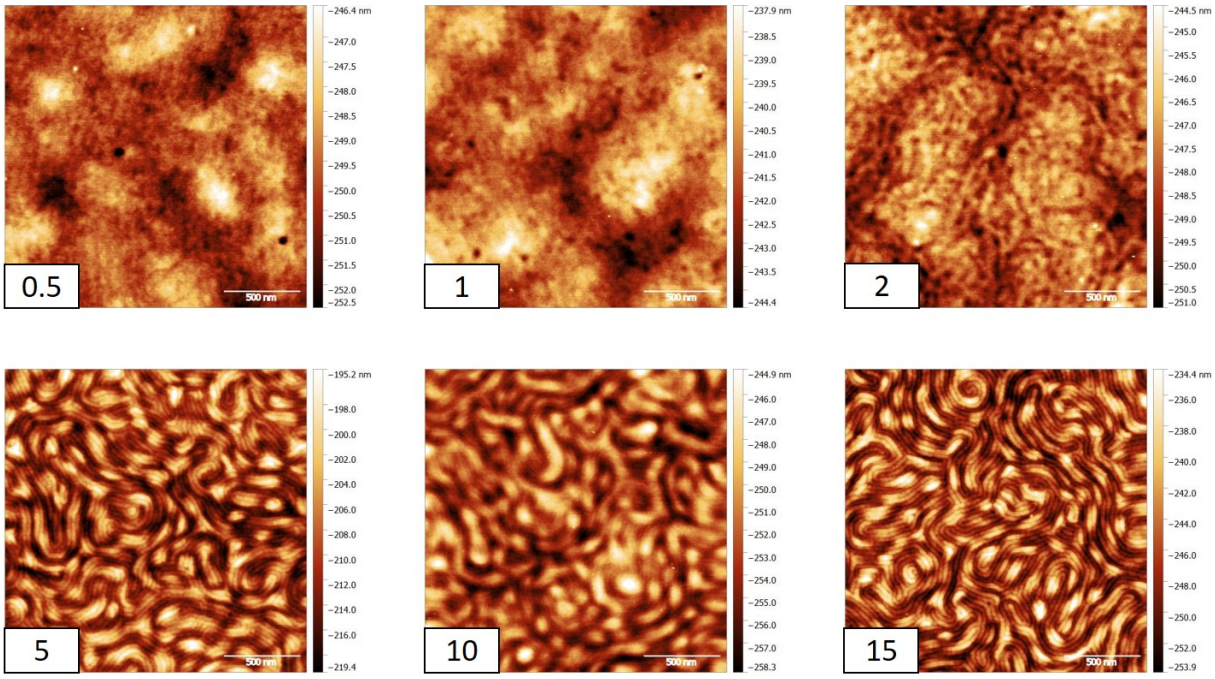

Figure V-19 Topographical AFM 2×2 µm² image of PS-b-P2VP film after dipping in tosylate bath and rinsing in butanol. The concentration of tosylate is given in the white square of each image.

In order to verify the incorporation of tosylate into the nanostructured films, XPS measurements have been performed on a PS-*b*-P2VP film dipped into a 15% tosylate solution. P2VP differs from PS as it contains a nitrogen atom in its repeating unit which allows us to follow the potential incorporation of tosylate into the P2VP domains via the interactions of the iron counter-ions with the nitrogen lone pair. Accordingly, precise scans of sulfur and nitrogen have been recorded in order to decipher the binding between these two elements and the results are displayed in Figure V-20.

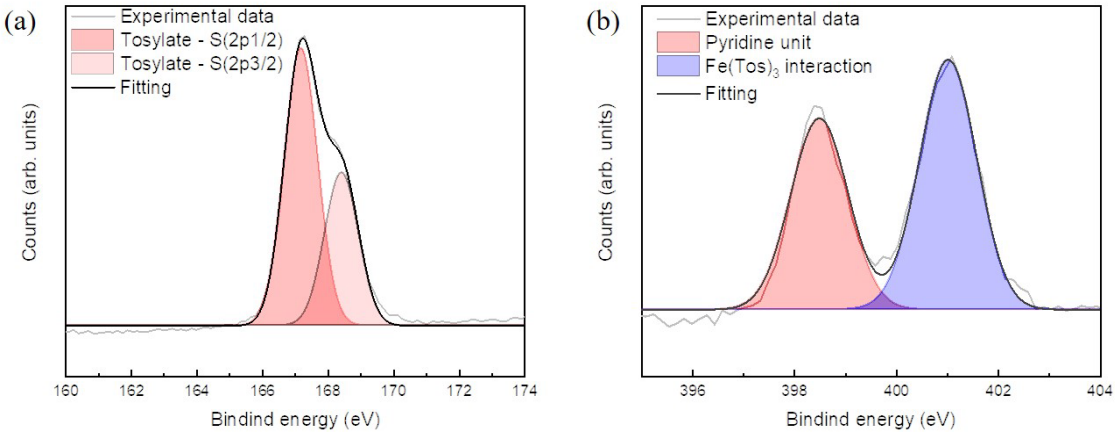

Figure V-20 XPS (a) S2p and (b) N1s spectra of PS-b-P2VP film after incorporation of tosylate

Two contributions can be extracted from the sulfur signal at 167.2 and 168.4 eV corresponding to the sulfur in the tosylate ion [34]. On the nitrogen spectrum, two contributions at 398.5 and 401.0 eV appear. The first one is linked to N in the pyridine unit while the second one can be attributed to the binding of iron ions with P2VP [35]. The shift of the contribution of the pyridine unit is linked to a thinning out of the electronic energy around this atom. By linking with nitrogen species, the Fe^{3+} ions appear to be reduced into Fe^{2+} species. As the Fe^{3+} ions are responsible for the oxidative polymerization of EDOT, the transformation from Fe^{3+} to Fe^{2+} is highly detrimental to the polymerization. Nevertheless, tosylate molecules are effectively inserted into the P2VP domains even if a proper quantification is missing. Our next step was thus to evaluate the propensity of EDOT to polymerize in such nano-templates as we cannot discard that some Fe^{3+} could be available to trigger the polymerization of EDOT monomers.

III-1-c- VPP OF TEMPLATED PEDOT:TOS

As said previously, tosylate in butanol is a viscous solution and dipping PS-*b*-P2VP film inside such a solution results in a layer of tosylate on top of the copolymer film. Two pathways to remove this layer were tested: the removal of the layer by rinsing in butanol or the flipping of the film followed by an etching step to reveal PEDOT:Tos.
As the best results on the incorporation of tosylate salts into the P2VP domains were obtained from a 15% tosylate solution, the aforementioned processes were applied to such structures. The resulting films were then employed as template for the VPP of EDOT monomers.

- *Removal of the tosylate salts layer by rinsing in butanol*

After being rinsed, the films were held above EDOT monomer droplets in the VPP set-up described in the previous chapters. The polymerization was performed for 5 minutes, 15 minutes or 1 hour at 100°C under static vacuum. After the VPP, the films were removed from the chamber and placed 5 minutes on a hot plate at 100°C, followed by a washing step with butanol. It is noteworthy that a mild plasma

treatment, inducing the cross-linking of the PS-*b*-P2VP layer was necessary in order to avoid the solubilization of the BCP film by the EDOT vapors. AFM characterization was performed after the VPP process to evaluate the morphological changes induced by the EDOT polymerization. Interestingly, the nanostructure observed after the dipping in the tosylate solution is preserved independently of the VPP duration with a periodicity of the lamellar structure of 33 nm as shown in Figure V-21. Nevertheless, we noticed that the topography of the films is modified with an accentuated roughness for the longer VPP duration. Such modification suggests an additive process of PEDOT materials templated by the BCP structure.

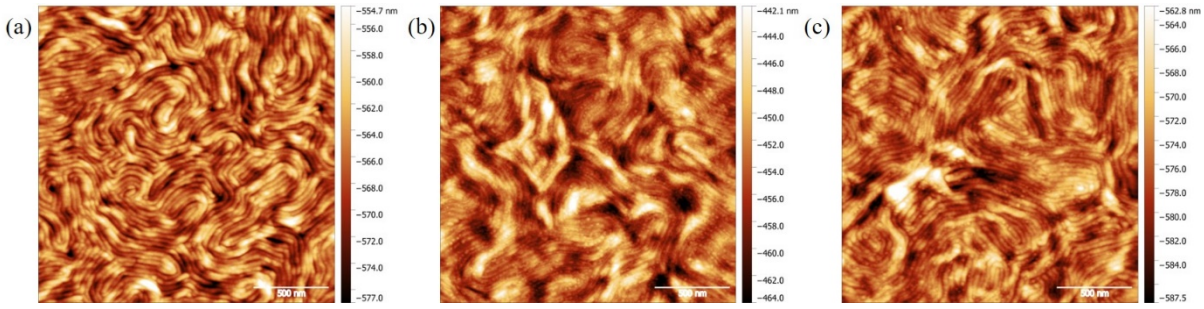

Figure V-21 Topographical AFM 2×2 µm² images of PS-b-P2VP film after dipping in tosylate bath and different VPP times. (a) 5 minutes (b) 15 minutes (c) 1 hour.

XPS measurements were carried in order to confirm these results. In the resulting S2p spectrum, Figure V-22, two peaks at 169.4 and 170.7 eV are retrieved and correspond to the sulfur unit link to oxygen in tosylate. Unfortunately, no signal from PEDOT could be resolved from this spectrum, underlining at best the weak efficiency of the VPP process. Further attempts to improve the process by tuning of the VPP parameters did not lead to conclusive results.

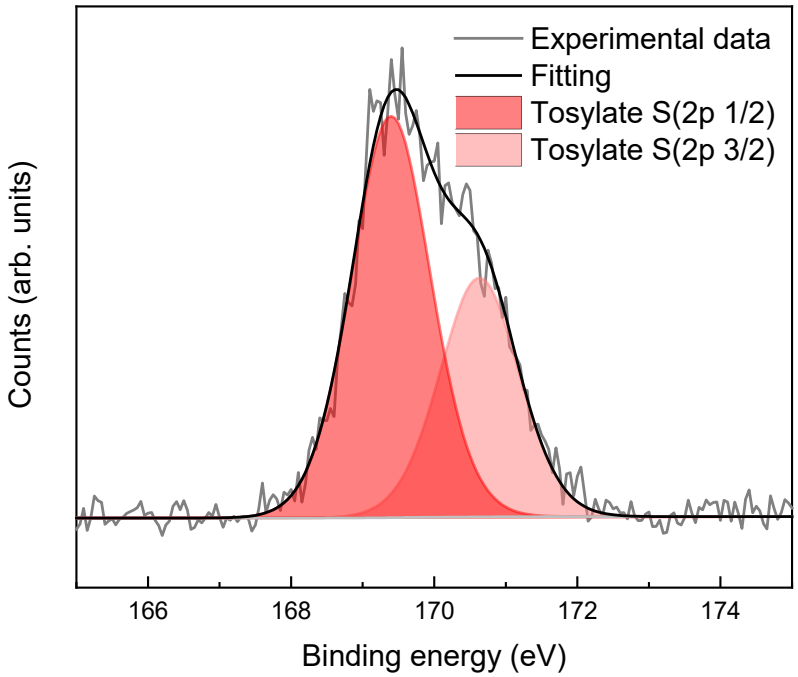

Figure V-22 XPS S2p spectra of PS-b-P2VP film dipped in tosylate bath after VPP. Red areas represent the signals linked to S2p in tosylate.

- *Flipping the film*

In order to verify that the VPP process did not take place in the bulk of the BCP structure or was inhibited through the final rinsing step with butanol, a PS-*b*-P2VP film loaded with tosylate (and exhibiting a thin tosylate layer on top of it) was used to perform the VPP of EDOT. The topographical AFM image in Figure V-23 shows the morphology of the PEDOT:Tos layer on top the nanostructured PS-*b*-P2VP film. The top surface of the film is characteristic of PEDOT:Tos with small dot features inherent to the nucleation and growth mechanism of PEDOT formation by VPP.

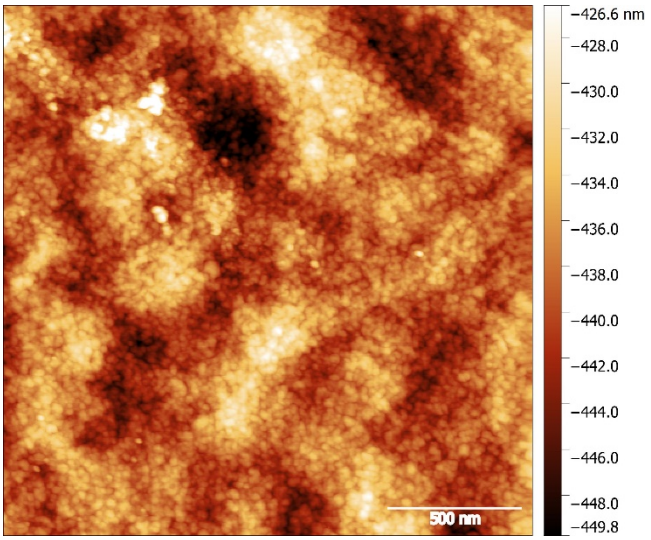

Figure V-23 Topographical AFM 2×2 µm² image of PS-b-P2VP film after dipping in a tosylate bath used for the VPP of EDOT.

The objective was now to flip the film in order to reveal the PS-*b*-P2VP structure. A solution of NaOH concentrated at 0.5 M was used to remove the film from the substrate. As the NaOH attacks the SiO_2 native oxide on top on the silicon substrate, the film is then peeled-off and floats onto the NaOH solution [36]. The floating film is then flipped on a new substrate to analyze it by AFM and the resulting image is displayed in Figure V-24 (a). The bottom surface of the film does not display the typical lamellar morphology of the PS-*b*-P2VP BCP but resembles a PEDOT:Tos-like structure. A blank test was also performed on a pristine PS-*b*-P2VP film and by dipping the film in NaOH the BCP structure was retrieved as shown in Figure V-24(b). In summary, even if it is possible to load the PS-*b*-P2VP structure with tosylate, the subsequent VPP process did not allow us to obtain nanostructured PEDOT:Tos structures. We hypothesize that the EDOT vapors are able to solubilize the BCP film during the VPP process and the plasma process used to counter-interact such solubilization leads to the inability for the EDOT vapors to penetrate the BCP structure loaded with tosylate.

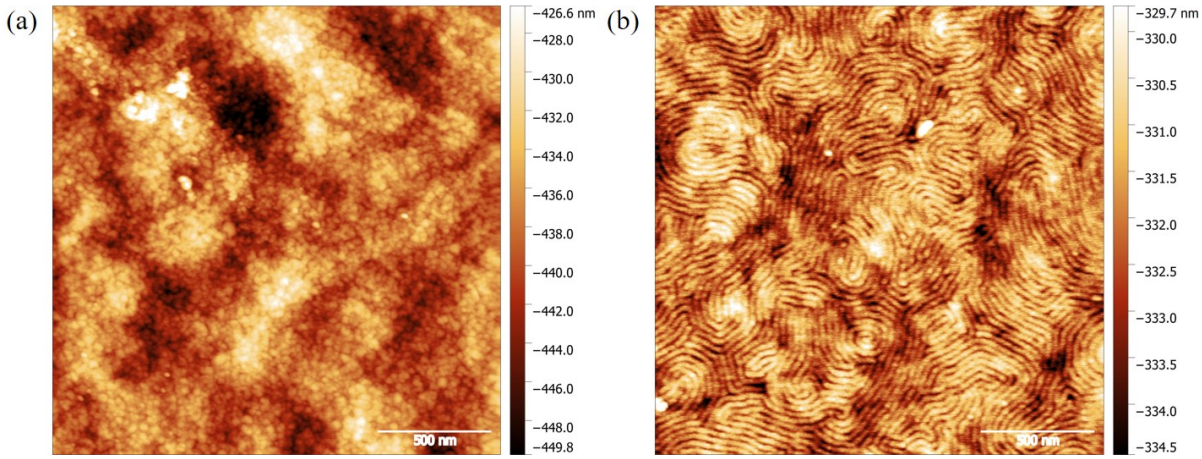

Figure V-24 Topographical AFM 2×2 µm² image of (a) PEDOT:Tos layer on top of PS-b-P2VP film after dipping in tosylate bath, vapor phase polymerized one hour at 100°C and flipping the film in NaOH. (b) PS-b-P2VP film dipped into NaOH 0.5 M solution.

III-2- Solution processing PS-*b*-P2VP:tosylate

Another pathway to pattern PEDOT:Tos polymer via BCP self-assembly is to directly deposit a mixture of BCP and tosylate in a thin film configuration . Accordingly, Lee *et al.* mixed tosylate salts with a PEO-*b*-PPO-*b*-PEO triblock copolymer [6] and after an annealing step, they concluded using GIWAXS that PEDOT:Tos can be confined into different BCP morphologies (lamellar, cylindrical and bi-continuous). It is noteworthy that a direct visualization of the structures was not provided.

Accordingly, a lamellar PS-*b*-P2VP BCP solution in PGEMA was loaded with tosylate (either in the form of iron tosylate salts or using a commercially available tosylate solution (Clevios)). The concentration of the mixture was kept at 2% and the ratio between the BCP and tosylate was varied. In the following we will use the notation *x*:*y* to describe the ratio between BCP and tosylate.

III-2-a- Mixing solutions process

Four solutions containing BCP and tosylate with ratios of 5:5, 6:4, 8:2 and 9:1 were prepared. These solutions were stirred for few hours and filtrated with a 0.22 µm PTFE filter. An underlayer was deposited on the silicon substrate to neutralize the surface with respect to the BCP domains then the mixture was spin-coated at 2000 RPM during 30 seconds. Prior to VPP, the films were treated with an Ar plasma (40 sccm, 40W and 15 s) to avoid the solubilization of PS-*b*-P2VP by the EDOT vapors. VPP

were carried out 5 min at 100°C. Following that, the films were annealed and rinsed in an ethanol bath prior to characterization. The process is displayed in Figure V-25.

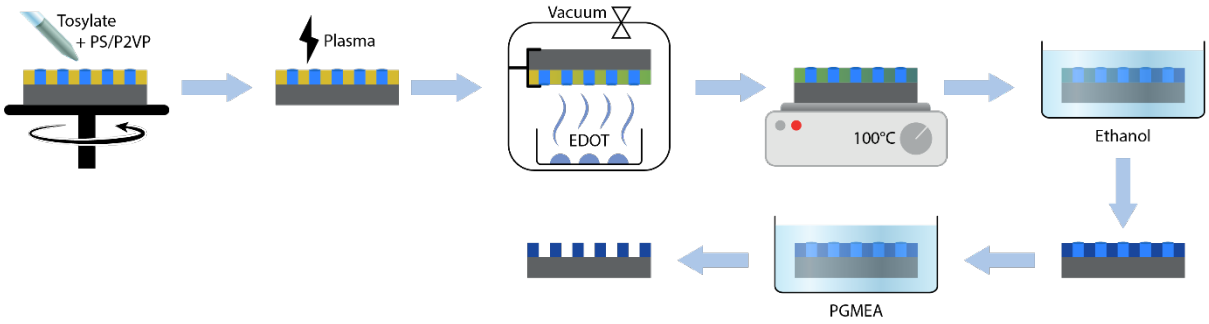

Figure V-25 Scheme of the process flow to polymerize EDOT in P2VP domains by dipping block copolymer into tosylate.

III-2-B- Results and discussion

The PS-*b*-P2VP BCP used in this study self-assembled in a lamellar configuration. By mixing with tosylate salts, the morphology of the BCP is modified, as displayed in Figure V-26. At a ratio of 5:5, it is possible to distinguish a segregation between the PS and P2VP domains but it is not possible to clearly identify the actual structure. At 6:4, the self-assembly is improved and it is now possible to distinguish isolated domains in a matrix even if the actual symmetry of the structure could not be established. As opposed, for the ratios 8:2 and 9:1, an out-of-plane cylindrical morphology can be observed. As the tosylate moieties have more affinity towards the P2VP block, its addition to the BCP system swells the P2VP domains leading to a morphological shift towards a hexagonally-packed PS cylindrical morphology embedded in a P2VP matrix. Indeed, such selective swelling induces an increase of the P2VP volume fraction inducing a shift in morphology from lamellar to cylindrical structures. The swelling of the BCP structure is further confirmed by an increase of the periodicity of the self-assembled structure, from 33 nm for the pristine PS-*b*-P2VP structure to 37.5 nm for the swelled structure.

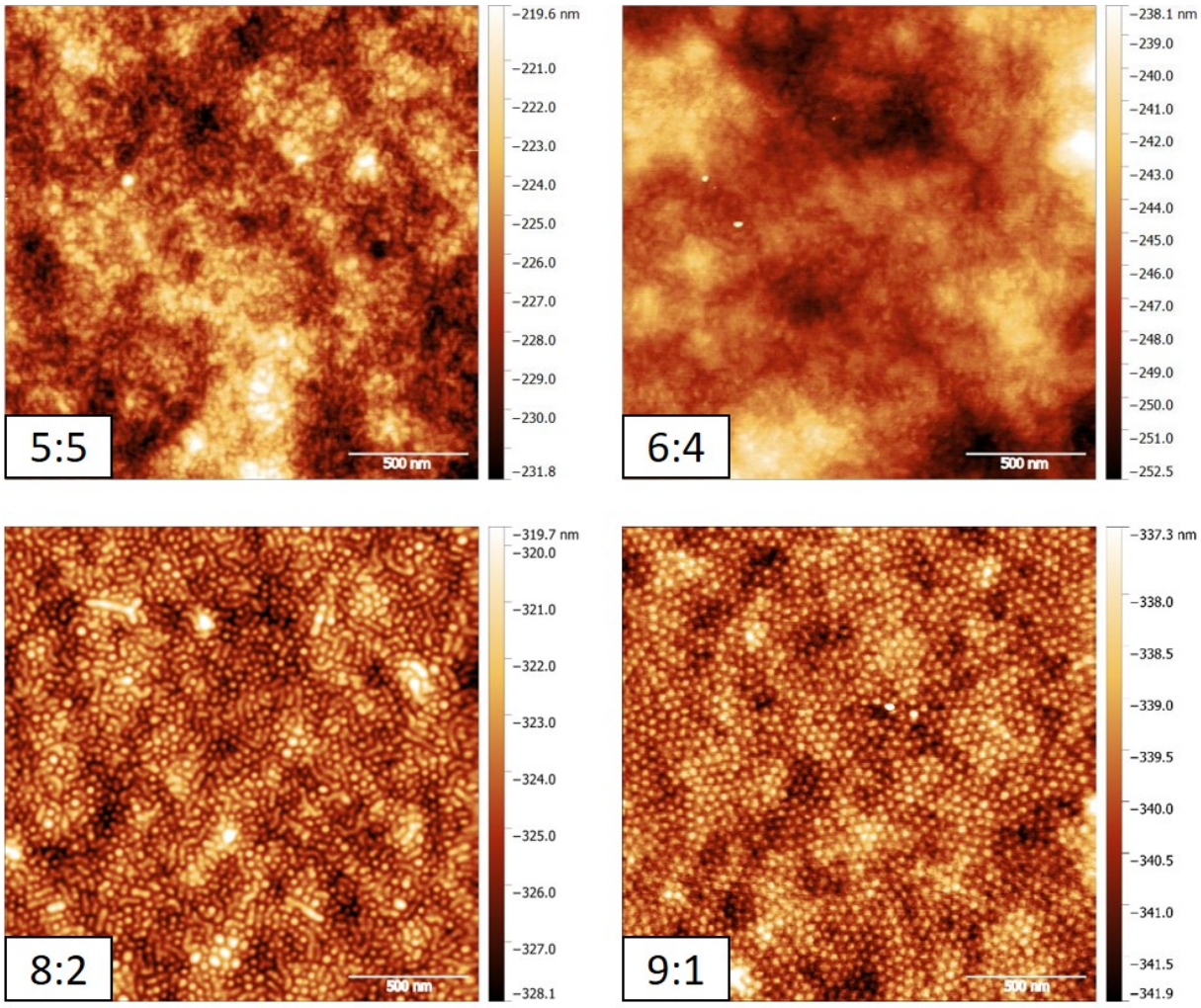

Figure V-26 Topographical AFM 2×2 µm² images of PS-b-P2VP:tosylate mixing films.

The 9:1 ratio was chosen to evaluate the influence of the addition of iron tosylate salts or Clevios on the self-assembly. The hybrid films (PS-*b*-P2VP + tosylate) were characterized by AFM and the results are displayed in Figure V-27. Interestingly, we did not notice any modifications of the morphological features as the nanostructured films are composed in both cases of PS cylinders inside a P2VP matrix.

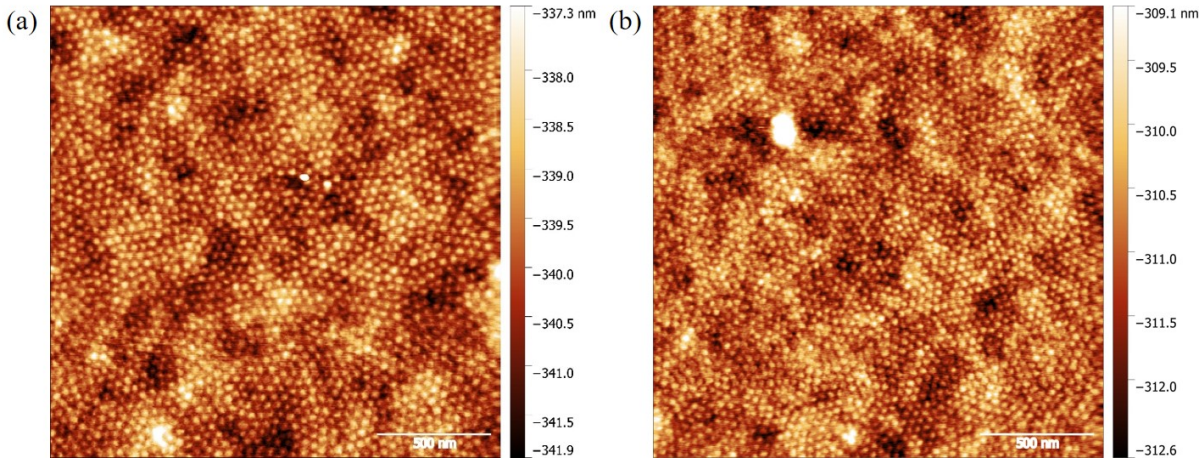

Figure V-27 Topographical AFM 2×2 µm² images of 9:1 PS-b-P2VP:tosylate mixing films. (a) using iron tosylate salts or (b) Clevios.

The resulting films were placed in the VPP chamber in order to template the polymerization of EDOT. In order to suppress the solubilization of the BCP film by EDOT vapors during the VPP process, either UV exposure (254 nm) during 30 seconds or Ar plasma treatments during 15 or 30 seconds were tested. Only the Ar plasma treatment during 30 seconds allows us to limit the extent of dewetting. The two first treatments were not efficient and led to a strong dewetting of the films under EDOT vapors. Accordingly, films treated with 30 seconds of Ar plasma were used for VPP.

- *Use of iron tosylate salts*

The films after VPP are not homogeneous, as it can be seen on the optical microscopy image shown in Figure V-28. The film is composed of areas with different thicknesses induced by film dewetting despite the use of the Ar plasma treatment. Figure V-28 displayed the morphological features obtained for three characteristic areas. Unfortunately, a strongly perturbed texture of the films were obtained even if hints of BCP structures could be observed. Despite the important modification of the self-assembled structures induced by the VPP process, we further analyzed the films by XPS in order to probe the formation of PEDOT:Tos.

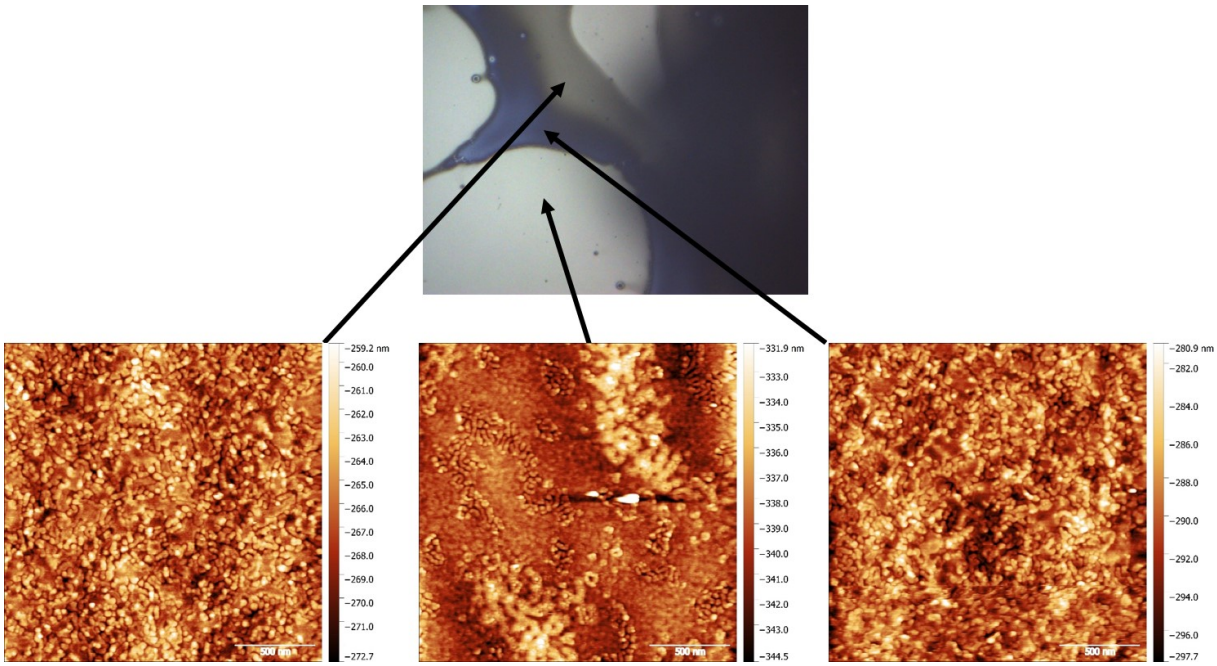

Figure V-28 Optical camera image and topographical AFM 2×2 µm² images of 9:1 PS-b-P2VP:tosylate mixing films with tosylate salts. The arrows pointed out the analyzing areas.

The survey spectrum confirms the presence of carbon, oxygen, nitrogen and sulfur linked to PS-*b*-P2VP, tosylate and/or PEDOT. The fitting of the sulfur XPS spectrum is shown in Figure V-29. Contributions of tosylate are clearly visible at 169.9 and 171.2 eV despite the low resolution of the spectrum. Two contributions at 165.6 and 167.6 eV can be tentatively assigned to sulfur signals in PEDOT even if the resolution is low.

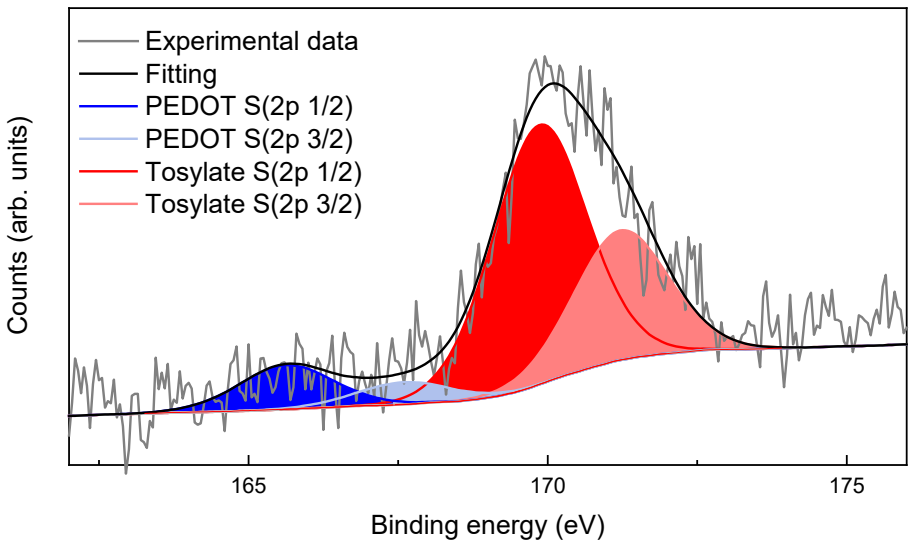

Figure V-29 XPS S2p spectra of mixing film (9:1) with tosylate salts. Blue and red areas represent the signals linked to S2p in PEDOT and S2p in tosylate, respectively.

- *Use of Clevios*

Interestingly, when applying the same route to BCP films processed with Clevios, the resulting films are more homogeneous with limited dewetting as shown in Figure V-30. Both islands and holes areas have been analyzed by AFM and the images are displayed in Figure V-30. The films are composed of small dots which displayed strong similarity with the texture of pristine PEDOT:Tos films made by VPP. Besides, BCP templating is evidenced as the BCP characteristic distance (32 nm in holes and 38 nm in islands) could be retrieved from the inverse power spectral density of the AFM images.

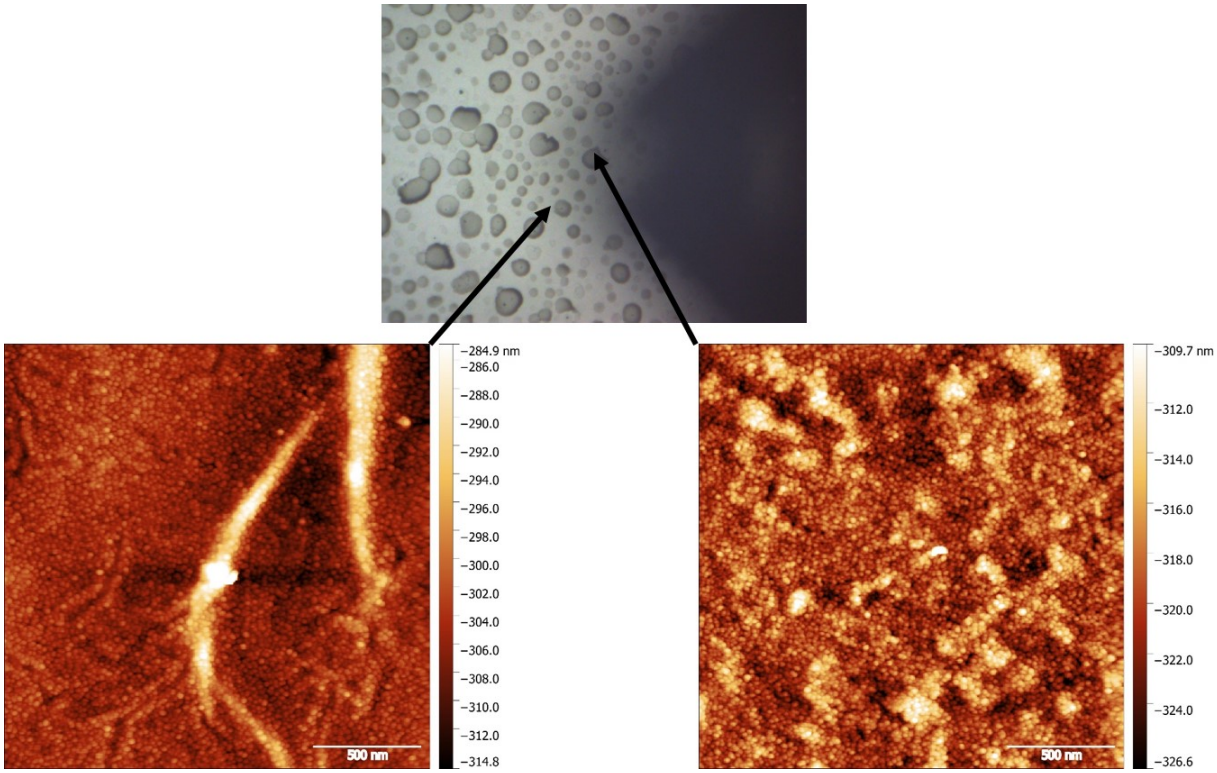

Figure V-30 Optical microscopy image and topographical AFM 2×2 µm² images of 9:1 PS-b-P2VP:tosylate obtained from Clevios. The arrows pointed out the analyzing areas.

The formation of PEDOT:Tos was also probed by XPS measurements. Spectra of the sulfur signal have been recorded with a large amount of scans but the intensity of the signal remains low as shown Figure V-31. The mains contributions at 169.9 and 171.2 eV correspond to the sulfur S2p signal from tosylate anions. Two others contributions at 164.7 and 166.4 eV can be attributed to sulfur S2p signals coming from PEDOT.

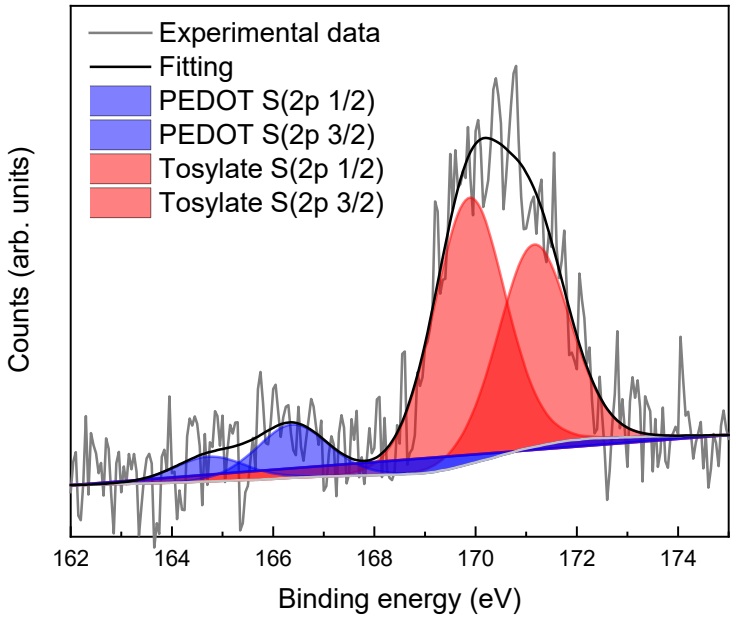

Figure V-31 XPS S2p spectra of mixing film (9:1) with Clevios. Blue and red areas represent the signals linked to S2p in PEDOT and S2p in tosylate, respectively.

One more time, the PEDOT signal is weak compared to the tosylate one. Moreover, the other contribution of PEDOT corresponding to charged PEDOT cannot be fitted. This result reveals that no delocalized charge (or a very small amount) are present along the polymer backbone. The absence of delocalized charges drastically decreases the electrical conductivity. To verify these assumptions, electrical conductivity measurements using 4 probes set-up have been performed and they did not reveal macroscopic transport in the samples.

IV- Conclusion

Block copolymers are interesting materials to nano-pattern other materials like PEDOT:Tos. In this study, we proved that lithography is an interesting way to obtain a matrix or lines of PEDOT:Tos with a conductivity around 60 $S.cm^{-1}$. Despite an important loss in electrical conductivity as compared to PEDOT:Tos films previously studied, lithography permits to transfer the BCP pattern to such conductive layer. An idea to increase the electrical conductivity should be to use a soft method to transfer the BCP pattern or to effectuate the patterning in a controlled atmosphere (without O_2) while re-doping the material after the plasma treatment.

On the other hand, dipping PS-*b*-P2VP films inside a solution of tosylate slightly modifies the morphology due to the interactions between the P2VP domains and the tosylate species. Unfortunately, we did not succeed to further polymerize PEDOT inside the P2VP domains loaded with tosylate moieties.

Finally, the direct mixing of BCPs with tosylate leads to a change in the morphology from lamellar to cylindrical, demonstrating the affinity of tosylate for the P2VP domains. However, after VPP, only traces of PEDOT:Tos could be retrieved. Even if this last pathway appears to be the most promising, we still need to improve the polymerization process in order to obtain nanostructured PEDOT:Tos layer at the nanometer scale

[1] J. Wang, K. Cai, H. Song, and S. Shen, "Simultaneously enhanced electrical conductivity and Seebeck coefficient in Poly (3,4-ethylenedioxythiophene) films treated with hydroiodic acid," *Synth. Met.*, vol. 220, pp. 585–590, 2016, doi: 10.1016/j.synthmet.2016.07.023.

[2] E. H. Khan *et al.*, "Environment-Friendly Post-Treatment of PEDOT-Tos Films by Aqueous Vitamin C Solutions for Tuning of Thermoelectric Properties," vol. 47, no. 7, 2018, doi: 10.1007/s11664-018-6279-5.

[3] J. Wang, K. Cai, and S. Shen, "A facile chemical reduction approach for effectively tuning thermoelectric properties of PEDOT films," *Org. Electron.*, vol. 17, pp. 151–158, 2015, doi: 10.1016/j.orgel.2014.12.007.

[4] R. Brooke, D. Evans, M. Dienel, P. Hojati-talemi, and P. Murphy, "Inkjet printing and vapor phase polymerization : patterned conductive PEDOT for electronic applications †," pp. 3353–3358, 2013, doi: 10.1039/c3tc30356j.

[5] B. Cho, K. S. Park, J. Baek, H. S. Oh, Y. E. Koo Lee, and M. M. Sung, "Single-crystal poly(3,4-ethylenedioxythiophene) nanowires with ultrahigh conductivity," *Nano Lett.*, vol. 14, no. 6, pp. 3321–3327, 2014, doi: 10.1021/nl500748y.

[6] Y. H. Lee, J. Oh, S. S. Lee, H. Kim, and J. G. Son, "Highly Ordered Nanoconfinement Effect from Evaporation-Induced Self-Assembly of Block Copolymers on In Situ Polymerized PEDOT:Tos," *ACS Macro Lett.*, vol. 6, no. 4, pp. 386–392, 2017, doi: 10.1021/acsmacrolett.7b00137.

[7] C. D. O'Connell, M. J. Higgins, H. Nakashima, S. E. Moulton, and G. G. Wallace, "Vapor phase polymerization of EDOT from submicrometer scale oxidant patterned by dip-pen nanolithography," *Langmuir*, vol. 28, no. 26, pp. 9953–9960, 2012, doi: 10.1021/la301724v.

[8] F. S. Bates and G. H. Fredrickson, "Block copolymers-designer soft materials," *Phys. Today*, vol. 52, no. 2, pp. 32–38, 1999, doi: 10.1063/1.882522.

[9] S. B. Darling, "Directing the self-assembly of block copolymers," *Prog. Mater. Sci.*, vol. 32, pp. 1152–1204, 2007, doi: 10.1016/j.progpolymsci.2007.05.004.

[10] T. Daniel *et al.*, "Patterning and Conductivity Modulation of Conductive Polymers by UV Light Exposure," 2016, doi: 10.1002/adfm.201601794.

[11] S. Park, C. W. Lee, and J. M. Kim, "Highly conductive PEDOT:PSS patterns based on photo-crosslinkable and water-soluble diacetylene diol additives," *Org.*

Electron., vol. 58, no. March, pp. 1–5, 2018, doi: 10.1016/j.orgel.2018.03.044.

[12] Z. Zhu, G. Yang, R. Li, and T. Pan, "Photopatternable pedot:Pss/peg hybrid thin film with moisture stability and sensitivity," *Microsystems Nanoeng.*, vol. 3, no. May 2016, pp. 1–9, 2017, doi: 10.1038/micronano.2017.4.

[13] S. Ouyang *et al.*, "Surface Patterning of PEDOT:PSS by Photolithography for Organic Electronic Devices," *J. Nanomater.*, vol. 2015, 2015, doi: 10.1155/2015/603148.

[14] C. M. Bates, M. J. Maher, D. W. Janes, C. J. Ellison, and C. G. Willson, "Block Copolymer Lithography," *Macromolecules*, vol. 47, no. 1, pp. 1–12, 2014, doi: 10.1016/B978-0-444-53874-1.00013-5.

[15] X. Gu, I. Gunkelk, and T. P. Russell, "Pattern transfer using block copolymers," *Philos. Trans. R. Soc. A Math. Phys. Eng. Sci.*, vol. 371, no. 2000, 2013, doi: 10.1098/rsta.2012.0306.

[16] K. Asakawa and T. Hiraoka, "Nanopatterning with microdomains of block copolymers using reactive-ion etching selectivity," *Jpn. J. Appl. Phys.*, vol. 41, no. 10, pp. 6112–6118, 2002, doi: 10.1143/jjap.41.6112.

[17] B. Charlot, G. Sassine, A. Garraud, B. Sorli, A. Giani, and P. Combette, "Micropatterning PEDOT:PSS layers," *Microsyst. Technol.*, vol. 19, no. 6, pp. 895–903, 2013, doi: 10.1007/s00542-012-1696-5.

[18] V. Kostianovskii, B. Sanyoto, and Y. Y. Noh, "A facile way to pattern PEDOT:PSS film as an electrode for organic devices," *Org. Electron.*, vol. 44, pp. 99–105, 2017, doi: 10.1016/j.orgel.2017.02.007.

[19] H. Hu, M. Gopinadhan, and C. O. Osuji, "Directed self-Assembly of block copolymers: A tutorial review of strategies for enabling nanotechnology with soft matter," *Soft Matter*, vol. 10, no. 22, pp. 3867–3889, 2014, doi: 10.1039/c3sm52607k.

[20] Y. Ting *et al.*, "Plasma etch removal of poly (methyl methacrylate) in block copolymer lithography," *J. Vac. Sci. Technol. B*, vol. 26, no. 5, p. 1684, 2008, doi: 10.1116/1.2966433.

[21] M. Fabretto, C. Jariego-moncunill, J. Autere, A. Michelmore, R. D. Short, and P. Murphy, "High conductivity PEDOT resulting from glycol / oxidant complex and glycol / polymer intercalation during vacuum vapour phase polymerisation,"

Polymer (Guildf)., vol. 52, no. 8, pp. 1725–1730, 2011, doi: 10.1016/j.polymer.2011.02.028.

[22] K. Z. Xing, M. Fahlman, X. W. Chen, O. Inganäs, and W. R. Salaneck, "The electronic structure of poly(3,4-ethylene-dioxythiophene): studied by XPS and UPS," *Synth. Met.*, vol. 89, no. 3, pp. 161–165, 1997, doi: 10.1016/S0379-6779(97)81212-X.

[23] C. Liu, M. J. Goeckner, and A. V. Walker, "Plasma polymerization of poly(3,4-ethylenedioxyethene) films: The influence of plasma gas phase chemistry," *J. Vac. Sci. Technol. A Vacuum, Surfaces, Film.*, vol. 35, no. 2, p. 021302, 2017, doi: 10.1116/1.4968017.

[24] A. M. Nardes, M. Kemerink, M. M. de Kok, E. Vinken, K. Maturova, and R. A. J. Janssen, "Conductivity, work function, and environmental stability of PEDOT:PSS thin films treated with sorbitol," *Org. Electron.*, vol. 9, pp. 727–734, 2008, doi: 10.1016/j.orgel.2008.05.006.

[25] J. Huang, P. F. Miller, J. S. Wilson, A. J. de Mello, J. C. De de Mello, and D. D. C. Bradley, "Investigation of the Effects of Doping and Post-Deposition Treatments on the Conductivity, Morphology, and Work Function of Poly (3,4-ethylenedioxythiophene)/ Poly (styrene sulfonate) Films," *Adv. Funct. Mater.*, vol. 15, no. 2, pp. 290–296, 2005, doi: 10.1002/adfm.200400073.

[26] L. Zhang, Y. Ju, A. Hosoi, and A. Fujimoto, "Measurement of electrical properties of materials under the oxide layer by microwave-AFM probe," *Microsyst. Technol.*, vol. 18, no. 11, pp. 1917–1922, 2012, doi: 10.1007/s00542-012-1512-2.

[27] S. A. Shamsudin, T. Mikihito, and H. Hirokazu, "Controlling Ordered Structures of PS-b-P2VP Block Copolymer Thin Film by Tuning Solvent Evaporation Rate," pp. 75–83, 2017, doi: 10.1002/masy.201600041.

[28] J. Q. Lu and S. S. Yi, "Uniformly sized gold nanoparticles derived from PS-b-P2VP block copolymer templates for the controllable synthesis of Si nanowires," *Langmuir*, vol. 22, no. 9, pp. 3951–3954, 2006, doi: 10.1021/la053377x.

[29] S. Z. Bas, C. Cummins, A. Selkirk, D. Borah, M. Ozmen, and M. A. Morris, "A Novel Electrochemical Sensor Based on Metal Ion In fi ltrated Block Copolymer Thin Films for Sensitive and Selective Determination of Dopamine," 2019, doi: 10.1021/acsanm.9b01794.

[30] Y. Wang, U. Gösele, and M. Steinhart, "Mesoporous block copolymer nanorods by swelling-induced morphology reconstruction," *Nano Lett.*, vol. 8, no. 10, pp. 3548–3553, 2008, doi: 10.1021/nl8022687.

[31] J. Chai, D. Wang, X. Fan, and J. M. Buriak, "Assembly of aligned linear metallic patterns on silicon," *Nat. Nanotechnol.*, vol. 2, no. 8, pp. 500–506, 2007, doi: 10.1038/nnano.2007.227.

[32] J. Chai and J. M. Buriak, "Using cylindrical domains of block copolymers to self-assemble and align metallic nanowires," *ACS Nano*, vol. 2, no. 3, pp. 489–501, 2008, doi: 10.1021/nn700341s.

[33] J. Yin, X. Yao, J. Y. Liou, W. Sun, Y. Sen Sun, and Y. Wang, "Membranes with highly ordered straight nanopores by selective swelling of fast perpendicularly aligned block copolymers," *ACS Nano*, vol. 7, no. 11, pp. 9961–9974, 2013, doi: 10.1021/nn403847z.

[34] M. Fabretto, K. Zuber, C. Hall, and H. J. Griesser, "The role of water in the synthesis and performance of vapour phase polymerised PEDOT electrochromic devices," pp. 7871–7878, 2009, doi: 10.1039/b912324e.

[35] J. G. Kennemur, "Poly(vinylpyridine) Segments in Block Copolymers: Synthesis, Self- Assembly, and Versatility," 2019, doi: 10.1021/acs.macromol.8b01661.

[36] A. Guliyeva, M. Vayer, F. Warmont, A. Takano, Y. Matsushita, and C. Sinturel, "Transition Pathway between Gyroid and Cylindrical Morphology in Linear Triblock Terpolymer Thin Films," *Macromolecules*, 2019, doi: 10.1021/acs.macromol.9b01263.

GENERAL CONCLUSION

Organic electronic has been in perpetual development to overcome the inherent limitations of organic materials in term of charge transport with respect to inorganic compounds. Nevertheless, organic/polymeric materials show some advantages inherent to their viscoelastic properties, low toxicity and abundance problem of synthesis and toxicity of inorganic compounds. Organic thermoelectric materials do not fail to the rule. While inorganic materials, and especially Bi_2Te_3, is the most studied compounds as it can reach high ZT, polymers have shown promise for their implementation in targeted thermoelectric applications (wearable, room temperature application). In particular, by doping PEDOT, it is possible to achieve ZT comparable to inorganic compounds.

In this thesis, we have thus explored the thermoelectric properties of PEDOT:Tos and the pathways to enhance the final applicative properties. Specifically, we were able to obtain an electrical conductivity of 2000 $S.cm^{-1}$ for optimized formulations of PEDOT:Tos, which is one of the highest value reported as today in the literature. Such result was obtained through the comparison of the thermoelectric, electronic and crystallographic properties of PEDOT:Tos films synthetized by either ISP or VPP which allows us to decipher the optimal pathway for the formation of highly conductive PEDOT:Tos layer. We demonstrated that films made by ISP have better transport properties than films made by VPP even if the oxidation level was found to be constant for both polymerization pathways. Such result clearly shows that the PEDOT:Tos structure (crystallinity and morphological features at the nanoscale) resulting from the polymerization is primordial in order to obtain high thermoelectric efficiency.
We further investigated PEDOT:Tos films made by VPP in order to analyze the role of additives and oxidant concentration. Pyridine and DMSO have been used to increase the arrangement of the polymers chains and so improve the thermoelectric properties. By playing also on the tosylate concentration, an electrical conductivity higher than 2000 $S.cm^{-1}$ was obtained with a Seebeck coefficient of 20.1 ± 0.8 µV.K-1.

This results of a high power factor of 105 ± 18 $\mu V.m^{-1}.K^{-2}$ which is higher than studies reported for PEDOT:Tos material.

Based on these promising results, we decided to use the VPP process in combination with block copolymer templating to generate nano-patterned PEDOT:Tos. Such nano-patterned layer could further be used to study the effect of confinement on the PEDOT:Tos transport properties (and fortunately demonstrate enhanced properties). We have shown the ability of BCP lithography to template PEDOT:Tos layer using PS-*b*-PMMA. Unfortunately, we observed a loss of the electronic properties due to the final etching step by plasma. In order to avoid such detrimental treatment, we have implemented a methodology based on the preferential interaction between P2VP and tosylate moieties in order to generate PEDOT:Tos inside nanostructured PS-*b*-P2VP structure. Our assumptions on the preferential loading of tosylate moieties inside the P2VP domains were verified by a combination of XPS and AFM measurements. Nevertheless, despite the presence of tosylate inside P2VP domains, the polymerization of EDOT by VPP inside the loaded P2VP domains was not successful, probably due to the poor diffusion of the EDOT vapors inside the nanostructured thin films.

In summary, we have demonstrated that PEDOT:Tos is a very promising material for thermoelectric applications. Its properties can be tuned on-demand by treating the films or directly during polymerization. We have also shown that VPP is the polymerization technique which affords the most potent tuning of the material properties. This could be further improved by designing a VPP set-up with advanced control of the temperature, the environment of polymerization (vacuum or atmosphere, humidity level) or the vapor pressure of EDOT in the chamber. Additionnaly, further details could be gathered by using an in-situ quartz microbalance in order to follow the growth rate of the films. These improvements should allow us to better understand the formation of PEDOT:Tos films and further improve the thermoelectric properties.

Such improvements would also allow us to better control the parameters needed to generate nano-structured PEDOT:Tos layer. Our results on the hybridization of BCP

structure with precursors of PEDOT:Tos are very promising and a fine tuning of the protocol should give us the opportunity to generate highly conductive nanostructured PEDOT:Tos. In particular, the BCP chemistry (for instance, PS-*b*-PEO or PEO-*b*-PPO-*b*-PEO) should be further engineered in order to permit both the loading of the tosylate into the BCP domains and the diffusion of the EDOT vapors inside the BCP domains. The use of sequential infiltration synthesis using atomic layer deposition technique could be envisaged in order to succeed in this pathway. For the direct patterning of PEDOT:Tos layer by BCP lithography, the use of mild treatments (for instance wet chemical etching or low energy plasma) to pattern the PEDOT:Tos layer should be investigated.

Titre : Polymères semi-métalliques pour des applications en thermoélectricité

Résumé : Les matériaux thermoélectriques (TE) ont le potentiel de convertir de grandes quantités de chaleur directement en électricité, et par conséquent de réduire la dépendance aux combustibles fossiles. En thermoélectricité, le concept d'un verre de phonons/cristal électronique est souvent utilisé pour décrire un matériau thermoélectrique idéal. Selon ce concept, un bon matériau TE devrait inhiber la conduction de phonons (ayant ainsi une faible conductivité thermique) tout en assurant efficacement une bonne conduction des porteurs de charges (conductivité électrique importante). Afin de quantifier l'efficacité des systèmes TE, la figure de mérite, ZT, est utilisée comme mesure de performance. Récemment, les polymères conducteurs ont gagné de l'élan dans la communauté TE pour des applications à température ambiante. Leur grand avantage est une conductivité thermique intrinsèquement faible à température ambiante (0.2-0.6 $W.m^{-1}K^{-1}$) qui est complétée par leur facilité de traitement et leur faible coût. Les films minces de dérivés de poly (3,4-éthylènedioxythiophène) (PEDOT) dopés avec des molécules de p-toluènesulfonate (Tos) peuvent présenter un ZT aussi élevé que 0,25 à température ambiante, soulignant ainsi le potentiel élevé de tels systèmes pour les applications futures. Dans cette thèse, nous nous sommes focalisés sur la compréhension des propriétés des films minces de PEDOT:Tos en jouant sur la méthode de polymérisation. Nous avons démontré que la conductivité électrique peut être améliorée en ajoutant des additifs dans la formulation du matériau. De plus, la concentration en p-toluènesulfonate est un paramètre permettant d'influencer la conductivité électrique sans modifier la valeur du coefficient Seebeck. Finalement, l'hybridation des précurseurs de PEDOT:Tos avec des copolymères à blocs a permis de concevoir des structures de PEDOT:Tos à l'échelle nanométrique.

Mots clés : Thermoélectricité – Polymères π-conjugués – Transport de charges – PEDOT:Tos

---

Title: Semi-metallic polymers for thermoelectric applications

Abstract: Thermoelectric (TE) materials have the potential to convert vast amounts of waste heat directly into electricity, therefore reducing the dependence on fossil fuel. In thermoelectricity, the concept of a phonon glass/electron crystal is often used to describe an ideal thermoelectric material. According to this concept, a good TE material should inhibit the conduction of phonons (thus having a low thermal conductivity) while efficiently conducting electronic charge carriers (high electrical conductivity). In order to quantify the efficiency of TE systems, the figure of merit, ZT, is used as a measure of performance. Recently, conducting polymers have gained momentum in the TE community for applications at room temperature. Their great advantage is an intrinsically low thermal conductivity at room temperature (0.2-0.6 $W.m^{-1}K^{-1}$) that is complemented by their easy processability and their low cost. Thin films of poly(3,4-ethylenedioxythiophene) (PEDOT) derivatives doped with p-toluenesulfonate (Tos) molecules can exhibit a ZT as high as 0.25 at room temperature underlining the high potential of such systems for future applications. In this thesis, we focused on the understanding of PEDOT:Tos thin films properties by playing on the polymerization method. We demonstrated that the electrical conductivity can be improved by adding additives to the formulation of PEDOT:Tos materials. Moreover, the concentration of p-toluenesulfonate is an important parameter to tune the electrical conductivity without changing the Seebeck coefficient. Finally, the hybridization of PEDOT:Tos precursors with block copolymers allows us to design PEDOT:Tos nanostructures.

Keywords: Thermoelectricity – π-conjugated polymers – Charge transport – PEDOT:Tos

---

Unité de recherche

Laboratoire de Chimie des Polymères Organiques (LCPO), UMR 5629,
Bâtiment B8, Allée Geoffroy Saint Hilaire, 33615 Pessac Cedex, France